Functional and behavioural characterisation of *C. elegans* acid-sensing DEG/ENaCs

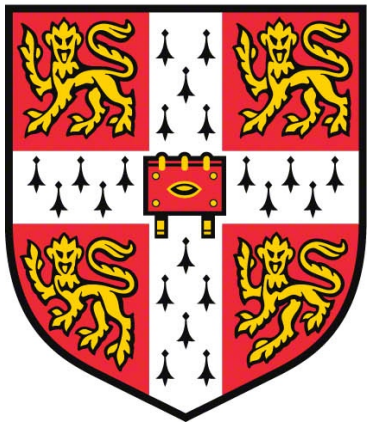

Eva Dorothea Kaulich

MRC Laboratory of Molecular Biology

Homerton College

This dissertation is submitted to the University of Cambridge

for the degree of Doctor of Physiology

March 2021

Declaration

This thesis is the result of my own work and includes nothing which is the outcome of work done in collaboration except as declared in the Preface and specified in the text. I further state that no substantial part of my thesis has already been submitted, or, is being concurrently submitted for any such degree, diploma or other qualification at the University of Cambridge or any other University or similar institution except as declared in the Acknowledgements and specified in the text. It does not exceed the prescribed 60 000 words in length (exclusive of tables, footnotes, bibliography, and appendices) for the Biology Degree Committee.

Summary of the thesis

The overarching aim of this thesis was to investigate how proton-sensitive members of the *C. elegans* DEG/ENaC family regulate cellular processes and drive behaviour. In the initial screen, I identified five *C. elegans* DEG/ENaCs subunits that can form proton-sensitive homomeric channels when expressed *in vitro* in *Xenopus* oocytes. These could be further clustered into two groups based on their response to neutral and low pH *in vitro*: One group that is inhibited by increasing concentrations of protons (ACD-5 and DEL-4, as well as the previously identified ACD-1 (Wang et al., 2008)) and the other one that can be activated by increasing concentrations of protons (ASIC-1, ACD-2 and DEL-9). Exploration of cellular expression pattern and amino acid sequence similarity revealed that *C. elegans* DEG/ENaCs can form clusters that reflect expression in neuronal or non-neuronal tissue but these clusters do not correspond to the electrophysiological properties presented here.

Further electrophysiological characterisation of candidate subunits showed that increasing concentrations of protons inhibit or activate the homomeric channels in a dose-dependent manner. The ACD-5 and DEL-4, which are inhibited by low pH, show specific pH ranges in which the channel is open or closed, which might reflect their physiological environment *in vivo*. A similar observation has been made for the human ENaC currents, they are regulated by a pH range that is comparable to the one in epithelia where ENaCs are expressed (Collier and Snyder, 2009). The electrophysiological characterisation confirmed previous results that the *C. elegans* DEG/ENaCs are highly diverse in their ion selectivity (Fechner et al., 2020). This again, is likely to reflect their diverse physiological function *in vivo*.

Based on expression pattern and *in vitro* electrophysiological evidence, I further characterised one candidates of each group in more detail, DEL-9 which belongs to the group that is activated by low pH and ACD-5 which is inhibited by low pH. Interestingly, both can be expressed in neuronal and non-neuronal tissue, suggesting that their proton-sensing properties are important for various physiological processes and are not restricted to neuronal functioning, and mutants of either gene show defects in rhythmic behaviours. This fits well with evidence across species that DEG/ENaCs and ASICs are involved in regulating cellular excitability and communication to modulate behaviour (Du et al., 2014, Wemmie et al., 2003, Wemmie et al., 2002, Voglis and Tavernarakis, 2008).

Finally, in the last chapter, I identified *daf-7*/TGFβ-like signalling as the regulatory genetic pathway for neuronal and global upregulation of ACD-5 in dauers and post-dauers. I have further explored the genetic relationship between *daf-7*/TGFβ and *acd-5* and explored potential behaviours relating to expression in ASK sensory neurons. Taking together the evidence presented suggests that at some level ACD-5 regulation depends on food and that ACD-5 is implicated in food-sensing: It is expressed in the chemosensory ASK neuron and in the intestine, it is implicated in food-sensing behaviours, and it is regulated by TGFβ-like signalling which again is a developmental pathway linked to food abundance.

Acknowledgements

A PhD is never a project in solitude. Without support and discussions, scientific research would be lonely and less rewarding. Therefore, I would like to acknowledge the following people and thank them for their advice and support at various stages during or throughout my PhD:

Professor William R. Schafer, my PhD supervisor, for his advice and support without whom this thesis would not have been possible.

Dr Denise S. Walker, for her encouragement and continuous support throughout the PhD, advice and discussions of this project.

Dr Ingo Greger, my second internal LMB supervisor, and Professor Julie Ahringer, my University supervisor.

All the current and past members of the Schafer lab, especially

Dr Yee Lian Chew, for being there in first year of my PhD, and setting up the microfluidic system together with me and Sol Ah Lee.

Dr Iris Hardege who taught me how to do Two-Electrode-Voltage Clamp.

Dr Yi-Quan Tang, Dr Iris Hardege and Dr Julia Morud-Lekholm for their advice on electrophysiology and general discussions about my project.

Patrick McCubbin, my Summer Student whom I supervised during my second year of the PhD and who constructed the EGAS plasmids for *Xenopus* oocyte expression.

Dr Laura Grundy, who started working on ASICs in her thesis.

Dr Amy Courtney for advice on the Sequence Similarity Network.

Lidia Ripoll-Sanchez who did some of the *C. elegans* microinjections.

The MRC LMB, in particular:

Dr Soudabeh Imanikia for sharing her knowledge and providing general help with qPCR and RNAi feeding experiments.

The LMB graduate administration, Dr Cristina Rada and Nikki Domingues.

The LMB Science and Support Facilities, in particular Ben Sutcliffe, Jonathan Howe and Nick Barry from the Light Microscopy Team, and Sue Hubbard and Martyn Howard and the Team from Media and Glass Wash.

MRC LMB Scholarship for funding.

My collaborators:

Dr. Yiquan Tang who conducted and analysed the Co-IP experiments.

Professor Brian Ackley (The University of Kansas, US) who conducted the experiments of the *C. elegans* intestinal lumen imaging.

Professor Kyuhyung Kim's lab (Daegu Gyeongbuk Institute of Science & Technology, Korea) for providing me with their *C. elegans* DEG/ENaC transcriptional reporter plasmids.

Lastly, I would like to extend my sincere thanks to

Dr Rosina Giordano-Santini, a friend and former colleague, who has always inspired me with her attention to detail and scientific reasoning.

The Hilliard lab, especially Professor Massimo Hilliard and Dr Xue Yan Ho for their support and advice.

Dr Denise S. Walker, Raquel A. Sandoval-Ortega (University of Bern, Switzerland), Dr Lisa Heinke, Dr Iris Hardege, Dr Yi-Quan Tang and Milan Stuermer for helpful advice and comments on various aspects of the thesis manuscript.

The Neurobiology Division, Taylor lab and the de Bono lab at the MRC LMB as well as the Beets lab, the Temmerman lab and Schoofs lab at the KU Leuven for general discussion in our joint meetings.

Professor Stefan A. Pless and his lab (University of Copenhagen) and Dr Ewan St. John Smith (University of Cambridge) for their insights on vertebrate ASICs.

The University of Cambridge and Homerton College.

My examiners Dr Howard Baylis and Dr QueeLim Ch'ng for their helpful comments and suggestions.

My Family, especially Milan, and all my friends around the world who have always supported me and believed in me.

Abbreviations list

aBoc – anterior body contraction

ASIC – acid-sensing ion channel

C. elegans – *Caenorhabditis elegans*

Cas9 – CRISPR associated protein 9

cDNA – complementary DNA

CGC – *Caenorhabditis* Genetics Centre

CRISPR – Cas9 nuclease from the microbial clustered regularly interspaced short palindromic repeats

cRNA – complementary ribonucleic acid

CTX – chemotaxis

daf – dauer formation defective

DEG/ENaC – Degenerin/Epithelial Sodium Channel

DMP – defecation motor programme

DNA – deoxyribonucleic acid

DOA – day old adult

EMC – enteric muscle contraction

E_{rev} – reversal (or equilibrium) potential of ions

ΔE_{rev} – reversal potential shift

GABA – gamma-amino butyric acid

gDNA – genomic deoxyribonucleic acid

GFP – green fluorescent protein

IC_{50} – half maximal inhibitory concentration

IQR – interquartile range

IV – current-voltage

KR35 – Kansas Red 35

MAT – maximum anterior transitions

NGM – nematode growth medium

pBoc – posterior body contraction

PCR – polymerase chain reaction

pH_{50} – half maximal activation/inhibitory pH

PPK – Pickpocket (protein)

RFP – red fluorescent protein

RNAi – ribonucleic acid interference

ROI – region of interest

RT-qPCR – real-time quantitative Polymerase Chain Reaction

SE – standard error

SEM – standard error of the mean

SSN – Sequence Similarity Network

TEVC – two-electrode voltage clamp

TGFβ – Transforming Growth Factor beta

vm – vulva muscle

Specific gene or protein abbreviations and descriptions of individual neurons are described in the main text and in the appendices of CHAPTER 1 and CHAPTER 3.

Table of Contents

List of Figures

Supplementary figures in Appendices

List of Tables

Supplementary Tables in Appendices

CHAPTER 1 – INTRODUCTION, LITERATURE REVIEW AND AIMS

1. 1. Introduction

One big question in neuroscience is to understand how behaviour is generated. This question can be addressed at different levels, such as the genetic and molecular level, cellular level, the level of local neuronal circuits and at the level of the entire organism. With recent advancements in neuronal connectomics and large sets of transcriptomics, scientist have moved towards trying to understand behaviour in terms of connections and molecules, believing that knowing these will allow us to probe for essential circuits and underlying molecular mechanisms, that, taken together, generate predicted behavioural outcomes.

The first complete synaptic connectome was mapped for the 302 neurons of the nematode *Caenorhabditis elegans* (White et al., 1986). More recently, a map of the fruit fly brain has been generated using electron microscopy and a collective effort of mapping each individual connection is ongoing (Scheffer et al., 2020, Zheng et al., 2018). Other collaborations are tackling even larger connectomic datasets, such as the Allen Brain Map, which includes anatomical references of mouse, human and non-human primate brain structures, taxonomy of cell types and new data from Patch-seq experiments that use morphological information combined with transcriptomics and electrophysiological characterisation (The Allen Institute for Brain Science: portal.brain-map.org).

Having the complete synaptic connectome for *C. elegans* has been a valuable resource to guide research by constraining circuit analysis through providing a list of pre- and postsynaptic connections for each neuron. For example, guided by this connectivity map, Martin Chalfie and colleagues in Sydney Brenner's lab have used laser ablations to identify two putative circuits responsible for escape responses to anterior or posterior body touch (Chalfie et al., 1985). Another example is mapping the GABAergic neurotransmitter system using expression studies in combination with laser ablation of GABAergic neurons; this provided insight into the control of muscles and evidence for an excitatory as well as inhibitory role of the neurotransmitter GABA (McIntire et al., 1993). These examples illustrate the advantage of having a complete

synaptic connectome as it enables the generation of testable hypotheses about general as well as specific roles of individual neurons.

However, 2013 Nobel Prize winner Thomas Südhof and many other scientist have argued that, despite having the complete synaptic connectome for *C. elegans*, "we still don't know how the neural networks of *C. elegans* 'work'" (Südhof, 2017). So, what is missing? Südhof addresses the discussions about the three shortcomings when trying to understand the brain by solely mapping synaptic connections (Südhof, 2017). Firstly, neglecting plasticity, which allows neurons to adapt and change in response to cellular and environmental stimuli.

Secondly, neglecting extra-synaptic communication including extra-synaptic and volume neurotransmission as well as peptides or diffusible messengers, which all can modulate neuronal functioning. This is what I will here consider as "wireless connectome" a network of neuromodulators that are act outside synapses (Bentley et al., 2016). Thirdly, he stresses the role of non-neuronal tissue, such as glia, which contribute to neuronal functioning. The underlying belief is, of course, that understanding the molecular mechanisms of the nervous systems will ultimately help us to understand the brain as a whole (Südhof, 2017). Other voices have gone even further, demanding a whole-body connectomics approach instead of just mapping the brain (which is the case for the fruit fly or mouse) (Lo and Chiang, 2016). The whole-body connectome has so far only been generated for the nematode *C. elegans* making it an excellent model to study. Finally, I would like to add to Südhof's points the concept of degeneracy which the ability of structurally different circuits to perform the same function as well as that networks are working in parallel to generate behaviour (for a comprehensive review on these thoughts see (Bargmann and Marder, 2013)).

The Schafer lab at the MRC Laboratory of Molecular Biology (Cambridge) has studied *C. elegans* connectomics at both the synaptic level with a focus on electrical and chemical synapses between individual neurons (e.g. (Rabinowitch and Schafer, 2015, Rabinowitch et al., 2014, Rabinowitch et al., 2013, Walker and Schafer, 2020, Chew et al., 2017)), as well as the "wireless connectome" with a focus on neuropeptides and monoamines (e.g. Morud, Hardege et al., unpublished, (Bentley et al., 2016, Chew et al., 2018)) with the aim to fully understand neural connectivity.

In this thesis, I take on the challenge to look at a less established form of transmitter, protons, with a focus on their receptors called Acid-Sensing Ion Channels (ASICs) and their role in modulating behaviour via neuronal and non-neuronal tissues.

The term ASICs has been mainly used to describe a mammalian, proton-sensitive subgroup of the diverse family of Degenerin/Epithelial Sodium Channels (DEG/ENaC), an amiloride-sensitive, non-voltage gated cation channel family. The *C. elegans* channels that I describe here are often only referred to as DEG/ENaCs, which might be partly due to a lack of electrophysiological characterisation, which I will also address (see CHAPTERs 3, 4, and section 1. 3. Aims and Objectives). As laid out in the following sections, one of the proposed functions for ASICs is proton sensing in the synapse, where protonergic neurotransmission has been described occurring in concert with classical neurotransmission (Du et al., 2014, Soto et al., 2018, Wemmie et al., 2002, Du et al., 2017, Uchitel et al., 2019).

Going back to Südhof's criticism above, ASICs present an interesting target to investigate, as they are activated by protons, which can be seen as diffusible messengers, but ASICs can also be modulated by a variety of stimuli including the classical neurotransmitter serotonin, as well as peptides and toxins (Vyvers et al., 2018, Besson et al., 2017, Diochot et al., 2012, Xie et al., 2003, Wang et al., 2013b). This is why they have also been referred to as "coincidence detectors". Furthermore, ASICs were shown to be involved in neuronal plasticity and modulating synaptic strength (Du et al., 2014, Voglis and Tavernarakis, 2008), raising further questions about their synaptic regulation under different environmental conditions and hence their influence on adaptations of behaviours.

As mentioned above, non-neuronal tissues have previously been shown to be important for neuronal functioning and appropriate behaviour. While the main focus here is on glia cells (and many scientist have also implicated protons secreted by glia in neuronal functioning (Deitmer and Rose, 1996, Wang et al., 2008)), *C. elegans* has provided us with evidence that protons can act as transmitters to generate behaviour independent of the nervous system (Beg et al., 2008). Investigating the role of ASICs as proton receptors therefore opens up new avenues for understanding the complex molecular mechanisms that contribute to the generation of behaviour, and potentially uncover translational conserved mechanisms of ASICs in driving behaviour in both neuronal and non-neuronal tissue.

1. 2. Literature Review

This thesis is divided into four chapters that describe my experimental data, each addressing one or multiple aims (see 'Aims and Objectives' below) with its own introduction, results and discussion section. However, the overarching focus is on members of the *C. elegans* DEG/ENaC family and how their proton-sensing properties translate into cellular processes and ultimately manifest themselves in behaviours. Therefore, in the following section, I will introduce the conserved DEG/ENaCs superfamily, with a focus on the ASICs, concentrating on and what is known about their proton-sensing role.

However, before diving into the world of ASICs and DEG/ENaCs, I will briefly introduce what is known about protons as signalling molecules and how this can inform our thinking about them as an unconventional form of neurotransmitter. In the current chapter, I will use the term "ASICs" to refer to the mammalian members and "*C. elegans* DEG/ENaCs" to refer to the nematode members of these acid-sensing channels. Finally, as I am using the nematode *C. elegans* as a model system to conduct my research, I will describe the advantages of using *C. elegans* to address the question of understanding the molecular and cellular mechanisms driving behaviour. (Abbreviations of *C. elegans* neurons and genes can be found in Appendix C 3. 5. 1. Abbreviation list of genes and neurons).

1. 2. 1. Protons as transmitters – protonergic (neuro)transmission

Proton concentrations in cellular environments and different cellular compartments are tightly controlled. For instance, pH of mammalian cells is actively maintained at pH 7.0-7.4 intracellularly, and at pH 7.1-7.3 extracellularly (Deitmer, 2007, Casey et al., 2010). Similarly, invertebrates such as the nematode *C. elegans* have an intracellular pH of around 7.4 (Mathew et al., 2014, Nehrke, 2003) implying that this is a suitable pH for cells to function. The proton equilibrium against the electrochemical gradient is maintained by a Na^+ gradient which drives the Na^+/H^+ exchanger, anion transporters and other acid/base transporters, thereby playing a major housekeeping role in maintaining proton homeostasis in a variety of tissues including in the gastro-intestinal tract (Deitmer, 2007, Ruffin et al., 2014, Sherman et al., 2005, Nehrke and Melvin, 2002). Therefore, protons have traditionally been seen as regulators of homeostatic processes essential for cellular functioning.

Besides having a homeostatic function, proton transients can be observed in neurons and glial, as well as extracellular spaces, in response to electrical and chemical stimulation (Deitmer and Rose, 1996, Deitmer, 2007, Chesler and Kaila, 1992). Therefore, proton signalling was previously compared to Ca^{2+} signalling but mainly acting on extracellular domains (Soto et al., 2018). However, unlike the dynamics of Ca^{2+} transients that increase and then recover, proton gradients can occur in two directions, becoming more acid or alkaline (Deitmer, 2007), suggesting a different level of complexity.

Cumulative evidence has since suggested that these rapid pH transients are likely to be signals rather than only a by-product of inadequate homeostatic pH regulation or neurotransmission (Du et al., 2014, Soto et al., 2018, Beg et al., 2008, Wemmie et al., 2002, Du et al., 2017, Deitmer, 2007, Highstein et al., 2014, Uchitel et al., 2019). The term 'protonergic neurotransmission' was adopted to describe the role of protons in interplay with classical mechanisms of synaptic transmission. While it has been well established that protons act as neuromodulators at the synapse, there is still an ongoing debate whether protons satisfy the criteria for neurotransmitters (Du et al., 2014, Soto et al., 2018, Beg et al., 2008, Wemmie et al., 2002, Du et al., 2017, Uchitel et al., 2019).

Here, I will briefly revisit the arguments that have been put forward (Du et al., 2017): Protons are present in the presynaptic cell, where they are co-packed in vesicles with other neurotransmitters by the action of the proton pump Vacuolar-type ATPase (V-ATPase) (Gowrisankaran and Milosevic, 2020). Upon stimulation of the presynaptic cell, protons are co-released from the acidic vesicles (pH 5.5) into the synaptic cleft, inducing a brief local drop in pH of 0.2 to 0.6 units (Miesenbock et al., 1998, Du et al., 2014, Zeng et al., 2015). This in turn simulates postsynaptic receptors. In the chemical synapse, protons can bind to specialised proton receptors, such as ASICs (see next section 1. 2. 2. Acid-sensing ion channels (ASICs) are proton receptors) and exogenous delivery of protons mimics the endogenous proton response and blocking the receptor leads to blockage of proton activity (Du et al., 2014, Soto et al., 2018, Beg et al., 2008, Wemmie et al., 2002, Du et al., 2017).

One issue that has been highlighted is that in the synapse protons are only co-released with neurotransmitters but independent regulated proton release at synapses has not been described (Soto et al., 2018). However, rhythmic release of protons via Na^+/H^+ exchanger has been described for *C. elegans* intestinal epithelial cells (Beg et

al., 2008). While the underlying mechanisms of protonergic (neuro)transmission inside but especially outside the nervous system are not well-understood, it has become clear that protons act as signalling particles that can affect general cellular excitability (Beg et al., 2008) and synaptic activity (Du et al., 2014, Highstein et al., 2014) in addition to maintaining homeostasis.

1. 2. 2. Acid-sensing ion channels (ASICs) are proton receptors

It has been long established that many molecules including transporters or enzyme as well as receptors and ion channels are modulated by changes in pH, and many acid-sensitive ion channels have been discovered which are reviewed elsewhere (Pattison et al., 2019, Holzer, 2009, Deitmer, 2007). Nevertheless, the strongest candidates for sole proton-receptors are the mammalian ASICs (Soto et al., 2018) which are the focus of this section. The first acid-sensing ion channel (ASIC3) was cloned in the 1990s (Waldmann et al., 1997) and was shown to be closely related to the previously described ENaCs and the *C. elegans* degenerins MEC-4 and DEG-1 (Canessa et al., 1993, Lingueglia et al., 1993, Driscoll and Chalfie, 1991).

1. 2. 2. 1. Acid-Sensing Ion Channels (ASICs) are part of the diverse family of Degenerin/Epithelial Sodium Channels (DEG/ENaC)

As the name suggests, the origin of the DEG/ENaC family dates back to the identification of sequence similarity between degenerins (DEG) from the nematode *C. elegans* and subunits of the mammalian epithelial sodium channel (ENaC) (Canessa et al., 1993, Lingueglia et al., 1993, Driscoll and Chalfie, 1991). This diverse family of non-voltage gated cation channels also includes the mammalian ASICs, *Drosophila* pickpockets (PPK) and an array of representatives from across animal phyla. Electrophysiological approaches, particularly expression in *Xenopus* oocytes, have played an essential role in establishing the physiology of channel properties of this diverse family (Zhang and Canessa, 2002, Li et al., 2009, O'Brodovich et al., 1993, Canessa et al., 1993, Canessa et al., 1994, Schild et al., 1997). The *C. elegans* DEGs, meanwhile, played a pivotal role in establishing genetic and behavioural approaches to their characterization *in vivo* (Driscoll and Chalfie, 1991).

As genome sequences became available, the DEG/ENaC family rapidly gained new members. In particular, it became clear that both *C. elegans* and *Drosophila*

melanogaster have vastly expanded numbers, with 30 and 31 members, respectively. As the Sequence Similarity Network (SSN) and phylogram in Figure 1A and B show, they form distinct homology groups, with the vertebrate ENaCs and ASICs clustering separately. However, it is not clear whether these clusters share functional characteristics.

In the phylogram (Figure 1A), MEC-4 and MEC-10 cluster with the mammalian ENaCs, and they share their mechanosensitive properties (Satlin et al., 2001, Carattino et al., 2004, Karpushev et al., 2010, Shi et al., 2016), whereas DEL-8 clusters with the mollusc and flatworm FaNaC and ENaC, some of which are proton-activated channels and some are peptide-activated ones (Golubovic et al., 2007, Schmidt et al., 2018). Indeed, the *C. elegans* DEG/ENaCs are the only group to cluster with members from multiple other phyla. The *Drosophila* pickpockets, on the other hand, form distinct, but diverse, clusters of their own, which is especially apparent in the SSN in Figure 1B. The vertebrate ASICs closely cluster with the TadNaCs from *Trichoplax adhaerens,* a basal multicellular animal lacking any internal organs and neurons, and both groups have members that are sensitive to changes in proton concentration (Zhang and Canessa, 2002, Elkhatib et al., 2019).

Visualising sequence similarity and phylogeny is a useful starting point to visualise different clusters within the family and generate functional hypotheses for those sequences whose molecular functions are currently unknown. In the following chapters, I will address this question by focussing on the *C. elegans* family of DEG/ENaCs and explore whether clusters according to sequence similarity within the *C. elegans* DEG/ENaCs reflect the molecular function of the particular channel subunit.

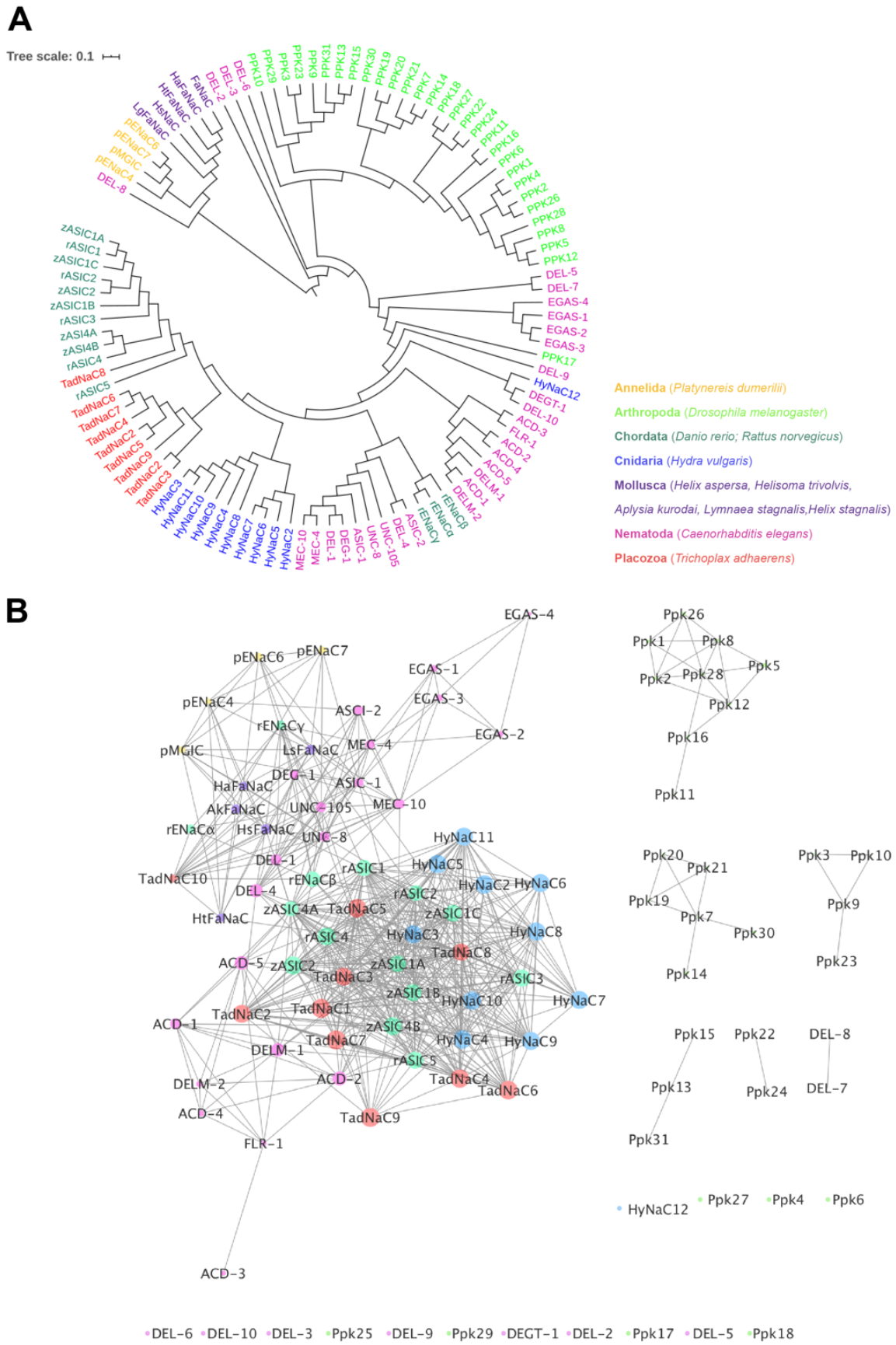

Figure 1: Phylogenetic analysis of the DEG/ENaC family.

(A) Polar view of a phylogenetic tree of the DEG/ENaC super-family. Protein sequences were aligned in MAFFT version 7 multiple alignment program using rough distance and average linkage UPGMA (unweighted pair group method with arithmetic mean) and the tree was visualized using iTOL (Ciccarelli et al., 2006, Letunic and Bork, 2019, Kuraku et al., 2013). Tree scale represents the amount of genetic change. (B) Sequence Similarity Network (SSN) of diverse members of the DEG/ENaC family. Generated using the web tool for SSNs for protein families (EFI-EST) developed by the Enzyme Function Initiative efi.igb.illinois.edu/ (Zallot et al., 2019, Zallot et al., 2018, Gerlt et al., 2015, Gerlt, 2017). Each symbol represents a protein (node), two nodes are connected by a line (edge) if they share >25% sequence similarity and lengths of edges correlate with the relative dissimilarities of each pair. Relative positioning of disconnected clusters and nodes has no meaning. Cytoscape (Shannon et al., 2003) is used to explore SSNs. Node sizes are determined by the degree of connectivity of the nodes (number of edges). The EFI-EST webtools use NCBI BLAST and CD-HIT to create SSNs. The computationally-guided functional profiling tool uses the CGFP programs from the Balskus Lab (https://bitbucket.org/biobakery/cgfp/src) and ShortBRED from the Huttenhower Lab (http://huttenhower.sph.harvard.edu/shortbred). The data used to build these networks originate from the UniProt Consortium databases and the InterPro and ENA databases from EMBL-EBI. Node colouring in A and B is according to phyla as indicated. Accession numbers can be found in the Appendix A, Supplementary Table 1.

1. 2. 2. 2. Chicken ASIC1 as a model for DEG/ENaC structural properties

Proteins that are encoded by DEG/ENaC genes range from 500-950 amino acids. The first crystal structure at low pH of a DEG/ENaC was cloned from chicken ASIC1 (cASIC1) after removal of both N-and C-terminal residues, here referred to as ∆cASIC1 (Jasti et al., 2007), and has since been used to inform a variety of structural studies as all DEG/ENaC family members share a common topology (Figure 2).

The authors of the original paper describe the ASIC structure as “chalice-like”, with each subunit comprising short cytoplasmic N- and C-termini, two transmembrane alpha-helices, a bound chloride ion and a large, disulphide-bond rich, multidomain extracellular loop which makes up approximately two thirds of the protein (Jasti et al., 2007). Using light-scattering and cross-linking, it was shown that ∆cASIC1 forms trimers (Jasti et al., 2007), even though recent biochemical evidence has suggested that tetrameric confirmation is also possible (van Bemmelen et al., 2015). Each of the subunits show extensive contacts in both extracellular as well as transmembrane domains, the latter may function in stabilisation and assembly of the channel (Jasti et al., 2007).

The first crystal structure also provided some evidence for proton-binding sites in the acidic pocket that were followed up with amino acid substitutions and electrophysiological experiments which confirmed that carboxyl-carboxylate pairs in the acidic pocket between the finger and thumb domains are indeed participating in pH-sensing (Jasti et al., 2007) (Figure 2).

The gating behaviour of ASICs is tightly regulated by the interplay between protons and cation concentrations, in particular Ca^{2+} ions, and is highly subunit specific. For instance, some ASICs are permeable for Ca^{2+} (Zhang and Canessa, 2002, Bässler et al., 2001, Hoagland et al., 2010) but others are inhibited by Ca^{2+} which can bind close to the channel pore (Paukert et al., 2004). Ca^{2+} can also allosterically modulate ASICs, changing their response to pH (Zuo et al., 2018, Immke and McCleskey, 2003, Babini et al., 2002, Paukert et al., 2004). Similarly, Zn^{+} also acts by altering the response to protons, potentiating the activation of ASIC2-containing channels (but not ASIC1a or ASIC3 homomers) by binding to the extracellular loop (Baron et al., 2001, Adams et al., 1999b). Further structural and mutation studies have revealed that the specific blocker of DEG/ENaCs, amiloride, an antihypertensive drug, binds within the open channel pore, on the extracellular acidic pocket (Schild et al., 1997, Kellenberger et al., 2003, Baconguis et al., 2014).

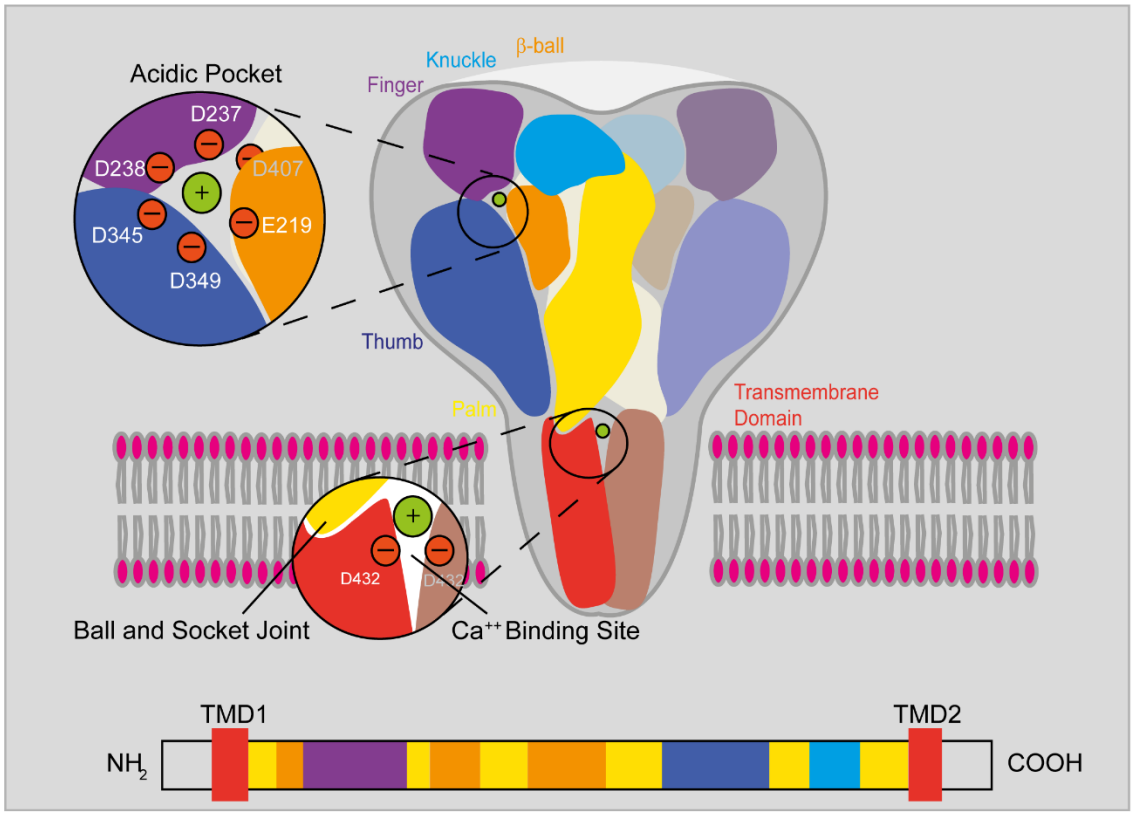

Figure 2: Schematic of the chicken ASIC1 structure as a model for DEG/ENaC structure.

Schematic of trimeric channel structure of chicken ASIC1. Each subunit has two transmembrane domains, with a large extracellular domain and relatively short N- and C-terminal cytoplasmic domains. Subdomains are indicated, along with key residues in the acidic pocket and at the entrance to the pore. Schematic below showing the location of residues contributing to each subdomain within the primary protein sequence. Figure generated by Laura Grundy with permission (in (Kaulich et al., unpublished)).

1. 2. 2. 3. ASICs proton-sensing and amiloride sensitive properties

As mentioned in the previous sections, acidosis, the increase in proton concentrations, can occur under healthy physiological conditions such as during synaptic transmission (Du et al., 2014), and cells monitor tissue acidosis though membrane proteins including ASICs (Vina et al., 2013, Ortega-Ramirez et al., 2017). Insights into pH-sensitivity of ASICs and other DEG/ENaCs are largely based on heterologous expression *in vitro*. Acid-evoked currents were first reported in cultured mouse and rat neurons (Gruol et al., 1980, Krishtal and Pidoplichko, 1980). Several years later, the gene encoding a channel with similar acid-dependent currents was cloned, later named as ASIC3 (Waldmann et al., 1997).

Acid-sensitive DEG/ENaC family members across species can be classified into two groups: One group shows activation and the other shows inhibition when encountering increasing proton concentrations. The former group includes mammalian ASICs (Waldmann et al., 1997, Zhang and Canessa, 2002), the zebrafish zASICs (Chen et al., 2007), the human ENaCs (Collier and Snyder, 2009) and the *Drosophila* PPK1 (Boiko et al., 2012).

Vertebrate ASICs are closed at neutral pH and generate proton-activated inward currents which increase with decreasing pH of the extracellular solutions. However, the precise concentration of protons required to activate the channels varies depending on the subunit, with the half activation pH varying from around 6.5 to 4.5 (Waldmann et al., 1997, Zhang and Canessa, 2002, Chen et al., 2007). Together they thus cover a significant range of pH, with relevance to a diverse array of biological processes and contexts. Heteromeric human αβγENaC channels, in contrast, are open at neutral pH with a maximal current at pH 6 and minimal current at pH 8.5 (Collier and Snyder, 2009). This *in vitro* data fits in well with the pH range in the collecting duct of the kidney and other epithelia where ENaCs are expressed. Rat

αβγENaC currents are not altered over the same range, indicating species differences in regulation by protons (Collier and Snyder, 2009). The *Drosophila* DEG/ENaC that has been shown to exhibit acid-evoked currents is PPK1 in cultured neurons (Boiko et al., 2012). Currently, there is no evidence from endogenous *C. elegans* channels that they can exhibit excitatory acid-evoked currents. However, *C. elegans* mutant UNC-105 or mutant UNC-8 currents are enhanced by low pH *in vitro* (Garcia-Anoveros et al., 1998, Jospin and Allard, 2004, Wang et al., 2013c).

The second group of protons-sensitive DEG/ENaC members are constitutively active when heterologously expressed, i.e. display inward currents at neutral pH in the absence of a stimulus, and are blocked by increasing extracellular proton concentrations. Current members are confined to mouse ASIC5 (also called brain liver intestine Na^+ channel (BLINaC)) (Wiemuth and Grunder, 2010), *Trichoplax* TadNaC6 (Elkhatib et al., 2019) and *C. elegans* ACD-1 (Wang et al., 2012, Wang et al., 2008). There might be an additional group consisting of the mouse ASIC5 and the rat ASIC1a which are also permeable for protons themselves (Wiemuth and Grunder, 2010, Chen and Grunder, 2007, Wiemuth et al., 2014). How proton permeability impacts cellular function has yet to be elucidated. Nevertheless, despite the expansion and known diversity of DEG/ENaCs in worms and flies many members lack functional characterization at the level of the channel.

With growing interest in the DEG/ENaCs as targets for pharmacological interventions (see section 1. 2. 3. below), the list of subunit-specific ligands, modulators and blockers of ASICs has expanded (Xiong et al., 2008, Kweon and Suh, 2013, Vullo and Kellenberger, 2020). Here, I briefly want to focus on amiloride, which is an antihypertensive drug acting on the human ENaCs in the kidney and is prescribed to patients to lower systemic blood pressure (Bhagatwala et al., 2014, Teiwes and Toto, 2007). Amiloride and its derivatives were shown to be potent and specific blockers for the DEG/ENaCs (Canessa et al., 1994, Palmer and Frindt, 1986, Bentley, 1968). However, compared to the block of its derivative benzamil (Fechner et al., 2020), the amiloride block is voltage-dependent (Bentley, 1968). This means that amiloride inhibition decreases as current nears the reversal potential, and lowers inhibition with outward current. The dependence on the membrane potential is a characteristic of pore blockers, and structural analysis and mutation studies have confirmed that amiloride is an open pore blocker and binds within the channel pore on the extracellular acidic pocket (Schild et al., 1997, Kellenberger et al., 2003, Baconguis

et al., 2014). In *C. elegans*, the amiloride derivative benzamil has been shown to inhibit mechanical currents of mutant MEC-4 homomeric or heteromeric channels in response to laminar shear stress (Shi et al., 2016). In mice, amiloride also inhibits ASIC1a postsynaptic neurons of lateral amygdala brain slices (Du et al., 2014). Similarly, amiloride can block acid-evoked currents of the *Drosophila* PPK1 in neurons (Boiko et al., 2012).

Amiloride has also been shown to enhance currents and even activate ASICs. This paradoxical phenomenon was firstly described in the human ASIC2 which showed that amiloride enhances currents induced by stimulation with extracellular Zn^{2+} (Adams et al., 1999b). A similar observation has been made for homomeric ASIC3 and heteromeric ASIC3/ASIC1b where amiloride acts as current-enhancing at mild acidosis and can open them at neutral pH (Li et al., 2011). One hypothesis drawn from chicken ASIC1 electron density maps derived from crystals soaked in amiloride is that the binding of two amiloride molecules in the acidic pocket might stimulate ASICs (Baconguis et al., 2014). Cations such as Na^{+} for hASIC-1b and Zn^{2+} and Ca^{2+} for αβγENaC also show a competitive interaction with amiloride (Qadri et al., 2010, Schild et al., 1997, Palmer and Andersen, 1989).

Other blockers include the nonselective potassium channel blocker tetraethylammonium (Sherwood et al., 2011, Adams et al., 1999a, Li et al., 2011), as well as toxins such as the spider venom peptide psalmotoxin-1 (PcTx1) (Escoubas et al., 2000), the sea anemone toxin (APETx2) (Diochot et al., 2004) and the black mamba venom peptide Mambalgin-1 (Diochot et al., 2012), and for some family members also Ca^{2+} (Paukert et al., 2004) or barium (Sherwood et al., 2011). Modulators include non-steroidal anti-inflammatory drugs (NSAIDs) (Voilley, 2004, Voilley et al., 2001, Fechner et al., 2020), extracellular Zn^{2+} (Adams et al., 1999b), 2-Guanidine-4-methylquinazoline (GMQ) (Yu et al., 2010), the neurotransmitter serotonin (Wang et al., 2013b), lactate (Immke and McCleskey, 2001) and endogenous (neuro)peptides (Vyvers et al., 2018, Grunder and Assmann, 2015, Durrnagel et al., 2012, Schmidt et al., 2018). Due to their susceptibility to modulation by different factors, ASIC channels have been proposed to be “coincidence detectors”.

1. 2. 3. Protons modulate and drive complex behaviours and rhythms

While this chapter will only focus on the proton-sensing properties and associated behaviours of members of the DEG/ENaC family, an overview and genetic insight into the diverse functions of the DEG/ENaC family can be found in the review by Kellenberger and Schild (Kellenberger and Schild, 2002). More recent work also showed the family's role in salt homeostasis (Hamm et al., 2010), involvement in mechanosensation and sensing shear stress (Fronius and Clauss, 2008, Shi et al., 2016, Huang and Chalfie, 1994), responses to chemosensory stimuli such as salt, water and pheromones in *Drosophila melanogaster* (Lin et al., 2005, Liu et al., 2003, Jaeger et al., 2018, Cameron et al., 2010) and salt sensation in mice (Spector et al., 1996), as well as their role in degeneration (Wang et al., 2013c, Brown et al., 2007). Below I will focus on behaviours in *C. elegans* that have been shown to be driven by proton signalling, as well as protonergic neurotransmission which has been proposed to drive neuronal plasticity and learning in rodents (Wemmie et al., 2003, Wemmie et al., 2002).

1. 2. 3. 1. Protons as drivers for the C. elegans defecation motor programme

The first evidence for protons as transmitters came from their role in eliciting muscle contractions as part of the *C. elegans* defecation motor program (DMP) (Beg et al., 2008). The DMP presents a valuable system for studying the molecular genetic analysis of short-period cellular oscillators and control of ultradian rhythms (Avery and Thomas, 1997, Thomas, 1990). It consists of a series of body contractions to expel gut contents. In wild-type animals that have a thick bacterial lawn and are undisturbed, the DMP is initiated approximately every 50 seconds with very high regularity (Thomas, 1990). Environmental factors such as temperatures below 19°C or above 30°C, food scarcity or mechanical stimulation can alter or reset the defecation cycle (Liu and Thomas, 1994).

Models of the genetic and molecular mechanism responsible for the DMP's highly rhythmic behaviour suggest that proton signalling presents an integral part. These mechanisms include the intestinal calcium wave (Dal Santo et al., 1999, Espelt et al., 2005) which is the main driver of rhythmic proton secretion from the intestinal basal membrane to the posterior muscles. These protons set off the posterior body contraction (pBoc) by protons activating the "cys-loop"-proton-gated cation channel

PBO-5/PBO-6 and mutants are defective in the pBoc step of the DMP (Beg et al., 2008). The anterior body contraction (aBoc) is elicited by the motorneuron AVL, and finally, GABA release from the neurons AVL and DVB, the latter being activated by the neuropeptide NLP-40, triggers to the enteric muscle contraction (EMC) and expulsion of gut contents ((Beg and Jorgensen, 2003, McIntire et al., 1993), Figure 3 and Figure 4).

Proton signalling also plays an important role inside the intestinal lumen as well as the intestinal cells. The pH of the intestinal lumen is weakly acidic at around pH 4, but rises to approximately pH 6 every 50 seconds during the DMP (Allman et al., 2009). Loss of the VHA-6 (Vacuolar H ATPase) protein on the apical membrane using *vha-6* RNAi knock-down increases pBoc period and variability and prevents full acidification of the intestinal lumen (Allman et al., 2009). The authors therefore suggest a role of VHA-6 in proton pumping from the intracellular space to the intestinal lumen. Their model is that protons leave from the intestinal lumen, pass through the intestinal cell and exit into the pseudocoelomic space during defecation via the Na^+/H^+ exchanger PBO-4/NHX-7 located on the surface of the intestinal membrane (Pfeiffer et al., 2008). Similarly, the Na^+/H^+ exchanger NHX-2 located at the apical membrane modulates defecation timing (measured in defecation cycle length) and proton flux by facilitating normal flow of protons between the intestinal lumen and the cytoplasm (Pfeiffer et al., 2008). Recently it has been shown that there is a wave of protons transitioning from the posterior to the anterior part of the intestinal lumen and it has been suggested that this might correspond to sequential activation of proton sensors along the length of the intestine rather than mechanical movement of the pBoc (Chauhan et al., 2013, Bender et al., 2013, Benomar et al., 2020). This in turn demonstrates that protons are an essential component of DMP signalling. Previous research has already implicated the *C. elegans* DEG/ENaC FLR-1 in controlling the rhythmicity and length of the DMP as well as generation of EMC and pBoc (Kwan et al., 2008, Take-Uchi et al., 1998), however, the underlying mechanisms are unclear.

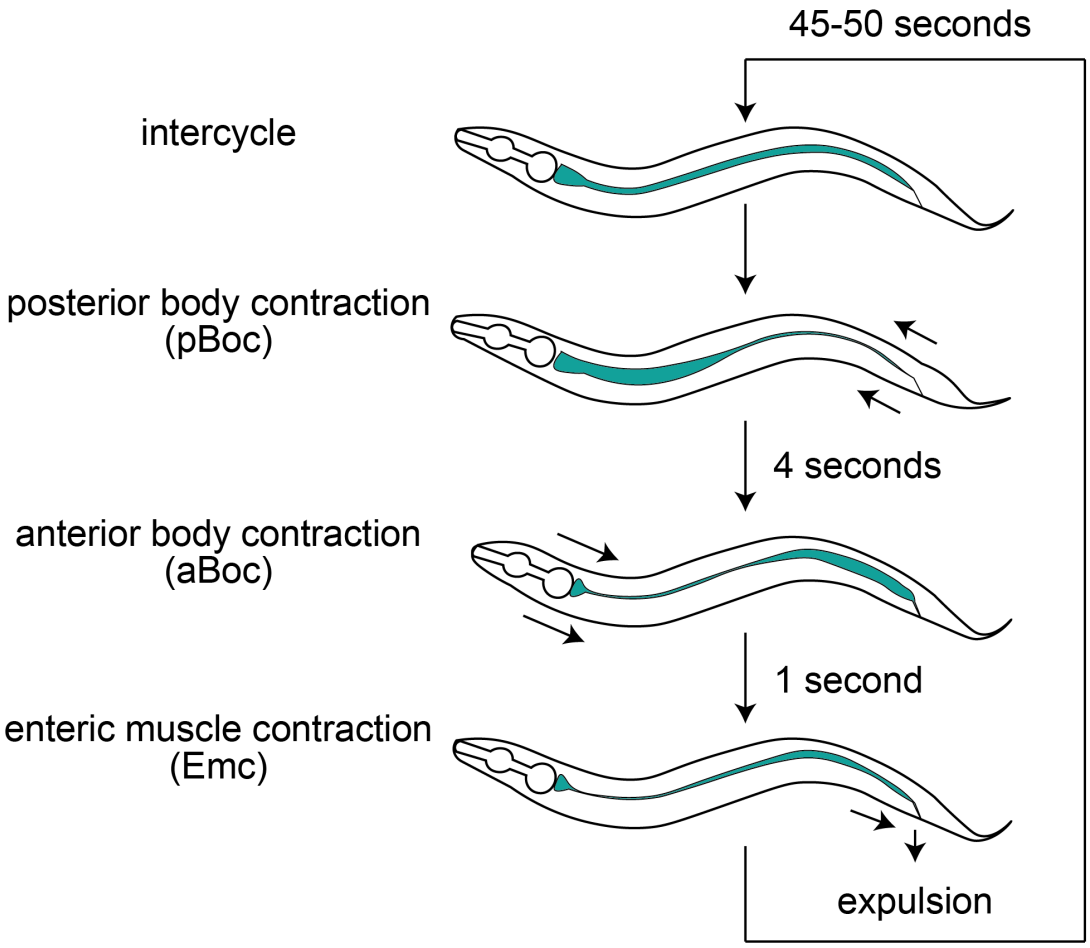

Figure 3: C. elegans Defecation Motor Programme.

Timeline of the three muscle contractions of the Defecation Motor Programme (DMP). Modified from (Kwan et al., 2008) with permission.

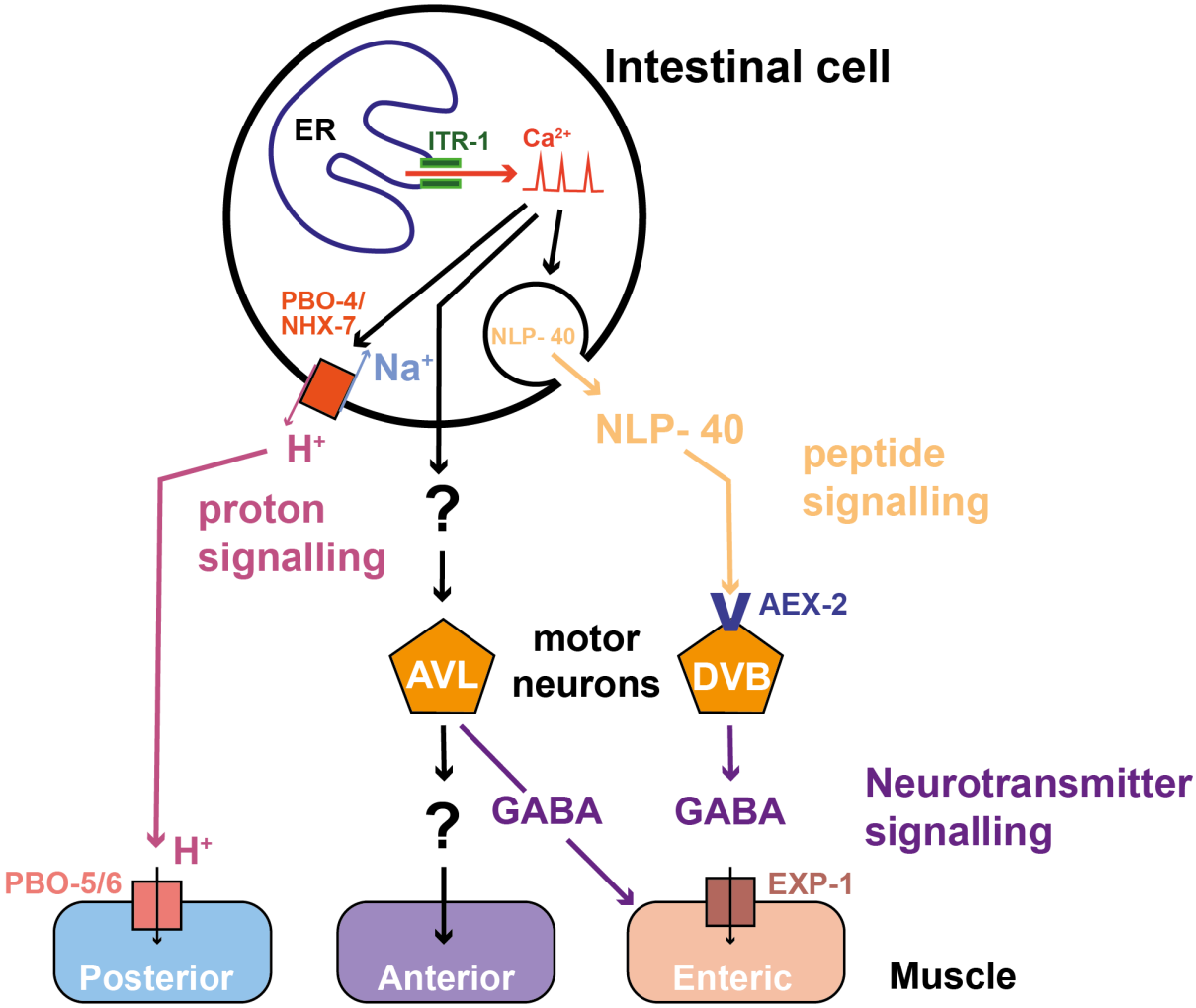

Figure 4: Circuitry and neurochemistry of the Defecation Motor Programme (DMP).

For references see main text. EXP-1 (EXPulsion defective (defecation), GABA-gated cation channel); PBO-4/NHX-7 (PBOc defective (defecation); PBO-5/6 (PBOc defective (defecation), 'cys-loop' proton gated ion channel); Na+/H+ exchanger); H+ (protons); Na+ (Sodium); Ca2+ (Calcium); ITR-1 (Inositol Triphosphate Receptor); NLP-40 (Neuropeptide Like Protein); AEX-1 (ABoc, EXpulsion (defecation) defective; punitive neuropeptide receptor). ER: Endoplasmic reticulum. Modified from (Zhao and Schafer, 2013).

1. 2. 3. 2. Evidence from across species that DEG/ENaCs are involved in modulating synaptic and neuronal function, learning and memory

Across species, knock-out mutants of DEG/ENaCs show deficits in neuronal modulation and synaptic transmission, mechanisms that underlie learning and memory. Rat ASIC1a is highly expressed in the nucleus accumbens (NAc), a brain

region known for its role in addiction linked to associative learning. *asic1a* knock-out rats showed an increased preference for the cocaine-conditioned environment, whereas overexpressing ASIC1a in the NAc reduced cocaine self-administration, suggesting that ASIC1 has a protective effect (Kreple et al., 2014). Another study used eyeblink conditioning, where a tone-conditioned stimulus is associated with a puff of air to the eye (shock) and then later tested in the absence of the air puff. Again, *asic1* knock-out animals performed poorer in making the association, they also showed defective spatial learning using the Morrison water maze (Wemmie et al., 2002). ASIC1 was found to be localized postsynaptically were it may contribute to strengthening of the synapse (as measured by Long Term Potentiation (LTP)) and synaptic plasticity, both of which are required for the acquisition of memory. However, this finding was contested in a recent study which failed to replicate the effect of *asic* knock-out on LTP suggesting that ASICs might not be essential for LTP to be generated (Wu et al., 2013). However, they agreed with previous studies that stimulating presynaptic neurons with low pH elicits postsynaptic ASIC currents in lateral amygdala pyramidal neurons and hippocampal pyramidal neurons in brain slices and that these acid-evoked currents were abolished in *asic1* knock-out mice (Wemmie et al., 2002, Du et al., 2014, Wu et al., 2013).

C. elegans ASIC-1 has also been shown to be required for associative learning. *asic-1* loss-of-function produced deficits in two learning paradigms where either cultivation temperature or a (food-associated) chemoattractant is paired with starvation such that the previously attractive temperature or olfactory/gustatory cue becomes aversive. ASIC-1 localizes at presynaptic terminals of dopaminergic neurons, so the working model is that protons released along with dopamine decrease the local pH and thus activate ASIC-1, which promotes sustained dopaminergic signalling. Dopamine release was reduced in *asic-1* mutants and the learning deficits could be mimicked by eliminating dopaminergic signalling, by ablation of the dopaminergic neurons or genetically blocking biosynthesis (Voglis and Tavernarakis, 2008).

In the harsh-touch mechanosensory PVD neurons, DEL-1, MEC-10 and UNC-8 localize to dendrites and modulate neuronal activity by inducing local Ca^{2+} increase and neuropeptide release (Tao et al., 2019). Similarly, the *Drosophila* PPK11 and PPK16 are involved in modulation of Ca^{2+}-dependent neurotransmitter release postsynaptically at neuromuscular junction (Younger et al., 2013), while the PPK29

regulates neuromuscular junction postsynaptically in baseline neurotransmission (Hill et al., 2017). Whether their function relies on (co-released) proton sensing is not clear.

In vivo voltage-clamp recordings showed that PPK1, expressed in mechanosensation neurons, also responds to acid, conducting a transient depolarizing current sufficient to elicit a burst of action potentials (Boiko et al., 2012), again suggesting a potential presynaptic role in modulating neurotransmitter release. Although these are very different functional contexts to the examples above, it will be interesting to see whether there are mechanistic parallels.

Finally, DEG/ENaCs can also exert an effect on neuronal function from surrounding glia. Two examples of this come from *C. elegans*. DEG-1 functions in acid sensation in the ASK amphid neurons and mutation of another DEG/ENaC, *acd-1,* expressed in the amphid socket cells, exacerbates these sensory deficits (Wang et al., 2012, Wang et al., 2008). Artificially increasing intracellular Ca^{2+} levels in one of these neurons bypassed the need for ACD-1, supporting the idea that ACD-1 modulates neuronal excitability (Wang et al., 2012, Wang et al., 2008). This idea is supported by the second example: DELM-1 and DELM-2 are expressed in the glia cells associated with some of the nose touch neurons, the OLQs and IL1, on which they appear to exert a similar effect (Han et al., 2013). Vertebrate ASICs are also expressed in glia and, for example, some of the roles identified in learning may in fact be glia-based (Hill and Ben-Shahar, 2018, Deitmer and Rose, 1996), so disentangling glial from neuronal functions represents an exciting avenue for future investigations. With the help of a combination of genetic, behavioural and electrophysiological approaches, there is now strong evidence for a wide variety of roles for DEG/ENaCs in the modulation of neuronal and synaptic function.

1. 2. 4. The role of DEG/ENaC and ASICs in pathological conditions

Over the past decades, increasing evidence has emerged linking DEG/ENaCs, especially ASICs and the *C. elegans* degenerins, to playing an important role in neuronal health and disease. The evidence will be briefly discussed below.

1. 2. 4. 1. Injury, Inflammation and neurodegeneration

Gain-of-function mutations in the *C. elegans* DEG-1, MEC-4 and UNC-8 subunits can cause neuronal degeneration which translate to phenotypes such as to touch

insensitivity or defective movement (Chalfie and Sulston, 1981, Wang et al., 2013c, Bianchi et al., 2004). Introducing the degenerative *mec-4* gain-of-function mutation into human ASIC2 also causes neuronal cell death in cultured neurons, suggesting that ASIC2 might be involved in neurodegeneration as well (Waldmann et al., 1996). This hypothesis has received attention since ASIC2 is upregulated in patients with Multiple Sclerosis (MS), an inflammatory neurodegenerative disease (Fazia et al., 2019). Mouse models of MS have provided further evidence that loss or pharmacological blocking of another ASIC, ASIC1, rescues clinical symptoms and inflammation *in vivo* and axonal degeneration *in vitro* further implying a role of ASICs in tissue injury (Friese et al., 2007).

1. 2. 4. 2. Pathological acidosis

Acidosis is a hallmark of pathological conditions including infection, inflammation and injury as shown above (Riemann et al., 2015, Dulai et al., 2021). Hypoxia and inflammation were shown to directly cause acidosis at the site of injury (Friese et al., 2007). This observation led to the hypothesis that ASICs as acid-sensors could play a critical role in tissue injury by detecting changes in proton concentrations. The protective effect seen for loss or pharmacological blocking of ASICs was proposed to be due to prevention of ASIC activation by pathological acidosis and the associated influx of cations into the vulnerable tissue (Friese et al., 2007). This is similar to what has been a proposed mechanism for the neurotoxic mutants of worm MEC-4 and UNC-8 (Wang et al., 2013c, Bianchi et al., 2004). Acidosis is also caused by the build-up of lactic acid which is common in ischemia, where blood and hence oxygen supply is disrupted. ASICs expression on sensory neurons innervating heart and skeletal muscles has been proposed to play a major role in detecting myocardial acidity that triggers ischemic pain (Yagi et al., 2006, Sutherland et al., 2001). Unsurprisingly, ASIC blockers exhibit a protective effect from ischemic injury (Xiong et al., 2004).

1. 2. 4. 3. A role of ASICs in sensing pain

The pharmacological characterisation *in vitro* has provided a repertoire of ASIC agonists and antagonists which have been used to investigate the role of ASICs in pain. For instance, injections of ASIC agonists such as 2-guanidine-4-methylquinazoline (GMQ), the Texas coral snake toxin MitTx or toxin mambalgin-1

into mouse paws increased pain-related behaviours in wild-type mice but not in *asic* mutant mice (Yu et al., 2010, Diochot et al., 2012, Bohlen et al., 2011). Increase in threshold to painful stimuli was also shown for *asic2* mutant animals (Fazia et al., 2019). While these experiments provide indirect evidence, they imply a role of ASICs in pain sensation.

Further pharmacological data have shown that ASICs as well as some *C. elegans* DEG/ENaCs containing the mec-4d gain-of-function mutation respond to non-steroidal anti-inflammatory drugs (NSAIDs), a diverse group of chemicals used to treat pain and inflammation (Voilley, 2004, Voilley et al., 2001, Fechner et al., 2020). The emerging evidence presented above and the finding that ASIC expression is altered following inflammation and injury has led to the suggestion of using ASICs as analgesic targets in pain therapy (for a recent review see (Dulai et al., 2021)).

1. 2. 5. *C. elegans* is a powerful model system to study molecular mechanisms underlying behaviour

The following sections addresses *C. elegans* as a model system and its advantages. More technical details of experiments conducted for this thesis can be found in CHAPTER 2 – Methods.

1. 2. 5. 1. C. elegans life cycle

Under favourable conditions, *C. elegans* larval hermaphrodite development encompasses four larval stages (L1, L2, L3, and L4) before moulting into reproductive egg-laying adults (Figure 5) which survive for approximately 3 weeks at 20°C in the laboratory (Byerly et al., 1976). However, low food availability and cold temperatures slow growing and larvae do not moult until they have reached a threshold in length (Uppaluri and Brangwynne, 2015). Under laboratory conditions, maintenance of *C. elegans* at temperatures between 15°C–25°C is considered physiological ((Brenner, 1974); www.wormbook.org). However, if L1s experience starvation, overcrowding (which can be sensed by the animals through an increase in pheromone concentration), or high temperatures, they may enter an alternative developmental stage, the L2d stage and then become dauer larvae (Golden and Riddle, 1984). The dauer larvae is a specialised non-feeding third larval stage that is adapted to endure unfavourable conditions over long periods of time and dauers can resume

reproductive development when suitable environmental conditions return, by moulting into post-dauer L4 larvae. For experiments, usually well-fed 1-day-old adult (1DOA) hermaphrodites are used, as sex, age, feeding status and life-cycle stages are important determinants of behaviour and morphology (www.wormbook.org). Males which occur spontaneously are generally only assayed when assessing male-specific behaviours.

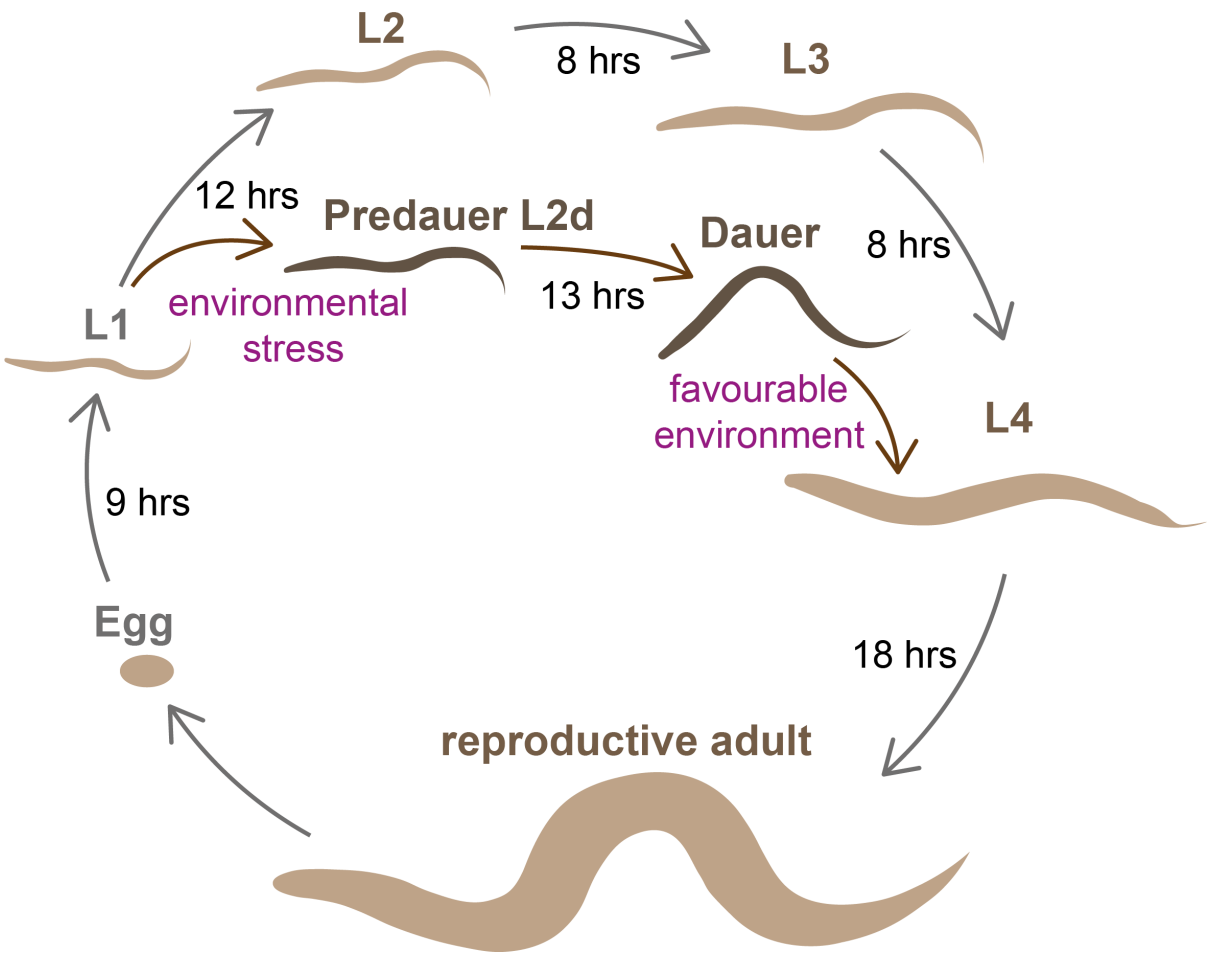

Figure 5: C. elegans life cycle under favourable conditions and under environmental stress.

L1 worms show a length of approximately 200 µm and grow to about 1 mm by adulthood. References for the illustration are found in the text above. Figure modified from Wormatlas (Wolkow and Hall, 2015).

1. 2. 5. 2. Advantages of C. elegans: Complete whole-body synaptic connectome, fully sequenced genome and single-cell RNA-sequencing data available

C. elegans bear many advantages as a genetic model. Firstly, they are self-reproducing hermaphrodite, meaning that they first produce sperm, which is stored in the spermatheca, and subsequently form oocytes (Brenner, 1974). Secondly, they are amenable to large-scale screens, due to a short generation time and the ease of growing large numbers. For such a screen, offspring of animals treated with a chemical mutagen can be manually screened for defects in morphology, movement and simple behaviours such as insensitivity to touch (Chalfie and Sulston, 1981, Waldmann et al., 1996, Brenner, 1974).

The *C. elegans* hermaphrodite has a stereotypic nervous system comprising 302 neurons (divided into somatic nervous system with 282 neurons and the pharyngeal nervous system with 20 neurons). This work was done by John Sulston and colleges who mapped out cell linages in the developing nervous system (Sulston and Horvitz, 1977, Sulston et al., 1983). The complete connectome of the *C. elegans* nervous system is also known and was further confirmed recently (Ward et al., 1975, White et al., 1986, Cook et al., 2019). The stereotypic development and having a complete connectome means that each neuron at any given position in the worm body can be identified based on its location and morphology and all physical connections are known. The *C. elegans* community has made a lot of use of these data sets linking many genes to functions within particular neurons and constructing functional circuits of neuronal clusters.

The *C. elegans* genome was also the first genome of a multicellular organism that was fully sequenced revealing over 19,000 genes with many of the predicted proteins showing significant homology in other organisms (C. elegans Sequencing Consortium, 1998). It also exposed that many gene families including ion channel families show *C. elegans*-specific expansions (Hobert, 2013). Very recently, datasets provided the complete single cell RNA-sequencing of every neuron class (Cao et al., 2017, Hammarlund et al., 2018, Taylor et al., 2020). These advances revolutionised the way in which hypotheses could be generated and tested and *C. elegans* has become the model system for the study of neural networks for reductionist neurobiology.

1. 2. 6. *C. elegans* technological toolbox

Another advantage is the powerful and varied technological toolbox available for use in *C. elegans,* including genetic tools for rapid generation of mutants and transgenic lines, optogenetics tools, and *in vivo* calcium imaging. It is also amenable to a variety of behavioural tests such as chemotaxis. These characteristics make it suitable for studying the function of ion channels such as the DEG/ENaC members and their role in various behaviours. These insights can help us to understand the consequences of sensory transduction failure, which is known to lead to a variety of impairments.

In the following section, I will briefly illustrate examples of techniques and behaviours that will be used to study DEG/ENaC function *in vivo* in the following chapters of this thesis – with the exception of the Defecation Motor Program (DMP) which has been described in detail in section 1. 2. 2. 1. above). Technical details are listed in CHAPTER 2 – Methods.

1. 2. 6. 1. C. elegans genetics and transgenics

There are two types of genetic screens that have traditionally been used: Firstly, as outlined above, forward generic screens and secondly, reverse genetic screens, in which candidate genes are tested for a particular phenotype. Recent advances have allowed for easier and targeted generation of mutants. For instance, some mutant strains described in this thesis were generated using RNA-guided Cas9 nuclease from the microbial clustered regularly interspaced short palindromic repeats (CRISPR) adaptive immune system (Jinek et al., 2012, Charpentier et al., 2015) to introduce targeted mutations in the *C. elegans* genome using the established protocol by the Mello lab (Dokshin et al., 2018). Another way to achieve targeted knock-down of particular genes is to use RNA interference (RNAi) by feeding (Fire et al., 1998, Fraser et al., 2000), where ingestion of bacteria producing double stranded RNA (dsRNA) leads to specific degradation of the corresponding mRNA.

For addressing the expression pattern of a gene or to rescue a particular mutant phenotype, a standard protocol for generating transgenic *C. elegans* has been microinjections of plasmids containing DNA of interest, essentially a form of heritable extrachromosomal DNA transformation (first described in (Stinchcomb et al., 1985)). These include transcriptional promoter-fluorophore fusions, tagged endogenous proteins as well as genes from other organisms. The original protocol for using

microinjections to generate transgenic animals was established by Craig Mello (Mello et al., 1991, Mello and Fire, 1995) and has since been widely used by the *C. elegans* community creating mosaic worms expressing extrachromosomal arrays.

Mosaicism refers to the process by which extrachromosomal arrays are lost during cell division. Therefore, different cells in the same animal have different numbers or arrangements of the extrachromosomal array which presents a disadvantage of this technique and explains variations that rescue lines can present. Different promoters and different injection concentrations can be used to generate a desired transgenic strain. Solutions to the issue of mosaicism include the so called MosSCI (Mos1-mediated Single Copy Insertion) system which leads to the insertion of a single copy of a transgene into a defined site in the genome (Frokjaer-Jensen et al., 2008), and more recently the use of CRISPR/Cas9 (Dokshin et al., 2018).

1. 2. 6. 2. In vivo visualisation of physiological states and processes

C. elegans are transparent which is advantageous for the visualisation of physiological processes *in vivo* in real time. Here I will focus on three examples. Firstly, the generation of transgenic strains as described above has the advantage that gene expression patterns can be tracked in different stages and within the same animal over a long period of time. Secondly, genetically encoded Ca^{2+} indicators such as GCaMP and Cameleon have made it possible to observe tissues, individual neurons or whole brains in action in ways that were previously unimaginable (Kerr et al., 2000, Suzuki et al., 2003, Nguyen et al., 2016, Cong et al., 2017, Ahrens et al., 2013, Nichols et al., 2017). Finally, feeding of sensors which can be imaged in the *C. elegans* intestinal lumen to measure intestinal lumen pH (Benomar et al., 2020, Bender et al., 2013, Chauhan et al., 2013) has improved our understanding of physiology.

GCaMP is a permuted GFP (N- and C-termini are fused) fused to calmodulin and M13 (peptide sequence from myosin light chain kinase). Upon increase in calcium in the cell calmodulin undergoes a conformational change and binds to M13 resulting in an increase in fluorescence (Nakai et al., 2001). In the absence of calcium GCaMP is only weakly fluorescent (Nakai et al., 2001). Cameleon on the other hand consists of two fluorophores, a yellow fluorescent protein (YFP) and cyan fluorescent protein (CFP) which are attached by a calmodulin binding domain and the M13 (Miyawaki et al., 1999, Kerr et al., 2000). In an experiment, light is used only for excitation of the

CFP, an increase in calcium concentration allowing fluorescence resonance energy transfer (FRET) to occur transferring energy from CFP to the YFP, hence increasing the YFP emission signal and reducing the CFP signal. Generation of transgenic lines that express one of the calcium indicators above in the neuron or tissue of interest is relatively easy in *C. elegans,* and due to being transparent, no invasive measures are required.

Another advantage of having a transparent model organism is that physiological processes such as ingestion of food and physiological pH within the intestinal lumen can be visualised using non-genetic fluorophores. For instance, a recent paper created a pH sensitive fluorophore, Kansas Red, to visualise dynamic proton waves in the intestinal lumen (Benomar et al., 2020, Bender et al., 2013). Kansas Red fluorophores show strong enhancement with decreasing pH and the fluorescence can be maintained throughout multiple defecation cycles (Bender et al., 2013). The authors found a dynamic proton wave in the intestinal lumen of *C. elegans* with a hot spot of acidity moving from posterior to anterior of the intestinal lumen where it becomes localized for approximately seven seconds every defecation cycle (Bender et al., 2013).

1. 2. 6. 3. Chemotaxis – contribution of a set of chemosensory neurons

C. elegans displays a remarkable repertoire of distinct behaviours some of which depend largely on particular neurons or discrete neuronal circuits. One of the formers is chemosensation which is used for attraction towards food, avoidance of noxious conditions, developmental- and mating cues. Chemotaxis is largely dependent on 24 ciliated sensory amphid neurons in the head of the animal and four phasmid neurons in the tail of the animal ((Ware et al., 1975, Ward et al., 1975), Figure 6). These are either directly or indirectly exposed to the outside environment through openings of glial cells called socket and sheath cells.

Due to the availability of the complete cell lineage of *C. elegans*, researcher have dissected chemosensory system by ablations of individual neurons and have generated a rich dataset for genetic mutations that impair chemosensory function (Bargmann et al., 1993, Bargmann and Horvitz, 1991, Hilliard et al., 2002). Using these techniques, it has been shown that the polymodal sensory neuron ASK, as an example, is involved in the attraction to amino acid lysine (Bargmann and Horvitz,

1991, Wakabayashi et al., 2009), and that ASK is also implicated in sensing dauer pheromones (via heterotrimeric GTP-binding protein G protein-coupled receptors (GPCRs)), which at high quantities signal unfavourable conditions and for L1 worms a cue to pursue the alternative developmental dauer pathway (as described in section 1. 2. 5. 1. C. elegans life cycle) (Macosko et al., 2009, Kim et al., 2009a). Chemotaxis is also subject to plasticity, as a result of feeding experience or other conditions (Jang et al., 2019, Saeki et al., 2001, Shimizu et al., 2019). These signals can come from neurons but chemotaxis behaviours have also been shown to be regulated by intestinal-derived neuropeptides, such as the insulin-like neuropeptide encoded by *ins-11* (Lee and Mylonakis, 2017). Consequently, chemosensory assays are a useful tool to understand how single neurons function and the immediate role of genes expressed in these neurons as well as to investigate physiological and behavioural adaptations to environmental context.

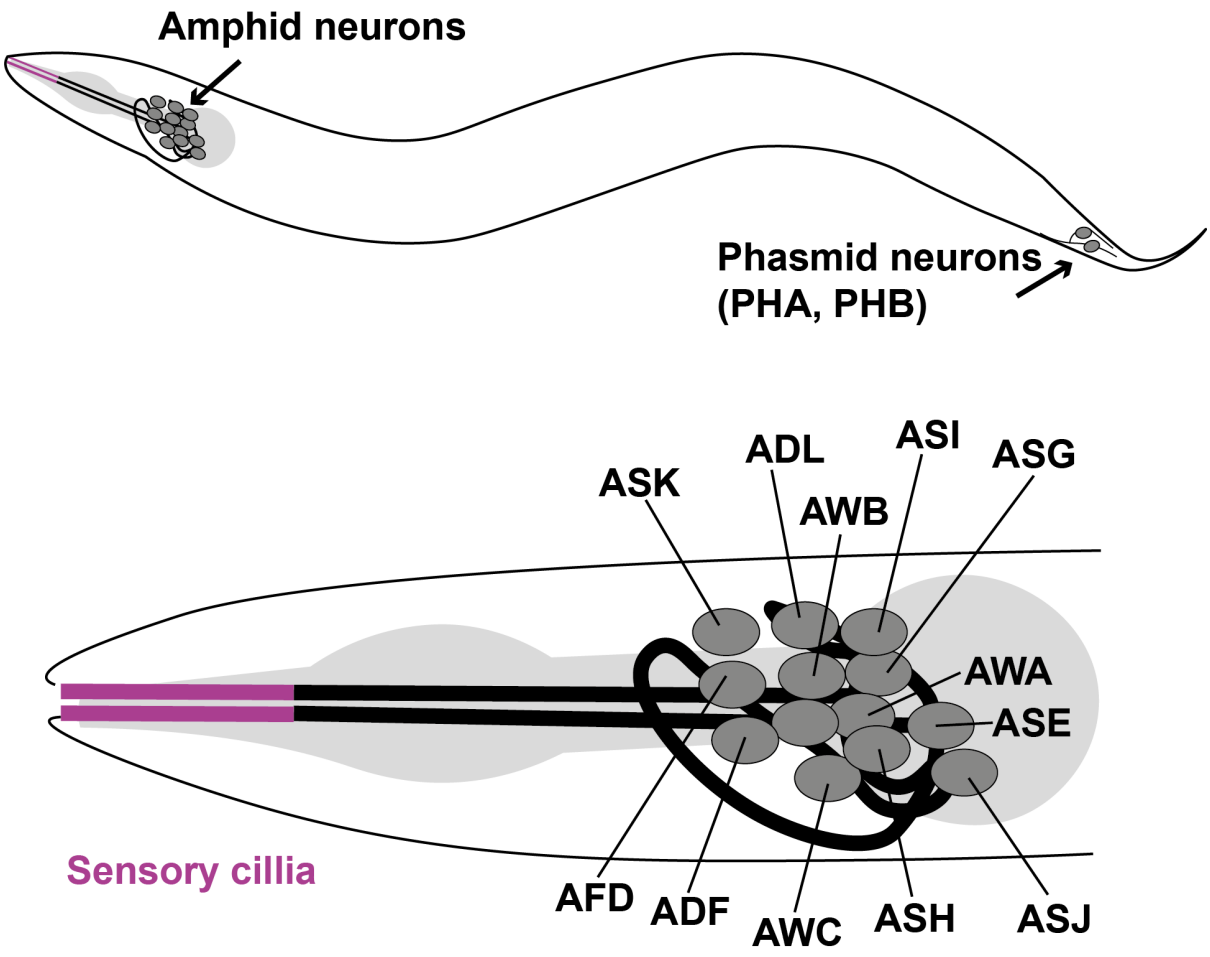

Figure 6: C. elegans chemosensory neurons.

Chemosensory neurons are located in the head (amphid neurons) and in the tail (phasmid neurons) of the worm. The two amphids consists of 12 chemosensory neurons (they are bilateral so one neuron on the left side of the animal has a corresponding one on the right side). Similarly, the two phasmids contain two chemosensory neurons each, PHA and PHB. (Figure adapted from wormbook.org)

1. 2. 6. 4. Egg-laying – a simple anatomical circuit between neurons and muscles

Another approach to assess neuronal function is to analyse behaviour at a circuit level where a variety of neurons (and tissues) are involved in generating a particular phenotype that can then be investigated or manipulated. As an example, I will use a circuit between neurons and muscles underlying the behaviour of egg-laying.

Young adult hermaphrodites accumulate an average of 10-15 fertilized eggs in the uterus (Brundage et al., 1996) and egg-laying occurs at particular time intervals allowing the egg-laying muscles to contract and eggs to be expelled. Egg-laying is controlled by a compact circuit, shown in Figure 7, consisting of two vulva muscles (vm1 and vm2) which receive synaptic input from the two serotonergic HSN (Hermaphrodite Specific Neuron) and six VC (Ventral class C neurons) both of which are hermaphrodite-specific (White et al., 1976), and further four neuroendocrine uv1 (uterine-vulval) cells (Jose et al., 2007). Mutants with abnormal HSN development or ablation of HSN neurons causes a strong reduction in the egg-laying rate (Trent et al., 1983, Waggoner et al., 1998).

Mutants have also provided insight into the control of egg-laying by at least two neurotransmitters, acetylcholine (ACh) and serotonin (5-HT) as well as neuropeptides (Schafer, 2006). Automated tracking of animals has further been used to show that egg-laying is a highly regulated, rhythmic behaviour that alternates between inactive states (no egg-laying) of approximately 20 min, and active states lasting several minutes during which eggs are laid (Waggoner et al., 1998). Environmental influences such as vibrations of the plates or lack of food can disrupt egg-laying patterns (Horvitz et al., 1982), again highlighting the delicate interplay between environment and physiology.

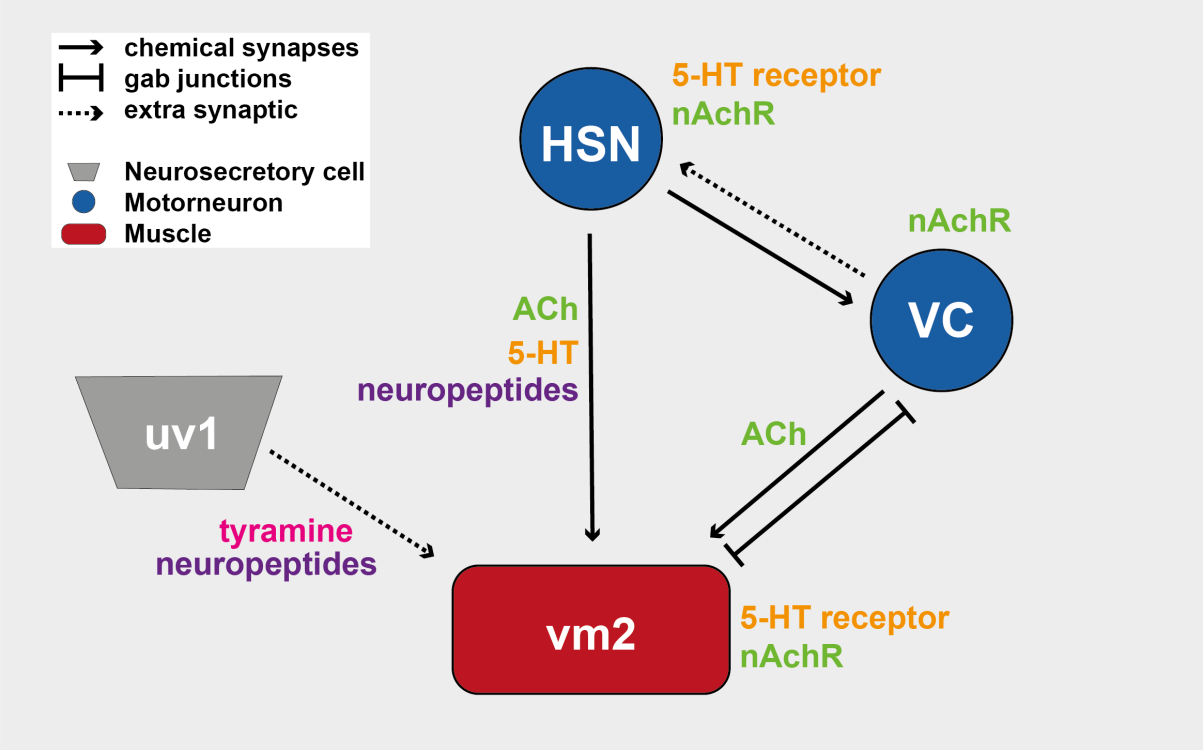

Figure 7: Model of connectivity and neurochemistry of the egg-laying circuit.

The main circuit consist of the HSN (Hermaphrodite Specific Neuron), VC (Ventral class C neurons) and uv1 (uterine-vulval cells). Signalling molecules including serotonin (5-HT), acetylcholine (Ach) as well as tyramine and neuropeptides and their potential receptors. References can be found in the text. Modified from (Schafer, 2006).

1. 3. Aims and Objectives

The overarching focus of this thesis is on the proton-sensitive members of the *C. elegans* DEG/ENaC family and how their proton-sensing properties translate into cellular processes and finally *C. elegans* behaviours.

Aim 1: Survey the diverse channel properties and expression patterns of the as yet uncharacterised *C. elegans* members of the DEG/ENaC family.

Using Two-Electrode Voltage Clamp (TEVC) recordings in *Xenopus* oocytes, the response of different DEG/ENaC subunits to increasing protons concentrations will be tested. Genetically encoded transcriptional promoter-fluorophore fusions combined with publicly available RNA-sequencing data are used to characterise *in vivo* expression patterns of *C. elegans* DEG/ENaCs. The relationship between phylogeny and sequence similarity and electrophysiological characteristics of the *C. elegans* DEG/ENaCs will also be explored.

Aim 2: Characterise electrophysiological properties of candidate proton-sensitive homomeric channels.

The proton-sensitive candidates from '*Aim 1*' above will be further characterised in terms of their electrophysiological properties, including ion substitution experiments of different cations to investigate ion selectivity, investigation of half-maximal inhibitory/excitatory proton concentration and use of the established DEG/ENaC antagonist, amiloride to block the proton-induced currents and investigate the half-maximal inhibitory concentration.

Aim 3: Determine the function of proton-sensitive *C. elegans* DEG/ENaCs *in vivo.*

Generation of transgenic *C. elegans* expressing transcriptional reporter-fluorophore fusions or fluorophore-tagged subunits of interest to visualise their subcellular localisation. Many neurons and tissues can be identified according to their morphology and location, or previously generated cell-specific markers can be obtained for particular neuron. Based on the expression pattern and previous research, hypotheses can be generated and particular behaviours can be tested. Rescues using overexpression of the gene of interest will be used to confirm these findings.

Aim 4: Explore likely subunit combinations of heteromeric channels.

Functional interactions between potential subunits will be explored, along with co-immunoprecipitation studies and tissue-specific co-expression, and behavioural studies of double mutants.

Aim 5: Identification of regulatory pathways.

Given conditional expression pattern in dauer, pathways that could conditionally regulate the expression of DEG/ENaCs will be explored.

1. 4. Appendix A

Supplementary Table 1: Accession numbers.

DEG/ENaC family members' name and accession numbers in Figure 1.

Organism	*Protein name (accession number)*
Caenorhabditis elegans	FLR-1 (UniProtKB/TrEMBL ID G5EGI5); ACD-1 (P91102); ACD-2 P91100); ACD-3 (G3MU02); ACD-4 (Q22970); ACD-5 (O01664); DELM-1 (O45402); DELM-2 (P91103); ASIC-1 (K7H9J0); ASIC-2 (Q22851); MEC-4 (P24612); DEL-4 (P91835); UNC-105 (Q09274); DEG-1 (P24585); DEL-1 (Q19038); MEC-10 (P34886); EGAS-1 (Q9U1T9); EGAS-2 (Q9U1T8); EGAS-3 (Q9XTS9); EGAS-4 (Q20852); DEGT-1 (Q19777); DEL-2 (G5ECD8); DEL-3 (Q93597); DEL-5 (G5EFH3); DEL-6 (Q8MPW0); DEL-7 (Q18651); DEL-8 (Q93205); UNC-8 (Q21974); DEL-9 (Q18077); DEL-10 (Q10025).
Drosophila melanogaster	PPK1 (Q7KT94); PPK2 (O46342); PPK3 (Q8MLR6); PPK4 (O61365); PPK5 (Q7KTW2); PPK6 (Q86LH3); PPK7 (Q9VME9); PPK8 (B7Z123); PPK9 (Q9W2B5); PPK10 (Q86LH1); PPK11 (Q9VL84); PPK12 (Q9W250); PPK13 (Q86LG9); PPK14 (Q86LG8); PPK15 (Q9VBF6); PPK16 (Q86LG7); PPK17 (Q9VJI4); PPK18 (Q9VL88); PPK19 (Q9VAJ3); PPK20 (Q86LG5); PPK21 (Q86LG4); PPK22 (Q8IMV2); PPK23 (Q9VX46); PPK24 (Q9V9Y5); PPK25 (A1Z6S4); PPK26 (Q9VS73); PPK27 (Q9VZN1); PPK28 (Q86LG1); PPK29 (A8DYP2); PPK30 (Q9VAJ5); PPK31 (A8JPJ8)
Rattus norvegicus	rASIC1 (P55926); rASIC2 (Q62962); rASIC3 (O35240); rASIC4 (Q9JHS6); rASIC5 (Q9R0W5); ENaCα (P37089); ENaCβ (P37090); ENaCγ (P37091)
Danio rerio	zAISC1A (Q708S7); zAISC1B (Q708S8); zAISC1C (Q708S6); zAISC2 (Q708S5); zAISC4A (Q708S4); zAISC4B (Q708S3)

Hydra vulgaris	HyNaC2 (A8DZR6); HyNaC3 (A8DZR7); HyNaC4 (A8DZR8); HyNaC5 (D3UD58); HyNaC6 (A0A0A0MP54); HyNaC7 (A0A0A0MP73); HyNaC8 (A0A0A0MP55); HyNaC9 (A0A0A0MP48); HyNaC10 (A0A0A0MP61); HyNaC11 (A0A0A0MP67); HyNaC12 (A0A0A0MP74)
Aplysia kurodai	FaNaC (Q4H3X6)
Platynereis dumerilii	pENaC4 (A0A2S1B6I2); pENaC7 (A0A2S1B6Q3); pENaC6 (A0A2S1B6R1); pMGIC (A0A2S1B6I3)
Lottia gigantean	LgFaNaC (V4C2H5)
Lymnaea stagnalis	LsFaNaC (Q9BJD0)
Helix aspersa	HaFaNaC (Q25011).
Helisoma trivolvis	HtFaNaC (Q9NBC7)
Trichoplax adhaerens	TadNaC1 (B3S0Z3); TadNaC2 (A0A5J6BSS6); TadNaC3 (A0A5J6BTF2); TadNaC4 (A0A5J6BSQ9); TadNaC5 (A0A5J6BSM6); TadNaC6 (A0A5J6BVG3); TadNaC7 (A0A5J6BSR6); TadNaC8 (A0A5J6BV03); TadNaC9 (A0A5J6BWR3); TadNaC10 (A0A5J6BSU1).

CHAPTER 2 – Methods

2. 1. Methods I – Phylogenetic and expression pattern analysis

2. 1. 1. Protein sequences and alignment

Databases and protein sequences. Un-aligned protein sequences of the DEG/ENaC superfamily were downloaded from UniProt, NBCI, Wormbase and Flybase and combined into one file using SnapGene software (from Insightful Science; available at snapgene.com). Due to the recent finding that removal of noisy or uncertain columns does not necessarily improve phylogenetic reconstruction (Tan et al., 2015), the complete amino acid sequences of the longest isoform (where applicable) were used for the phylogenetic estimation of protein similarity.

Generation of alignment of protein sequences. In order to address the issue that variable regions tend to be over-aligned, and consequently, might lead to biases, the robust aligners PRANK ((Loytynoja and Goldman, 2010) data not shown) and MAFFT (Katoh et al., 2002, Katoh and Standley, 2013) were used and confidence in the individual alignment columns was assessed using GUIDANCE2. Both alignments generated were similar. I decided to use MAFFT (Katoh et al., 2002, Katoh and Standley, 2013) as it allows re-adjustment alignment to reflect information from sequences aligned later compared to other alignment strategies such as ClustalW (Larkin et al., 2007).

2. 1. 2. Phylogram

Phylogenetic tree generation and visualisation. Generated alignment were entered into the BioNJ tool (www.phylogeny.fr) for tree generation and visualised using FigTree v1.4.4 software (Rambaut, 2010). The analysis was performed on the Phylogeny.fr platform and comprised the following steps: The phylogenetic tree was reconstructed using the neighbour joining method implemented in the BioNJ program for the *C. elegans* DEG/ENaCs (Settings: Bootstraps: 100) (Felsenstein, 1989, Gascuel, 1997, Dereeper et al., 2008, Elias and Lagergren, 2007, Dereeper et al., 2010). For visualisation of the DEG/ENaC super-family, protein sequences were

aligned in *MAFFT version 7 multiple alignment program* using rough distance and average linkage UPGMA (unweighted pair group method with arithmetic mean) and the tree was visualized using iTOL (Ciccarelli et al., 2006, Letunic and Bork, 2019, Kuraku et al., 2013).

2. 1. 3. Sequence Similarity Network

Sequence Similarity Network (SSN) were generated using the web tool for SSNs for protein families (EFI-EST) developed by the Enzyme Function Initiative (EFI; accessed at efi.igb.illinois.edu/) (Zallot et al., 2019, Zallot et al., 2018, Gerlt et al., 2015, Gerlt, 2017). Each symbol represents a protein (node), two nodes are connected by a line (edge) if they share pairwise sequence similarity that exceeds the indicated threshold. Within each cluster the sequences show high similarity and the lengths of connecting edges correlate with the relative dissimilarities of each pair. Relative positioning of disconnected clusters and nodes has no meaning. Cytoscape (Shannon et al., 2003) was used to explore SSNs. The EFI-EST webtools use NCBI BLAST and CD-HIT to create SSNs. The computationally-guided functional profiling tool uses the CGFP programs from the Balskus Lab (https://bitbucket.org/biobakery/cgfp/src) and ShortBRED from the Huttenhower Lab (http://huttenhower.sph.harvard.edu/shortbred). The data used in these analyses originated from the UniProt Consortium databases and the InterPro and ENA databases from EMBL-EBI.

2. 1. 4. Clustergram and heatmap visualization of neuronal expression data

The neuronal expression data was downloaded for the available DEG/ENaC single-cell RNA sequencing data from the CenGen.org app (Hammarlund et al., 2018, Taylor et al., 2020). Hierarchical clustering of rows and columns were generated in using the Clustergrammer web tool developed by the Ma'ayan lab using the Scipy library in Python, using cosine distance and average linkage (Fernandez et al., 2017).

2. 2. Methods II – Two Electrode Voltage Clamp (TEVC) in Xenopus oocytes

2. 2. 1. Sub-cloning of *C. elegans* DEG/ENaC cDNA into KSM vector for *Xenopus oocyte* expression

cDNA generation. C. elegans cDNA was obtained from growing N2 wild-type animals on fifteen 6cm NGM plates until the food was diminished, and subsequently extracted and purified using the TRIzol Direct-zol RNA Miniprep (Catalogue #R2051, Zymo Research). cDNA was generated using the Invitrogen™ SuperScript™ III First-Strand Synthesis System (Catalogue # 18080051).

Primer design. Primers were designed using SnapGene 5.0.4. (Hifi-Cloning of two fragments) based on the cDNA gene sequence found on wormbase.org, and ordered from Integrated DNA Technologies Inc (IDT) (Leuven Belgium) or Sigma-Aldrich (Merck Life Science UK Limited, Dorset, UK). The cDNA inserts were sub-cloned into the KSM vector under the control of the T7 promoter containing 3' and 5' untranslated regions (UTRs) of the *Xenopus* beta-globin gene and a poly(A) tail. The forward primer *agatctggttaccactaaaccagcc* and reverse primer *tgcaggaattcgatatcaagcttatcgatacc* were used to amplify the KSM vector. NEB T_m Calculator was used to determine annealing temperatures. For generation of mutations and deletions, the NEBaseChanger™ tool to generate primer sequences and an annealing temperature. A full set of primers can be found in Appendix B, 2. 6. 2. Key resource tables. The *acd-5(ok2657)* was based on the *acd-5(ok2657)* mutant allele generated by *C. elegans* Gene Knockout Consortium (CGC).

Polymerase Chain Reaction (PCR). Q5® High-Fidelity DNA Polymerase 2x Master Mix (Catalogue # M0492S) was used to amplify vectors and inserts from genomic DNA or cDNA. For the following constructs synthetic genes were ordered from Sigma-Aldrich: *egas-1, egas-2, del-5*. The obtained fragments were visualised on a 1% w/v agarose TAE gel at 100V for 25min, to obtain a single band of the correct molecular weight, and gel-purified using Zymoclean Gel DNA Recovery Kit (Catalogue # D4007/D4008).

Vector Assembly. The NEBuilder HiFi DNA Assembly Reaction Protocol was used to assemble the KSM vector and cDNA inserts using NEBuilder® HiFi DNA Assembly Master Mix (Catalogue # E2621L) and a vector:insert ratio 1:2 (0.5pmol vector and the corresponding amount of insert using NEBiocalculator). The following constructs were generated using the NEB Q5® Site-Directed Mutagenesis Kit (Catalogue # E0554S): pEK172 [acd-5(ok2657)::KSM]; pEK273 [asic-1(Y601P)::KSM]; pEK274 [ASIC-1(Y601G)::KSM]; pEK275 [ASIC-1(Y601K)::KSM]; pEK276 [ASIC-1(Y601K and small deletion)::KSM]; pEK277 [ASIC-1(Y601K and large deletion)::KSM]; pEK279 [ASIC-1 (△495-597)::KSM]; pEK280 [ASIC-1 (△517-521)::KSM]; pEK281 [ASIC-1 (△549-552)::KSM]; pEK282 [ASIC-1 (3xGly 549-552)::KSM]; pEK283 [ASIC-1 (△CRISPR)::KSM].

Cloning of plasmids into E. coli. In order to amplify the generated plasmids, 2 µl of the assembly product was transformed into NEB 10-beta (Catalogue # C3019I) chemically competent cells, and the High Efficiency Transformation Protocol was followed. For extraction of the plasmid, the PureLink™ Quick Plasmid Miniprep Kit (Catalogue # K210010) was used. Restriction digestion followed by Sanger sequencing (SourceBioscience, Cambridge) of the insert(s) was used to confirm the plasmid sequence.

RNA Synthesis and Microinjection. The approximately 1ug of KSM plasmid containing the DEG/ENaC cDNA insert was lineralised by a 30 mins enzyme digest with NotI-HF (Catalogue # R3189S) in CutSmart Buffer in a 20 µl reaction. Digestion efficiency was confirmed by running 1µl of the digest mixture on a 1% w/v agarose TAE gel at 100V for 25min, to obtain a single band of the correct molecular weight. The remaining digestion mixture was then purified by column purification using Zymo Research DNA Clean & Concentrator-5 (Catalogue # D4013). Linear plasmid DNA was used as the template for *in vitro* RNA synthesis from the T7 promoter using the mMessage T3 kit (Ambion # AM1348), producing 5' Capped RNA. The reaction was carried out using half volume of manufacturer's protocol, in a total of 10µl, with 3µl linear plasmid DNA. Subsequently, the mix was incubated at 37°C for 2h, resulting RNA was purified by RNeasy clean up kit (Qiagen #74104), and eluted in 15µl RNase free water. Concentration of RNA was determined by Nanodrop spectrophotometry.

2. 2. 2. Two-Electrode Voltage Clamp (TEVC) in *Xenopus oocytes*

Xenopus oocyte injection. Xenopus laevis oocytes of at least 1mm in size were obtained from EcoCyte Bioscience (Dortmund, Germany). They were de-folliculated by collagenase treatment and maintained in standard 1xND96 solution (96mM NaCl, 2mM $MgCl_2$, 5mM HEPES, 2mM KCl, 1.8mM $CaCl_2$, pH7.4, see Appendix B, 2. 6. 1. Standard solutions and recipes). Oocytes were injected with 25µl of RNA solution at a total concentration of approximately 500 ng/µl using the Roboinject (MultiChannel Systems). Oocytes were kept at 16°C in 1xND96 prior to TEVC.

Two-Electrode Voltage Clamp in Xenopus oocyte. The theory of two-electrode voltage clamping is discussed in detail in Finkel and Gage (Finkel, 1985) and (MolecularDevices, 2012). Briefly, in a two-electrode voltage clamp experiment, two intracellular microelectrodes are inserted into the *Xenopus* oocyte: One electrode holds the membrane potential constant (also called “clamped”) while the other one measures the current flowing through the membrane. For the experiments described here, TEVC was performed 1-2 days post injection at room temperature using the Roboocyte2 (MultiChannel Systems). *Xenopus* oocytes were clamped at −60 mV, using ready-to-use Measuring Heads from MultiChannel Systems filled with 3M KCl. All channels were tested using the Roboocyte2 (MultiChannel Systems). For all current-voltage steps (I-V) experiments, measurements were obtained in each solution once a steady-state current was achieved and the background leak current was subtracted (background subtraction).

Ion Selectivity. As millimolar concentrations of Ca^{2+} and other divalent ions except Mg^{2+} have been shown to partially inhibit ENaC channel activity (Garty et al., 1987) and Ca^{2+} can block ASICs (Paukert et al., 2004), I used the following Ca^{2+}-free buffers for substitution experiments of monovalent cations: For constitutively open channels I used a modified protocol from (Hardege et al., 2015): 96mM XCl, 1mM $MgCl^2$, 5mM HEPES, pH adjusted to 7.4 with XOH, where X was Na^+, K^+ or Li^+, respectively. For testing ion permeability for Ca^{2+}, the following protocol was used as in (Wang et al., 2008) replacing Na^+ with equimolar Ca^{2+}. If necessary, D-Glucose was used to adjust osmolarity. The osmolarity was checked and confirmed to be within the error of 210 mosm (Awayda and Subramanyam, 1998). For testing pH sensitivity, 1x ND96 solutions was used; for solutions with a pH 5 or lower, MES was used instead of

HEPES and adjusted with HCl. I-V relationships for ion selectivity were calculated by subtracting the background leak current in the presence of 500 μM amiloride from the current observed in the absence of amiloride in order to get the actual current. By contrast, I-V relationships for pH-activated channels were calculated as previously reported (Yang and Palmer, 2014) by subtracting background currents measured at pH 7.4 from those measured during activation of the channels for ACD-2 and ASIC-1 and pH 4 for DEL-9. In noninjected oocytes the difference between these currents was negligible. Actual current IV curves for each individual oocyte were fitted to a linear regression line and the x intercept was compared between solutions to calculate an average reversal potential (E_{rev}). Reversal potential shift (ΔE_{rev}) when shifting from an NaCl to a KCl, LiCl or $CaCl_2$ solution was calculated for each oocyte.

pH sensitivity. In order to test the responses to pH, the channel-expressing *Xenopus* oocytes were perfused with 1x ND96 (using HEPES for buffering pH above 5.5 and MES for pH below 5), pH was adjusted with HCl and ranged from pH 7.4 (neutral pH of the ND96 solution) to pH 3.8 or pH 4. Background currents measured at pH 7.4 were subtracted from those measured during activation of the channels. For analysis, currents were normalized to maximal currents (I/I_{max}) and best fitted with the Hill's equation (Variable slope).

2. 3. Methods III – *C. elegans* experiments

C. elegans growth and maintenance. Standard techniques were used for *C. elegans* strain maintenance and genetic manipulations (Brenner, 1974). All experiments were performed at room temperature (22°C) on hermaphrodite animals. All animals were kept at 22°C unless otherwise stated. Strains with dauer-constitutive alleles (*daf-1(m40); daf-2(e1370); daf-4(e1364ts); daf-7(e1372); daf-9(m540); daf-11(ks67); daf-16(mu86)*) are temperature-sensitive (ts) and form dauer larvae at a restrictive temperature regardless of environmental conditions (Golden and Riddle, 1984), and were thus kept at the permissive temperature of 15°C where they undergo reproductive development. The experiments to test dauer formation (CHAPTER 6) at restrictive temperatures were synchronised and grown at 25°C to induce dauer formation.

Generation of genetically modified C. elegans strains. Appendix B (2. 6. 2. Key resource tables) lists the strains and mutations used in the current thesis. Mutations used were 6x outcrossed with the N2 wild-type, and transgenic strains were generated by microinjection of plasmid DNA into the worm creating mosaic worms expressing extrachromosomal arrays (Mello et al., 1991). Mosaicism refers to the process by which extrachromosomal arrays are lost during cell division. Therefore, different cells in the same animal have different numbers or arrangements of the extrachromosomal array. In order to generate CRISPR mutations, the protocol established by the Mello lab was used (Dokshin et al., 2018). Guide RNAs (crRNA) and homology arms were ordered from IDT (Leuven Belgium) or Sigma-Aldrich (Merck Life Science UK Limited, Dorset, UK). In order to confirm neuronal identity, the following strains were used: For confirming ASK neuronal identity the strain AQ3093 *ljEx543[sra-9::YC3.60;unc-122::rfp]* was used. For confirming AVL neuronal identity the strain was used AQ4583 *ls[unc-47:NLS-mCherry]*. For subcellular localisation for ACD-5 to the apical membrane localisation the strain KWN246 *pha-1(e2123) III; rnyEx133 [pKN114 (opt-2p::opt-2(aa1-412)::GFP) + pCL1 (pha-1+)]* was used. Other neurons, cells and tissues were identified based on location and characteristic morphology (e.g. PVD, FLP, muscle, intestine). Some strains were provided by the CAENORHABDITIS GENETICS CENTER CGC, which is funded by NIH Office of Research Infrastructure Programs (P40 OD010440). These strains are annotated in the main text.

SDS protocol for dauer larvae. The protocol described by Cassada and Russell was used to do select dauer larvae from a starved plate (Cassada and Russell, 1975). Briefly, worms were washed off plates (with M9) and put in a 1.5ml Eppendorf tube and pelleted (by centrifugation on the bench), and resuspend in 1% SDS. The worms were then incubated in 1% SDS for 30 minutes with gentle agitation. The samples were then spun down, supernatant was removed and 1ml M9 was added. After a second spin, supernatant containing non-dauers was taken off and the rest containing the dauer larvae was poured onto a plate seeded with OP50.

2. 3. 1. Molecular Biology

Genotyping. Primers for genotyping (Appendix B, 2. 6. 2. Key resource tables) were designed using PrimerBlast and sequences amplified using either Phire Tissue Direct

PCR Master Mix (Catalogue # F170S) to visualise directly on a 1% w/v agarose TAE gel (100V for 25min), or Q5® High-Fidelity DNA Polymerase 2X Master Mix (Catalogue # M0492S) when amplified for Sanger sequencing (SourceBioscience, Cambridge).

Vector assembly. For *acd-5* promoter constructs Gateway cloning was performed. Briefly, gene fragments were either cloned from genomic DNA or lysis for genomic fragments or promoter sequences, or from cDNA using primers designed in SnapGene with the attB-flanked DNA fragment. These fragments were amplified by PCR and an entry clone was generated by BP reaction combination into the appropriate attP-containing donor vector (depending on the position for the final vector). The following MultiSite Gateway® LR recombination reaction between multiple entry clones (attL4-5′ element-attR1 + attL1-gene of interest-attL2 + attR2-3′ element-attL3) and the pDEST™ R4-R3 Vector II vector was done using LR Clonase II Plus. For all other constructs the NEBuilder HiFi DNA Assembly Reaction Protocol was used to assemble the vector and inserts using NEBuilder® HiFi DNA Assembly Master Mix (Catalogue # E2621L) and a vector:insert ratio 1:2 (0.5pmol vector and the corresponding amount of insert using NEBiocalculator). I constructed the following promoter-fluorophore fusions: *acd-5* promoter consisting of 4.763kb promoter upstream of the start of the gene which is the distance to the next gene, the *asic-1* promoter containing 3kb promoter upstream of the start of the gene and the *acd-4* promoter with 1kb promoter including 655 bp upstream sequence from the start of the gene and the first two exons and *delm-1* promoter with 2kb promoter including 1707bp upstream sequence from the start of the gene and the first two exons. The latter two constructs were based on plasmid maps from the Kim lab (see below). Dr. Laura Grundy constructed the plasmid and reporter line for *asic-2* (Grundy, 2018). The rest of the plasmids for *C. elegans* DEG/ENaC transcriptional reporter were a kind gift from Professor Kyuhyung Kim's lab (Daegu Gyeongbuk Institute of Science & Technology (DGIST), Korea) who had also done a preliminary expression analysis on the *C. elegans* DEG/ENaCs. The plasmids from the Kim lab contain an approximately 3kb transcriptional promoter including upstream sequences from the start of the gene and partial exons. A list of all plasmids generated and used is attached in (Appendix B, 2. 6. 2. Key resource tables). For rescue in the vulva muscles, the vulva muscle specific promoter unc-103e was amplified from genomic DNA by PCR as previously described, a ~2.6 kb DNA fragment upstream of the *unc-103e* start site was amplified (Collins

and Koelle, 2013). *unc-47* (~1.7kb) and *rab-3* (~1.2kb) promoters were amplified from plasmids previously generated in the lab, pWRS25 and pWRS2328, respectively.

2. 3. 2. Microscopy

DiI staining to visualize environmentally exposed neurons. The following protocol was modified using DiI (Thermofisher, Calalog # D282) (Schultz and Gumienny, 2012, Tong and Burglin, 2010) to stain environmentally exposed amphid and IL2 neurons. A stock solution of DiI 2 mg/ml in dimethyl formamide was diluted 1:200 in M9 for the staining of the amphid neurons and diluted in water for staining of the IL2 neurons (Tong and Burglin, 2010). Worms were either washed off an NGM plate or picked with an eyelash into a 1.5 mL Eppendorf tube containing 150 µl working solution and incubated for 3 hours at room temperature wrapped in foil with gentle agitation. After incubation, worms were emptied out onto a non-seeded patch on a seeded plate with *E. coli* OP50 for about 1 hour to de-stain in the bacteria before they were imaged by confocal microscopy.

Confocal microscopy. Worms were mounted on 3% agar pads (3% agar solution in M9) in a 3 µl drop of M9 containing 25 mM sodium azide (NaN_3). Images were acquired using a Leica TCS SP8 STED 3X confocal microscope at 63x or 40x resolution unless otherwise specified and Z stacks generated using Fiji (ImageJ).

2. 3. 3. Quantitative RT-qPCR

C. elegans preparation. The following protocol was used (Imanikia et al., 2019): Animals were synchronised by letting ten one-day old adults (1DOA) crawl on a 90 mm OP50 seeded NGM plate for 5 hours. Adults were then picked off the plate and the first generation (F1s) was grown at 15 °C (which is the permissive temperatures for the dauer-constitutive mutants, see above). The end of the synchronisation time is timepoint zero (t_0). Larval stage 3 (L3) animals were harvested at 65 hours post-t_0 at 15 °C and larval stage 4 (L4) animals were harvested 80 hours post post-t_0 by washing the animals off the plate with M9 Buffer into 15ml Falcon tubes. Tube were subsequently spun down at 3000rpm to pellet the animals at the bottom of the tube. Samples were washed 2 more times with M9 Buffer. After the last wash, they were collected into a 1.5ml Tube and frozen in 1ml Trizol and metal beads.

Dauer larvae formed at 15°C were collected from 90mm NGM plates (initially containing 10 1DOAs), 5 days after the food had run out. Dauer larvae were SDS-treated (incubated in 1% SDS for 30min) (Albert and Riddle, 1988) and sucrose-flotation was performed to select the living dauer as previously described (Karp, 2018). Half of selected dauers were put on OP50 seeded NGM plate for recovery and harvested 24 hours after recovery as post-dauer L4s and further processed as described above.

Three independent samples from different animal populations at different days were taken for each stage. The following housekeeping genes were used as controls due to their previously shown stable expression pattern: *pmp-3, cdc-42* and *Y45F10D.4* (Hoogewijs et al., 2008). Primers were designed with https://qpcr.probefinder.com/ and ordered from Sigma-Aldrich (Merck Life Science UK Limited, Dorset, UK) (Appendix B, 2. 6. 2. Key resource tables). RNA was extracted using TRIzol Direct-zol RNA Miniprep (#R2051, Zymo Research). 2 ng of purified RNA was used for cDNA synthesis using the Invitrogen™ SuperScript™ III First-Strand Synthesis System (Catalogue # 18080051). SYBRGreen quantitative RT-PCR was performed using a Vii7 Real-Time PCR machine (ThermoFisher Scientific). Data from 3 biological repeats were analysed using the comparative 2ΔΔCt method.

2. 3. 4. Behavioural assays

Developmental timing and brood count of acd-5 mutant and wild-type animals. The protocol described by (Rollins et al., 2017)) was used: Briefly, animals were synchronised by allowing adults to lay eggs for one hour on an *E. coli* OP50 seeded 60mm NGM plate. After hatching animals were randomly picked onto individual 20 µl *E. coli* OP50 seeded NGM plates. Time (in hours) was counted from laid egg to egg-laying adulthood. To assess brood size (here: hatched progeny), adult animals were transferred to a fresh plate every day until egg-laying stopped. Hatched progeny and unfertilized oocytes were counted for each plate 48 hours after removal of the egg-laying adult. The animals were kept at 20°C for the duration of the assay.

Food racing assay. The following protocol was adapted and modified for the food racing assay (Calahorro et al., 2019). 9 cm (30ml) NGM plates were poured the day before the assay and kept overnight at room temperature. These plates were seeded

with a spot of 50 µl *E. coli* OP50 (which had been freshly grown over night) displaced 2 cm from the edge of the plate and incubated overnight. The day before the assay 50-100 L4 larvae were picked onto NGM *E. coli* OP50 plates and kept at 22˚C. The day of the assay, the animals were washed twice in M9 buffer to remove residual bacteria and added in a minimal volume 2 cm from the edge opposite to the food patch using a glass pipette to avoid the worms sticking to the filter tips. The clock was started when the M9 had dried up. The number of animals reaching food was recorded every 10 min for of time of 2 h. The cumulative number that reached the food spot within that time frame was calculated. Assay plates were blinded.

Assessing and Scoring Defecation Motor Program. Defecation was assayed as previously described (Thomas, 1990). Briefly, animals were staged to 1DOA. Stageing was done by letting ten 1DOA mothers crawl on an *E. coli* OP50 seeded 60mm NGM plate for ~ 3 hours to lay eggs and then mothers were picked off leaving eggs laid within this time on the plate. The worms were grown at 22°C to 1DOA. On the day prior to the assay transgenics were picked to a new plate (where applicable) and plates were blinded for scoring. Five cycles of the DMP for each animal were observed on a dissecting stereomicroscope at 50X magnification. Following a two-minute acclimation period on the microscope the time elapsed between posterior body wall contractions (pBoc) was measured and both the pBoc and EMC step was recorded. The aBoc response was scored separately. Each assay was conducted at least 3 times (N > 15) and wild-type and mutants were always scored alongside as a control.

The RNAi feeding experiments were performed as described (Kamath and Ahringer, 2003, Kamath et al., 2003, Kamath et al., 2001). Standard NGM plates were prepared by supplementation of agar with 100 µg/mL carbenicillin and 1mM IPTG after autoclaving and were poured 1-3 days before use (Imanikia et al., 2019). For feeding RNAi experiments the L4440 empty vector was used as a negative control and the following RNAi bacterial strains from the Ahringer *C. elegans* RNAi collection on SourceBioscience (X-6G10 (FLR-1); X-5E18 (DEL-5); X-6L08 (ACD-3); X-2G20 (DEL-9)) were used to knock-down the respective genes. The bacterial strains were freshly grown overnight in LB + 50 µg/ml ampicillin and 24 hours prior to each assay plates were seeded with 100 µL of overnight bacterial culture. Stageing and scoring were done as described in the previous paragraph.

Survival assay. Animals were staged until L4. Larvae were then picked onto OP50 seeded 60mm NGM plates (day 0; 100 animals per genotype (10 animals per plate)). The animals were kept at 20°C for the duration of the assay and were moved onto fresh plates every second day until egg lying stopped. Animals were scored every day. Death was determined by gentle touch with a sterilized platinum wire, worms that did not respond to the touch were counted as dead. The death was scored every day. The assay was repeated three times.

Recording and Analysis of C. elegans Egg-Laying Behaviour. For experiments with *del-9* mutants: Animals were staged to 1DOA. Stageing was done by letting ten 1DOA mothers crawl on an *E. coli* OP50 seeded 60mm NGM plate (seeded the night before) for ~ 3 hours to lay eggs and then mothers were picked off leaving eggs laid within this time on the plate. For experiments with *daf-7* and *acd-5* mutants (due to significant difference in developmental timing) animals were grown at 15°C (as the *daf-7* mutants are temperature sensitive and go into dauer stage at higher temperatures) and picked at L4 and then transferred to 22°C overnight to reach adulthood (1DOA). 60mm NGM plates (poured approximately 3 days before using) were dried overnight on the bench and seeded with 5 µl OP50 in the centre of the plate. These plates were dried and the OP50 could grow at 37°C for 30 mins and then cooled to room temperature for another 30 min on the bench. This procedure was necessary to achieve a sufficiently dense bacterial lawn to allow egg laying while not impeding visibility of laid eggs on a overgrown lawn. If the bacterial lawn is too thin, worms will leave the food patch and they will not lay many eggs there, however, if it is overgrown, then egg-laying is not visible. One animal per plate was picked to the food patch using an eyelash to avoid damage. Worms are acclimatised to the plate for 10 min, transferred to the tracker and left for approximately another 10 min before starting the video collection. The Dino-Lite Edge (AM7515MZT Digital Microscope, USB, 5MP, AMR, 20x-220x) camera set-up was used for video acquisition (10 fps, Shutter: 1/30 s, Brightness settings: 128, Contrast settings: 22). Egg-laying events were counted by eye and intervals of events were analysed with a program previously developed by (Waggoner et al., 1998) showing the log tail probability for intervals generated by a three-state model. Wild-type and mutants were always scored together on the same day.

C. elegans egg-retention behaviour. Animals were staged to 1DOA. Stageing was done by letting ten 1DOA mothers crawl on an *E. coli* OP50 seeded 60mm NGM plate (seeded the night before) for ~ 3 hours to lay eggs and then mothers were picked off leaving eggs laid within this time on the plate. Plates were then blinded for analysis. The hatched worms were grown at 22°C for ~ 80 hours to 1DOA. For counting eggs retained in the uterus a modification of a previously published protocol was employed (Gardner et al., 2013). Briefly, a 20% bleach solution pipetted (approximately 200 µl) on an NGM plate (without food) and worms were picked into the bleach solution and the bleach was left to dry for approximately 15 min allowing the cuticle (eggs are unaffected by bleach) to dissolve to burst the worm open and expelling the eggs. The eggs for each bleached worm were then counted using a dissecting microscope. Wild-type and mutants were always scored together on the same day. Each assay was repeated >3 times.

Imaging intestinal lumen pH. The experiments were done by Brian Ackley at the University of Kansas (US) but I analysed the blinded data. KR35 feeding, imaging and image analysis was carried out as previously described (Benomar et al., 2020, Bender et al., 2013). Briefly, worms were raised to young adults on OP50. Prior to acquisition of videos, the animals were transferred to NGM plates supplemented with 10 µM KR35 and OP50 for 15–30 minutes, and then transferred and imaged on NGM plates without the fluorophore. All animals were treated with equivalent conditions on all days of imaging, including feeding the KR35 dye to animals of each genotype from the same source plate (one condition at a time) to avoid differences in dye concentration, immediately prior to imaging.

Imaging and image analysis were done as previously described (Benomar et al., 2020, Bender et al., 2013). Videos of free-moving animals fed with KR35 and KR54 dyes were acquired on a Leica M165FC microscope using a Leica DFC3000G CCD Camera via the Leica Application Suite software (v 4.40) (Leica Microsystems (Switzerland) Limited). Image sequences were acquired at 5x zoom, with 10x gain, and at 10 frames per second. Illumination was via a Leica Kubler Codix source equipped with an Osram HXP 120W lamp. Images were opened in Fiji (ImageJ), converted to 8-bit, scaled from 0–255 to a dynamic range of 10–120, and a rainbow RGB look-up table applied. Movies were converted to AVI using FIJI based on an approximately 30 s clip that corresponded to ~10–15 seconds before and after a

Maximum Anterior Transitions (MAT) (where one occurred). Movies were acquired for ~2 minutes, to include 1–2 MAT. Movies were opened in ImageJ, and a circular ROI of 25x25 pixels was used to measure the fluorescence of the anterior-most intestine during a MAT. 1-2 measurements were taken per animal, and the data transferred to Excel and GraphPad Prism for graphing and statistical analysis.

Pharyngeal pumping rate was assessed using the Android app "Tap Frequency Counter" (Dystopia Entertainment), following the pumping for approximately 30 seconds. Animals were picked the day before as L4 and were grown over night on freshly seeded NGM plates and then scored on the plate as young adults. After picking, the plates were blinded before scoring pharyngeal pumping the next day.

Assessing Chemotaxis, scoring and analysis. For benzaldehyde attraction and repulsion, low peptone 55 mm NGM plates were used. Plates were left to dry for one hour at room temperature (22°C) immediately before the experiment. The underside of the plate was divided into four equal quadrants in which the two opposite ones were test or control quadrants, respectively (Margie et al., 2013). For facilitating counting worms, 0.5M sodium azide (NaN_3) was used to paralyze worms on the test and control spots.

In order to test attraction to lysine, a previous protocol was used for a single worm chemotaxis assay on CTX plates as lysine is a weak attractant (Bargmann and Horvitz, 1991): 24h before the assay, an agar plug was soaked in 0.5M Lysine (pH 6.0) for 3 hours and was then placed at the "test" side of the assay plate to create a gradient while a "control" plug soaked in water was put on the opposite side, both agar plugs were removed from the plate before the start of the assay.

Animals were synchronised to 1DOA. For the benzaldehyde assays, the worms were washed off a plate with 2ml S-basal buffer (100mM NaCl, 0.05M phosphate buffer pH 6.0, 5 µg/mL cholesterol), and then washed 3 times with S-basal to clean them from any bacteria. Between 50 and 250 animals were put in the middle of the plate using a glass pipet. The assay started once the S-basal had evaporated completely. After one hour, worms were counted such that only worms in each quadrant were considered that had completely crossed the 0.5 cm inner circle to prevent immobile worms from skewing the data. The chemotaxis (CI) index was calculated as follows: Chemotaxis Index = (# Worms in Both Test Quadrants - #

Worms in Both Control Quadrants) / (Total # of scored Worms). CI of 1 indicates maximal attraction; CI of -1 indicates maximal repulsion. For the lysine assay, individual animals were picked onto a 90mm plate using an eyelash. *deg-1(u38u421)* mutants which are impaired in lysine sensing (Wang et al., 2012) were used as a negative control. After one hour, attraction was scored as either attracted (when the animal reached the test plug) or not attracted (when the animal did not reach the test plug), and the percentage of animals that reached the test plug was calculated. Both assays were conducted at room temperature (22°C) and repeated at least 3 times and plates were blinded.

Calcium imaging experiments. Calcium imaging was performed on 2 DOA in a custom-designed microfluidic device as previously described (Chew et al., 2018, Cho et al., 2017, Cho et al., 2018). Experiments were performed on a Leica Axiovert 135 inverted microscope using a 40x air objective (N.A. 0.75). Video sequences were captured using a Hamamatsu ORCA-R2 (C10600-10B) camera with 100 ms exposure time. Simultaneous dual colour imaging was performed using an OptoSplit II (Andor Technology) beamsplitter containing a GFP(520 nm)/RFP(605 nm) filter set. CoolLED's pE-300white was used as a light source for fluorescent imaging. Imaging was carried out in S-basal buffer (100mM NaCl, 0.05M phosphate buffer pH 6.0, 5 µg/mL cholesterol). Stimuli were delivered as a 10 s pulse of 1/5 diluted crude pheromone extract or 30mM Lysine in S-basal at t = 5 s after recordings were started. Videos were recorded for 25s following stimulus delivery.

For analysis of calcium transients, fluorescence intensities for each frame were extracted using a custom MATLAB script (Cho et al., 2018, Cho et al., 2017). The GCaMP3/tagRFP ratio (R) between intensity values was computed to minimize movement artefacts. GCaMP3 and tagRFP intensities were measured as the mean pixel intensity of the 100 brightest pixels in a circular region of interest (ROI) with a 14-pixel radius. Calcium traces were computed as the change in R from the baseline value which were computed as the mean R prior to stimulus onset and quantification is provided as the ratio of GCaMP3 to tagRFP fluorescence intensity (Chew et al., 2018, Cho et al., 2017, Cho et al., 2018). The following transgenic lines were used for Calcium imaging: AQ4259 (*ljEx1186 [Psra-9::GCaMP3::SL2-tagRFP (pWRS1483) (50ng/µl); unc-122::RFP(50ng/µl)]*) and for the mutant AQ4447 (*acd-5(ok2657) I; ljEx1186 [Psra-9::GCaMP3::SL2-tagRFP(pWRS1483); Punc-122::RFP]*)

2. 4. Methods IV – Co-immunoprecipitation and pull-down assays (by Yi-Quan Tang)

I constructed the plasmids for C-terminally V5-tagged ACD-5 in which the ACD-5 cDNA was cloned into the pcDNA3.1D/V5-His-TOPO® vector using the pcDNA™3.1/V5-His TOPO™ TA Expression Kit (Invitrogen, K480001). The C-terminally 3xFLAG- tagged ACD-3, DEL-5 and FLR-1 constructs were cloned using the NEBuilder Hifi DNA Assembly Reaction Protocol as described above.

The Co-immunoprecipitation experiment in HEK293T cells were done by Dr. Yi-Quan Tang using the same protocols and reagents as in following paper (Tang et al., 2020): Transfected HEK293T cells were washed three times with ice cold PBS and lysed in lysis buffer (150 mM NaCl, 25 mM Tris-HCl, 1% NP-40, 1 mM EDTA, 5% glycerol and proteinase inhibitor cocktails, pH 7.4) on ice for 30 min with extensively pipetting every 10 min. The insoluble fraction was removed by centrifugation at 16,000 3 g for 10 min and the lysates were split into two aliquots, one for immunoblot analysis and the other for coIP. Equal amounts of proteins were immunoprecipitated with 25 mL anti-V5 agarose affinity gel (A7345, Sigma-Aldrich) overnight at 4 °C with gentle tumbling. The agarose beads were extensively washed four times with wash buffer (150 mM NaCl, 50 mM Tris-HCl, 0.1% NP-40, 0.5 mM EDTA, pH 7.4). The immunoprecipitated protein complexes were eluted using SDS-PAGE sample loading buffer for 5 min at 95 °C. The samples were resolved in SDS-PAGE and transferred to PVDF membranes (Bio-Rad), then subjected to western blot analysis with mouse monoclonal anti-V5-HRP antibody (1:5000, R961- 25, Thermo Fisher Scientific) or mouse monoclonal anti-FLAG M2-HRP antibody (1:2000, A8592, Sigma-Aldrich).

For pull-down assays, V5-tagged fusion protein lysate was incubated with anti-V5 agarose affinity gel (A7345, Sigma-Aldrich) for 3 hours at 4 °C with gentle tumbling. After extensive washing, V5-tagged fusion protein coated beads were further incubated with lysate of HEK293T cells expressing the 3xFLAG fusion proteins (either ACD-3 or DEL-5 or FLR-1) overnight at 4 °C. The beads were then extensively washed four times with wash buffer. The pull-down protein complexes were eluted using SDS-PAGE sample loading buffer for 5 min at 95 °C. The samples were resolved in SDS-PAGE and transferred to PVDF membranes (Bio-Rad), then subjected to western blot analysis.

2. 5. Methods V – Statistical Analysis

Statistical Analysis was done in GraphPad Prism version 9.0.2 for macOS, GraphPad Software, San Diego, California USA (www.graphpad.com). Normality (if the data follows a normal/Gaussian distribution) was assessed by a Shapiro-Wilk test. If the data followed a normal distribution, a parametric test was deployed, if not, the non-parametric equivalent was chosen. Appropriate post-hoc tests were always used for multiple comparisons (Bonferroni correction). The parameters and statistical test used are indicated in each figure description.

Statistical Reporting was done using the guidelines of the American Psychological Association (APA) statistical referencing style.

2. 6. Appendix B

2. 6. 1. Standard solutions and recipes

M9 Buffer

3 g KH_2PO_4, 6 g Na_2HPO_4, 5 g NaCl, 1M $MgSO_4$, (1 ml) H_2O to 1 litre. Sterilize by autoclaving.

S-Basal Buffer

5.85 g NaCl, 1 g $K_2 HPO_4$, 6 g KH_2PO_4, 1 ml cholesterol (5 mg/ml in ethanol), H_2O to 1 litre. Sterilize by autoclaving.

Freezing buffer

150 ml 100% glycerol, 25 ml 1M KPO_4 (pH6), 3.85g NaCl, fill up to 500 ml with MilliQ water, then add 500 ml M9. (add bacto agar at 0.4% for agar freezing stock solution). Autoclave.

NGM

3 g NaCl, 17 g agar, 2.5 g peptone, add 975 ml H_2O. Autoclave for 50 min. Cool flask to 55°C. Add 1 ml 1 M $CaCl_2$, 1 ml 5 mg/ml cholesterol in ethanol, 1 ml 1 M $MgSO_4$ and 25 ml 1M KPO_4 buffer pH 6.0 (108.3 g KH2PO4, 35.6 g K2HPO4, H2O to 1 litre).

CTX Agar

Difco Bacto Agar 20g, MPW 1L. Autoclave, allow to cool to around 55°C, and the add 1M $CaCl_2$ (1ml);1M $MgSO_4$ (1ml); 1M KPHOS (pH 6) (5ml).

LB plates

10g Tryptone, 5g Yeast Extract, 10g NaCl, 15g Agar, make to 1 litre with milli-q water. Autoclave at 121°C for 15mins at 15psi. Final pH 7.0±0.2 at 25°C.

1x TAE

40mM Tris, 20mM Acetate and 1mM EDTA

10x ND96

960mM NaCl, 10mM $MgCl_2$, 50mM HEPES (or MES), 18mM $CaCl_2$, 20mM KCl, pH 7.4 with NaOH. Do not autoclave.

1X NMDG

96mM NMDG, 2mM KCl, 1.8mM $CaCl_2$, 5mM HEPES, 1mM $MgCl_2$, pH 7.4 with HCl. Do not autoclave.

2. 6. 2. Key resource tables

Supplementary Table 2: Bacterial strains, chemicals, peptides and recombinant proteins.

REAGENT OR RESOURCE	SOURCE	IDENTIFIER
Bacterial strains		
E. coli OP50	CGC	OP50

REAGENT OR RESOURCE	SOURCE	IDENTIFIER
Chemicals, Peptides and Recombinant proteins		
Amiloride hydyrochloride	Sigma-Aldrich	
Direct-zol RNA Miniprep	Zymo Research	
Power SYBR Green PCR Master Mix-1	Life Technologies Ltd	
SuperScript™ II Reverse Transcriptase	Invitrogen™	
pUCIDT-KAN-egas-1 cDNA	IDT	pEK308
pUCIDT-KAN-egas-2 cDNA	IDT	pEK309
pUCIDT-KAN-del-5_F9F3.4	IDT	pEK155
Alt-R® S.p. Cas9 Nuclease V3	IDT	
Reagents for CoIP and pull-down experiments (see Tang et al., 2020)		

Supplementary Table 3: Strains used in this thesis.

REAGENT OR RESOURCE	**SOURCE**	**IDENTIFIER**
Experimental Models: Organism and Strains		
C. elegans var. Bristol N2	Caenorhabditis Genetics Center (CGC)	N2 (wild-type)
ljEx1225 [Pacd-5::mKate2 (50ng/µl)]	This thesis	AQ4335
daf-2(e1370) III	Caenorhabditis Genetics Center (CGC)	CB1370
acd-5(ok2657) I	Caenorhabditis Genetics Center (CGC)	AQ4339
daf-4(e1364) III	Caenorhabditis Genetics Center (CGC)	CB1364
daf-9(m540) X	Caenorhabditis Genetics Center (CGC)	DR2281
acd-5(ok2657) I; ljEx1225[Pacd-5::mKate2 (50ng/µl)]	This thesis	AQ4394
acd-5(ok2657) I; ljEx1249 [Pacd-5::acd-5 cDNA; Punc-122::GFP (50ng/µl)]	This thesis	AQ4401
daf-2(e1317) II; ljEx1225[Pacd-5::mKate2 (50ng/µl)]	This thesis	AQ4442
acd-5(ok2657) I; ljEx1186[Psra-9::GCaMP3::SL2-tagRFP(pWRS1483); Punc-122::RFP]	This thesis	AQ4447

daf-11(ks67) V	Caenorhabditis Genetics Center (CGC)	FK183
daf-16(mu86) I	Caenorhabditis Genetics Center (CGC)	CF1038
daf-16(mu86) I; ljEx1225[Pacd-5::mKate2 (50ng/µl)]	This thesis	AQ4494
daf-4(e1364) III; ljEx1225[Pacd-5::mKate2 (50ng/µl)]	This thesis	AQ4495
ljEx1248 [Pacd-5::acd-5 cDNA; Punc-122::GFP (50ng/µl)]	This thesis	AQ4496
ljEx1249 [Pacd-5::acd-5 cDNA; Punc-122::GFP (50ng/µl)]	This thesis	AQ4497
osm-6(p811)V; ljEx1225[Pacd-5::mKate2 (50ng/µl)]	This thesis	AQ4534
dpy-21(e428) V; ljEx1225[Pacd-5::mKate2 (50ng/µl)]	This thesis	AQ4535
daf-9(rh50) X	Caenorhabditis Genetics Center (CGC)	RG1228
dbl-1(ok3749) V	Caenorhabditis Genetics Center (CGC)	VC3044
unc-129(ev554)IV; ljEx1225[Pacd-5::mKate2 (50ng/µl)]	This thesis	AQ4569
dbl-1(ok3749) V; ljEx1225[Pacd-5::mKate2 (50ng/µl)]	This thesis	AQ4570
daf-9(rh50) X; ljEx1225[Pacd-5::mKate2 (50ng/µl)]	This thesis	AQ4593
daf-7(e1372) III	Caenorhabditis Genetics Center (CGC)	CB1372
daf-1(m40) IV	Caenorhabditis Genetics Center (CGC)	AQ4636
deg-1(u38u421)	(Wang et al., 2008)	AQ1319
ljEX1344 [Pacd-2::GFP (50ng/µl); Punc-122::GFP (50ng/µl)]	This thesis	AQ4647
ljEX1345[Pacd-3::GFP; Punc-122::GFP]	This thesis	AQ4648
ljEX1347 [Pdelm-2::GFP (50ng/µl); Punc-122::GFP (50ng/µl)]	This thesis	AQ4650
ljEx1349[Pdel-5::GFP (50ng/µl); Punc-122::GFP (50ng/µl)]	This thesis	AQ4652
ljEx1350[Pdel-1::GFP (50ng/µl); Punc-122::GFP (50ng/µl)]	This thesis	AQ4653
ljEx1352[Pdel-2::GFP (50ng/µl); Punc-122::GFP (50ng/µl)]	This thesis	AQ4655
ljEx1355[Pdel-4::GFP (50ng/µl); Punc-122::GFP (50ng/µl)]	This thesis	AQ4664
acd-5(lj122) I	This thesis	AQ4667
ljEx1361 [Pdel-9::GFP (50ng/µl); Punc-122::GFP (50ng/µl)]	This thesis	AQ4672
ljEx1362 [Pdel-10::GFP (50ng/µl); Punc-122::GFP (50ng/µl)]	This thesis	AQ4673

ljEx1363 [Pegas-1::GFP (50ng/µl); Punc-122::GFP (50ng/µl)]	This thesis	AQ4674
ljEx1364 [Pegas-2::GFP (50ng/µl); Punc-122::GFP (50ng/µl)]	This thesis	AQ4675
acd-3(ok1335) X	Caenorhabditis Genetics Center (CGC)	VC1047
ljEX1368 [Pegas-3::GFP (25ng/µl); Punc-122::GFP (50ng/µl)]	This thesis	AQ4684
ljEX1369 [Pegas-4::GFP (25ng/µl); Punc-122::GFP (50ng/µl)]	This thesis	AQ4685
acd-5::GFP(lj126) I	This thesis	AQ4723
ljEx1386 [Pacd-4::GFP (50ng/µl); Punc-122::GFP (50ng/µl)]	This thesis	AQ4724
acd-5(lj122) I; ljEx1248 [Pacd-5::acd-5 cDNA; Punc-122::GFP (50ng/µl)]	This thesis	AQ4759
acd-5(lj122) I; ljEx1249 [Pacd-5::acd-5 cDNA; Punc-122::GFP (50ng/µl)]	This thesis	AQ4760
ljEx1432 [Pdel-9::del-9 cDNA (5ng/µl); Punc-122::GFP (50ng/µl)]	This thesis	AQ4794
del-9(ok2353) X	Caenorhabditis Genetics Center (CGC)	AQ4797
del-5(lj138) X	This thesis	AQ4802
ljEx1437[Pdel-9::del-9 genomic DNA(25ng/µl); Punc-122::GFP (50ng/µl)]	This thesis	AQ4804
del-9(lj142) X	This thesis	AQ4809
del-9(ok2353) X; ljEx1432 [Pdel-9::del-9 cDNA (5ng/µl); Punc-122::GFP (50ng/µl)]	This thesis	AQ4812
ljEx1448 [Pasic-1::mKate2 (10ng/µl) ; Punc-122::GFP (50ng/µl)]	This thesis	AQ4840
daf-7(e1372) III; ljEx1225[Pacd-5::mKate2 (50ng/µl)]	This thesis	AQ4858
ljEx1463 [Pdel-9::del-9 cDNA::mKate2 (10ng/µl); Punc-122::RFP (50ng/µl)]	This thesis	AQ4864
ljEx1464 [Pdel-9::del-9 cDNA::mKate2 (10ng/µl); Punc-122::RFP (50ng/µl)]	This thesis	AQ4865
ljEx1465 [Pdel-9::del-9 cDNA::mKate2 (10ng/µl); Punc-122::RFP (50ng/µl)]	This thesis	AQ4866
ljEx1470 [Pacd-5::acd-5(no stop) cDNA::mKate2 (10ng/µl) ; Punc-122::GFP (50ng/µl)	This thesis	AQ4872
daf-7(e1372) III	Caenorhabditis Genetics Center (CGC)	AQ4919
daf-4(e1364ts) III; acd-5 (lj122) I	This thesis	AQ4920
daf-7(e1372) III; acd-5 (lj122) I	This thesis	AQ4922

ljEx1507 [Pges-1::acd-5(ok2657) (stop) (10ng/µl) ; Punc-122::RFP (50ng/µl)]	This thesis	AQ4925
acd-5(lj122)I; del-9(lj140) X	This thesis	AQ4926
acd-5(lj122)I; acd-3(ok1335) X	This thesis	AQ4930
acd-5(lj122)I; del-9(ok2353) X	This thesis	AQ4931
ljEx1500 [Pacd-5::acd-5(ok2657) cDNA (no stop) (10ng/µl) ; Punc-122::RFP (50ng/µl)	This thesis	AQ4934
ljEx1503 [Pacd-5::acd-5(ok2657) cDNA (no stop) (10ng/µl) ; Punc-122::RFP (50ng/µl)	This thesis	AQ4940
ljEx1504 [Pacd-5::acd-5(ok2657) cDNA (no stop) (10ng/µl) ; Punc-122::RFP (50ng/µl)	This thesis	AQ4941
ljEx1505 [Pges-1::acd-5(ok2657) (stop) (10ng/µl) ; Punc-122::RFP (50ng/µl)	This thesis	AQ4942
ljEx1506 [Pges-1::acd-5(ok2657) (stop) (10ng/µl) ; Punc-122::RFP (50ng/µl)	This thesis	AQ4943
unc-25(e156) III	Caenorhabditis Genetics Center (CGC)	CB156
del-9(ok2353) X; ljEx1533 [Prab-3::del-9 gDNA (10ng/µl); Punc-122::GFP (50ng/µl)	This thesis	AQ4981
del-9(ok2353) X; ljEX1534 [Prab-3::del-9 gDNA (10ng/µl); Punc-122::GFP (50ng/µl)	This thesis	AQ4982
del-9(lj142) X; ljEX1535 [Prab-3::del-9 gDNA (10ng/µl); Punc-122::GFP (50ng/µl)	This thesis	AQ4983
del-9(ok2353) X; ljEX1536 [Prab-3::del-9 gDNA (10ng/µl); Punc-122::GFP (50ng/µl)]	This thesis	AQ4984
del-9(lj142) X; ljEX1537 [Prab-3::del-9 gDNA (10ng/µl); Punc-122::GFP (50ng/µl)]	This thesis	AQ4985
del-9(ok2353) X; ljEX1538 [Punc-47::del-9 gDNA (10ng/µl); Punc-122::GFP (50ng/µl)]	This thesis	AQ4986
acd-3(ok1335) X; acd-5(ok2657)I	This thesis	AQ4999
del-5(lj138) X; acd-5(ok2657)I	This thesis	AQ5000
del-5(lj138) X; acd-5(lj122) I	This thesis	AQ5001
del-9(ok2353) X; ljEx1437[Pdel-9::del-9 genomic DNA(25ng/µl); Punc-122::GFP (50ng/µl)]	This thesis	AQ5002
ljEx1546 [Pdel-9::del-9::mKate2 (25ng/µl) ; Punc-122::GFP (50ng/µl)]	This thesis	AQ5004
del-9(lj142) X; ljEx1547 [Punc-47::del-9 gDNA (10ng/µl); Punc-122::GFP (50ng/µl)]	This thesis	AQ5005
del-9(lj142) X; ljEX1548 [Punc-47::del-9 gDNA (10ng/µl); Punc-122::GFP (50ng/µl)]	This thesis	AQ5006
del-9(ok2353) X; ljEx1549 [Punc-47::del-9 gDNA (10ng/µl); Punc-122::GFP (50ng/µl)]	This thesis	AQ5007
pbo-4(ok583) X		RB793

del-9(lj142) X; ljEx1437 [Pdel-9::del-9 genomic DNA(25ng/µl); Punc-122::GFP (50ng/µl)]	This thesis	AQ5016
del-9(lj142) X; pbo-4(ok583) X	This thesis	AQ5031
del-9(ok2353) X; pbo-4(ok583) X	This thesis	AQ5032
itr-1(sa73) IV; acd-5(ok2657) I	This thesis	AQ5048
acd-5(ok2657) I; pbo-4(ok583) X	This thesis	AQ5050
del-9(lj142) X; ljEx1591 [Punc-103e::del-9 cDNA (25ng/µl); Punc-122::RFP (50ng/µl)]	This thesis	AQ5051
acd-5(lj122) I; pbo-4(ok583) X	This thesis	AQ5074
del-9(ok2353) X; ljEx1579 [Punc-103e::del-9 cDNA (25ng/µl); Punc-122::RFP (50ng/µl)]	This thesis	AQ5120
del-9(ok2353) X; ljEx1582 [Pdel-9 (empty)(25ng/µl); Punc-122::GFP (50ng/µl)]	This thesis	AQ5131
del-9(lj140) X; ljEx1583 [Pdel-9 (empty)(25ng/µl); Punc-122::GFP (50ng/µl)]	This thesis	AQ5132
del-9(lj140) X; ljEx1589 [Punc-103e (empty)(25ng/µl); Punc-122::RFP (50ng/µl)]	This thesis	AQ5147
del-9(ok2353) X; ljEx1590 [Punc-103e (empty)(25ng/µl); Punc-122::RFP (50ng/µl)]	This thesis	AQ5148
itr-1(sa73) IV	Caenorhabditis Genetics Center (CGC)	JT73
ljEx543 [sra-9::YC3.60;unc-122::rfp]	(Tang et al., 2020)	AQ3093
Is [Punc-47::NLS-mCherry]	This thesis	AQ4583
pha-1(e2123) III; rnyEx133 [pKN114 (opt-2p::opt-2(aa1-412)::GFP) + pCL1 (pha-1+)]	Caenorhabditis Genetics Center (CGC)	KWN246
[Pasic-2::GFP::UTR;Pelt-2::RFP::UTR]	(Grundy, 2018)	AQ3478

Supplementary Table 4: Primers used for plasmid construction

REAGENT OR RESOURCE		**SOURCE**	**IDENTIFIER**
Primers for cloing promoters, gDNA and cDNA			
KSM Hifiuni F	AGATCTGGTTACCACTAAACCAGCC	This thesis	backbone for all KSM vectors if not stated otherwise
KSM hifiuni R	TGCAGGAATTCGATATCAAGCTTATCGATACC		
Pacd-5 Fwd	GGGGACAACTTTGTATAGAAAAGTTGTAagaaaaattatcacatttttgtagatgaaac	This thesis	pEK163
Pacd-5 Rev	GGGGACTGCTTTTTTGTACAAACTTGTcctggaacaactccactttcaaacctg		
acd-5_cDNA_attB1_F	GGACAAGTTTGTACAAAAAAGCAGGCTTAATGCGACGCGTAAGAAACCT	This thesis	pEK262

Pacd-5_R	CTGCTTTTTTGTACAAACTTGTcctggaacaactccactttca aacctg		
Pacd-5_F	CAACTTTGTATAGAAAAGTTGTAagaaaaattatcacatttttgta gatgaaaccgtaatatgac		
acd-5_cDNA_attB1_R	CCACTTTGTACAAGAAAGCTGGGTTTTATGCTTCATGTA TCACAGCTGGC		
acd-5 fragment_KSM_F	TTGGGCCCCTCGAGGTCGACATGCGACGCGTAAGA AACC	This thesis	pEK171
acd-5 fragment_KSM_R	CTCCATTCGGGTGTTCTTGATTATGCTTCATGTATCA CAGCTGGC		
KSM vector_acd-5_F	AGGTTTCTTACGCGTCGCATGTCGACCTCGAGGGG CC		
KSM vector_acd-5_F	CTGTGATACATGAAGCATAATCAAGAACACCCGAATG GAGTCTCT		
acd-5(ok2657) mut_F	tgTCAAGAACACCCGAATGG	This thesis	pEK172
acd-5(ok2657) mut_R	caTTCATATGCGGAATCGTC		
Pacd-4+HindIII_F	ggccAAGCTTgatgcagtttgaaaagccataag	This thesis	pEK206
Pacd-4+XmaI_R	cgcGGGCCCttgagatagtgtaggtttgg		
acd-2_KSM_F	TTGGGCCCCTCGAGGTCGACATGCATCTCGAGGAC GGTC	This thesis	pEK214
acd-2_KSM_R	CTCCATTCGGGTGTTCTTGATTAACGAGGAGACAAGG ATGATGGTAAAG		
KSM_acd-2_R	GGACCGTCCTCGAGATGCATGTCGACCTCGAGGGGC		
KSM_acd-2_F	CATCCTTGTCTCCTCGTTAATCAAGAACACCCGAATGG AGTCT		
F28A12.1_ACD-4_KSM_F2	TATCGAATTCCTGCAATGAATAGAAAACGAAAATTAT CGTGCTTTGTATCTGTC	This thesis	pEK252
F28A12.1_ACD-4_KSM_R2	GTGGTAACCAGATCTTCATAGTTTTATAATAATTCCC AGATC		
Y69H2.2_egas-3_KSM_F1	CTTGATATCGAATTCCTGCAATGATTTTCCTGCTTTT CCTCATATTCCC	This thesis	pPM003

Y69H2.2_egas-3_KSM_R1	GTTTAGTGGTAACCAGATCTCTACTTTTCATATTTCTGGCACAAAACCATAAACA		
Y69H2.11_egas-1_KSM_F	GTTTAGTGGTAACCAGATCTTCACTTTCCATACTTCTTACAACATAACGTGAATAG	This thesis	pPM001
Y69H2.11_egas-1_KSM_R	CTTGATATCGAATTCCTGCAATGCTACTATTCCTCTTCTTTTTCCCGG		
Y69H2.12_egas-2_KSM_F	CTTGATATCGAATTCCTGCAATGATTTTCCTGCTTTTCCTCATATTCCC	This thesis	pPM002
Y69H2.12_egas-2_KSM_R	GTGGTAACCAGATCTTCACTTTCTACAACATATTGTCAAAACTCCGAAC		
F55G1.13_egas-4_KSM_F	CTTGATATCGAATTCCTGCAATGTTGCTGCTATGGTTTTTTCTTCCG	This thesis	pPM004
F55G1.13_egas-4_KSM_R	GTTTAGTGGTAACCAGATCTTCAAAGACGTTTGTTGAACAAAAGTATGAC		
T28B8.5_del-4_KSM_F	CTTGATATCGAATTCCTGCAATGGGTGTATTTTGGACCGGC	This thesis	pEK230
T28B8.5_del-4_KSM_R	GTTTAGTGGTAACCAGATCTTCAATCATTAGAATGAGGCTTTGGTGGAAC		
F16F9.5_KSM_F	CGAATTCCTGCAgtacaaaattcaaaaaATGAATCGAAACCCGC	This thesis	pEK253
F16F9.5_mec-10_KSM_R	GTTTAGTGGTAACCAGATCTTCAATACTCATTTGCAGCATTTTCTC		
C47C12.6_deg-1_KSM_R	GTGGTAACCAGATCTTTATATTGATACGAAAGCGTCTGACTTTCGCC	This thesis	pEK251
C47C12.6_deg-1_KSM_F	CGAATTCCTGCAGCCCGGGGGATCCACTAGTATGTCGAACCATCACAGTAAAAC		
E02H4.1_del-1_KSM_F	GATATCGAATTCCTGCAATGGCAAGGAAGTATATTGATATTTTAAAAAAATCAAAAATG	This thesis	pEK329
E02H4.1_del-1_KSM_R	GTTTAGTGGTAACCAGATCTTCAATTATTATTTGTGGATACTCCTTTTTCCGCA		
F59F3.4_del-5_KSM_F1	CTTGATATCGAATTCCTGCAATGACGAGTGTCTCGTTTGGT	This thesis	pEK228
F59F3.4_del-5_KSM_R1	GTTTAGTGGTAACCAGATCTTTAAAAATCATTCATAGGCATATTTTTGGTGAATGCT		
F_T28D9.7_del-10_KSM	CTTGATATCGAATTCCTGCAATGGTCCGCATGGCTGAG	This thesis	pEK229
R_T28D9.7_del-10_KSM	GTTTAGTGGTAACCAGATCTCTACACGTAAGAATGTTTATCATCATCCTCTTCG		
R_del-9_C18B2.6_KSM	GTTTAGTGGTAACCAGATCTTCATATGGGAGGCGTCGTTTCT	This thesis	pEK219
F_del-9_C18B2.6_KSM	CTTGATATCGAATTCCTGCAATGTACATGAATGGAAATTTTCCCGAGAC		

R13A1.4c_KSM_F	TCGAATTCCTGCATGATTCCAAAATATACATTTCCACGTCGC	This thesis	pEK285
R13A1.4c_unc-8c_KSM_R1	GTGGTAACCAGATCTCTATTTGCTCATTAACTCCTTTGTTGATTCATTTG		
F25D1.4_degt-1_F	CTTGATATCGAATTCCTGCAATGCCTCGAAAAAGAAGATCTGAAGAC	This thesis	pEK254
F25D1.4_degt-1_R	GTTTAGTGGTAACCAGATCTTTATATAAATTGTGGTTTTAGGAATATATTACTTTTCTTTCGTTCAC		
F58G6.6a_del-2a_F	CTTGATATCGAATTCCTGCAATGTTCTGCTTTCTGCAGTTACCG	This thesis	pEK247
F58G6.6a_del-2a_R	GTTTAGTGGTAACCAGATCTTCACATATTGTCAGGCAAGTTTCTTCTGG		
F58G6.6b_del-2b_F	CTTGATATCGAATTCCTGCAATGAAAGGGCACACAGATTTTGATG	This thesis	pEK248
F58G6.6b_del-2b_R	GTTTAGTGGTAACCAGATCTTCACATATTGTCAGGCAAGTTTCTTCTGG		
asic-2_KSM_F	CTTGATATCGAATTCCTGCAATGCGCGGTGGCG	This thesis	pEK264
asic-2_KSM_R	GTTTAGTGGTAACCAGATCTTTATTTCTTCTTTTTCTCCTCATCTCCTTTATTCTCGA		
C27C12.5b_KSM_F1	CCCTCGAGGTCGACGGATGACTGAAACTTCAAATTGCTCCAG	This thesis	pEK207
C27C12.5b_KSM_R1	CTTAGAGACTCCATTCGGGTTTAGAAATCACAATTTCCGAGATACACAGAATTTCTTTT		
T28B8.5_del-4_KSM_F	CTTGATATCGAATTCCTGCAATGGGTGTATTTTGGACCGGC	This thesis	pEK230
T28B8.5_del-4_KSM_R	GTTTAGTGGTAACCAGATCTTCAATCATTAGAATGAGGCTTTGGTGGAAC		
ZK770.1_KSM_F	TATCGAATTCCTATGGGAAAGAACAGCTTAAAACGGG	This thesis	pEK234
ZK770.1_KSM_R	GTAACCAGATCTATCAATTATCAAGATTAAACCCGTCTTTGTTTAAATTATAATCAG		
del-3_KSM_F	CTTGATATCGAATTCCTGCAATGTGGCTCCGAGGACTTTT	This thesis	pEK236
del-3_KSM_R	GTTTAGTGGTAACCAGATCTTTATGTGTCTCCTGAAGCTACATCTTGAC		
del-7_KSM_F	CTTGATATCGAATTCCTGCAATGAATTGTAGCTGTGGTCATCAAACAG	This thesis	pEK237
del-7_KSM_R	GTTTAGTGGTAACCAGATCTTTATAGATCCATTTCGCGATTTTCTCGAA		
C24G7.4_KSM_F	TGATATCGAATTCCTGCAGCATGCATCTCGAGGACGGTC	This thesis	pEK216

C24G7.4_KSM_R1	TCCATTCGGGTGTTCTTGAGTTAACGAGGAGACAAGGATGATGGTAAAGAGG		
F02D10.5_KSM_F1	AGCTTGATATCGAATTCCTGATGGAAACGGAGACGGAAAGTG	This thesis	pEK215
F02D10.5_KSM_R1	TTCTTGAGGCTGGTTTAGTGTCAAATTAATTGTGATTTGAATATGGAGGATGTTGAAACT		
mKate2_Hifiuni_F	TCCGAGCTCATCAAGGAGAACATGCACAT	This thesis	pEK240
pasic-1_Hifi_F	ACACAGGAAACAGCTATGACttagctgccaataaataaaaactccaattttcaaaaaaatatttt		
pasic-1_Hifi_R	TTCTCCTTGATGAGCTCGGAcatttggtggcctgaaatttgatcaaaaa		
Kim_lab_vector_unihifi_F	cattcgtagaattccaactgagcg		
asic-1_Y601K_F	GCCTGCTCCAaagGGAGATTGTG	This thesis	respective point mutations: pEK273; pEK274; pEK275; (pEK276; pEK277 - random mutations)
asic-1_Y601G_F	GCCTGCTCCAggcGGAGATTGTG		
asic-1_Y601P_F	GCCTGCTCCAcccGGAGATTGTGTTC		
asic-1_uni_R	AGGCGGACCATTGATTTC		
asic-1_D495-597_F	CCTGCTCCATATGGAGATTG	This thesis	pEK279
asic-1_D495-597_R	TTTCATAATAAAATCAGACTTATTATAAGAAATC		
asic-1_D515-520_F	TATGGCCAGAAGCTGGGC	This thesis	pEK280
asic-1_D515-520_R	CGTTGGATCAAGGTATTCCACG		
asic-1_D549-552_F	ACGACTGAGGCAGCTGGA	This thesis	pEK281
asic-1_D549-552_R	AGTTACATTCACAAAAACTTCTAGTCGAAG		
asic-1_3xG_549-552_F	ggtggtACGACTGAGGCAGCTGGA	This thesis	pEK282
asic-1_3xG_549-552_R	accaccAGTTACATTCACAAAAACTTCTAGTCGAAG		

asic-1_CRISPR-del_F	CAGAGAAGTTGTATTCAAAAAC	This thesis	pEK283
asic-1_CRISPR-del_R	GGACCGTTCATTCGTATTATTG		
Pacd-5_acd-5_no stop_R	CTCCTTGATGAGCTCGGACATTTTTTCTACCGGTACTTTCTGATCTACTCCGCCGACTT	This thesis	pEK190
Pacd-5_acd-5_no stop_F	CCAAGCTCGGACACCGTTAATCCAATTACTCTTCAACATCCCTACATGC		
mKate2_fragment_F	TCGGCGGAGTAGATCAGAAAGTACCGGTAGAAAAAATGTCCGAGC		
mKate2_fragment_R	GATGTTGAAGAGTAATTGGATTAACGGTGTCCGAGCTTGGA		
del-9_cDNA_mK_R	TTCTCCTTGATGAGCTCGGATATGGGAGGCGTCGTTTCTG	This thesis	pEK210
mKate_Hifiuni_F	TCCGAGCTCATCAAGGAGAACATGCACAT		
mKate_unihifi_stop_R2	TTAACGGTGTCCGAGCTTGGATGGGAGGTC		
Kimlab_uni_mKate2_F	CCAAGCTCGGACACCGTTAAcattcgtagaattccaactgagcg		
Kim_lab_vector_unihifi_F	cattcgtagaattccaactgagcg	This thesis	pEK232; pEK235
del-9_hifi_F	agatcgacaatccgaagaacATGTACATGAATGGAAATTTTCCCGAGAC		
del-9_hifi_R	cagttggaattctacgaatgTCATATGGGAGGCGTCG		
del-9_Kimlab_vector_R	AAATTTCCATTCATGTACATgttcttcggattgtcgatcttctctga		
acd-5(ok2657)_F	tgGTCCAATTACTCTTCAACATC	This thesis	pEK286, pEK287
acd-5(ok2657) mut_R	TTCATATGCGGAATCGTC		
flr-1_F	GGTACCGAGCTCGGATCCACATGGAAACGGAGACGGAAAGTGA	This thesis	pEK288
flr-1_noStop_R	TCGAATTCCACCACACTGGAAATTAATTGTGATTTGAATATGGAGGATGTTGAAACT		
pcDNA3.1(+)_F	TCCAGTGTGGTGGAATTCGACTAC		
pcDNA3.1(+)_R	GTGGATCCGAGCTCGGTACCA		

acd-3_F	GGTACCGAGCTCGGATCCACATGACTGAAACTTCAAATTGCTCCAGC	This thesis	pEK289
acd-3_noStop_R	TCGAATTCCACCACACTGGAGAAATCACAATTTCCGAGATACACAGAATTTCT		
pcDNA3.1(+)_F	TCCAGTGTGGTGGAATTCGACTAC		
pcDNA3.1(+)_R	GTGGATCCGAGCTCGGTACCA		
del-5_F	GGTACCGAGCTCGGATCCACATGACGAGTGTCTCGTTTGGT	This thesis	pEK290
del-5_noStop_R	TCGAATTCCACCACACTGGAAAAATCATTCATAGGCATATTTTTGGTGAATGCT		
pcDNA3.1(+)_F	TCCAGTGTGGTGGAATTCGACTAC		
pcDNA3.1(+)_R	GTGGATCCGAGCTCGGTACCA		
acd-5_F	CACCATGCGACGCGTAAGAAACCTCTC	This thesis	pEK291
acd-5_R	TGCTTCATGTATCACAGCTGGC		
ok2657_v1_F	AGGTCAAGACAATTCTGCAG	This thesis	pEK292
ok2657_v1_R	TTCATATGCGGAATCGTCC		
Prab-3_F	aatgaaataagcttgcatgcgatcttcagatgggagcagtggac	This thesis	pEK297
Kimlab_vector_rab-3_R	actgctcccatctgaagatcgcatgcaagcttatttcatttccaagttg		
del-9_gDNA_F	tacagtagccctattttcagATGTACATGAATGGAAATTTTCCCGAGAC		
prab-3_R	AAATTTCCATTCATGTACATctgaaaatagggctactgtagatttattttaaaagagca		
Punc-47L_F	aatgaaataagcttgcatgcAAAGTTGACAAAACAACTTTCTTGGAAAAAAAG	This thesis	pEK298
Punc-47L_R	AAATTTCCATTCATGTACATGGTCATGAGGTGGGGGATTTGA		
KV_R	AAAGTTGTTTTGTCAACTTTgcatgcaagcttatttcatttccaagttg		
KV_F	AAATCCCCCACCTCATGACCATGTACATGAATGGAAATTTTCCCGAGAC		
Punc-103e_F	cgtggaccttgtcagaactgtgcatgcctattttatatttacaatattttagttattg	This thesis	pEK321
Punc-103e_R	AAATTTCCATTCATGTACATaccaccaccaccacaaccaccg		
vector_R	taaaataggcatgcacagttctgacaaggtccacgatttagca		
del-9cDNA_F	gtggttgtggtggtggtggtATGTACATGAATGGAAATTTTCCCGAGAC		
Kim_lab_vector_unihifi_F	cattcgtagaattccaactgagcg	This thesis	pEK322
Pdel-9_mK_R	TCCTTGATGAGCTCGGAcatgttcttcggattgtcgatcttctct		
Punc-103e_F3	tgctggaagatggcgattagatctcgcgcccgtg	This thesis	pEK323

Punc-103e_R3	accttcctcttcttcttgggaccaccaccaccacaacc

Supplementary Table 5: CRISPR/Cas9 reagents

REAGENT OR RESOURCE	SOURCE	IDENTIFIER	
CRISPR reagents			
Ce.Cas9.DPY-10.1.AQ	GCTACCATAGGCACCACGAG + AltR2	IDT	co-CRISPR
ssODN_dpy-10			
CD.Cas9.VZPJ2357.AN	GTTTGATCTGAAAGATATCA + AltR2	IDT	acd-5(lj122)
Ce.Cas9.ACD-5.1.AK	TTTGTATAACGACGGACCGA + AltR2	IDT	
ssODN_acd-5	aacctattattcacaccgttcagAAACCTCTCACTAGGATCAAATAACACG TGGAAGGGCTGCATCAATG	IDT	
CD.Cas9.SNTV1186.AA	TATGCTTCATGTATCACAGC + AltR2	IDT	acd-5(lj126)
3'Homology_Arm_ACD-5GFP_R	taagagagtgtttgccacaaacccaaaaaaacatacaacacattaaaaacgttttcattag aaaacagataccggtatctacatacacatatgtatatttaattctcatctctctacttacttgtaga gctcgtccattc	IDT	
5'Homology_Arm_ACD-5GFP_F	acaattttgccgtttgatctgaaagatatcaaggatcaaataacacgtggaagggctgcatc aatgtttcgaagtcggcggagtagatcagaaacagcgcgagctgtgatacatgaagcaA TGagtaaaggagaagaatt	IDT	
ssODN_DEL-9	agccagctgtgtgATGTACATGAATGGAAATTTTCACAGATGCTTCA AGCCTTAGTGACAGTTCAGATGA	IDT	del-9(lj142)
Ce.Cas9.DEL-9.1.AC	CTAAGGCTTGAAGCATCTGT + AltR2	IDT	
Ce.Cas9.DEL-9.1.AN	CTTCGGACCACGGTGGTCTC + AltR2	IDT	
ssODN_del-5_new	GACTCTCAATTTCAAAGTCTTGATCCAGCTCCTGGCTTGCCTA GTTTTCTACATTATGGTGgtgagtgat	IDT	del-5(lj38)
Ce.Cas9.DEL-5.1.AW	AATGTAGAAAACTAGGCAAG + AltR2	IDT	
Ce.Cas9.DEL-5.1.AD	CAAAGTCTTGATCCAGCTCC + Alt2	IDT	
Ce.Cas9.DEL-5.1.AE	ACCAATCATTATTTTCGAGC + Alt2	IDT	

Supplementary Table 6: Primers for genotyping.

Primers for genotyping	
acd-5(ok2657)_F	cgcagctagagtttcacagc
acd-5(ok2657)_R	cagagctttaacattgagatgcc
daf-11(ks67)_F	ATGGGACCAACATGCTCCAG
daf-11(ks67)_R	CTAGTTATCTGGAATAGTTGAAGCTTG
daf-4(e1364ts)_F	gagaacgaaagctccgtaag
daf-4(e1364ts)_R	ggcaacctccgtatgatgaacc
daf-16(mu86)_F	catagacgatttcgaaaagttc
daf-16(mu86)_R	caatagtattggatcgttcacg
dpy-21(e428)_F	gctagcctatagccattctg
dpy-21_(e428)_R	gtgaagaaggatccaccagc
ceh-17(mp1)_F	gacatagagacacattcagcacgg
ceh-17(mp1)_R	ctacagaagttcgcttttgg
daf-9(m540)_F	cgttagtgttctgtgctggc
daf-9(m540)_R	gctgccattcgaagtcaggg
osm-6(p811)_F	caagaaacctgcttcttcgc
osm-6(p811)_R	ctagtagttcctttcccagg
daf-7(e1372)_F	AGCTGAACATGAAAGAGGCACC
daf-7(e1372)_R	CGGAGAAATTGTGAACCAACTG
daf-1(m40)_R	ctgcagatgtgctcattgtgc
daf-1(m40)_F	cggatgcatggacgagaaatc
dbl-1(ok3749)_F	gatatgtccagtggctgcct
dbl-1(ok3749)_R	ctcacTGGGTGCCATAATCC
daf-9(rh50)_F	gGTTCCGTACTATTTTGGAAGAAC
daf-9(rh50)_R	CCGAAAGAGTGGCTCTCAC
unc-129(ev554)_F	CTCGATTCCATTGGATAATGATG
unc-129(ev554)_R	cactataacgaaagaaaaataataaac
daf-11(ks67)_F	GAATCTGACAGCATACACTC
daf-11(ks67)_R	cagcctatagttttgacgcg
flp-6(ok3056)_F	ggtgaaaaaccaacctcatgtaggc
flp-6(ok3056)_R	ggtactccccctcatccaaattc
del-5(lj138)_F	aATGACGAGTGTCTCGTTTG
del-5(lj138)_R	CGTTGATTCTCATAAAACTGGG
del-9(ok2353)_F	GCCCgtaagtgcactgatttt
del-9(ok2353)_R	GGCGTCGTTTCTGATGTGTG
del-9(lj142)_F	ctttgtgtttcctgtcatcttag
del-9(lj142)_R	CAACTATCCTCCTCATCGAATAC
flr-1(ut11)_F	cagacgttgaaaaagatgg
flr-1(ut11)_R	gagaaagcggttctaatgatac
acd-3(ok1335)_F	catgaaagtactaacttccagattcg
acd-3(ok1335)_R	gagatccatggatacttccg
itr-1(sa73)_F	TCAAAGGGACGTAGTTCTGACAGC
itr-1(sa73)_R	TGAAGAGCTGAATATGGCGCTTC

pbo-4(ok583)_F	ACTAGATGAGAGTTGGCGAGA
pbo-4(ok583)_R	AGTCGTGTGGTAAAGCTCCG
pbo-4(ok583)_v2_F	CGAGTTGGTGCTCACCCTAT

Supplementary Table 7: Plasmids used in this thesis.

REAGENT OR RESOURCE	SOURCE	IDENTIFIER
Recombinant DNA (Plasmids)		
pENTR_Pacd-5 (4.763 kb)	This thesis	pEK163
Pacd-5(4.763kb)::mKate2	This thesis	pEK165
pENTER acd-5 cDNA	This thesis	pEK168
Pacd-5(4.763kb)::acd-5	This thesis	pEK169
ACD-5::KSM	This thesis	pEK171
acd-5(ok2657)::KSM	This thesis	pEK172
Pacd-2::GFP	This thesis	Kyuhyung Kim Lab
Pacd-3::GFP	This thesis	Kyuhyung Kim Lab
Pdel-10::GFP	This thesis	Kyuhyung Kim Lab
Pacd-5::acd-5 cDNA (no stop)::mKate2	This thesis	pEK190
Pdel-1::GFP	This thesis	Kyuhyung Kim Lab
Pdel-2::GFP	This thesis	Kyuhyung Kim Lab
Pdel-4::GFP	This thesis	Kyuhyung Kim Lab
Pdel-5::GFP	This thesis	Kyuhyung Kim Lab
Pdel-8::GFP	This thesis	Kyuhyung Kim Lab
Pdel-9::GFP	This thesis	Kyuhyung Kim Lab
Pdelm-2::GFP	This thesis	Kyuhyung Kim Lab
Pegas-1::GFP	This thesis	Kyuhyung Kim Lab
Pegas-2::GFP	This thesis	Kyuhyung Kim Lab
Pegas-3::GFP	This thesis	Kyuhyung Kim Lab
Pegas-4::GFP	This thesis	Kyuhyung Kim Lab
Pacd-4::GFP	This thesis	pEK206
acd-3::KSM	This thesis	pEK207
Pdel-9::del-9 cDNA::mKate2	This thesis	pEK210
acd-2::KSM	This thesis	pEK214
flr-1::KSM	This thesis	pEK215
acd-1::KSM	This thesis	pEK216
del-9::KSM	This thesis	pEK219
del-5::KSM	This thesis	pEK228
del-10::KSM	This thesis	pEK229
del-4::KSM	This thesis	pEK230
Pdel-9::del-9 gDNA	This thesis	pEK232
asic-1::KSM	This thesis	pEK234

Pdel-9::del-9 cDNA	This thesis	pEK235
del-3::KSM	This thesis	pEK236
del-7::KSM	This thesis	pEK237
Pasic-1 (3.5kb)::mKate2	This thesis	pEK240
del-2a::KSM	This thesis	pEK247
del-2b::KSM	This thesis	pEK248
deg-1::KSM	This thesis	pEK251
acd-4-4::KSM	This thesis	pEK252
mec-10::KSM	This thesis	pEK253
degt-1::KSM	This thesis	pEK254
egas-1::KSM	This thesis	pPM001
egas-2::KSM	This thesis	pPM002
egas-3::KSM	This thesis	pPM003
Pacd-5::acd-5 cDNA	This thesis	pEK262
asic-2::KSM	This thesis	pEK264
egas-4::KSM	This thesis	pPM004
unc-8 (isoform c)::KSM	This thesis	pEK285
Pacd-5::acd-5(ok2657) cDNA (no stop)	This thesis	pEK286
Pges-1::acd-5(ok2657) cDNA (stop)	This thesis	pEK287
flr-1::3xFLAG pcDNA 3.1(+)	This thesis	pEK288
acd-3::3xFLAG pcDNA 3.1 (+)	This thesis	pEK289
del-5::3xFLAG pcDNA 3.1 (+)	This thesis	pEK290
acd-5 pcDNA 3.1 V5 His TOPO	This thesis	pEK291
acd-5(ok2657) pcDNA 3.1 V5 His TOPO	This thesis	pEK292
Prab-3::del-9 gDNA	This thesis	pEK297
Punc-47L::del-9 gDNA	This thesis	pEK298
Punc-103e::del-9 cDNA	This thesis	pEK321
Pdel-9 (empty)	This thesis	pEK322
Punc-103e (empty)	This thesis	pEK323
ASIC-1(Y601P)::KSM	This thesis	pEK273
ASIC-1(Y601G)::KSM	This thesis	pEK274
ASIC-1(Y601K)::KSM	This thesis	pEK275
ASIC-1(Y601K (Δ597Δ599))::KSM	This thesis	pEK276
ASIC-1(Y601KΔ370-597)::KSM	This thesis	pEK277
ASIC-1 (△495-597)::KSM	This thesis	pEK279
ASIC-1 (△517-521)::KSM	This thesis	pEK280
ASIC-1 (△549-552)::KSM	This thesis	pEK281
ASIC-1 (3xGly 549-552)::KSM	This thesis	pEK282
ASIC-1 (△CRISPR)::KSM	This thesis	pEK283
del-1::KSM	This thesis	pEK329

Supplementary Table 8: Software, Algorithms and other equipment.

Software and Algorithms	
Graphpad	GraphPad Software inc
Roboocyte2+	Multichannel Systems inc.
SnapGene	Insightful Science
GUIDANCE2	Sela et al., 2015
MAFFT	Katoh et al., 2002, Katoh and Standley, 2013
BioNJ	www.phylogeny.fr
FigTree	Rambaut, 2010
iTOL	Ciccarelli et al., 2006, Letunic and Bork, 2019, Kuraku et al., 2013
EFI-EST	Enzyme Function Initiative (efi.igb.illinois.edu/)
Programme for Three-State Stochastic Model for Egg-Laying Behavior	Waggoner et al., 1998
Programme for Caclium imaging Analysis	Cho et al., 2017

Other	
Roboocyte	Multichannel Systems inc.
Roboinject	Multichannel Systems inc.
Dino-Lite Edge	AnMo Electronics Corporation
Tap Frequency Counter	Dystopia Entertainment

CHAPTER 3 – Systematic *in vivo* and *in vitro* characterisation of *C. elegans* DEG/ENaCs

3. 1. Introduction

3. 1. 1. DEG/ENaCs contribute to a variety of *C. elegans* behaviours

C. elegans has played a pivotal role in the discovery and genetic characterisation of the DEG/ENaC superfamily. To date, 17 of the 30 *C. elegans* DEG/ENaC subunits have been characterised to varying extents and have shown to play a role in a variety of different functions *in vivo*, including mechanosensation, proprioception, chemosensation and learning and memory (Takagaki et al., 2020, Tao et al., 2019, Han et al., 2013, Wang et al., 2012, Wang et al., 2008, Voglis and Tavernarakis, 2008, Goodman et al., 2002).The first *C. elegans* DEG/ENaC family members, *deg-1*, *mec-4* and *mec-10,* were identified in a forward genetic screen looking for touch insensitive mutants and were later shown to cause neuronal degeneration of touch receptor neurons (Chalfie and Wolinsky, 1990, Driscoll and Chalfie, 1991, Huang et al., 1995) (summary of abbreviations can be found in Appendix C, 3. 5. 1. below). Since then, many more *C. elegans* DEG/ENaC mutants have shown to cause defects linked to mechanical touch and proprioception. For instance, neuronal calcium imaging and behavioural analysis have shown that mutations in the subunits *degt-1, del-1, mec-10, unc-8* and *asic-1* abolish or decrease the animal's touch sensitivity which correlates with a decrease in calcium transients in the nociceptive PVD neurons (Chatzigeorgiou et al., 2010, Husson et al., 2012, Tao et al., 2019). Furthermore, DEG-1 has recently also been proposed to act as an ambient temperature (mechano)sensor in the ASG sensory neurons, which are part of a neural circuit underlying cold tolerance (Takagaki et al., 2020). There are further examples of *C. elegans* DEG/ENaCs that are involved in mechanosensation but are expressed in non-neuronal tissue such as *delm-1* and *delm-2* which are expressed in glia where they are required cell-autonomously for nose-touch responses (Han et al., 2013).

Many mutants also display altered motor behaviours, such as *unc-8* which is expressed in GABAergic motor neurons, *unc-8* mutants display both an abnormal locomotion behaviour as well as a neurodegenerative phenotype caused by neuronal

swelling and neuronal death (Miller-Fleming et al., 2016, Brenner, 1974, Shreffler et al., 1995, Tavernarakis et al., 1997). Additional genes have been identified in screens for locomotion abnormalities, including *acd-5, asic-1, asic-2, egas-2*, *del-4, del-7* and *del-9,* which may be indicative of proprioceptive roles of these channel subunits (Yemini et al., 2013, Brown et al., 2013). There is also evidence for involvement of DEG/ENaCs in other motor behaviours than locomotion, for instance, *unc-105* acting in muscle cells, which when mutated causes hypercontraction and paralysis, and mutants for the intestinal *flr-1* show an altered behaviour in executing the defecation motor program (Park and Horvitz, 1986, Take-Uchi et al., 1998).

Some worm DEG/ENaC family members have also shown to be involved in regulating chemosensory behaviours. For instance, *deg-1,* expressed in ASK neurons, modulates chemosensory attraction and repulsion, and mutant deficits can be exacerbated by mutations in glial *acd-1* (Wang et al., 2008, Wang et al., 2012). *del-3* and *del-7* are enriched in NSM neurons that are involved in driving behavioural responses to food indigestion and are activated by bacteria (Rhoades et al., 2019). Both channel subunits localise close to the site of bacterial lysis raising the possibility that they could directly be involved in sensing bacterial components (Rhoades et al., 2019).

Finally, as shown in CHAPTER 1, ASIC-1 has shown to localise to presynaptic sites in dopaminergic neurons where it plays a role in associative learning (Voglis and Tavernarakis, 2008). Synaptic expression has also been described for DEL-1 in PVD and UNC-8 in GABAergic neurons (Tao et al., 2019, Miller-Fleming et al., 2016). As shown the *C. elegans* DEG/ENaCs are expressed in a variety of tissues and neurons and contribute to a vast array of behaviours which can provide a starting point for investigating their physiological roles.

3. 1. 2. In vitro characterisation of *C. elegans* DEG/ENaC function

As mentioned above, characterisation of the worm DEG/ENaCs has relied heavily on genetic and behavioural studies, but often lack electrophysiological characterisation. This presents a major limitation when inferring molecular channel functioning from genetic evidence alone. Similar to the DEG/ENaCs in other species, electrophysiological properties of the *C. elegans* members have been studied in *Xenopus* oocytes using TEVC, as electrophysiology in worms is challenging and time

consuming. As we will see below, the electrophysiological evidence available focussed on constitutively active homomeric channel (Wang et al., 2008, Han et al., 2013). Being constitutively active in this case means that the channel is in an open state and the oocyte shows currents that can be blocked using a channel blocker. For those *C. elegans* DEG/ENaCs that are not constitutively active *in vitro*, mutations based on the degeneration-causing *mec-4(a713t)* mutation are usually introduced that constitutively open the channels (at neutral pH) in order to investigate channel function (Fechner et al., 2020, Goodman et al., 2002).

3. 1. 2. 1. Proton-sensitivity

We have seen in CHAPTER 1, that the DEG/ENaC superfamily can be divided into two groups based on whether they are blocked or activated by increasing extracellular proton concentrations *in vitro*. The homomeric ACD-1 is blocked at low pH, similarly the mutant MEC-4 and mutant DEGT-1 expressed in oocytes also show a small decrease in response to pH 6.4, while mutant UNC-105 and mutant UNC-8 currents are potentiated (Wang et al., 2008, Garcia-Anoveros et al., 1998, Fechner et al., 2020, Wang et al., 2013c). Despite the expansion and known diversity of the *C. elegans* DEG/ENaCs, many members have not undergone a detailed electrophysiological characterisation in heterologous expression systems, and this limitation will be addressed over the course of this thesis.

3. 1. 2. 2. Amiloride is a potent channel-pore blocker

I introduced the most commonly used pharmacological DEG/ENaC- specific blocker amiloride in CHAPTER 1 (Canessa et al., 1994, Palmer and Frindt, 1986, Bentley, 1968). The amiloride block is voltage-dependent which is a characteristic of blockers that bind within the channel pore (Fechner et al., 2020, Bentley, 1968). The potency of its block strongly depends on the expression system (e.g. *Xenopus* oocytes, mammalian cell lines, tissue or slices) but also on the on the channel itself, and amiloride concentrations of up to 500 µM were needed for completely blocking some members of the DEG/ENaC family (Baron et al., 2002). However, at high concentrations, amiloride can also enhance currents and even activate vertebrate ASICs. Structural evidence has suggested that this might be due to multiple amiloride

molecules binding within the acidic pocket holding the pore open (Adams et al., 1999b, Li et al., 2011, Baconguis et al., 2014).

3. 1. 2. 3. Ion selectivity

In vitro characterisation of DEG/ENaCs across species has provided insight into their ion selectivity revealing that ion permeability varies significantly amongst members of the superfamily. For instance, mammalian ENaCs are permeable to Na^+ and Li^+, vertebrate ASICs show measurable K^+ permeability, the mammalian ASIC1 is also permeable for Ca^{2+} and the neuropeptide-gated *Hydra* channel (HyNaC) even forms a Ca^{2+} channel (Palmer and Frindt, 1986, Carattino and Della Vecchia, 2012, Zhang and Canessa, 2002, Bässler et al., 2001, Hoagland et al., 2010, Durrnagel et al., 2012). Table 1 summarises the ion selectivity of previously characterised *C. elegans* DEG/ENaCs. It is likely that the difference in ion permeability for different channels reflects their functional requirements *in vivo*. However, more direct evidence is needed to explore how *in vitro* characteristics translate into *in vivo* function, and the CHAPTERS 4 and 5 will survey ion selectivity for selected proton-sensitive *C. elegans* DEG/ENaCs.

The overall aim of the current chapter was to generate a starting point for further investigation, by identifying subunits that could form functional homomeric channels *in vivo* and to generate an overview of the protein similarity and *in vivo* expression pattern for the worm DEG/ENaCs, in order to then generate hypotheses about potential channel functioning and their cellular role which will be investigated in the subsequent chapters.

Table 1: Ion selectivity of previously characterised C. elegans DEG/ENaCs.

Channel subunit	Ion Selectivity	Reference
UNC-105	slightly selective for Na^+ and Li^+ over K^+ and Cs^+ Impermeable to Ca^{2+} and Mg^{2+}	(Garcia-Anoveros et al., 1998)
DELM-1	Li^+ followed by Na^+ and K^+	(Han et al., 2013)
ACD-1	Na^+ followed by Li^+ and K^+ Impermeable for Ca^{2+}	(Wang et al., 2008)
MEC-4d	permeable for Na^+ and Li^+ Ca^{2+} and to a lower degree K^+ and Cs^+	(Goodman et al., 2002, Bianchi et al., 2004, Fechner et al., 2020)
UNC-8d	Li^+ and Na^+ followed by K^+ and Cs^+	(Fechner et al., 2020, Wang et al., 2013c)
DEGT-1d	equally permeable for Na^+, K^+ and Cs^+ and lower for Li^+	(Fechner et al., 2020)

d = contain the mutation based on MEC-4d (or MEC-4(A713T)) which opens the channel.

3. 2. Results

3. 2. 1. Exploration of the *C. elegans* DEG/ENaC protein sequences

Compared to its vertebrate homologues, the *C. elegans* family has undergone an expansion with 30 channels currently known, most of whom only encode one isoform. The *C. elegans* DEG/ENaCs are a diverse family of ion channels within them, they share 30-76% identity and 40-85 % sequence similarity as assessed with local

alignment (Smith-Waterman, in the SnapGene software) (Daily, 2016). Figure 8 shows the phylogenetic relationships of the *C. elegans* DEG/ENaCs, generated using a neighbour-joining phylogenetic tree and a Sequence Similarity Network (SSN). Both are useful starting points to visualise different clusters within the family and generate hypotheses for those sequences whose molecular functions and expression patterns are currently unknown.

The phylogram identifies roughly three clusters within the *C. elegans* DEG/ENaC family (Figure 8A). The first and biggest cluster consist of ASIC-1, ASIC-2, DEG-1, DEL-1, DEL-4, MEC-4, MEC-10, UNC-8 and UNC-105. Then there is a smaller tight second cluster ACD-1, ACD-2, ACD-4, ACD-5, DELM-1 and DELM-2. Further distant but on the same branch are FLR-1, DEL-5, ACD-3 and finally there is DEL-3 which might also belong to this cluster but is most distant from this second cluster. The third cluster consists of the four subunits EGAS-1, EGAS-2, EGAS-3 and EGAS-4. Within the *C. elegans* DEG/ENaCs they form a distinct family as they present not only the ASC domain (Pfam: PF00858) but also the EGF domain (Pfam: PF00008). DEL-8 is also on the same branch but more distant. Finally, there are miscellaneous sequences that do not form a distinct cluster with others. These include DEGT-1, DEL-2, DEL-6, DEL-7, DEL-9 and DEL-10.

To further explore the similarities among the *C. elegans* DEG/ENaC proteins, I generated an SSN which has the advantage over the phylogram that it visualises functional clusters of sequences making it easier to reveal outliers (Atkinson et al., 2009). The SSN for the *C. elegans* DEG/ENaC family is shown in Figure 8B. Each node represents a DEG/ENaC protein and two nodes are connected by an edge if they share pairwise sequence similarity above a 30% threshold. The SSN clearly identifies three distinct clusters of *C. elegans* DEG/ENaCs, and a pair of only two subunits: The first cluster consists of ASIC-1, ASIC-2, DEG-1, DEL-1, DEL-4, MEC-4, MEC-10, UNC-8 and UNC-105, I will call this group the ASIC-1 group. The second cluster ACD-1, ACD-2, ACD-4, ACD-5, DELM-1, DELM-2 and FLR-1, which I will call the ACD-1 group, and the third cluster, the EGAS group, which is made up of the four EGAS proteins. There is one further pair consisting of only DEL-7 and DEL-8. The following proteins could not be grouped with any other proteins: ACD-3, DEGT-1, DEL-2, DEL-3, DEL-5, DEL-6, DEL-9 and DEL-10. Based on the clustering of amino acid sequences in the phylogram and the SSN, there are at least three distinct clusters of *C. elegans* DEG/ENaCs, and from now on they will be referred to, and colour-coded

as, ASIC-1 group (green), ACD-1 group (orange) and EGAS group (purple) as shown in Figure 8. In the following sections, I will use expression pattern data as well as data from two electrophysiological screens in order to functional characterise the *C. elegans* DEG/ENaCs to explore whether these clusters reflects tissue-specific expression pattern or electrophysiological properties.

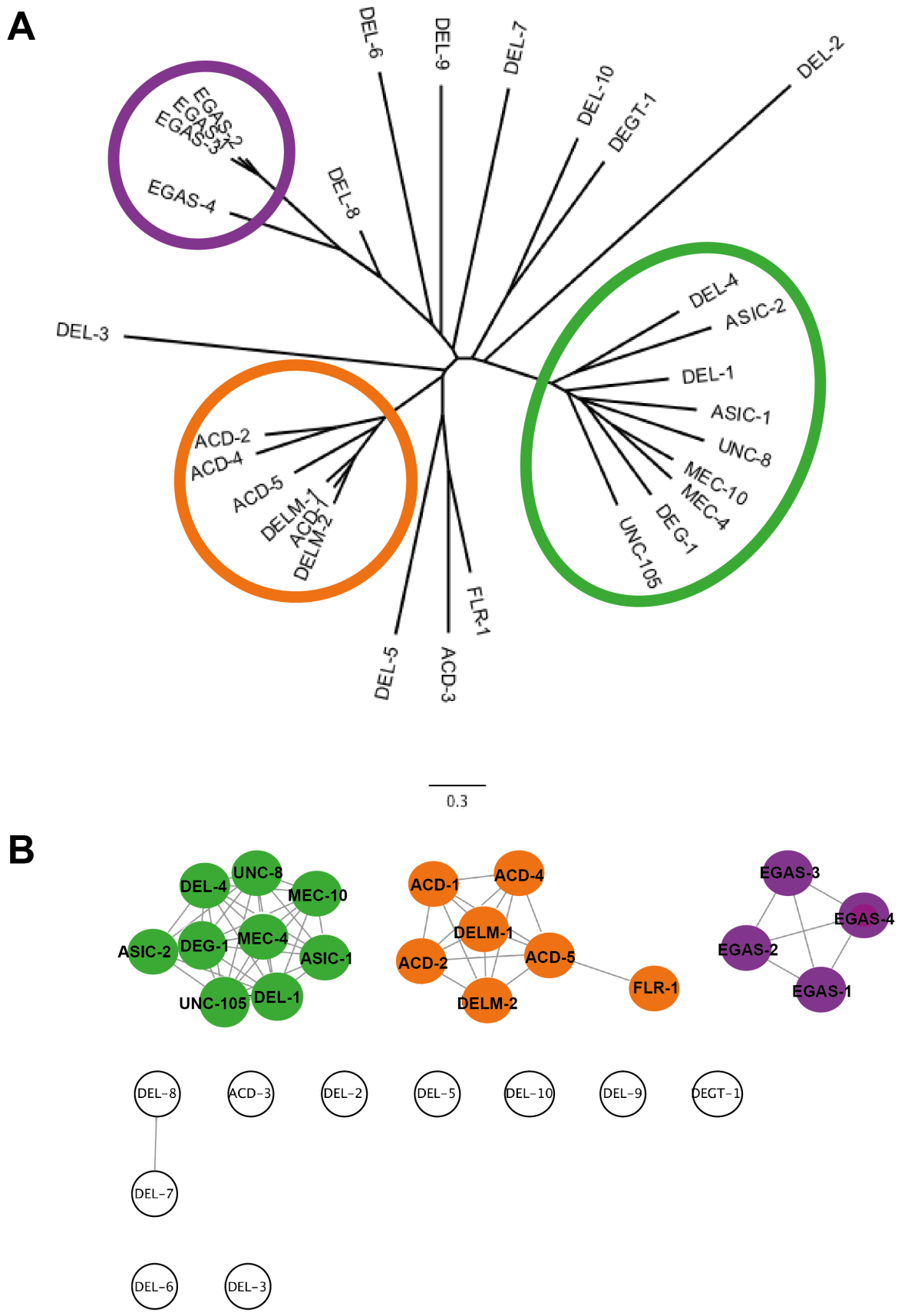

Figure 8: Phylogenetic analysis of the 30 C. elegans DEG/ENaCs.

Phylogenetic analysis of the 30 *C. elegans* DEG/ENaCs shows three distinct groups: The ASIC-1 group (green), ACD-1 group (orange) and EGAS group (purple). (A) Neighbour-joining tree of all 30 members of the *C. elegans* DEG/ENaCs generated using MAFFT (Katoh and Standley, 2013, Katoh et al., 2002) confidence in the individual alignment columns was assessed using GUIDANCE2 (Sela et al., 2015), BioNJ (www.phylogeny.fr, (Felsenstein, 1989, Gascuel, 1997, Dereeper et al., 2008, Elias and Lagergren, 2007, Dereeper et al., 2010), see Methods) was used for tree generation and Figtree 1.4.4 Software (Rambaut, 2010) for visualisation. The scale bar represents 0.3 genetic distance in substitutions per nucleotide. (B) Sequence Similarity Network (SSN) visualized and analysed in Cytoscape12 (cytoscape.org/) using a force-directed layout (Shannon et al., 2003). The SSN was generated using the web tool for generating sequence similarity networks (SSNs) for protein families (EFI-EST) developed by the Enzyme Function Initiative (EFI; accessed at efi.igb.illinois.edu/) (Zallot et al., 2019). Each *C. elegans* DEG/ENaC represents a node (circle), two nodes are connected by a line ('edge') if they share pairwise sequence similarity that exceeds the 30% threshold. Within each cluster the sequences show high similarity and the lengths of connecting edges correlate with the relative dissimilarities of each pair. Relative positioning of disconnected clusters and nodes has no meaning. Accession numbers are listed in the Appendix C 3. 5. 2.

3. 2. 2. Expression pattern of *C. elegans* DEG/ENaCs *in vivo*

While many members of the family have had some level of expression analysis, I set out to perform a comprehensive characterisation of expression pattern of all family members. I used transcriptional reporters of the *C. elegans* DEG/ENaCs. I generated the plasmids for the *acd-5, asic-1, acd-4* and *delm-1* reporters, the *asic-2* reporter was generated by Dr Laura Grundy (Grundy, 2018) and the rest were a kind gift from Professor Kyuhyung Kim's lab (Daegu Gyeongbuk Institute of Science & Technology, Korea). In order to generate transgenic lines, the plasmids were injected into wild-type worms.

I grouped the expression patterns into the clusters generated by the SSN above. For the ASIC-1 group, I found *del-4* expression in anterior neurons in the head region in addition to known IL2 and *asic-1* expression in FLP and ventral cord neurons (Figure 9) in addition to ADE, CEP, PVQ, PDE and PVD that had previously been described (Voglis and Tavernarakis, 2008, Husson et al., 2012, De Stasio et al., 2018). I also confirmed *asic-2* expression pattern in the six IL2 neurons (Wang et al., 2015, Grundy, 2018). Taking together evidence from current and previous expression patterns most members of this group are expressed in neuronal tissue.

For the ACD-1 group shown in Figure 10, my data showed expression of *delm-2* in neurons in the head and in the tail as yet to be identified, in addition to the previous expression in glia (Han et al., 2013). *acd-4* is expressed in anterior neurons in the head as well as in the pharyngeal-intestinal valve and the intestinal-rectal valve. *acd-5* is strongly expressed in the intestine. And finally, the *acd*-2 transcriptional reporter shows faint expression in anterior neurons or glia in the head. For the ACD-1 group, a common trend might be that this subgroup that many of them are expressed in non-neuronal tissue.

The smallest cluster consisting of the EGAS-genes, EGAS-1 has previously been reported to be expressed in IL2 quadrant neurons (Wang et al., 2015) which is consistent with my reporter lines. Transcriptional reporters for *egas-2* and *egas-4* also show expression in neurons in the head which are likely to be IL2 neurons (Figure 11), while *egas-3* shows expression in anterior neurons in the head, hypodermal cells in the tail as well as seam cells (Figure 11).

Finally, there are the miscellaneous members that could not be clustered with other subunits in the SSN. However, in the phylogram shown in section 3. 2. 1. Exploration of the *C. elegans* DEG/ENaC protein sequences, ACD-5 and particularly FLR-1 closely cluster with ACD-3 and DEL-5 which are all expressed in the intestine (Figure 12 and (Take-Uchi et al., 1998)). Based on their expression pattern, these four DEG/ENaCs make good candidates for forming a heteromeric channel together, this possibility will be explored in CHAPTER 5. Other miscellaneous members include DEGT-1, DEL-2, DEL-3, DEL-6, DEL-7, DEL-9 and DEL-10. My expression data showed that *del-2* is expressed in head and tail neurons or glia, *del-9* is expressed in anterior and posterior body wall muscles, vulva muscles as well as head and tail neurons, and *del-10* shows strong expression in body-wall muscles (Figure 12). Expression patterns are summarised in the figures below and a final summary combining my data with previous characterisation and single-cell RNA sequencing data (CenGen.org) can be found in Figure 13 and Table 3.

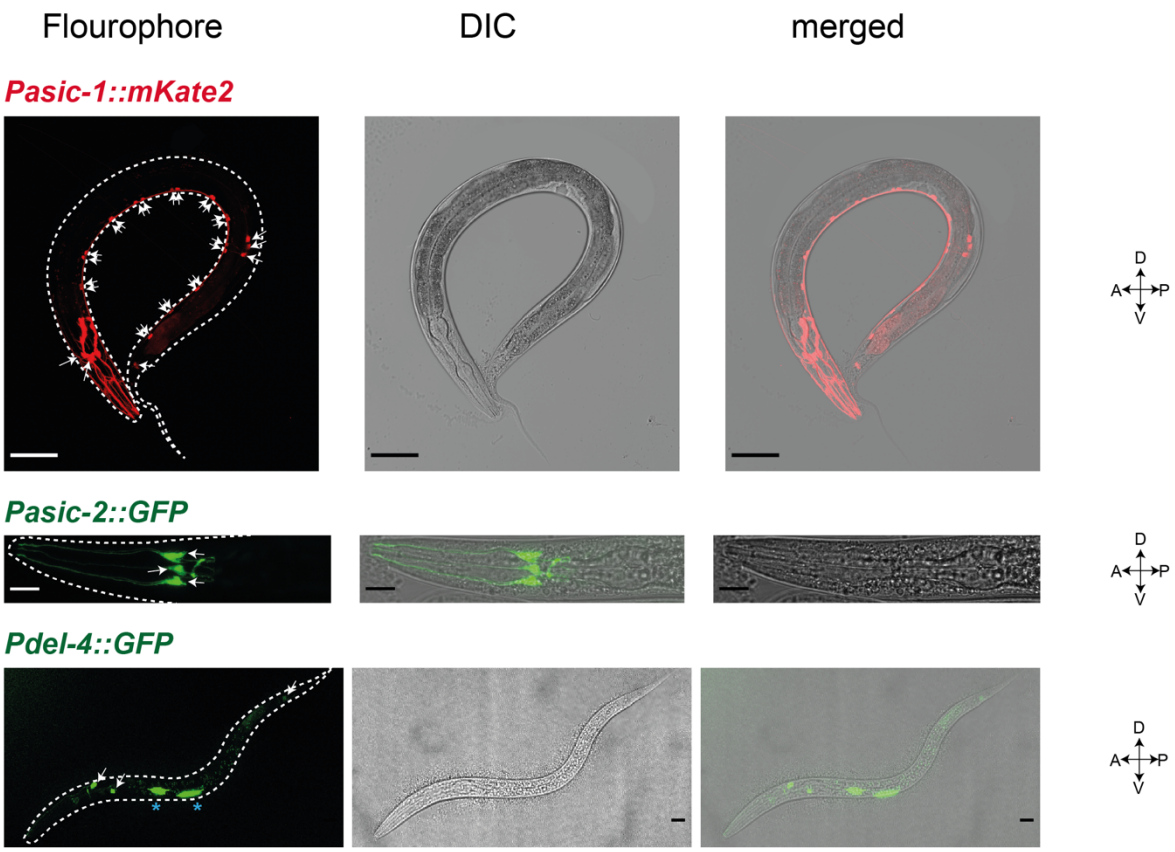

Figure 9: Expression pattern of the ASIC-1 group of C. elegans DEG/ENaCs.

Transgenic animals expressing the respective transcriptional reporters. Potential neurons or cluster of neurons are marked by a white arrow and non-neuronal tissues are marked by a yellow arrow. The blue asterisk marks the coelomocytes (*Punc-122::GFP*) which are used as co-injection marker. *ljEx1448* [*Pasic-1::mKate2] (*ADE, CEP, PVQ, PDE, PVD, FLP, ventral cord)*, ljEx[Pasic-2::GFP] (IL2)* and *ljEx1357* [*Pdel-4::GFP] (neurons in the head)*. Scale bars are 10 µm.

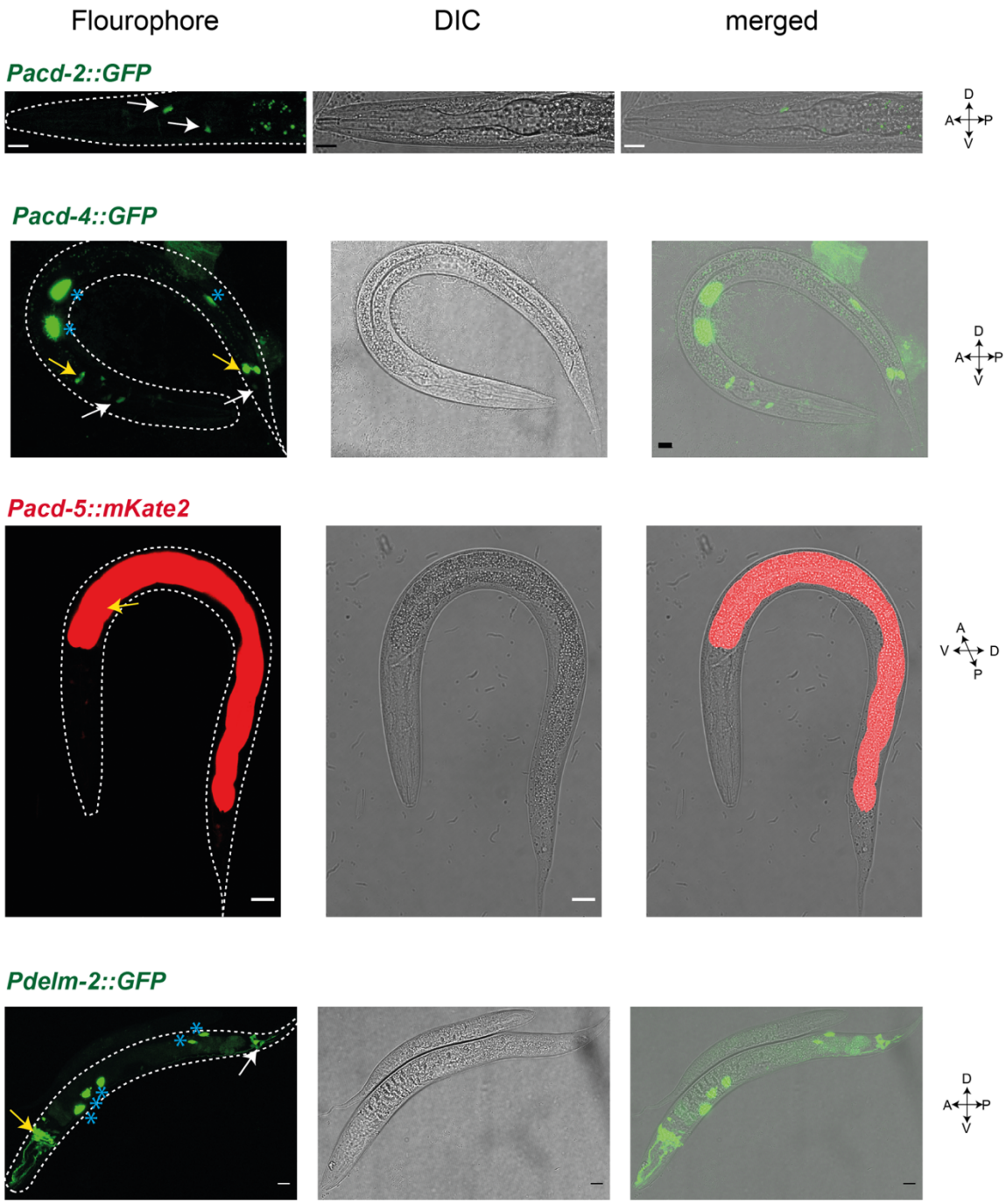

Figure 10: Expression pattern of the ACD-1 group of C. elegans DEG/ENaCs.

Transgenic animals expressing the respective transcriptional reporters. Potential neurons or cluster of neurons are marked by a white arrow and non-neuronal tissues are marked by a yellow arrow. The blue asterisk marks the coelomocytes (*Punc-122::GFP*) which are used as co-injection marker. *ljEx1344[Pacd-2::GFP] (weak expression in neurons in the head), ljEx1386[Pacd-4::GFP]* (neurons in the head, pharyngeal-intestinal valve, intestinal-rectal valve), *ljEx1225[Pacd-5::mKate2] (strongly expressed in the intestine*) and *ljEx1347[Pdelm-2::GFP] (head and tail neurons and glia).* Scale bars are 10 µm.

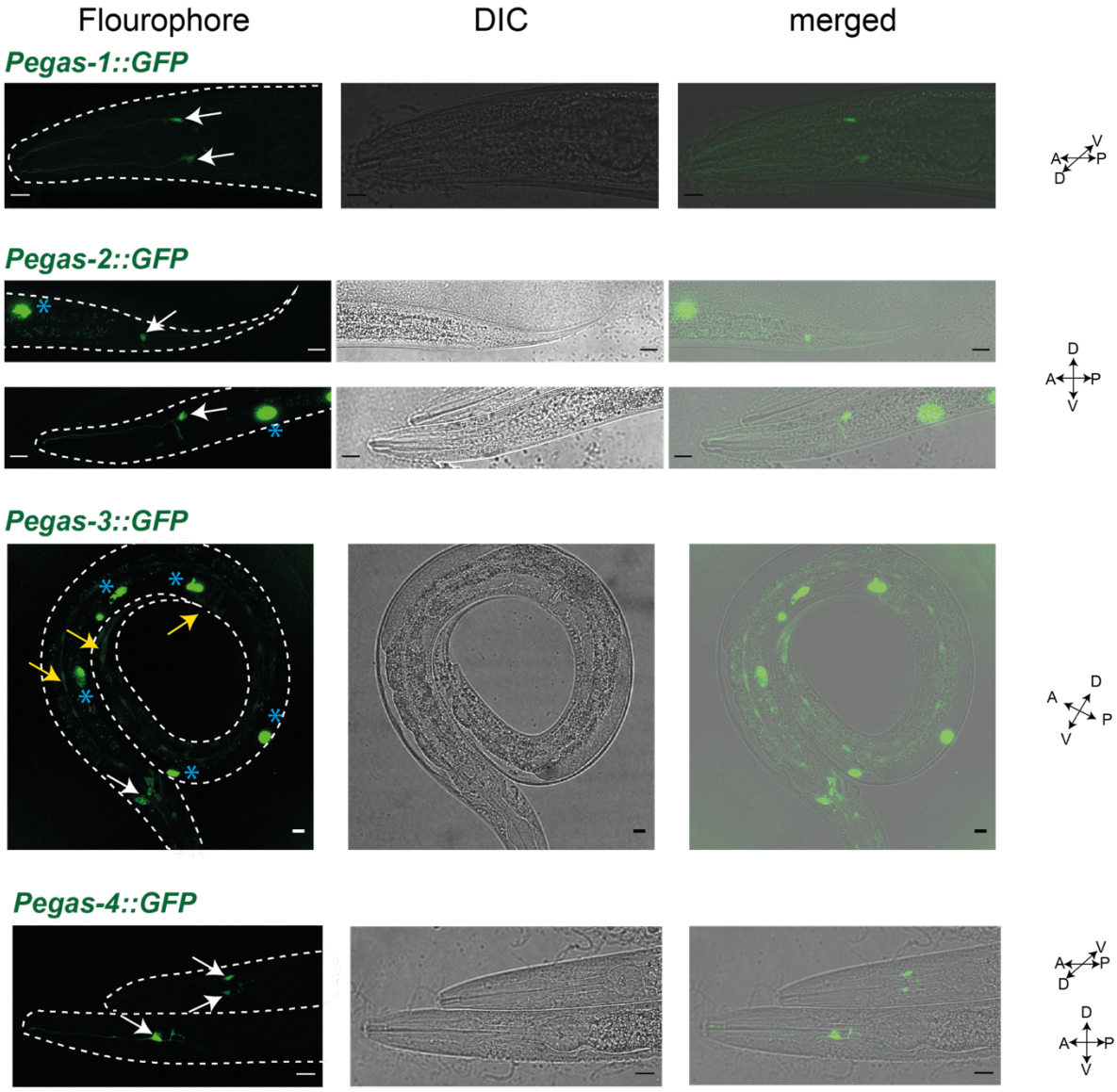

Figure 11: Expression pattern of the EGAS group of C. elegans DEG/ENaCs.

Transgenic animals expressing the respective transcriptional reporters. Potential neurons or cluster of neurons are marked by a white arrow and non-neuronal tissues are marked by a yellow arrow. The blue asterisk marks the coelomocytes (*Punc-122::GFP*) which are used as co-injection marker. *ljEx1363[Pegas-1::GFP] (IL2), ljEx1364[Pegas-2::GFP] (IL2, head/anterior neurons, tail neurons), ljEx1368[Pegas-3::GFP] (IL2, anterior/head neurons, hypodermal cells in the tail, seam cells)* and *ljEx1369[Pegas-4::GFP] (IL2).* Scale bars are 10 µm.

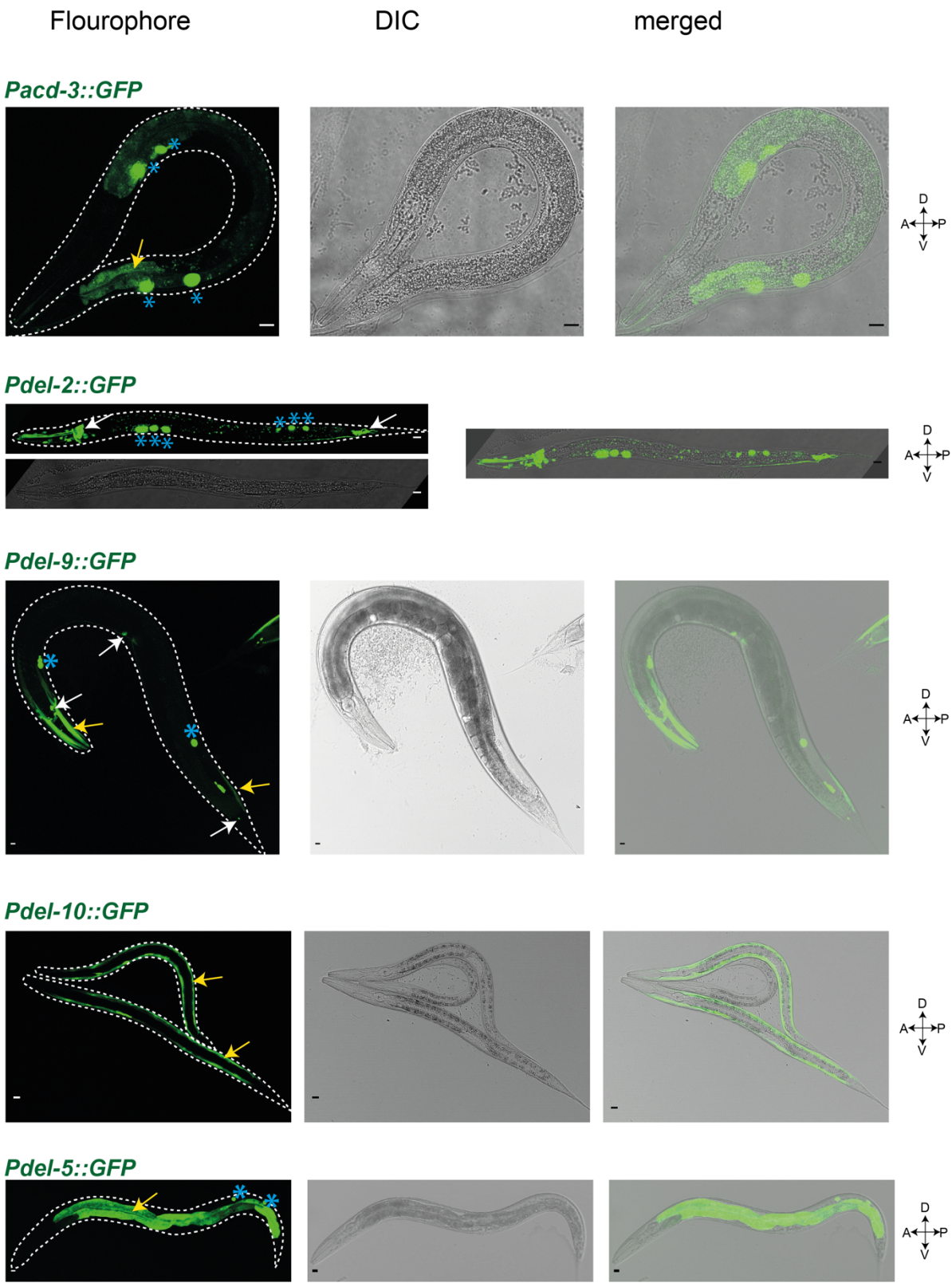

Figure 12: Expression pattern of the miscellaneous members of C. elegans DEG/ENaCs.

Transgenic animals expressing the respective transcriptional reporters. Potential neurons or cluster of neurons are marked by a white arrow and non-neuronal tissues are marked by a yellow

arrow. The blue asterisk marks the coelomocytes (*Punc-122::GFP*) which are used as co-injection marker. *ljEx1345[Pacd-3::GFP] (intestine), ljEx1352[Pdel-2::GFP] (*neurons or glia (head/tail, anterior/posterior)*, ljEx1361[Pdel-9::GFP] (head- and tail- body wall muscles, vulva muscles head and tail neurons)*, *ljEx1362[Pdel-10::GFP] (body-wall muscles)* and *ljEx1349[Pdel-5::GFP] (intestine)*. Scale bars are 10 µm.

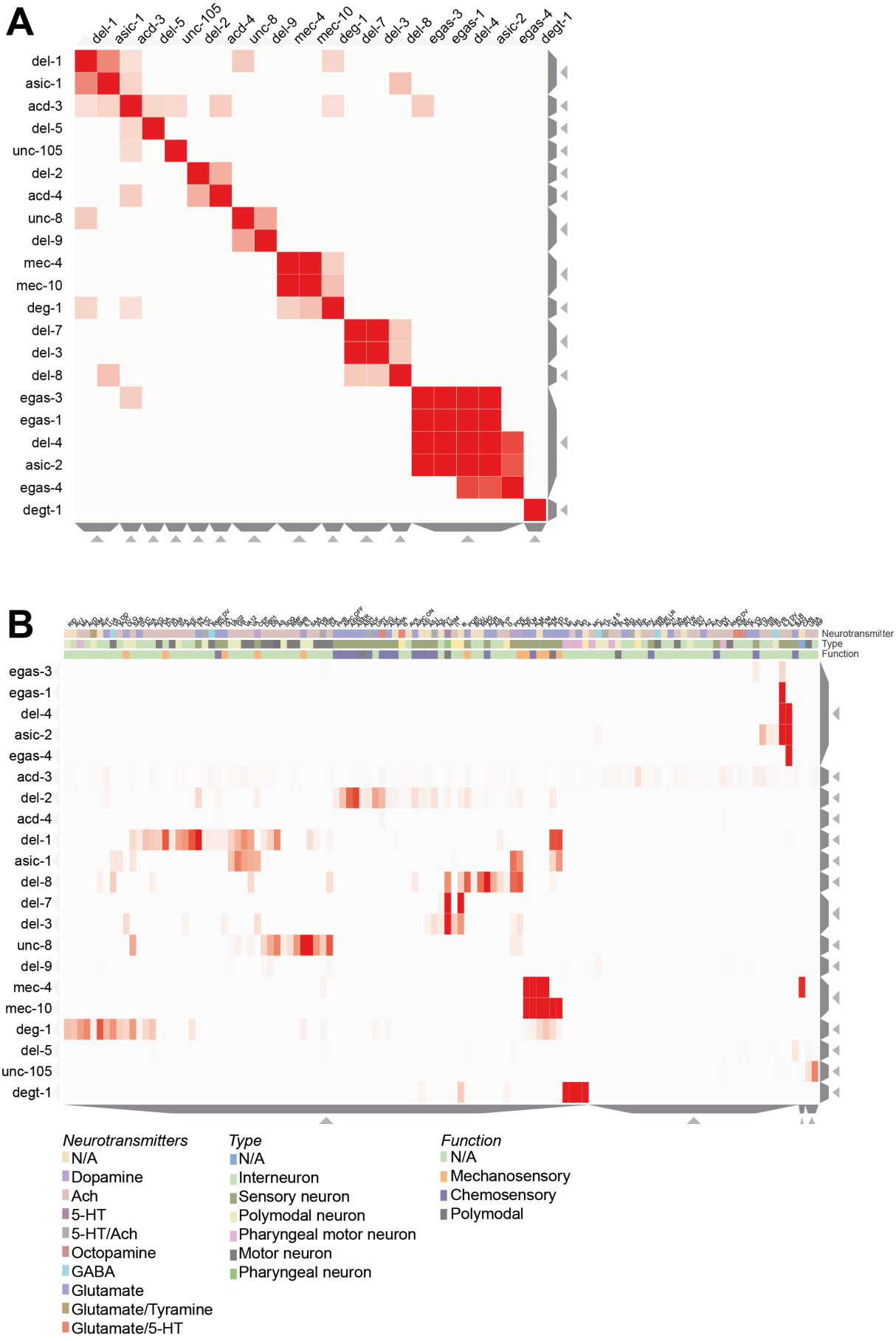
A
del-1
asic-1
acd-3
del-5
unc-105
del-2
acd-4
unc-8
del-9
mec-4
mec-10
deg-1
del-7
del-3
del-8
egas-3
egas-1
del-4
asic-2
egas-4
degt-1
B
Neurotransmitter
Type
Function
Neurotransmitters
N/A
Dopamine
Ach
5-HT
5-HT/Ach
Octopamine
GABA
Glutamate
Glutamate/Tyramine
Glutamate/5-HT
Type
N/A
Interneuron
Sensory neuron
Polymodal neuron
Pharyngeal motor neuron
Motor neuron
Pharyngeal neuron
Function
N/A
Mechanosensory
Chemosensory
Polymodal

Figure 13: Co-expression of C. elegans DEG/ENaCs using the CenGen.org single cell RNA sequencing expression dataset (threshold 2).

(A) Similarity matrix of the co-expression for DEG/ENaC from the single neuron RNA sequencing data (from Cengen.org). The cells in the matrix represent the similarity between genes, where red represent positive similarity (measured as 1 - cosine-distance). Poential clusers are indicated by the grey shadows. (B) Clustergram/heatmap visualization of neuronal expression data matrix. The rows and columns have been hierarchically clustered, using the Scipy library in Python, using cosine distance and average linkage. Red cells in the matrix represent positive values in the matrix. N/A meaning that to my knowledge this has not been investigated. Both panels were created using the Clustergrammer web tool developed by the Ma'ayan lab (Fernandez et al., 2017). The visualization interactive (zoomable, reorderable, filterable) can be found under the following link: maayanlab.cloud/clustergrammer/viz_sim_mats/60b39933fe6520000e1de1f9/20210530_new.tsv

3. 2. 3. Identification of *C. elegans* acid-sensing DEG/ENaCs

Unlike what has been shown for the mammalian ASICs which are activated in response to a drop in pH, *C. elegans* proton-sensitive subunits expressed *in vitro* in X*enopus* oocytes have shown to be constitutively active at neutral pH and inhibited by low pH (Wang et al., 2008). For mutant subunits there is some limited evidence for current potentiation as a consequence of a drop in pH (see section 3. 1. 3. 1. above). However, currently it is unknown if wild-type *C. elegans* DEG/ENaC family members can display acid-evoked currents similar to mammalian homologues.

In order to systematically test this, I performed a screen using TEVC and perfused *Xenopus* oocytes injected with cRNA from 25 *C. elegans* DEG/ENaCs with solutions of different pH. I suggested above that there are two groups of acid-sensing ion channels based on their response to low pH when heterologously expressed *in vitro*. Here I found more channels belong to each of the two groups: ASIC-1, ACD-2 and DEL-9 which can be (further) opened in response to decreasing pH (Figure 14), and ACD-5 and DEL-4 subunits that can form homomeric channels that are open at neutral pH and are inhibited by low pH (Figure 15). Candidates of both groups will be followed up in detail in CHAPTER 4 and CHAPTER 5, respectively. DEL-10, DEGT-1 and DEG-1 which showed very variable responses to low pH which might be due to difficulty in expressing them *in vitro*. DEL-10 might belong to the second group that can be inhibited by low pH (see trace Figure 15), and DEGT-1 and DEG-1 occasionally showed increased currents at pH 4 which suggests that it could belong to the first group that can be activated by low pH (see traces Figure 14). Finally, there were 17

remaining candidates that were insensitive to pH 4 (Figure 16). The summary of oocytes injected with each construct in Table 2 and Figure 17 showed that while some oocytes are insensitive to pH, they display larger inward currents at neutral and low pH compared to the water controls. These include ACD-3, DEL-7 and FLR-1. By contrast, the remaining ones did not differ from the control (Figure 16). This could have multiple reasons which will be addressed in the in the discussion section (3. 3.) below. Colour coding based on clusters identified previously, clearly illustrates that proton-sensitivity is not confined to one cluster.

Previous research has described and successfully predicted proton binding sites in the rat ASIC1a (Shaikh and Tajkhorshid, 2008, Paukert et al., 2008, Li et al., 2009, Grunder and Chen, 2010). In order to look for potentially conserved sites between the well-characterised rASIC1a and the here described proton-sensitive *C. elegans* DEG/ENaCs, I compared sequence similarity and identity using a local alignment (Appendix C, 3. 5. 3. below). However, the individual amino-acids did not seem to correlate with pH sensing between rASIC1a and the proton-sensitive *C. elegans* DEG/ENaCs and hence it is difficult to draw any conclusion about function from the amino acid sequences. Nevertheless, I have demonstrated for the first time that there are *C. elegans* acid-sensing ion channels that can be activated by low pH similar to their vertebrate homologues.

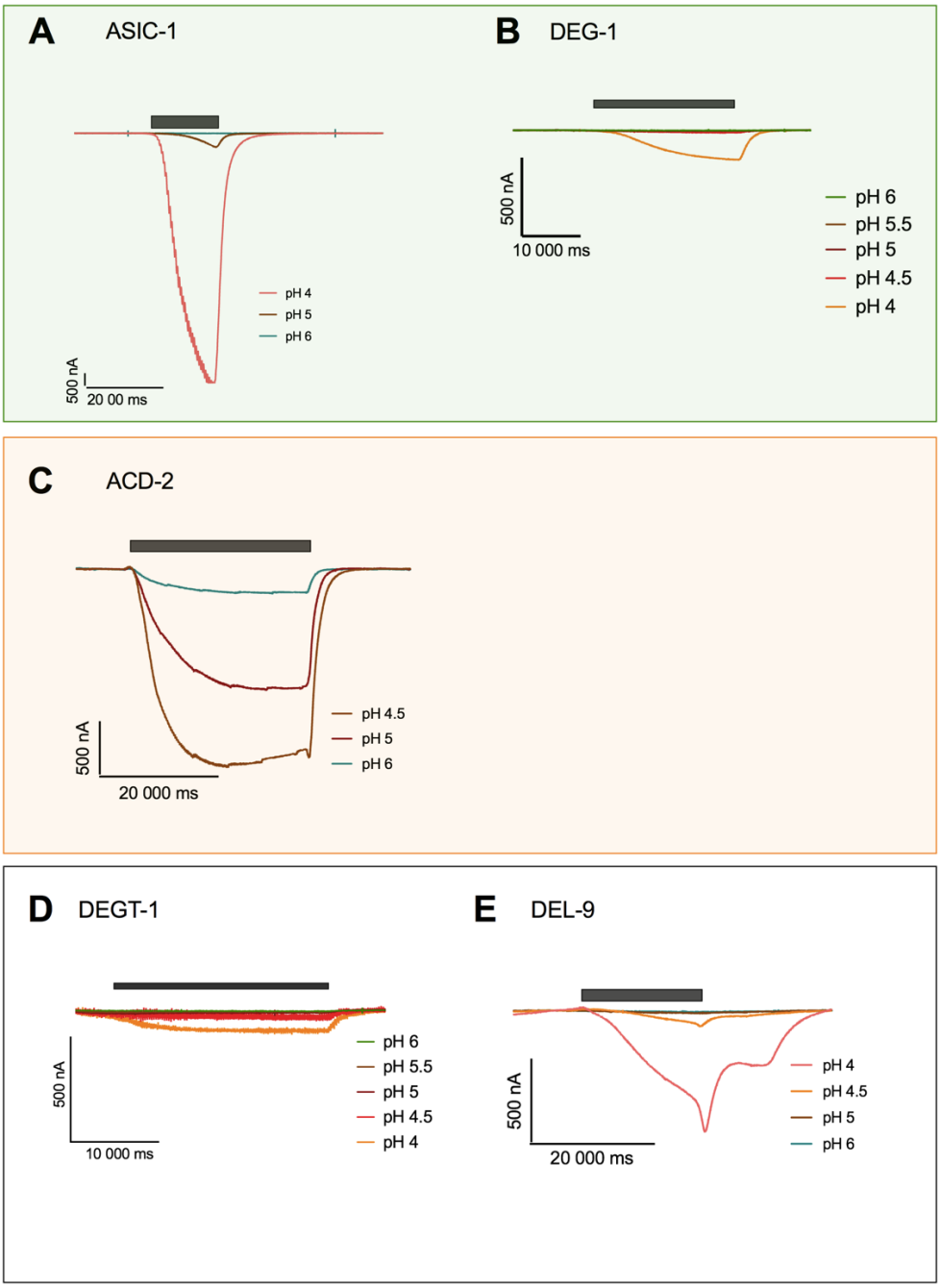

Figure 14: Raw representative traces from the initial screen for pH-activated C. elegans DEG/ENaCs.

Shown are raw representative traces of *Xenopus* oocytes expressing the *C. elegans* DEG/ENaC (A) ASIC-1; (B) DEG-1, (C) ACD-2, (D) DEGT-1 (E) DEL-9, perfused with low pH as indicated and colour coded. The grey bar above the traces indicates the length of the perfusion with the indicated pH solution when switched from the basal solution (ND96) of pH 7.4. Scale bars are indicated: actual current in nA (y-axis) and time in ms (x-axis). The background of the panel indicates which group it belongs to (ASIC-1 group (green); ACD-1 group (orange) or miscellaneous (black)). For representation, the currents were baseline subtracted and drift correction was applied in the Roboocyte2+ software.

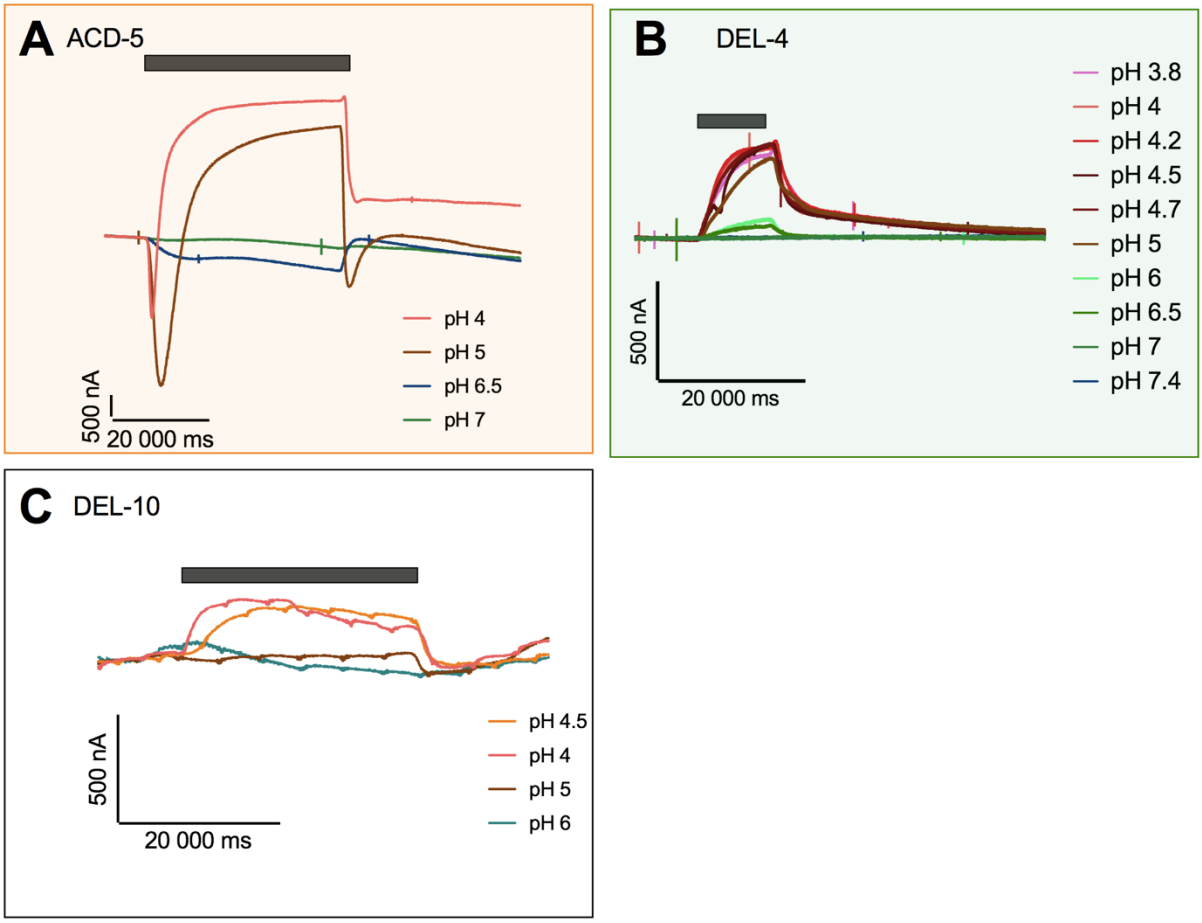

Figure 15: Raw representative traces from the initial screen for pH-inhibited C. elegans DEG/ENaCs.

Shown are raw representative traces of *Xenopus* oocytes expressing the *C. elegans* DEG/ENaC (A) ACD-5; (B) DEL-4 and (C) DEL-10, perfused with low pH as indicated and colour coded. The grey bar above the traces indicates the length of the perfusion with the indicated pH solution when switched from the basal solution (ND96) of pH 7.4. Scale bars are indicated: actual current in nA (y-axis) and time in ms (x-axis). The background of the panel indicates which group it belongs to (ASIC-1 group (green); ACD-1 group (orange) or miscellaneous (black)). For representation, the currents were baseline subtracted and drift correction was applied in the Roboocyte2+ software.

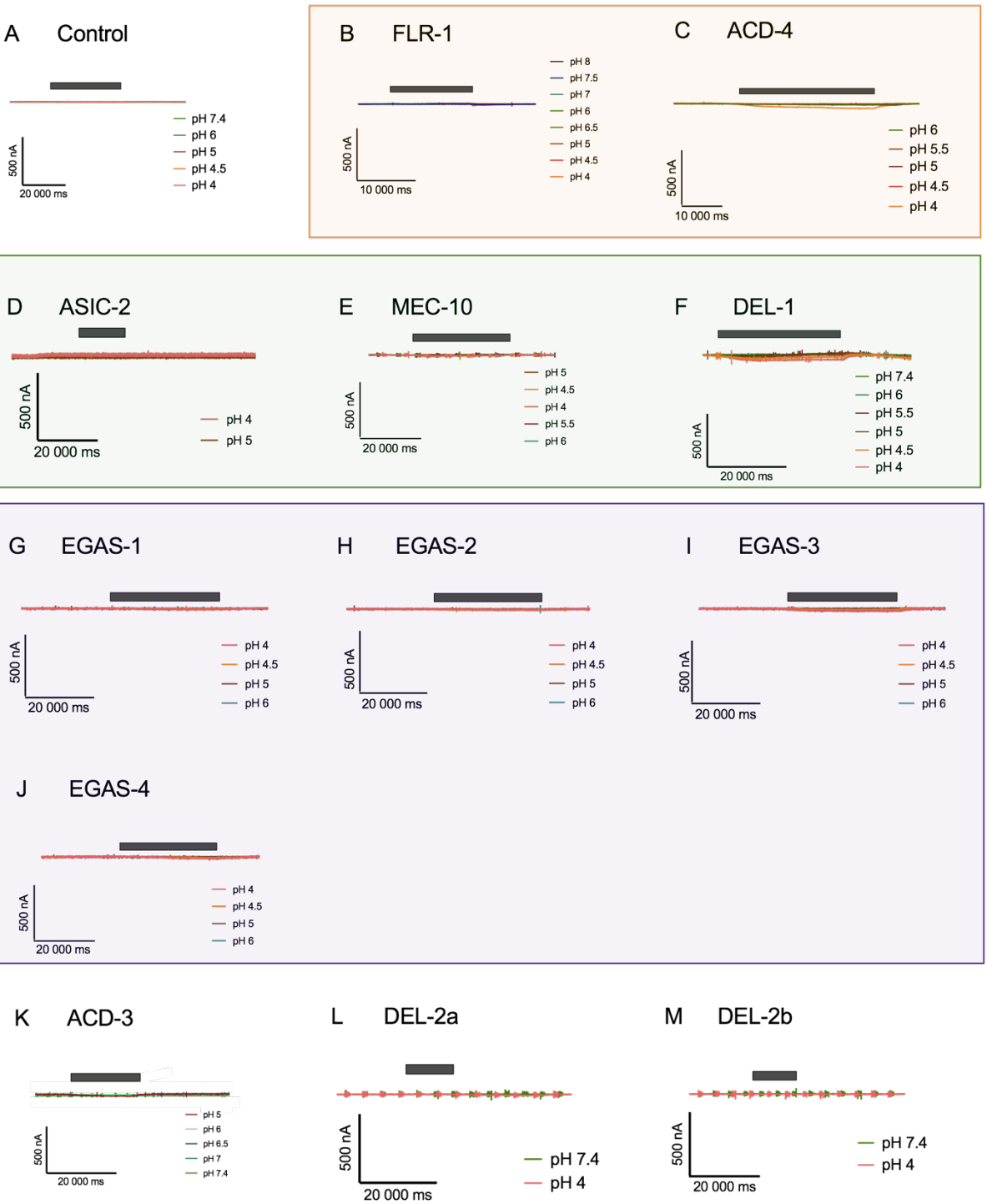
A Control
pH 7.4
pH 6
pH 5
pH 4.5
pH 4
500 nA
20 000 ms
B FLR-1
pH 8
pH 7.5
pH 7
pH 6
pH 6.5
pH 5
pH 4.5
pH 4
500 nA
10 000 ms
C ACD-4
pH 6
pH 5.5
pH 5
pH 4.5
pH 4
500 nA
10 000 ms
D ASIC-2
pH 4
pH 5
500 nA
20 000 ms
E MEC-10
pH 5
pH 4.5
pH 4
pH 5.5
pH 6
500 nA
20 000 ms
F DEL-1
pH 7.4
pH 6
pH 5.5
pH 5
pH 4.5
pH 4
500 nA
20 000 ms
G EGAS-1
pH 4
pH 4.5
pH 5
pH 6
500 nA
20 000 ms
H EGAS-2
pH 4
pH 4.5
pH 5
pH 6
500 nA
20 000 ms
I EGAS-3
pH 4
pH 4.5
pH 5
pH 6
500 nA
20 000 ms
J EGAS-4
pH 4
pH 4.5
pH 5
pH 6
500 nA
20 000 ms
K ACD-3
pH 5
pH 6
pH 6.5
pH 7
pH 7.4
500 nA
20 000 ms
L DEL-2a
pH 7.4
pH 4
500 nA
20 000 ms
M DEL-2b
pH 7.4
pH 4
500 nA
20 000 ms

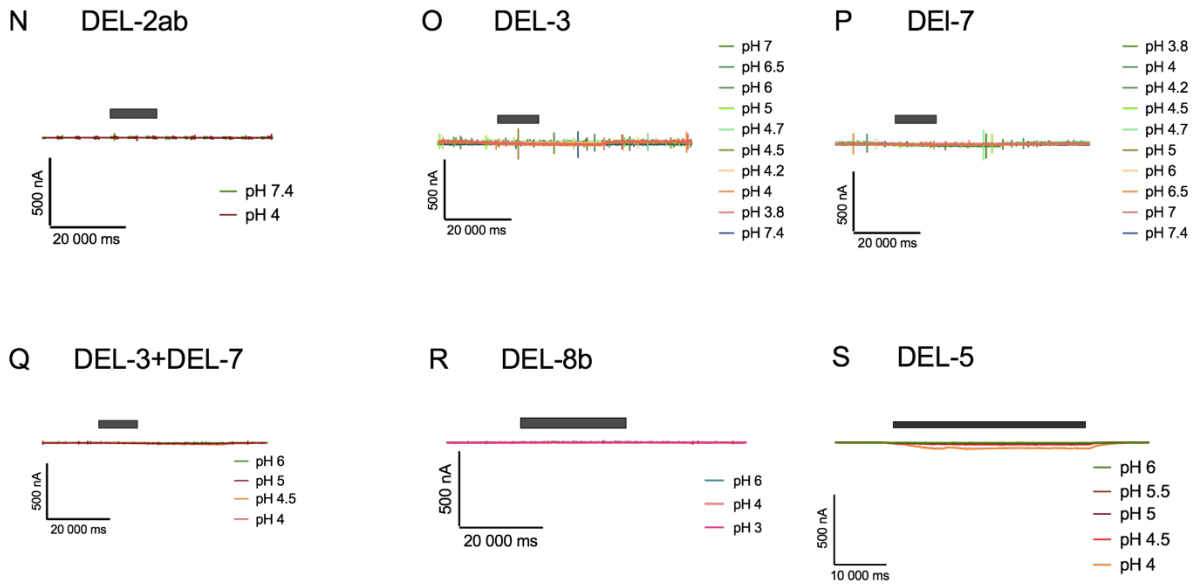

Figure 16: Raw representative traces from the initial screen for pH-insensitive C. elegans DEG/ENaCs.

(A)-(S) Shown are raw representative traces of *Xenopus* oocytes expressing the *C. elegans* DEG/ENaC perfused with low pH as indicated and colour coded. The grey bar above the traces indicates the length of the perfusion with the indicated pH solution when switched from the basal solution (ND96) of pH 7.4. Scale bars are indicated: actual current in nA (y-axis) and time in ms (x-axis). The background of the panel indicates which group it belongs to (ASIC-1 group (green); ACD-1 group (orange) or miscellaneous (black)). For representation, the currents were baseline subtracted and drift correction was applied in the Roboocyte2+ software.

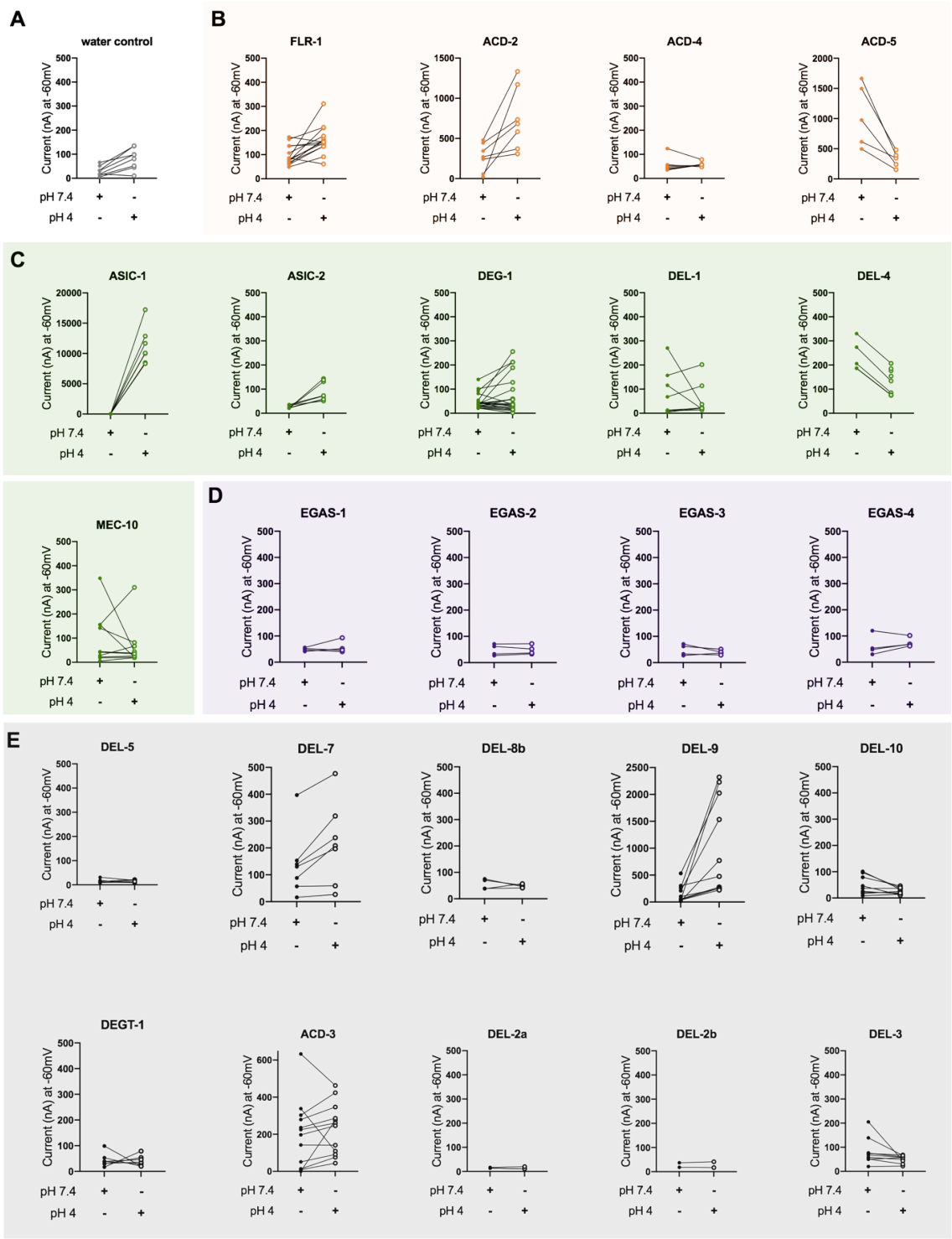

Figure 17: Quantification of current at pH 7.4 and pH 4.

(A) Nuclease-water injected control oocytes. Individual before-after lines connect data from each oocyte. Colours represent belonging to the following groups (B) ACD-1 group (orange), (C) ASIC-1 group (green); (D) EGAS group (purple) and (E) miscellaneous members (grey). Axis labels: y= actual current in nA; x = perfusion with either pH 7.4 (closed circle) or pH 4 (open circle) as indicated. Holding potential was -60mV. Number of oocytes screened, Mean ± SEM can be found in Table 2 below.

Table 2: Actual current of C. elegans DEG/ENaCs expressed in Xenopus oocytes.

Number of oocytes screened, Mean ± SEM for the particular construct in Figure 17 above.

Name	**N**	**Mean$_{pH7.4}$ ± SEM (in nA)**	**Mean$_{pH4}$ ± SEM (in nA)**
water control	8	-82 ± 16	-30 ± 7.3
FLR-1	14	-97 ± 11	-160 ± 16
ACD-2	7	-265 ± 67	-740 ± 146
ACD-4	8	-54 ± 10	-58 ± 3.8
ACD-5	5	-1050 ± 232	-323 ± 57
ASIC-1	7	-27 ± 2.5	-11233 ± 1171
ASIC-2	8	-31 ± 4	-91 ± 14
DEL-4	9	-408 ± 72	-130 ± 18
DEG-1	24	-252 ± 154	-250 ± 150
DEL-1	8	-80 ± 34	-56 ± 24
MEC-10	11	-63 ± 25	-160 ± 71
EGAS-1	4*	-49 ± 3.2	-58 ± 12
EGAS-2	4*	-48 ± 11	-49 ± 8.8
EGAS-3	4*	-45 ± 7.4	-39 ± 4.6
EGAS-4	4*	-63 ± 20	-75 ± 9
DEL-2A	3	-15 ± 1	-14 ± 3
DEL-2B	2	-29 ± 12	-28 ± 9.5
DEL-3	10	-82 ± 17	-108 ± 58
DEL-5	6	-16 ± 3.4	-16 ± 2.3
DEL-7	7	-218 ± 58	-140 ± 47
DEL-8B	5	-56 ± 9.9	-48 ± 3.4
DEL-9	10	-159 ± 53	-1037 ± 282
DEL-10	10	-530 ± 482	-360 ± 16
DEGT-1	8	-188 ± 144	-266 ± 225
ACD-3	14	-757 ± 400	-689 ± 238

*EGAS-1-4 subunits were also screened by my Summer student Patrick McCubbin and he found similar results (Data not shown).

3. 2. 4. Amiloride is a pore blocker for both proton-inhibited and proton-activated *C. elegans* DEG/ENaCs

Based on the results from the previous screen and analysis of the data, I picked twelve interesting candidates and performed a second screen using the ten channels that displayed a leak current at neutral pH regardless of whether they were affected by pH or not, with the aim to see whether the leak current could be blocked by amiloride. In addition, I also tested the three candidates that displayed currents at low pH. As introduced in CHAPTER 1, the amiloride block is voltage-dependent as amiloride is binding to the channel pore (Kashlan and Kleyman, 2011). To examine the voltage dependence of amiloride inhibition, I investigated current-voltage (I-V) relationships using voltage ramps between -150 mV and 75 mV in the absence and presence of amiloride (Figure 18). ACD-1 was used as a positive control because it is known from previous research that it can be blocked by amiloride at neutral pH 7.4 (Wang et al., 2008). At neutral pH 7.4 the following constructs could be blocked by amiloride indicative that amiloride binds to the channel pore: ACD-1, ACD-5, DEL-4, DEL-9 and DEL-10, while the following ones were insensitive to amiloride FLR-1, ACD-2, ACD-3 and DEL-7. DEL-5 and DEL-8b transient currents are enhanced in the presence of amiloride. The acid-induced currents of ASIC-1 and ACD-2 could be blocked by amiloride and the acid-evoked currents of DEL-9 were also enhanced in the presence of amiloride (Figure 19). These results show that similar to what has been described for vertebrate ASICs, amiloride can also both block and enhance currents of *C. elegans* DEG/ENaCs at neutral and low pH. The type of response to amiloride is not confined to a particular cluster.

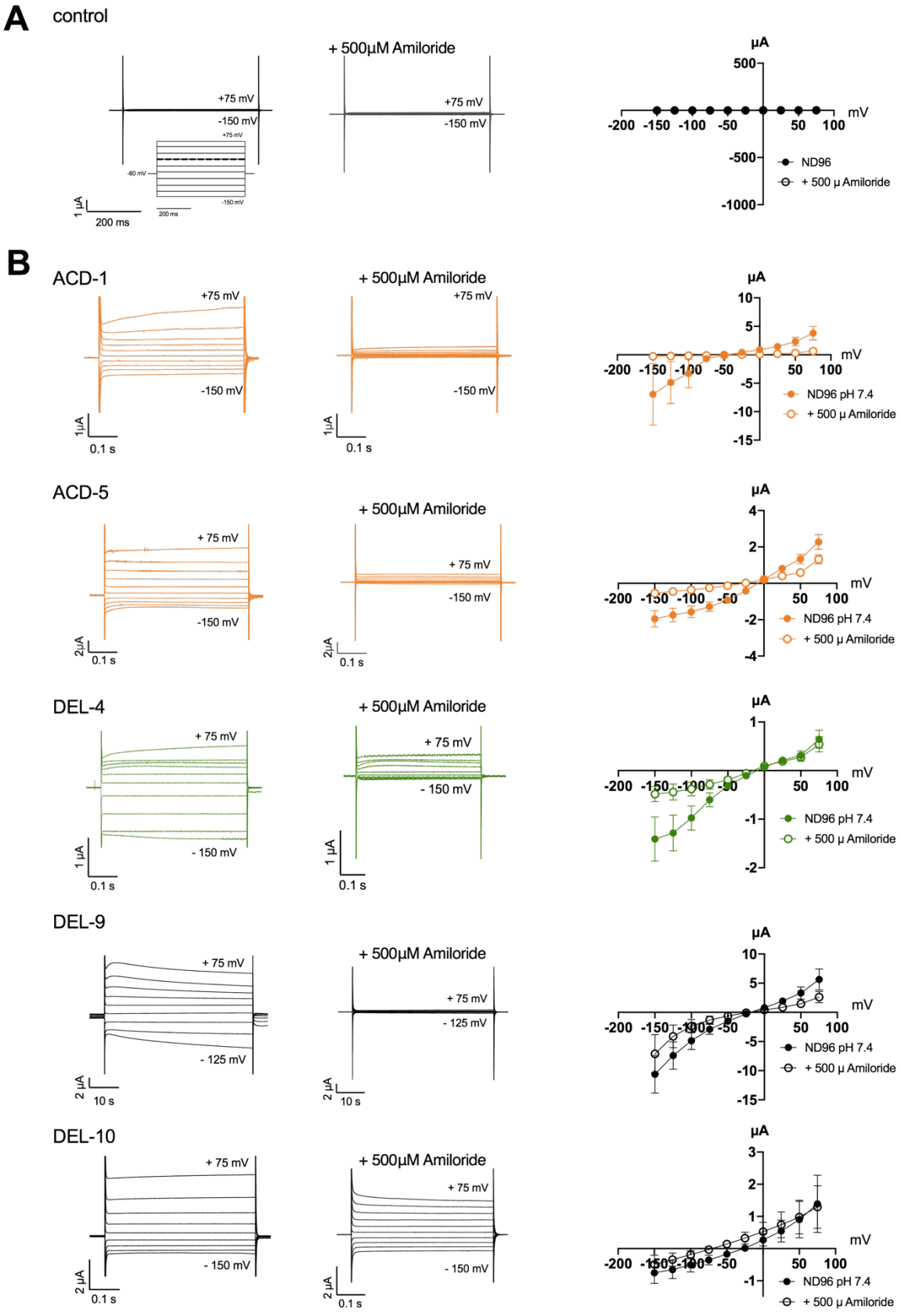
A
control
+75 mV
-150 mV
1 µA
200 ms
+ 500µM Amiloride
+75 mV
-150 mV
µA
500
-500
-1000
mV
-200 -150 -100 -50 50 100
ND96
+ 500 µ Amiloride
B
ACD-1
+75 mV
-150 mV
1µA
0.1 s
+ 500µM Amiloride
+75 mV
-150 mV
1µA
0.1 s
µA
10
5
-5
-10
-15
mV
-200 -150 -100 -50 50 100
ND96 pH 7.4
+ 500 µ Amiloride
ACD-5
+ 75 mV
-150 mV
2µA
0.1 s
+ 500µM Amiloride
+ 75 mV
-150 mV
2µA
0.1 s
µA
4
2
-2
-4
mV
-200 -150 -100 -50 50 100
ND96 pH 7.4
+ 500 µ Amiloride
DEL-4
+ 75 mV
- 150 mV
1 µA
0.1 s
+ 500µM Amiloride
+ 75 mV
- 150 mV
1 µA
0.1 s
µA
1
-1
-2
mV
-200 -150 -100 -50 50 100
ND96 pH 7.4
+ 500 µ Amiloride
DEL-9
+ 75 mV
- 125 mV
2 µA
10 s
+ 500µM Amiloride
+ 75 mV
- 125 mV
2 µA
10 s
µA
10
5
-5
-10
-15
mV
-200 -150 -100 -50 50 100
ND96 pH 7.4
+ 500 µ Amiloride
DEL-10
+ 75 mV
- 150 mV
2 µA
0.1 s
+ 500µM Amiloride
+ 75 mV
- 150 mV
2 µA
0.1 s
µA
3
2
1
-1
mV
-200 -150 -100 -50 50 100
ND96 pH 7.4
+ 500 µ Amiloride

C DEL-5

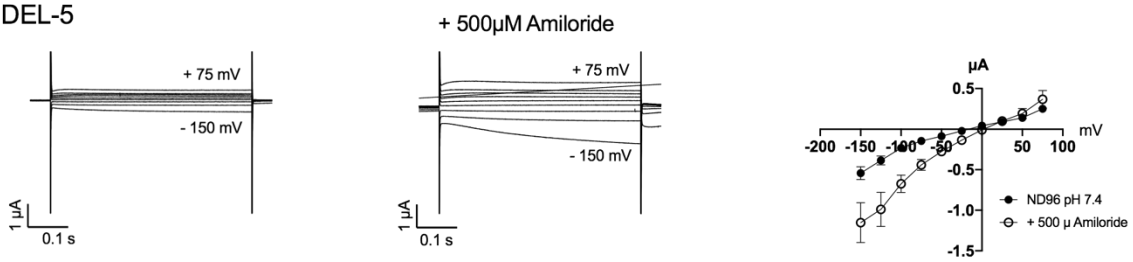

DEL-8B

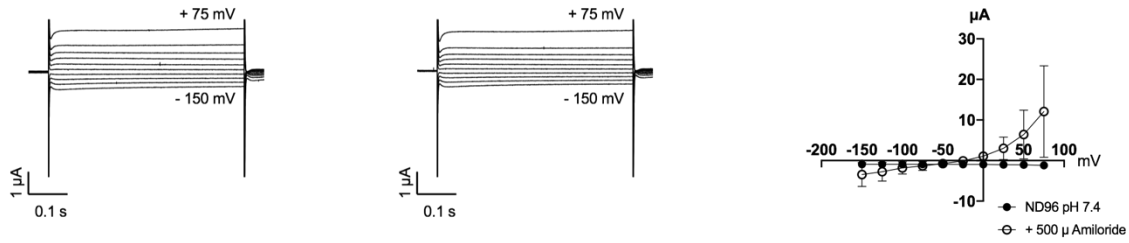

D

FLR-1

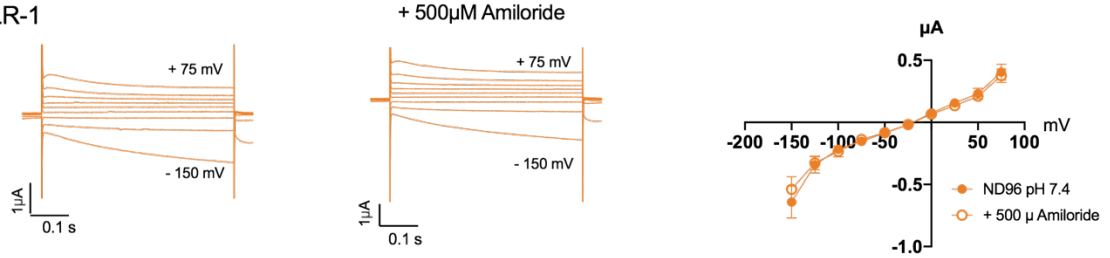

ACD-2

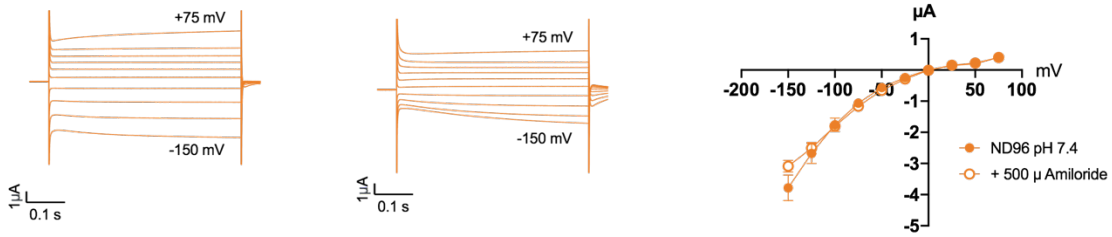

ACD-3

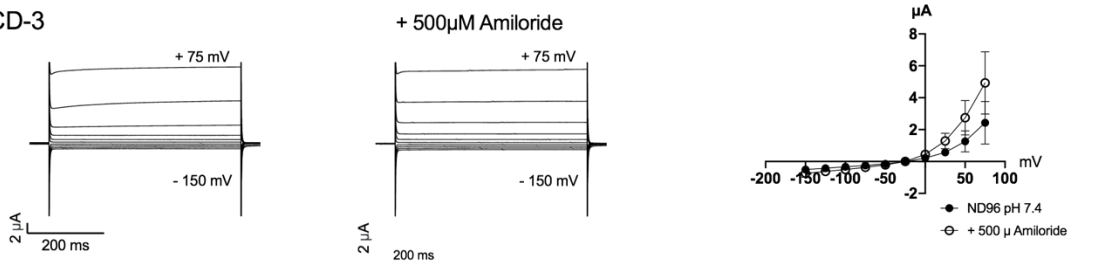

DEI-7

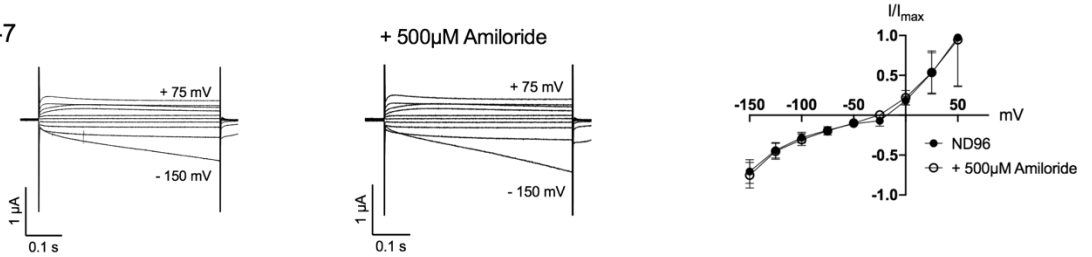

Figure 18: Representative current traces and IV relationships in the absence and presence of 500 µM amiloride at pH 7.4.

Representative transient currents and current–voltage (IV) relationships in the absence (left) and presence of 500 µM amiloride (middle) at pH 7.4. (A) Nuclease-free water-injected oocytes (negative control) are unaffected by amiloride. (B) Amiloride block. ACD-1 (positive control, N=7), ACD-5, DEL-4 (N=10), DEL-9 (N=8) and DEL-10 (N=4) transient currents can be blocked by amiloride. (C) Amiloride current-potentiation. DEL-5 (N=6) and DEL-8b (N=3) transient currents are enhanced in the presence of amiloride. (D) Amiloride insensitive. FLR-1 (N=15), ACD-2 (N=4), ACD-3 (N=10) and DEL-7 (N=8) transient currents are insensitive to amiloride as currents cannot be blocked. *Xenopus* oocytes are perfused with a basal solution (ND96) only (filled circles), and in presence of the DEG/ENaC channel blocker amiloride (open circles). The oocyte membrane was clamped at −60 mV and voltage steps from -150 mV to +75 mV were applied as indicated. Currents are actual currents in µA (y-axis), voltage steps in mV (x-axis) as indicated. Error bars represent Mean ± SEM.

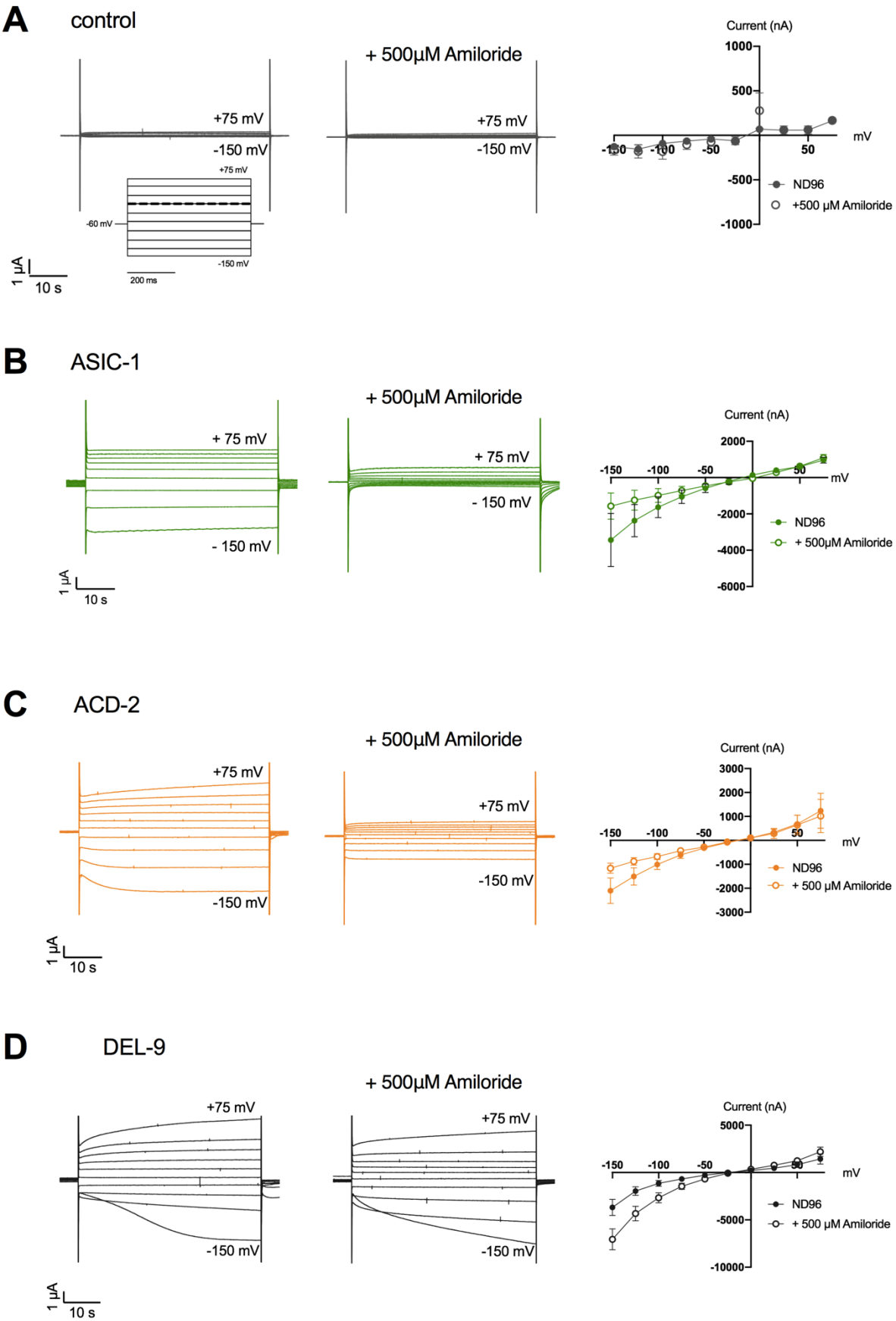
A
control
+75 mV
-150 mV
+75 mV
-60 mV
-150 mV
200 ms
1 µA
10 s
+ 500µM Amiloride
+75 mV
-150 mV
Current (nA)
1000
500
-500
-1000
-150
-100
-50
50
mV
ND96
+500 µM Amiloride
B
ASIC-1
+ 75 mV
- 150 mV
1 µA
10 s
+ 500µM Amiloride
+ 75 mV
- 150 mV
Current (nA)
2000
-2000
-4000
-6000
-150
-100
-50
50
mV
ND96
+ 500µM Amiloride
C
ACD-2
+75 mV
-150 mV
1 µA
10 s
+ 500µM Amiloride
+75 mV
-150 mV
Current (nA)
3000
2000
1000
-1000
-2000
-3000
-150
-100
-50
50
mV
ND96
+ 500 µM Amiloride
D
DEL-9
+75 mV
-150 mV
1 µA
10 s
+ 500µM Amiloride
+75 mV
-150 mV
Current (nA)
5000
-5000
-10000
-150
-100
-50
50
mV
ND96
+ 500 µM Amiloride

Figure 19: Representative current traces and IV relationships in the absence and presence of 500 µM amiloride at low pH.

Representative acid-evoked transient currents and current–voltage (IV) relationships in the absence (left) and presence of 500 µM amiloride (middle) at pH_{50}. (A) Nuclease-free water-injected oocytes (negative control) are unaffected by amiloride or low pH. (B) ASCI-1 (N=6) and (C) ACD-2 (N=11) pH_{50}-evoked transient currents can be blocked by amiloride (for pH_{50} of each channel see CHAPTER 4, Figure 20). (D) DEL-9 (N=10) transient currents are enhanced in the presence of amiloride. *Xenopus* oocytes are perfused with a basal solution (ND96) only (black circles), and in presence of the DEG/ENaC channel blocker amiloride (open circles). The oocyte membrane was clamped at −60 mV and voltage steps from -150 mV to +75 mV were applied as indicated. Currents are actual currents in nA (y-axis), voltage steps in mV (x-axis) as indicated. Error bars represent Mean ± SEM.

3. 3. Discussion

Based on analysis of phylogeny and sequence similarity, I identified three clusters within the *C. elegans* DEG/ENaC family. The ASIC-1 group (ASIC-1, ASIC-2, DEG-1, DEL-1, DEL-4, MEC-4, MEC-10 and UNC-105), ACD-1 group (ACD-1, ACD-2, ACD-4, ACD-5, DELM-1, DELM-2 and FLR-1), and the EGAS group (EGAS-1, EGAS-2, EGAS-3 and EGAS-4). Based on the evidence presented here, it is most likely that these clusters correlate with expression patterns of the respective proteins. For instance, I and others have found that members of the ASIC-1 group and EGAS-group are almost exclusively expressed in neurons (Voglis and Tavernarakis, 2008, Wang et al., 2015, Geffeney et al., 2011, Tao et al., 2019, Driscoll and Chalfie, 1991). By contrast, my expression analysis and that of others found that members of the ACD-1 group are largely expressed in non-neuronal tissue (Wang et al., 2008, Han et al., 2013). One limitation of the current characterisation is that both the single-cell RNA sequencing data (from CenGen.org) as well as my reporter strains were imaged at late L4/young adult stages in development, however, some *C. elegans* DEG/ENaCs are more highly expressed in larvae compared to adults (personal observation and for *del-4* (De Stasio et al., 2018)). Cellular location and timing of DEG/ENaC expression during development might be a point for further investigation to fully understand the function of these channels and their impact on behaviour.

I have presented the results from two electrophysiological screens using TEVC in *Xenopus* oocytes, screening 25 previously uncharacterised *C. elegans* DEG/ENaCs for proton-sensitivity. I found five acid-sensing DEG/ENaC that can be split into two

groups based on their acid-sensing properties *in vitro* in *Xenopus* oocytes. I showed that one group consists of ACD-5 and DEL-4 in addition to the previously described *C. elegans* ACD-1 (Wang et al., 2008). These channels are constitutively open at neutral pH and inhibited by low pH. There is one additional candidate that showed a large variability in expression but is likely to belong to the first group, this is DEL-10. I have also for the first time described a group of *C. elegans* acid-sensing DEG/ENaCs, ASIC-1, ACD-2 and DEL-9, which show increasing inward currents in response to increasing concentrations of protons. Two additional candidates, DEGT-1 and DEG-1, are likely to belong to this group despite displaying smaller response to low pH. A possible explanation for the variability for DEGT-1, DEG-1 or DEL-10 above could be poor trafficking, low level of translocation to the membrane or inability to form fully functional homomeric channels *in vitro*. Consequently, further optimisation and experiments are needed to confirm their properties. I have also demonstrated that neither proton-sensitivity nor type of proton-sensitivity is confined to one particular cluster based on phylogeny or SSN.

As mentioned above, the pore-blocker amiloride has been a useful pharmacological tool to investigate channel functioning. I tested amiloride-sensitivity of selected candidates identified in the first screen and I found that at neutral pH, ACD-5, DEL-4, DEL-9 and DEL-10 currents can be inhibited by amiloride. Acid-evoked currents of ASIC-1 and ACD-2 can likewise be blocked by amiloride. These findings show that amiloride can function as a pore-blocker for these homomeric channels. The screen revealed three additional homomeric channels which show enhanced inward currents in the presence of amiloride, these are DEL-5 and DEL-8b at neutral pH and DEL-9 at low pH. This property of amiloride acting as an agonist has been described for the homomeric human ASIC2 as well as for homomeric rat ASIC3 and heteromeric rat ASIC3/ASIC1b where the action of amiloride is pH dependent (Adams et al., 1999b, Li et al., 2011, Yagi et al., 2006): Amiloride enhances rat ASIC3 currents evoked at pH 7.0 but blocks currents evoked at pH 6.0 and below (Yagi et al., 2006). Enhancement of currents by amiloride could have multiple explanations including the conformational changes that the channel might undergo in response to proton binding, or that protons and amiloride compete for a similar binding site, for instance, due to multiple amiloride molecules binding within the acidic pocket (Baconguis et al., 2014). It would be interesting to explore this further as it implies that there are some

conserved functions between the mammalian ASICs and *C. elegans* DEL-5, DEL-8b and DEL-9.

Further optimisation is also needed to explore the conditions for expression of ACD-4, ASIC-2, EGAS-1, EGAS-2, EGAS-3, EGAS-4, and DEL-3 which, when injected into oocytes, did not show any responses to varying proton concentrations or amiloride, and FLR-1, ACD-3 and DEL-7 which showed elevated inward currents in the initial screen but are unaffected by low pH or amiloride. A similar observation of amiloride insensitive currents has been described for DELM-2 when expressed *in vitro* in *Xenopus* oocytes (Han et al., 2013). The authors' interpretation for this observation was that DELM-2 on its own cannot form a functional channel (Han et al., 2013). While this could explain the observation for FLR-1, ACD-2, ACD-3 and DEL-7 amiloride-insensitive currents, an alternative explanation is that another blocker is required to block these channels. Therefore, other subunit-specific blockers could be used to test this hypothesis such as tetraethylammonium which has shown to block ASIC1a/2b currents, non-steroidal anti-inflammatory drugs (NSAIDs) which inhibits ASIC3 and ASIC1a or specific toxins (Sherwood et al., 2011, Adams et al., 1999a, Voilley, 2004, Voilley et al., 2001, Diochot et al., 2004, Diochot et al., 2012).

Another explanation might be that these subunits are unable to form functional homomers but might require additional channel subunits or auxiliary subunits such as stomatin-like genes. For instance, the rat ENaC where the beta- and gamma-subunits do not form functional channels when expressed alone or in combination but the alpha-ENaC subunit does (Canessa et al., 1994). The MEC-4 and MEC-10 mechanotransduction complex requires stomatin-like proteins for anchoring in the membrane (Goodman et al., 2002). Other explanation for a lack of function are that the expression is affecting the health of the *Xenopus* oocyte, or poor translocation to the membrane. As injections are done automatically by the Roboinject (Mutlichannel Systems) it is unlikely that small variations in volume of cRNA injected could be the reason for the observed expression level. However, we noticed that expression success varies between different batches of oocytes which cannot be controlled. Finally, it might be that subunits are not expressed or are require a ligand (other than protons) or stimulus for activation. Endogenous ligands might include (neuro)peptides as it is the case for some Hydra Na^+ channel (HyNaC) and DEG/ENaC homologues in Platynereis (Durrnagel et al., 2012, Schmidt et al., 2018). Other stimuli could involve mechanical stimulation or shear stress which have been shown to trigger the opening

of MEC-4/MEC-10 heteromeric channels, or temperature which has been previously suggested to activate DEG-1 in *Xenopus* oocytes (Shi et al., 2016, Takagaki et al., 2020).

Finally, there are still open questions that needed to be addressed about the *in vivo* state of the channels. First of all, while I have shown that some *C. elegans* DEG/ENaCs can form functional homomeric channels *in vitro* in *Xenopus* oocytes that are sensitive low pH, it is likely that *in vivo* they form heteromeric channels and it is unknown whether they are open or closed under physiological conditions. One way to investigate whether they form heteromeric channels is to use proximity labelling using for instance TurboID or pull-down of epitope-tagged DEG/ENaC subunits and subsequent mass-spectrometry (Zanin et al., 2011, Branon et al., 2018). Secondly, it would be interesting to connect *in vitro* data to *in vivo* channel function. In order to do this, it is necessary to obtain full expression data including subcellular localisation. This data together with the electrophysiological results might be able to identify physiological functions of the subunits *in vivo.*

Understanding the functional diversity of the DEG/ENaC family is crucial for investigating their cellular role. In this chapter, I have shown for the first time that *C. elegans* ASICs exist and that they can be activated by low pH, like the mammalian ASICs. I have also shown that there are further similarities between the *C. elegans* DEG/ENaCs and the mammalian homologues in terms of their electrophysiological profiles. For instance, *C. elegans* DEG/ENaCs can be blocked by amiloride similar to the ASICs and ENaCs (Kashlan and Kleyman, 2011) and that the *C. elegans* DEL-5, DEL-8 and DEL-9 currents can be enhanced in the presence of amiloride which has previously been shown for human ASIC2, homomeric rat ASIC3 and heteromeric rat ASIC3/ASIC1b (Adams et al., 1999b, Li et al., 2011). These findings in turn suggest that at a physiological level DEG/ENaCs functions are conserved between species. The following chapters will build on these findings, including further characterising these candidate homomeric channels *in vitro* in *Xenopus* oocytes as well as in *C. elegans in vivo*.

3. 4. Summary of *C. elegans* DEG/ENaC properties with other information

Differential gene expression defines individual neuron types and knowing the genes expressed in neurons allows us to probe for circuit physiology and interpret behaviour. As mentioned in the introduction to this chapter, *C. elegans* research has traditionally relied on transcriptional reporter expression data and behavioural analysis when probing the molecular function of homomeric or heteromeric DEG/ENaC of interest. However, one drawback of using transcriptional reporter is that depending on the length of the promoter used the expression pattern can vary and no expression of the reporter does not exclude that the gene of interest is not expressed in the respective tissue. To address this limitation, recent efforts such as the CenGen project (CenGen.org) have used neuronal single cell RNA sequencing to establish a neuronal gene expression atlas of the larva stage L4 worms. However, for experimental research, there are obvious limitations such as that the data generated are a snapshot in pre-adult development as well as the focus on neurons over non-neuronal tissue. In the light of the current research, the latter is important as many DEG/ENaCs are expressed in non-neuronal tissue in addition to neurons. There are further limitations with this approach they both are related to predicting channel functioning. The first limitation is that (as for many molecules) it is critical where in the cell a channel is expressed: Is the ion channel expressed in the synapse or extra-synaptic? If we take the localisation of an acid-sensing DEG/ENaC, it is important to know its physiological environmental pH to hypothesise how it would function under physiological conditions. In later chapters of the thesis, I will demonstrate how the environment such as the synapse or the intestinal cells are important for generating testable hypothesis about the function of a channel. The second limitation is the difficulty to predict the response of a channel to stimulus without electrophysiological data. For cellular processes and downstream signalling, it is important to know not only the stimulus of a channel but also the ion-selectivity, for instance. The latter limitations were partially addressed in this chapter with the screen for acid-sensitive DEG/ENaCs. Another limitation of only gene expression studies or single cell RNA sequencing data is that information of homomeric and heteromeric channels are impossible to know which again is an issue given that homomeric and heteromeric channels are likely to have different electrophysiological properties and could lead to different behavioural outputs.

Being aware of these limitations, I now want to draw together DEG/ENaC electrophysiological channel properties, expression patterns, behavioural and developmental data from this thesis and previous research. The summary table below can hence serve as a starting point for further experiments and guide experimental hypothesis as shown in the following chapters of the thesis. Therefore, one aim of generating the summary table and the heat map was to investigate trends and generate hypotheses about possible combinations of channels functioning together in a particular cell, e.g. do channels that have overlapping expression in the same cell have similar phenotypes of properties? As will be discussed below in particular examples as well as in later chapters, co-expression data provides a useful guide for finding candidate subunits that could potentially act together. Nevertheless, it is challenging to show that these subunits indeed form a heteromeric channel and participate together in the same behaviour.

There are some examples where co-expression and behavioural data has discovered DEG/ENaC subunits that act as a heteromeric channels to generate a particular behaviour. The most famous examples are MEC-4 and MEC-10 acting together in the touch receptor neurons and mutants of either gene are defective in their response to mechanical touch (Driscoll and Chalfie, 1991). Other examples include DELM-1 and DELM-2 both expressed in glial socket cells function together in responding to nose touch, and DEL-7 and DEL-3 both expressed in NSM are involved slowing of movement in response to food (Han et al., 2013, Rhoades et al., 2019). However, subcellular co-localisation of the latter example channels has not yet been shown but the characterisation relies exclusively on behavioural phenotypes.

A recent study has illustrated that it is necessary to use experimental approaches to investigate subunit-specific functioning in the same neuron. The authors identified two parallel processes in the PVD neurons both relating to mechanosensation which they classified as nociception and proprioception (Tao et al., 2019). *mec-10, del-1, degt-1* and *unc-8* are expressed in PVD and *mec-10, degt-1* and *unc-8* have been linked to mechanosensitive functions (Chatzigeorgiou et al., 2010, Smith et al., 2010, Tavernarakis et al., 1997). However, while they are all expressed in PVD, they are not all involved in the same processes in PVD but proprioception depends on DEL-1, MEC-10 and UNC-8 while mechanonociception depends on DEGT-1 (Tao et al., 2019). While there is research that has also shown a nociceptive role for MEC-10 (Chatzigeorgiou et al., 2010), the different functions make sense if

one considers the subcellular localisation DEGT-1 is expressed in 4° dendrites in a position where it can activate downstream command interneurons. By contrast, DEL-1 localises in puncta along 1°-3° dendrites and activation of DEL-1, MEC-10 and UNC-8 induces a local calcium increase which triggers dendritic release of a neuropeptide (Tao et al., 2019). Interestingly, *del-1, mec-10* and *unc-8* also share a locomotion phenotype which can be rescued by expressing the wild-type gene in PVD (Tao et al., 2019). However, this study ignored the other DEG/ENaC expressed in PVD, ASIC-1, and while it does not have a visible (proprioceptive) locomotion defect, it is involved in potentiating PVDs' output as well as enhancing synaptic release of dopamine in dopaminergic neurons (Voglis and Tavernarakis, 2008, Husson et al., 2012). The CenGen dataset also identifies *del-2* and *del-8* as being also expressed in PVD which makes the dataset even more complicated. Nevertheless, the research highlights the complications and importance of experimental approaches in order to fully understand and make sense of gene expression data.

I will focus the discussion below on the here identified acid-sensing DEG/ENaCs, namely ACD-5, DEL-4, DEL-9 and ASIC-1 (unfortunately, there is not enough data available for ACD-2), as further exploration is beyond the scope of the thesis. However, Table 3 might be a useful summary for future researchers for further investigation into the diverse family of the *C. elegans* DEG/ENaC members.

acd-5 demonstrates the limitations of the CenGen dataset as it is expressed in the intestine and therefore not in the dataset. However, my transcriptional promoter expression data shows that it is co-expressed with *acd-3, flr-1* and *del-5* in the intestine. While ACD-5 and FLR-1 are both expressed at the apical membrane throughout the intestine (see above, and (Take-Uchi et al., 1998)) and therefore are at the correct location to form a heteromeric channel. They also cluster together in the SSN in Figure 8 indicating that they share a similar amino acid sequence. It is not known if ACD-3 and DEL-5 are expressed on the apical or basal intestinal membrane or whether they are expressed equally throughout the intestine. Therefore, even if they all participate in the DMP, it is difficult to dissect whether they act together as a heteromeric channel or in which subunit combination. Biochemical approaches are needed to address this issue and *in vivo* expression data can provide further evidence. However, expression in the intestine, electrophysiological properties and further experiments (see CHAPTER 5) show that ACD-5 localises at a site where it can sense protons in the intestinal lumen which influences the DMP.

del-4 and *asic-2* are highly expressed in the with *egas-1* and *egas-3* and possibly *unc-105* in the dorsal and ventral IL2 as well as with *egas-4* and possibly *del-1* in the left and right IL2. This data is difficult to interpret, however, interestingly, all candidates, *del-4, asic-2, egas-2* and *del-1* show a locomotion defect (Yemini et al., 2013). *del-4, asic-2, unc-105* and *del-1* also show some sequence similarity as they are part of the neuronally expressed ASIC-1 cluster (green) and the *egas* subunits also share a high degree of sequence similarity and hence they could fulfil similar functions in the IL2s. The role of DEL-4 is unknown but based on its expression and response to protons, it might be involved in modulation by protons secreted from the surrounding glia cells, as glia have previously been proposed to use proton-signalling to modulate neuronal functioning (Deitmer and Rose, 1996).

del-9 is expressed in both neurons and muscles and the wide expression pattern suggests that it might be able to form heteromeric channels with a variety of other subunits. When exploring expression in muscles, there are only two other DEG/ENaCs that are expressed in muscle tissue, these are *del-10* as described above and *unc-105* (Jospin and Allard, 2004, Garcia-Anoveros et al., 1998, Park and Horvitz, 1986). *del-9* mutants showed decreased amplitude in midbody bends and *unc-105* mutants were significantly faster than wild-type in backward midbody speed and increase in eccentricity (Yemini et al., 2013). There is no data available for *del-10*.

Further exploration of *del-9* in neurons revealed that it is co-expressed in the DB ventral cord motor neurons with *del-1* and both mutants show a similar locomotion phenotype (Yemini et al., 2013) as well as in the VD ventral cord motor neurons with *asic-1* which, as shown above, is an acid-sensing DEG/ENaC. In the VD neurons, it is also co-expressed with *unc-8* which has shown to be important for developmental synapse remodelling (Miller-Fleming et al., 2016). As shown above, *del-1* and *unc-8* are involved in the release of neuropeptides (Tao et al., 2019). Interestingly *del-9* is also co-expressed with *asic-2* in the GABAergic neuron AVL which also expressed various neuropeptides (CenGen.org). Consequently, based on this data, it is likely that *del-9* participates in synaptic functioning in both neuronal and non-neuronal tissue. This hypothesis will be further explored in CHAPTER 4.

The CEP, ADE, and PDE dopaminergic neurons all express *asic-1* (Voglis and Tavernarakis, 2008). In the CEPs, and according to the CenGen data, *asic-1* is co-expressed with *del-2, del-3* and possibly *acd-3*, while in ADE and PDEs it is co-expressed with *del-2, del-3* and *del-8.* By contrast, as shown before in the PVD and

FLP neurons which are similar in both morphology and function to mammalian nociceptors, *asic-1* is co-expressed in PVD with *del-2, del-8, mec-10, del-1, degt-1* and *unc-8* according to the combined data of previously research and CenGen.org, and in the FLPs with *mec-10, del-1* and *unc-8*. Based on previous research (Tao et al., 2019, Voglis and Tavernarakis, 2008) it is likely that *asic-1*, *mec-10, del-1* and *unc-8* are involved in regulating synaptic release of neurotransmitters or neuropeptides in both PVD and this might be the case for FLP as well, however, weather on in which combination they form heteromeric channels needs to be investigated. Interestingly, when considering neuronal identity *asic-1* seems to be expressed in dopaminergic neurons such as the CEP, ADE, and PDE neurons as well as glutamatergic neurons such as FLP and PVD with a characteristic other subunit which might be a good starting point for investigating a synaptic role of a potential heteromeric channel *in vivo* as well as *in vitro* in *Xenopus* oocytes.

To summarise is section, drawing together the findings of this chapter, the information provided in Table 3 and Figure 13 it becomes apparent that there is not a clear pattern for DEG/ENaC subunit co-expression in particular neurons. However, based on the examples of acid-sensitive DEG/ENaCs from the TEVC screen above as well as other information provided by previous research or as part of this thesis, it supports the hypothesis that the acid-activated DEG/ENaCs are likely to be involved in modulation and potentiation of neuronal signalling at the synapse as they are co-expressed with previously identified synaptically localised DEG/ENaCs or DEG/ENaCs involved in the secretion of neuromodulators. However, based the summary also suggests that in order to find out how exactly the respective homomeric or heteromeric channels might function *in vivo*, one has to dissect each individual neuron as subunits are expressed with a varying subunit which could act together, in parallel or in different functions in each neuron.

Table 3: Summary of C. elegans DEG/ENaC information.

Summary of *C. elegans* DEG/ENaC expression pattern taking together expression data from previous research, neuronal single-cell RNA sequencing data and expression patterns described in this chapter. Fields marked with N/A are not found in the CenGen.org dataset. Hyphens indicate that the particular expression pattern has not been investigated in the current thesis and blank boxes indicated that there is no evidence found in the literature. Accession numbers of genes and description of the neurons can be found in (Appendix 3. 5. 1. Table 9 and Table 10 at the end of

this chapter). For the CenGen dataset: The following genes turned up results: *acd-3, acd-4, asic-1, asic-2, mec-4, del-4, unc-105, deg-1, del-1, mec-10, egas-1, egas-3, egas-4, degt-1, del-2, del-3, del-5, del-7, del-8, unc-8, del-9, del-10*, while for the following genes expression pattern could not be found *flr-1, acd-1, acd-2, acd-5, delm-1, delm-2, egas-2, del-6*. This could have several reasons, for instance these genes might not be expressed in L4 animals, they might not be expressed in neurons (which would be supported by the expression data shown above), or their expression might be very low (not detected) or very high (excluded from the dataset). Behavioural and developmental data was taken from previous research as indicated or from this thesis. Colours indicate the clusters identified in the SSN above.

DEG/ ENaC gene	**Reported Expression pattern**	**CenGEN.org expression pattern (threshold 2)**	**Behavioural phenotype**	**Developmental phenotype**	**Electrophysiology** (individual subunit expression in *Xenopus* oocytes)	**Reference**
flr-1	Intestine	N/A	defects in defecation rhythm, high variability between cycles, missing pBoc and EMCs	defects in dauer formation (in *unc-3/osm-1/tax-2* mutant background	does not respond to low pH or amiloride	Take-Uchi et al., 1998, this thesis
acd-1	Amphid sheath cells (glia)	N/A	chemosensory deficits (in sensitised *deg-1* mutant background)	-	Constitutively open Na^+ channel (Na^+>Li^+~K^+), impermeable for Ca^{2+}, blocked by pH 5 and intracellular pH, amiloride-sensitive	Wang et al., 2008, 2012, this thesis
acd-2	Neurons (head/ anterior)	N/A	-	-	pH sensitive (activated by increasing amount of protons), amiloride-sensitive	this thesis

acd-3	Intestine	RIP, AFD, URB, M1, LUA, VC, VA12, RME_LR, RME, ASG, RIF, PLN, AVG, PQR, BAG, RMH, RMD, PVW, RIH, RIR, RIC, DVB, ASJ, VB02, AIA, VB, VC, VB01, DB, AIB, PDE, RIV, CEP, IL2_LR, NSM, IL2, AWB, DA, AWC_ON, AVE, I5, M2, AUA, SMB, PHA, AQR, AIZ, MI, PVP, RID, DB01, AVK, RIM, ADF, M5, VA, AVJ, SIA, AVF, I4, RIG, AIY, ASER, SAB, AWA, PVQ, ASH, URX, AVM, AIM, ASK, AVH	Locomotion phenotype, missing pBoc and EMCs	-	does not respond to low pH or amiloride	Brown et al., 2013; Yemini et al., 2013, this thesis
acd-4	Neurons (head/ anterior), pharyngeal-intestinal valve, intestinal-rectal valve	ASG, M1, PHA, ASH, AIM	-	-	does not respond to low pH or amiloride	this thesis
acd-5	Intestine	N/A	Locomotion phenotype, higher intestinal lumen pH, increased defecation cycle intervals	expression of *acd-5* in ASK in dauers and post-dauers, may affect dauer-formation	pH sensitive, amiloride-sensitive	Brown et al., 2013; this PhD thesis; Grundy (2018)

delm-1	Glial socket cells (of OLQ and IL1)	N/A	neuronal excitability: mechano-sensory defects related to nose touch & foraging	-	amiloride-sensitive, ion-selectivity: $Li^+>Na^+\sim K^+$	Han et al., 2013, this thesis
delm-2	Glial socket cells (of OLQ and IL1); rectal gland cells; neurons or glia (head/tail, anterior/posterior)	N/A	neuronal excitability - mechanosensory defects related to nose touch & foraging	-	does not respond to amiloride	Han et al., 2013, this thesis
asic-1	ADE, CEP, PVQ, PDE, PVD, FLP, ventral cord; dopaminergic neurons	PDE, VB. FLP, ADE, VA12, VA, CEP, VB02, PVD, SAB	involved in associative learning (presynaptic, enhancing activity in dopaminergic neurons), locomotion phenotype; potentiation of PVD output	-	pH sensitive (activated by increasing protons concentrations), amiloride-sensitve	Voglis and Tavernarakis, 2008; Yemini et al., 2013; Husson et al 2012, this thesis
asic-2	six IL2 neurons (cilia), two fainter OLs	IL2_DV, IL2_LR, URB, RIR, DVB, AVL	Locomotion phenotype	may affect dauer-formation	does not respond to low pH or amiloride	Wang et al., 2015; Yemini et al., 2013; De Stasio et al., 2018; Grundy, 2018, this thesis

mec-4	ALM, AVM, PLM, PVM	PLM, ALM, AVM, PVM, CAN, HSN	mechanosensation, neuronal degeneration	-	neuronal degeneration (mec-4(d) causes necrosis through increase in intracellular Ca^{2+} and calpain activation)	Driscoll and Chalfie, 1991; Huang and Chalfie, 1994; Garcia-Aiioveros et al., 1995; Bianchi et al., 2004; O'Hagan, Chalfie and Goodman, 2005 Goodman et al., 2002, Fechner et al., 2020
del-4	ASE, AIY, ASG (fainter), AIA, PHA, PQR (up to three neurons in tail)	IL2	Locomotion phenotype	age-dependent expression in ASE, ASG, and several other unidentified neurons, decrease from eight ciliated sensory neurons in L1-L2 larvae to four in adults. daf-19(m86) alters expression pattern (DAF-19 activates del-4 expression in ASE and in AIY interneurons)	Constitutively open Na_+ channel, blocked by pH 5, amiloride-sensitive	Yemini et al., 2013; De Stasio et al., 2018, this thesis
unc-105	Act in muscles	RIF, URA, IL2, M1, CAN	mutation become small, severely hyper-contracted and paralyzed; genetic interaction with collagen let-2	-	slightly selective for Na^+~Li+ > K^+ > Cs^+, impermeable to Ca^{2+} and Mg^{2+}	Park and Horvitz, 1986, Liu et al 1996, Garcia-Anoveros et al., 1998)

deg-1	ASH, ASK, IL1 and AVG neurons	AVF, AVD, VD, SAB, M4, LUA, RID, AVM, AVJ, AVG	mechanosensation, chemo-sensory defects, neuronal degeneration, acid avoidance thermo-sensation/ cold tolerance	-	slight increase in currents at low pH	Geffeney et al., 2011; Wang et al., 2008; Garcia-Aiioveros et al.,1995; Chalfie and Wolinsky, 1990; Huang and Chalfie, 1994, Takagaki et al 2020, this thesis
del-1	PVD; FLPs and the VA and VB Motor Neurons	PHC, FLP, PVD, PVN, AS, VA12, AVE, VA, SIA	Locomotion phenotype (putative mechanosensation: co-expressed with unc-8); proprioception in PVD and release of neuropeptide	-	slight increase in currents at low pH	Tavernarakis et al., 1997; Yemini et al., 2013; Tao et al., 2019, this thesis
mec-10	ALM, AVM, PLML, PVM, PVD	AVM, PVM, PLM, ALM, PVD, FLP	neuronal degeneration, mechanosensation; proprioception in PVD and release of neuropeptide	-	-	Huang and Chalfie, 1994; Chatzigeorgiou et al., 2010;; Tao et al., 2019
egas-1	Two IL2	IL2	-	-	does not respond to low pH or amiloride	Wang et al., 2015, this thesis
egas-2	Neurons (head/anterior) possibly two IL2, tail neurons	N/A	Locomotion phenotype	-	does not respond to low pH or amiloride	Yemini et al., 2013, this thesis
egas-3	Neurons (head/ anterior) and hypodermal cells in the	IL2_DV, AFD, HSN	-	-	does not respond to low pH or amiloride	this thesis

	tail, seam cells					
egas-4	Two IL2 (not the same as *egas-1*)	IL2_LR	-	-	does not respond to low pH or amiloride	this thesis
degt-1	PVD	M5, MI, M3, I4, I6, ASI, I3	harsh touch; mechanonociception	-		Chatzigeorgiou et al., 2010; Tao et al., 2019, Fechner et al., 2020, this thesis
del-2	Neurons or glia (head/tail, anterior/ posterior)	ASER, ASEL, URY, ASG, AWC, PHC, ADL, PQR, ADF, ASH, PVD, PHB, ASI, CEP, ASK, ADE, ASJ, AWA, I6, NSM, PHA, LUA, I5, AQR, PDE, AVK, BDU, I3	-	-	does not respond to low pH or amiloride	wormbook.org; this thesis
del-3	NSM and 8 other neurons	NSM, I6, I1, OLQ, CEP, ADL, ADE, PVT, PDE, OLL, AVE, ASJ	Mediate Food Responses in an Enteric Serotonergic Neuron that Controls Foraging Behaviors. Probably not mechanosensation - nanobeads do not activate; heat sensitive bacterial component required	-	does not respond to low pH or amiloride	Rhoades et al., 2019; this thesis

del-5	Intestine	BAG, URA, PDE, PQR, RIC, AVG, HSN, DVB	DMP defects: missing pBoc and EMCs	-	does not respond to low pH but currents enhanced by amiloride	this thesis
del-6	-	-	-	-	-	-
del-7	NSM	NSM, I6, PVT	Locomotion phenotype; mediate food responses in NSM neurons that controls foraging behaviours		does not respond to low pH or amiloride	Yemini et al., 2013; Rhoades et al., 2019; this thesis
del-8	-	AQR, ADE, PRQ, PDE, RMG, NSM, AIB, VD_DD, I6, VA, DA, PVP, AWC_ON, AVF, I3, BDU, PVD	-	-	-	-
unc-8	VD and DD GABAergic neurons; ASH and FLP neurons, cholinergic motor neurons		locomotion phenotype (mechanose nsation), mutant version causes neuronal swelling; proprioceptio n in PVD and release of neuropeptide	removal of synapses in remodelling GABAergic neurons	Na^+ permeable channel	Miller-Fleming et al., 2016; Wang et al., 2013c; Tavernarakis et al., 1997, Yemini et al., 2013; Tao et al., 2019; Fechner et al., 2020
del-9	Head- and tail- body wall muscles, AVL, PVQ and other head and tail neurons	DB, AVL, DB01, DA, M1, AVF, MC, RMD, PVQ, VB02, MI	Locomotion phenotype, missed EMCs during DMP	-	pH sensitive (activated by increasing proton cncentrations), amiloride-insensitive at low pH but amiloride-sensitive at neutral pH	Yemini et al., 2013; this thesis
del-10	Body wall muscles	-	-	-	might close in response to low pH, constitutively open	this thesis

					at neutral pH amiloride-sensitive	

3. 5. Appendix C

3. 5. 1. Abbreviation list of genes and neurons

Supplementary Table 9: Abbreviation list of genes.

Abbreviations of *C. elegans* DEG/ENaC taken from wormbase.org. As most *C. elegans* genes, the names are either based on homology or on mutant phenotypes associated with a particular gene. (wormbase.org)

Name	
ACD-1	**AC**id-sensitive **D**egenerin
ACD-2	
ACD-3	
ACD-4	
ACD-5	
ASIC-1	**A**cid-sensing/**A**miloride-**S**ensitive **I**on **C**hannel family
ASIC-2	
DEG-1	**DEG**eneration of certain neurons
DEGT-1	**DEG**enerin-related **T**ouch-involved channel
DEL-1	**DE**generin **L**ike
DEL-2	
DEL-3	
DEL-4	
DEL-5	
DEL-6	
DEL-7	
DEL-8	
DEL-9	
DEL-10	
DELM-1	**DE**generin **L**inked to **M**echanosensation
DELM-2	
EGAS-1	**EG**F plus **AS**C domain ion channel
EGAS-2	
EGAS-3	
EGAS-4	

FLR-1	**FL**uoride **R**esistant phenotype
MEC-4	**MEC**hanosensory abnormality, due to neuronal degeneration
MEC-10	
UNC-8	**UNC**oordinated, meaning atypical uncoordinated crawling
UNC-105	

Supplementary Table 10: Abbreviations of C. elegans neuron names.

Abbreviations of neuron names taken from wormatlas.org. Each neuron in *C. elegans* has its own name and can be identified according to its characteristic morphology and location. (wormatlas.org)

Neuron	Description
ADE	Anterior deirid, sensory neuron
ADF	Amphid neuron
ADL	Amphid neuron
AFD	Amphid finger cell
AIA	Amphid interneuron
AIB	Amphid interneuron
AIM	Ring interneuron
AIY	Amphid interneuron
AIZ	Amphid interneuron
ALM	Anterior lateral microtubule cell
AQR	Neuron, basal body. not part of a sensillum, projects into ring
AS	Ventral cord motor neuron, innervates dorsal muscles, no ventral counterpart
ASE	Amphid neurons, single ciliated endings
ASG	Amphid neurons, single ciliated endings
ASH	Amphid neurons, single ciliated endings
ASI	Amphid neurons, single ciliated endings
ASJ	Amphid neurons, single ciliated endings
ASK	Amphid neurons, single ciliated endings
AUA	Neuron, process runs with amphid processes but lacks ciliated ending
AVD	Ventral cord interneuron
AVE	Ventral cord interneuron, like AVD but outputs restricted to anterior cord

AVF	Interneuron
AVG	Ventral cord interneuron
AVH	Neuron, mainly postsynaptic in ventral cord and presynaptic in the ring
AVJ	Neuron, synapses like AVHL/R
AVK	Ring and ventral cord interneuron
AVL	Ring and ventral cord interneuron and an excitatory GABAergic motor neuron for rectal muscles. Few synapses
AVM	Anterior ventral microtubule cell, touch receptor
AWA	Amphid wing cells, neurons having ciliated sheet-like sensory endings closely associated with amphid sheath
AWB	Amphid wing cells, neurons having ciliated sheet-like sensory endings closely associated with amphid sheath
AWC	Amphid wing cells, neurons having ciliated sheet-like sensory endings closely associated with amphid sheath
BAG	Neuron, ciliated ending in head, no supporting cells, associated with ILso
BDU	Neuron, process runs along excretory canal and into ring, unique darkly staining synaptic vesicles
CAN	Process runs along excretory canal, no synapses, essential for survival
CEP	Cephalic neurons, contain dopamine
DA	Ventral cord motor neurons, innervate dorsal muscles
DB	Ventral cord motor neurons, innervate dorsal muscles, reciprocal inhibitor
DVB	An excitatory GABAergic motor neuron/interneuron located in dorso-rectal ganglion. Innervates rectal muscles
FLP	Neuron, ciliated ending in head, no supporting cells, associated with ILso
HSN	Hermaphrodite specific motor neurons (die in male embryo), innervate vulval muscles, serotonergic
I1	Pharyngeal interneurons: ant sensory, input from RIP
I3	Pharyngeal interneuron, ant sensory

I4	Pharyngeal interneuron
I5	Pharyngeal interneuron, post sensory
I6	Pharyngeal interneuron, post sensory
IL2	Inner labial neuron
IL1	Inner labial neuron
LUA	Interneuron, short process in post ventral cord
M1	Pharyngeal motorneuron
M2	Pharyngeal motorneurons
M3	Pharyngeal sensory-motorneurons
M4	Pharyngeal sensory-motorneurons
M5	Pharyngeal motorneuron
M6	Pharyngeal motorneuron
MC	Pharyngeal neurons that synapse onto marginal cells
MI	Pharyngeal motor neuron/interneuron
NSM	Pharyngeal neurosecretory motorneuron, contain serotonin
OLL	Lateral outer labial neurons
OLQ	Quadrant outer labial neuron
PDB	Motor neuron, process in dorsal cord, cell body in pre-anal ganglion
PDE	Neuron, dopaminergic of postderid sensillum
PHA	Phasmid neurons, chemosensory
PHB	Phasmid neurons, chemosensory
PHC	Neuron, striated rootlet in male, possibly sensory in tail spike
PLM	Posterior lateral microtubule cells, touch receptor neurons
PLN	Interneuron, associated with PLM
PQR	Neuron, basal body, not part of a sensillum, projects into preanal ganglion
PRQ	Sensory neuron, oxygen sensing
PVD	Neuron, lateral process adjacent to excretory canal, nociceptor
PVM	Posterior ventral microtubule cell, touch receptor
PVN	Interneuron/motor neuron, post. vent. cord, few synapses
PVP	Interneuron, cell body in preanal ganglion, projects along ventral cord to nerve ring

PVQ	Interneuron, projects along ventral cord to ring
PVT	Interneuron, projects along ventral cord to ring
PVW	Interneuron, posterior ventral cord, few synapses
RIC	Ring interneuron
RID	Ring interneuron, projects along dorsal cord
RIF	Ring interneuron
RIG	Ring interneuron
RIH	Ring interneuron
RIM	Ring motor neuron
RIP	Ring/pharynx interneuron, only direct connection between pharynx and ring
RIR	Ring interneuron
RIV	Ring interneuron
RMD	Ring motor neuron/interneuron, many synapses
RME	Ring motor neuron
RMF	Ring motor neuron/interneuron
RMG	Ring interneuron
RMH	Ring motor neuron/interneuron
SAA	Ring interneuron, anteriorly projecting process that runs sublaterally
SAB	Ring interneuron, anteriorly projecting process that runs sublaterally, synapses to anterior body muscles in L1
SDQ	Post. lateral interneuron, process projects into ring
SIA	Receive a few synapses in the ring, have posteriorly directed processes that run sublaterally
SMB	Ring motor neuron/interneuron, has a posteriorly direct ed process that runs sublaterally
URA	Ring motor neuron
URB	Neuron, presynaptic in ring, ending in head
URX	Ring interneuron
URY	Neuron, presynaptic in ring, ending in head
VA	Ventral cord motor neuron, innervates vent. body muscles
VA12	Ventral cord motor neuron, innervates vent. body muscles, but also interneuron in preanal ganglion

VB	Ventral cord motor neuron, innervates vent. body muscles
VC	Hermaphrodite specific ventral cord motor neuron innervates vulval muscles and ventral body muscles
VD	Ventral cord motor neuron, innervates vent body muscles, reciprocal inhibitor

3. 5. 2. Accession numbers

Supplementary Table 11: Accession numbers for C. elegans DEG/ENaCs.

Name	**Gene stable ID**	**WormBase CDS ID**	**UniProtKB/TrEMBL ID**
ACD-1	WBGene00016064	C24G7.2	P91102
ACD-2	WBGene00016066	C24G7.4	P91100
ACD-3	WBGene00007775	C27C12.5	G3MU02
ACD-4	WBGene00017879	F28A12.1	Q22970
ACD-5	WBGene00020903	T28F2.7	O01664
ASIC-1	WBGene00022815	ZK770.1	K7H9J0
ASIC-2	WBGene00012137	T28F4.2	Q22851
DEG-1	WBGene00000950	C47C12.6	P24585
DEGT-1	WBGene00009109	F25D1.4	Q19777
DEL-1	WBGene00000952	E02H4.1	Q19038
DEL-2	WBGene00000953	F58G6.6	G5ECD8
DEL-3	WBGene00009144	F26A3.6	Q93597
DEL-4	WBGene00012116	T28B8.5	P91835
DEL-5	WBGene00010334	F59F3.4	G5EFH3
DEL-6	WBGene00011891	T21C9.3	Q8MPW0
DEL-7	WBGene00016699	C46A5.2	Q18651
DEL-8	WBGene00007518	C11E4.3	Q93205
DEL-9	WBGene00015957	C18B2.6	Q18077

DEL-10	WBGene00020897	T28D9.7	Q10025
DELM-1	WBGene00009073	F23B2.3	O45402
DELM-2	WBGene00016063	C24G7.1	P91103
EGAS-1	WBGene00013486	Y69H2.11	Q9U1T9
EGAS-2	WBGene00013487	Y69H2.12	Q9U1T8
EGAS-3	WBGene00013480	Y69H2.2	Q9XTS9
EGAS-4	WBGene00018906	F55G1.13	Q20852
FLR-1	WBGene00001465	F02D10.5	G5EGI5
MEC-4	WBGene00003168	T01C8.7	P24612
MEC-10	WBGene00003174	F16F9.5	P34886
UNC-8	WBGene00006748	R13A1.4	Q21974
UNC-105	WBGene00006832	C41C4.5	Q09274

3. 5. 3. Homology of *C. elegans* proton sensitive DEG/ENaCs to rat ASIC1

Previous research has described and successfully predicted proton binding sites in the rat ASIC1a (rASIC1a) (Shaikh and Tajkhorshid, 2008, Paukert et al., 2008, Li et al., 2009, Grunder and Chen, 2010). Some sites are located in the extracellular loop region including the thumb domain (rASIC1a P200-F410). These potentially proton sensing sites were determined by amino acid substitution studies (e.g. E219Q, D237N, E238Q (Paukert et al., 2008), P286/W287 (Li et al., 2009)). Furthermore, there are some residues that are part of the acidic pocket (e.g. E219, D237, E238, D349, D407 (Grunder and Chen, 2010)) which are implicated in proton sensing. Furthermore, residues in the first transmembrane (TM1) region are predicted to be proton sensing sites (Shaikh and Tajkhorshid, 2008). Additionally, there are predicted and experimentally confirmed proton sensing sites in the linker regions between the TM1 and the extracellular loop of rASIC1a, for instance, E63 (Paukert et al., 2008, Shaikh and Tajkhorshid, 2008), Y71 (Paukert et al., 2008, Li et al., 2009), H72/H73 and D78 (Shaikh and Tajkhorshid, 2008)).

In order to look for potential conserved sites in the *C. elegans* acid-sensing ion channels and the well-characterised rASIC1a (Shaikh and Tajkhorshid, 2008, Paukert et al., 2008, Li et al., 2009, Grunder and Chen, 2010), I compared sequence similarity and identity using a local alignment method (Smith-Waterman in the SnapGene Software) (Daily, 2016). *C. elegans* DEG/ENaC amino acid sequence identity to the rASIC1a was found to be ranged between 21-28% while the amino acid similarity was ranged between 40-56%. For the particular proton-sensitive DEG/ENaCs shown below, the precise amino acid sequence identities and similarities are as followed: ACD-2 (Identity: 27.6 %; Similarity: 44.5 %); ACD-5 (Identity: 26.5 %; Similarity: 44.5 %); ASIC-1 (Identity: 28.0 %; Similarity: 46.3 %); DEG-1 (Identity: 28.0 %; Similarity: 47.8 %); DEL-4 (Identity: 23.3 %; Similarity: 43.2 %); DEL-9 (Identity: 22.8 %; Similarity: 40.58 %); DEL-10 (Identity: 21.0 %; Similarity: 41.7 %). However, the individual amino-acids did not seem to correlate with pH sensing between ASIC1a and the *C. elegans* DEG/ENaCs and hence it is difficult to draw any conclusion about function from the amino acid sequences.

TM1

```
Cons.    (149)  RXXW-XLIXXXXLXXXXXQXXXXXXXYXXXXXXXXXXXXXX
rASIC1a  (43)   RALW-ALCFLGSLAVLLCVCTERVQYYFCYHHVTKLD-EVA
acd-2    (103)  RAFW-MLIVGLALAMLCFQIFILLQMYFSKPTVTKLD-EVA
acd-5    (134)  CVFW-VFIWISSMIMLLTQVTSLISMYISKPTVSQVSFLLS
asic-1   (37)   RYMW-LLCFLFCLSCFGHQAYLIVERFNRNDIIVGVEIKFE
del-4    (36)   RAFW-ILVVVVSIALFIWQFITLLTNYLSFSVNTETTLQFA
deg-1    (80)   KLMWGLIIFSFLL-MFAYQASKLIFKFSAHEKITDISLKFD
del-9    (104)  RMVW-VLIVILALFMTFQGCYQIMDEYSMRRIVVSYFIQEA
del-10   (94)   RGLW-CMIIIAFVILVLVQCYSQIKLYISEPVATNIEAEYP
```

Extracellular loop

```
Cons.    (699)  -XDXXXXXXXXXXGXXXGLRXXXXXXXXEYXX-XXEXXXXX
rASIC1a  (200)GQDGRPRLKTMKGGTGNGLEIMLDIQQDEYLPVWGETDETS
acd-2    (267)  NLAPEWMRKQISPGSEAGLQIVVDAQLEEELK--GENDDAK
acd-5    (298)  GSDKSWMKMQTEPGIAAGLQIILDSHLEEQFD--SETDGVT
asic-1   (522)  -QKLGNN-TNERSGPAYGLRLEVFVNVTEYLP-TTEA----
del-4    (192)  -TD--GMYSSSRAGPLYGLRMVMRTDQDTYLP-WTEA----
deg-1    (467)  -YDVNNNYTSSRAGPMYGIRVLLFVNTSDYMS-TSES----
del-9    (258)  ------GIKQEIAGFGNGDRYVIDLPEEYYNPGINQM----
del-10   (239)  -TDPHNPYEVTGSGEGHGLRLLLNVESYERVDACTKHFRTK
```

Extracellular loop region

```
Cons.    (785)  XXXLXX-PXGXCXXXX-XXDX--XXXXXXXX-XYXX
rASIC1a  (280)LIYLPS-PWGTCNAV--TMDS------DFFD-SYSI
acd-2    (351)  HNLLNRGNWGNCS------ENW-PEGYNTFL-SYSA
acd-5    (382)  YILLSSNAWGNCS------DSW-PRGYDYSF-PYTS
asic-1   (594)  MVRLPA-PYGDCVREGKTED------FIYTQKAYNT
del-4    (263)  TTRLSK-PYGSCTTKTKLKT------THYTG-TYTV
deg-1    (540)  MQRLPA-PYGECVETKKVVDR----NYIYAGYDYHP
del-9    (327)  FEFMNDPPRYECEED--------PHG------NYSR
del-10   (319)  RSKLTG---VHCIEEN---DEQIEASTDFNN-PENI
```

Thumb domain

```
Cons.    (480)  -------XPX-YXXXX---XXXXCXXXXX--XXCX-------DXXXXXXXXXX--XXXXXX
rASIC1a(325)MVHMPGDAPY-------------CTPEQY--KECA-------DPALDFLVEKD--------
acd-2    (396)  -------APFTYNVDG---RKKICAPYES--ITCM-------DNHMLKKVNGT--DYLELP
acd-5    (427)  -------SPSIYNHLN---RFNDCTPYET--FICM-------DTKMKKVVNQS--FNIEMP
asic-1   (641)  -------DPR-FPPYR---ESKNCPVDDPYKRECI-------KNEM----------HVATR
del-4    (309)  -------YPA-Y-----------SHASNTTQYVSC-------DNGVQTLSNLNCVDLINSA
deg-1    (589)  -------DPR-FPVPE---GYRHCSAFNATARTCL-------EKNIGSVGDF---HHITQK
del-9    (368)  PAAAQ--NPA-Y-------PDKLCTATQL--YHCFFTKLFPEDSNLSKAIVDA--------
del-10   (367)  LRRA-------YTSNSTDVKMKACNVDQY--FGCA-------QKAMQRIREEG--------
```

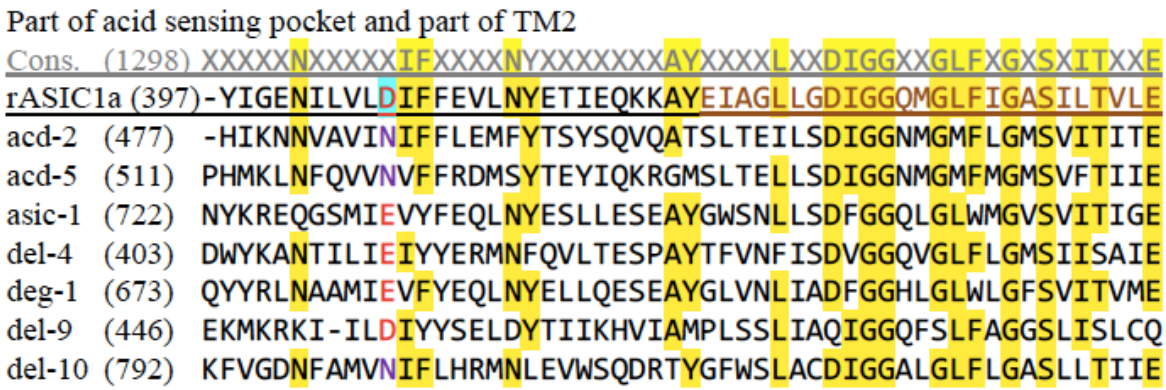

Supplementary Figure 1: Amino acid alignment of the C. elegans acid-sensing DEG/ENaCs to the rat ASIC1 (rASIC1).

ACD-2, ACD-5, ASIC-1, DEG-1, DEL-4, DEL-9 and DEL-10 alignment to rat ASIC1a was generated with MAFFT integrated in the SnapGene Software. Transmembrane region (TM1) of rASIC1a is shown in brown. Consensus (Cons.) alignment is highlighted in yellow. Amino acids previously implicated in pH sensitivity in rASIC1a highlighted in turquoise. Colour indication: orange (small nonpolar: G, A, S, T); green (hydrophobic: C, V, I, L, P, F, Y, M, W); magenta (polar: N, Q, H); red (negatively charged: D, E); blue (positively charged: K, R).

CHAPTER 4 – DEL-9, a novel *C. elegans* acid-sensing DEG/ENaC is driving muscle contractions

4. 1. Introduction

A major aim in neuroscience is to understand how behaviour is generated and the underlying molecular mechanisms involved. In CHAPTER 1, I have outlined the evidence for protonergic signalling in- and outside of the nervous system in modulating behaviour. I have further outlined there is an increasing consensus that protons satisfy the criteria for chemical transmitters and that the synaptic acid-sensing ion channels (ASICs) have been put forward as the main proton-receptors (Du et al., 2014, Soto et al., 2018, Beg et al., 2008, Wemmie et al., 2002, Du et al., 2017, Uchitel et al., 2019). The major criticism is that, in the synapse, protons are only co-released with neurotransmitters but regulated, independent proton release at synapses has not been described (Soto et al., 2018). However, rhythmic release of protons via Na^+/H^+ exchangers has been described from *C. elegans* intestinal cells (Beg et al., 2008).

The intestine is one of the largest organs in *C. elegans*, and as the worm does not have a vascular system, it is responsible for the distribution and production of many signalling molecules and hence modulates and generates behaviour (Lee and Mylonakis, 2017, Beg et al., 2008, Imanikia et al., 2019). For instance, the highly rhythmic defecation motor program (DMP) is initiated by the Na^+/H^+ exchanger PBO-4 (also called NHX-7) expressed on the basal intestinal membrane acidifying the pseudocoelomic space between the intestine and the posterior muscle prior to the pBoc which in turn activates receptors on the posterior muscle (Beg et al., 2008). This is followed by the aBoc dependent on the motorneuron AVL, and finally, GABA release from the motoneurons AVL and DVB initiates the EMC and expulsion of gut contents (Beg and Jorgensen, 2003, McIntire et al., 1993). While activating mechanisms for the posterior muscle and DVB are known, DVB is activated by a neuropeptide (Wang et al., 2013a), the mechanisms by which AVL is activated has not been described (see CHAPTER 1, Figure 4).

A recent micropublication pointed out the synaptic and behavioural relationship between the expulsion of an egg during egg-laying and the expulsion step of the DMP (Ravi et al., 2019). These two circuits are synaptically connected as both the HSN

command neurons and VC4/5 motor neurons that regulate egg-laying make and receive synapses from AVL (White et al., 1986). Egg-laying is a stochastic behaviour characterised by active and inactive states, were eggs are expelled or retained in the uterus, respectively (Schafer, 2006, Waggoner et al., 1998, Trent et al., 1983). Interestingly, mutant worms lacking the HSN command neurons still lay eggs as the vulva muscles are still contracting, indicating that other mechanisms can induce egg-laying (Collins et al., 2016). Here, I am testing the hypothesis that both expulsive behaviours could be controlled by proton signalling.

My research has revealed for the first time that there are at least three acid-sensing DEG/ENaCs in *C. elegans*, however, how their proton-sensing properties translate to cellular function and behaviour have not been investigated. In the current chapter I will deepen the characterisation of the electrophysiological properties of ASIC-1, ACD-2 and DEL-9 that exhibited proton-activated currents in response to low pH. I will then focus on the role of DEL-9 as proton-receptor in the two contexts mentioned above, defecation and egg-laying, in order to understand how DEL-9 can contribute to the generation of muscle contractions in both neuronal and non-neuronal tissues.

4. 2. Results

4. 2. 1. ASIC-1, ACD-2 and DEL-9 can form proton-activated homomeric channels *in vitro*

Mammalian ASICs are activated by increasing amounts of protons with a characteristic half maximal activation at pH (pH_{50}) depending on the subunit compositions (Hesselager et al., 2004). Building on the findings described in CHAPTER 3, I investigated the responses to increasing proton concentrations of the homomeric ASIC-1, ACD-2 or DEL-9 channels by perfusing differing pH solutions over the oocytes expressing the respective construct. Results showed that for all three constructs acid-evoked currents increased in a concentration-dependent manner and reached an excitatory pH_{50} of 4.49 for ASIC-1, pH_{50} of 5.03 for ACD-2 and pH_{50} of 4.27 for DEL-9. (Figure 20). ASIC-1 co-expression with other subunits as well as several point mutations with the aim to alter pH sensitivity have been created but had little impact on the pH_{50} (Appendix D, Supplementary Figure 2, Supplementary Figure 3,

Supplementary Figure 4). All three homomeric channels do not desensitize but reach a plateau after several seconds, ASIC-1 and ACD-2 reach the plateau much faster than DEL-9 as shown by the timescale in Figure 20, which is not an artefact of the perfusion rate as the same perfusion rate was used for all oocytes and conditions. ACD-2 partially desensitises from proton concentrations at pH 4 (and below) which might reflect the channel's physiological pH range (Appendix D, Supplementary Figure 5).

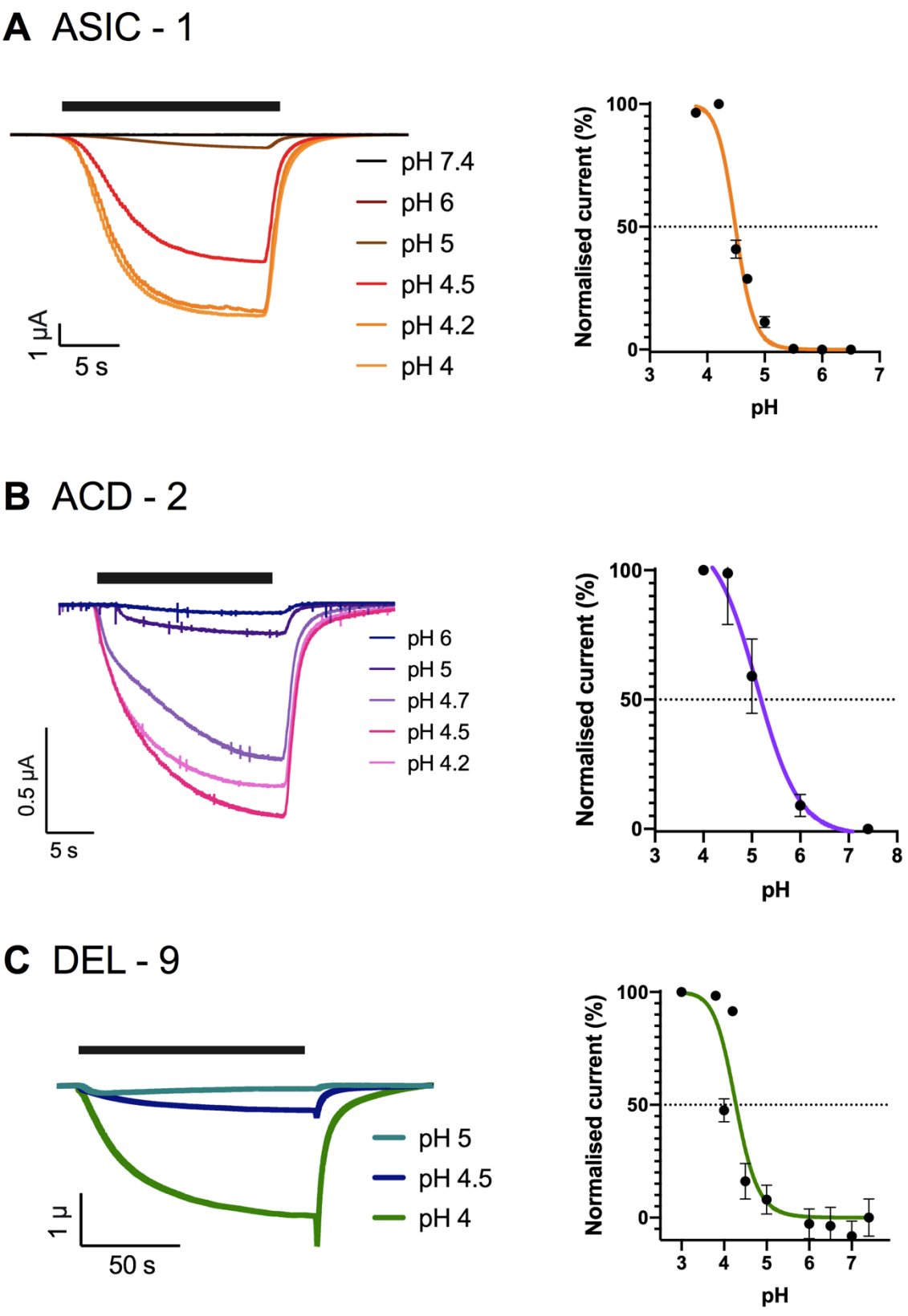

Figure 20: ASIC-1, ACD-2 and DEL-9 can form proton-activated homomeric channels in vitro.

Left: Representative traces of oocytes expressing the respective construct when perfused with solutions of different pH, lowering of pH (black bar) from a holding pH of 7.4. *Right:* Sensitivity to extracellular pH, dotted line presents the pH_{50}. (A) ASIC-1 is closed at neutral pH and gives rise to a non-desensitising current at low pH. Sensitivity of ASIC-1 to extracellular pH with a pH_{50} of 4.49 ± 0.02 (N = 13). (B) ACD-2 subunits can form proton-activated homomeric channels in *Xenopus* oocytes with a pH_{50} of 5.028 ± 0.109 (N = 6). (C) DEL-9 subunits can form proton-activated homomeric channels in *Xenopus* oocytes. Heterologously expressed DEL-9 homomeric channel perfused with solutions of differing pH with and pH_{50} of 4.27 ± 0.07 (N = 10). The channel is open at 100% current and completely closed at 0% current. Currents were recorded at a holding potential of – 60mV, normalized to maximal currents (I/I_{max}) and best fitted with the Hill's equation (Variable slope). Error bars represent Mean ± SEM.

4. 2. 2. ASIC-1 and ACD-2 homomeric channels can be blocked by amiloride

Amiloride is a potent blocker for DEG/ENaC channels (Schild et al., 1997, Kellenberger et al., 2003, Baconguis et al., 2014) and preliminary results in CHAPTER 3 have shown that amiloride can block acid-evoked currents of ASIC-1 and ACD-2 but not the acid-evoked currents of DEL-9. Here, I further investigated the nature of this block using dose-responses to varying concentrations of amiloride at pH_{50} concentrations (see Figure 20 for reference). Results showed that amiloride can block ASIC-1 acid-evoked currents with an IC_{50} of 134 µM and ACD-2 acid-evoked currents with an IC_{50} of 84 µM (Figure 21A, B).

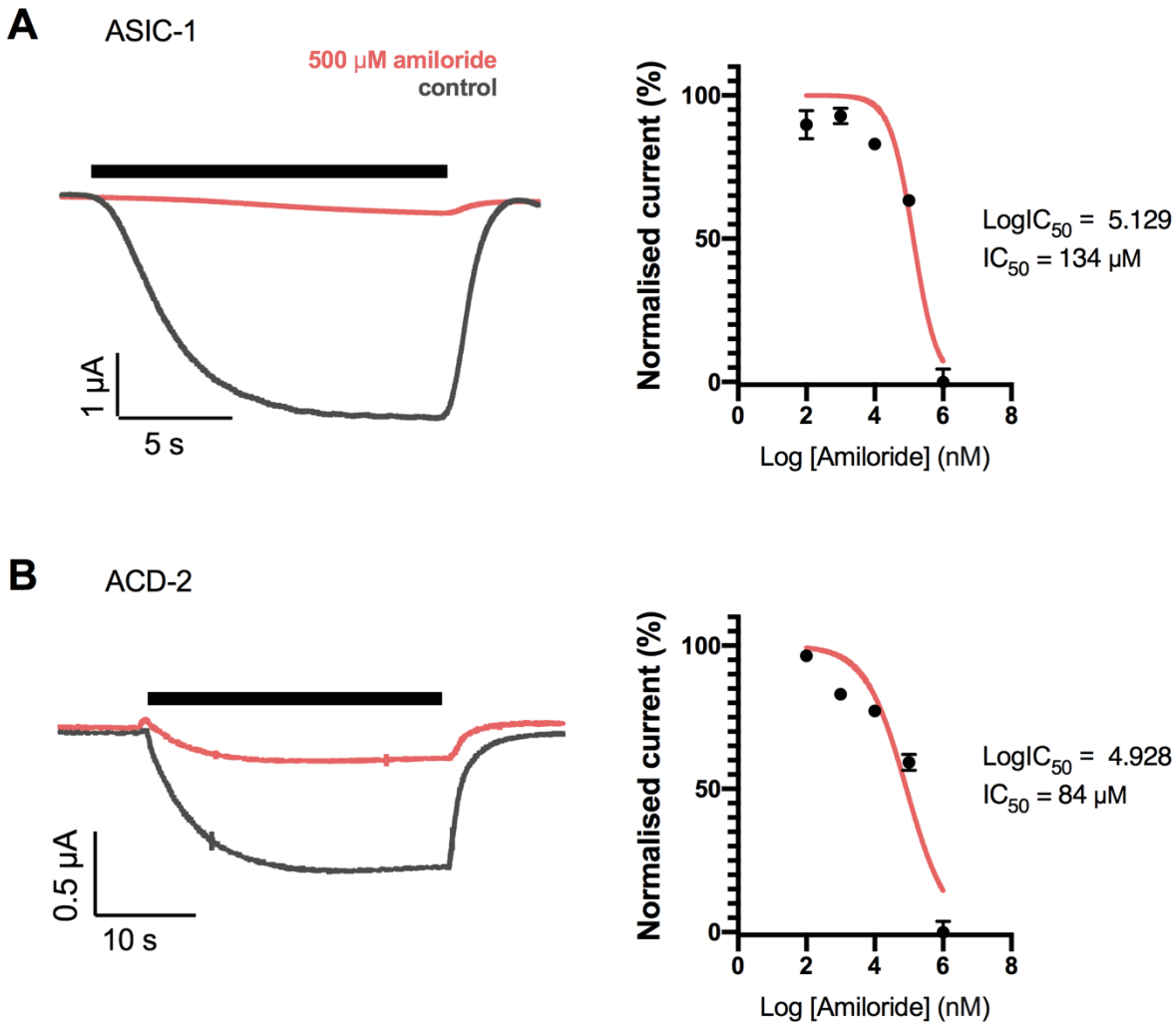

Figure 21: ASIC-1 and ACD-2 acid-evoked currents can be blocked by amiloride in a dose-dependent manner.

The black bar represents the time of perfusion of the solution at pH_{50} concentrations (black bar, see Figure 20 for reference) from basal condition of pH 7.4. Traces show perfusion with the control solution only (grey trace) or in presence of amiloride (light red trace). The channel is open at 100% current and completely closed at 0% current. Currents were recorded at a holding potential of - 60mV and are normalised to the maximum current (I_{max}) calculated for each oocyte individually, and best fitted with the Hill's equation (Variable slope). Error bars represent Mean ± SEM. (A) Left: Representative traces of ASIC-1 cRNA injected *Xenopus* oocytes. Right: Amiloride dose-response of ASIC-1 with an IC_{50} of 134 µM amiloride (N = 10). (B) *Left*: Representative traces of ACD-2 cRNA injected *Xenopus* oocytes. *Right*: Amiloride dose-response of ACD-2 with an IC_{50} of 84 µM amiloride (N = 12).

4. 2. 3. Proton-activated DEG/ENaCs channels are cation channels

I next investigated the ion selectivity of the proton-activated channels by carrying out ion substitution experiments. The experiments were performed at low pH at pH_{50} concentrations (see Figure 20 for reference) and the shift in reversal potential (ΔE_{rev}) was assessed after substituting NaCl with either KCl or LiCl in the solution containing 96mM NaCl, 1mM $MgCl_2$, 5mM MES based on a previous protocol (Hardege et al., 2015). The osmolarity was checked and if needed, D-Glucose was used to adjust osmolarity until within the error margins of 210 mosm (Awayda and Subramanyam, 1998). All ion-substitution experiments were conducted in the absence of Ca^{2+} as Ca^{2+} has shown to be able to block ASIC channels (Paukert et al., 2004). Results showed that ASIC-1 shows a preference of K^+ and Li^+ over Na^+ with a median positive shift in E_{rev} of 12.2 mV when shifting from a NaCl solution to a KCl or LiCl solution (Figure 22A, D). By contrast, the ACD-2 homomeric channel is a sodium channel that has a high preference for Na^+ and Li^+ over K^+ with no change in E_{rev} when switching from a NaCl to a LiCl solution, but a large median negative shift in E_{rev} of -43.3 mV when shifting from a NaCl solution to a KCl solution (Figure 22B, D). DEL-9 is cation unselective showing almost no shift in reversal potential when switching between solutions (Figure 22C, D).

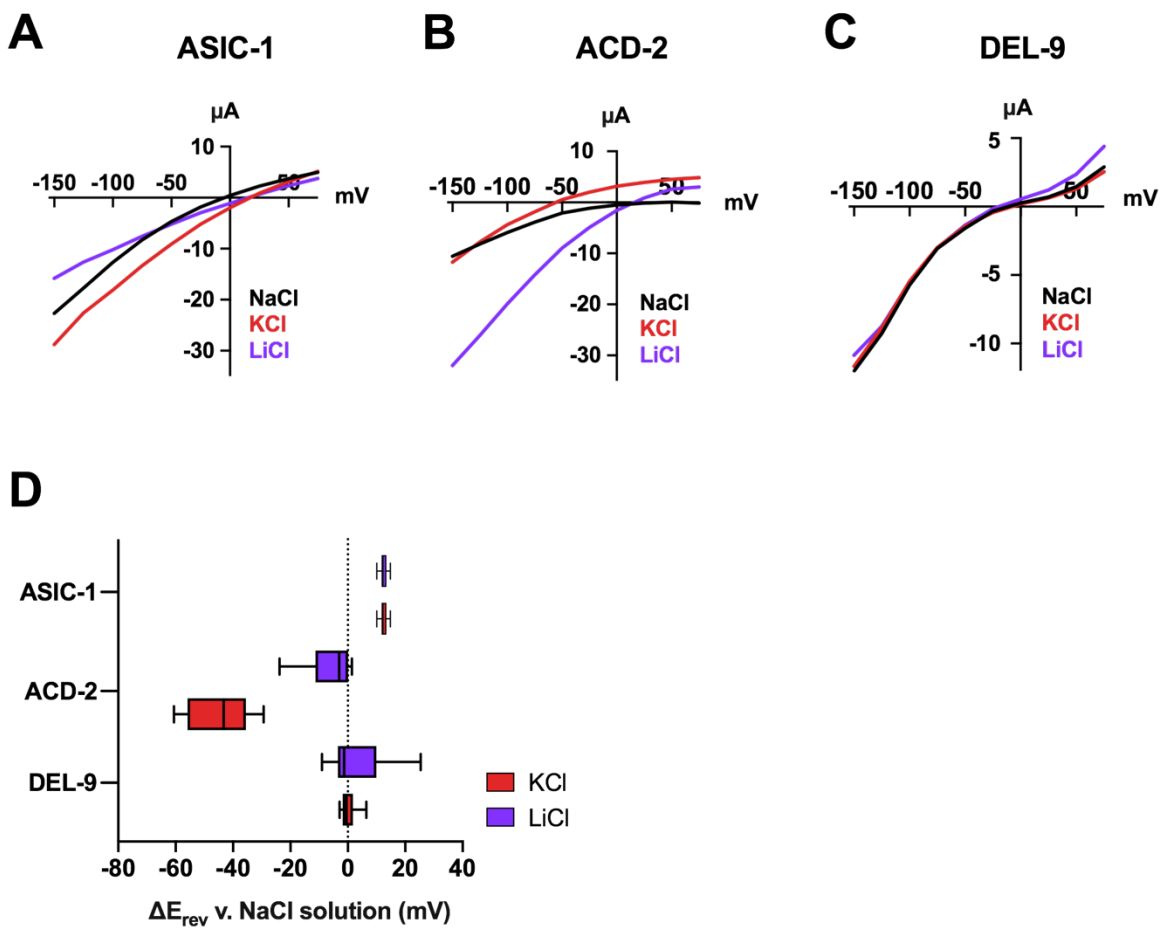

Figure 22: Ion selectivity of ACD-2, ASIC-1 and DEL-9.

(A)-(C) Representative current-voltage (IV) relationships for *Xenopus* oocytes expressing ASIC-1, ACD-2 and DEL-9. Actual current for each oocyte and baseline current subtracted from acid-evoked current at pH_{50} concentrations (see Figure 20 for reference). (D) Average calculated from 4<N<12 oocytes for each construct of ΔE_{rev} when shifting from a NaCl solution to KCl or LiCl solution. A negative shift of E_{rev} indicating a preference for Na^+ over the respective ion and a positive shift indicating a preference of the respective ion over Na^+. Data is presented as box-plots (hinges of the plot are the 25th to 75th percentiles) with Median and whiskers of 1.5IQD (inter-quartile distance, as calculated by the Tukey method).

4. 2. 4. DEL-9 is involved in execution of the rhythmic muscle contraction during the defecation motor program

Based on the expression of DEL-9 in the AVL neuron that participates in the DMP (Figure 23A), I examined the rhythmicity of DMP muscle contractions in animals expressing either of the two mutant alleles *del-9(ok2353)* or *del-9(lj142)* (Figure 23B, C). The *del-9(ok2657)* mutation was obtained from the CGC and is a deletion that removes the extracellular loop, but parts of the N- and C-termini are still in frame with

each other, so they might still be able to form a protein. By contrast, the *del-9(lj142)* allele was created by me using CRISPR/Cas9 as a method to generate a deletion that removes the predicted N-terminal fragment, with the remainder of the gene lacking a start site and being out of frame, so it is expected that no protein is generated. Findings showed that the DMP average cycle length was similar to the wild-type (Figure 23D), however, on average in 19% and 13% of the cycles, *del-9(lj142)* and *del-9(ok2353)* mutants completely lacked a visible EMC (Figure 23E). Overexpression of the DEL-9 subunit in wild-type could mimic this phenotype and increased the frequency of missed EMCs to on average in 8.5 % (Figure 23E). This phenotype is consistent with a role of DEL-9 in the AVL neuron showing that DEL-9 is involved in the execution of the EMC. The missed EMCs could only be rescued in *del-9(lj142)* mutants by expressing *del-9* genomic DNA (gDNA) under its endogenous promoter (Figure 24A). In order to determine if *del-9* was cell-autonomously required in neurons or in the GABAergic AVL neuron, I used a pan-neuronal promoter (*Prab-3*) and the *unc-47* promoter expressed in the GABAergic neurons driving *del-9* genomic DNA for the rescue experiments (AVL, DD, DVB, RIS, RME and VD (McIntire et al., 1993)). Neither of the neuronal promoters was able to rescue the missed EMCs and some of the overexpression lines disrupt the frequency of EMCs even further (Figure 24A, B). This finding suggests that level of expression of *del-9* is important for wild-type functioning which could explain why the rescues were unsuccessful. Furthermore, ectopic expression of *del-9* when using a pan-neuronal promoter or GABAergic neuron-specific promoter could further complicate matters. However, *del-9* might not exclusively be required in neurons but might additionally act in muscles to elicit EMCs.

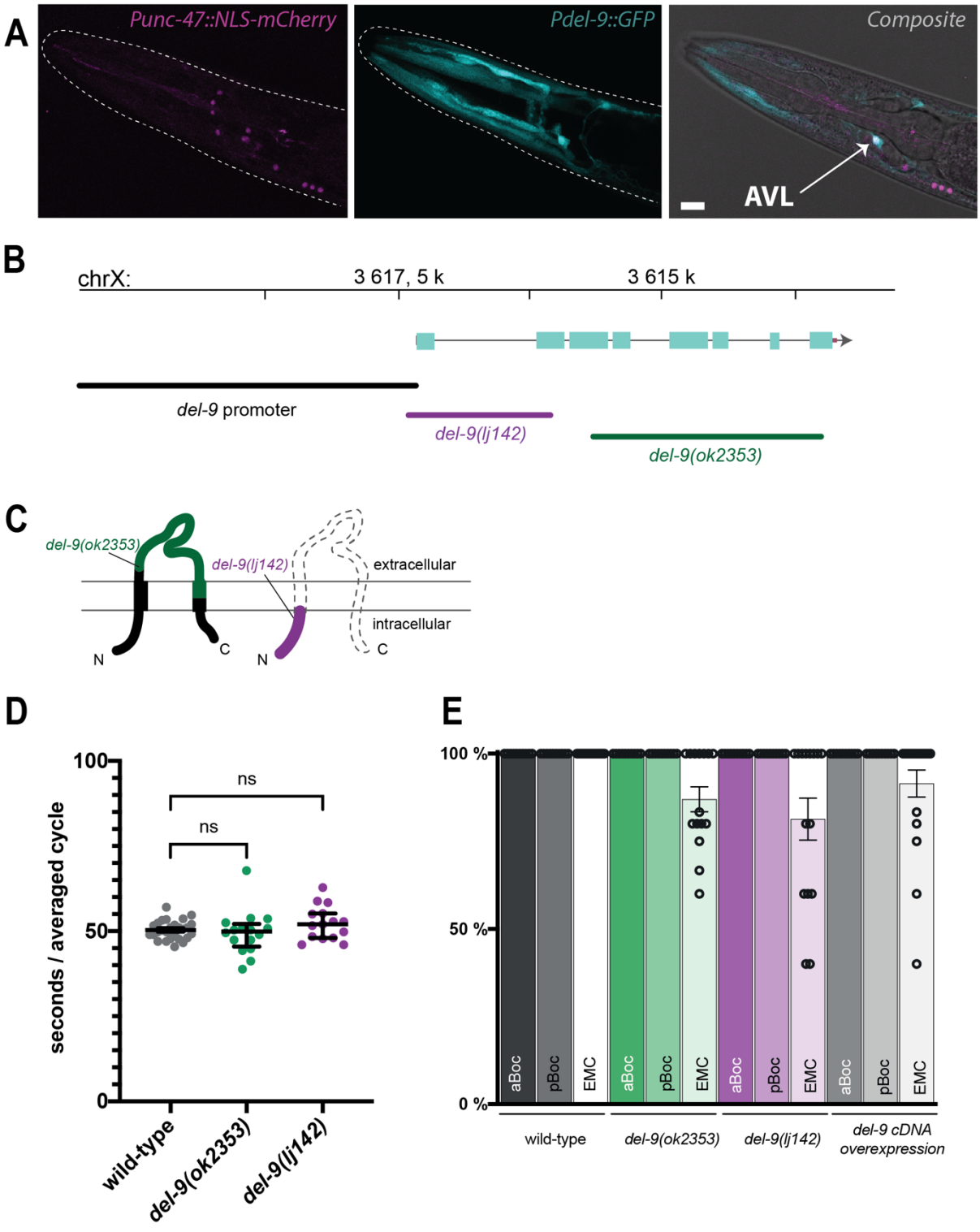

Figure 23: DEL-9 is involved in initiating the expulsion step during the rhythmic contractions of the DMP.

(A) DEL-9 is expressed in AVL. Overlap of the *del-9* promoter driving GFP (*ljEx1361[Pdel-9::GFP])* in the cytoplasm and a *Punc-47* promoter driving a nuclear localization signal (NLS) fused mCherry (*Punc-47::NLS-mCherry)* in the nucleus of the AVL neuron in the head of the animal. Scale bars are 10 µm. (B) *del-9* genomic region on chromosome X. Boxes indicate exons and lines indicate introns. Endogenous promoter region and mutations used in the study are shown. (C) Schematic of predicted DEL-9 protein structure with two transmembrane domains, and cytosolic N- and C-termini and an extracellular loop, typical of DEG/ENaC subunits. Mutations used in the study are indicated in green for *del-9(ok2657)*. The *del-9(lj142)* mutation, in purple, is a putative null-mutation deleting the start codon, the first exon and part of the second exon. (D) Defecation cycle interval length is not affected by either *del-9* mutant allele as indicated by a Kruskal-Wallis test (H = 2.82, p=0.245, ns; $Mdn_{wild\text{-}type}$= 50.2 sec; $Mdn_{del\text{-}9(lj142)}$ = 49.9 sec; $Mdn_{del\text{-}9(ok2353)}$= 52 sec). (E) Behavioural characterization of DMP muscle contraction. aBoc (anterior body contraction), pBoc (posterior body contraction) and EMC (enteric muscle contraction) in wild-type, *del-9(lj142)* and *del-9(ok2353)* mutants and overexpression of *del-9* genomic DNA (*ljEx1437*) in the wild type. Five defecation cycles in day 1 adult animals were scored for the presence or absence of each muscle contraction (n ≥ 15 for each genotype). Mean ± SEM are represented.

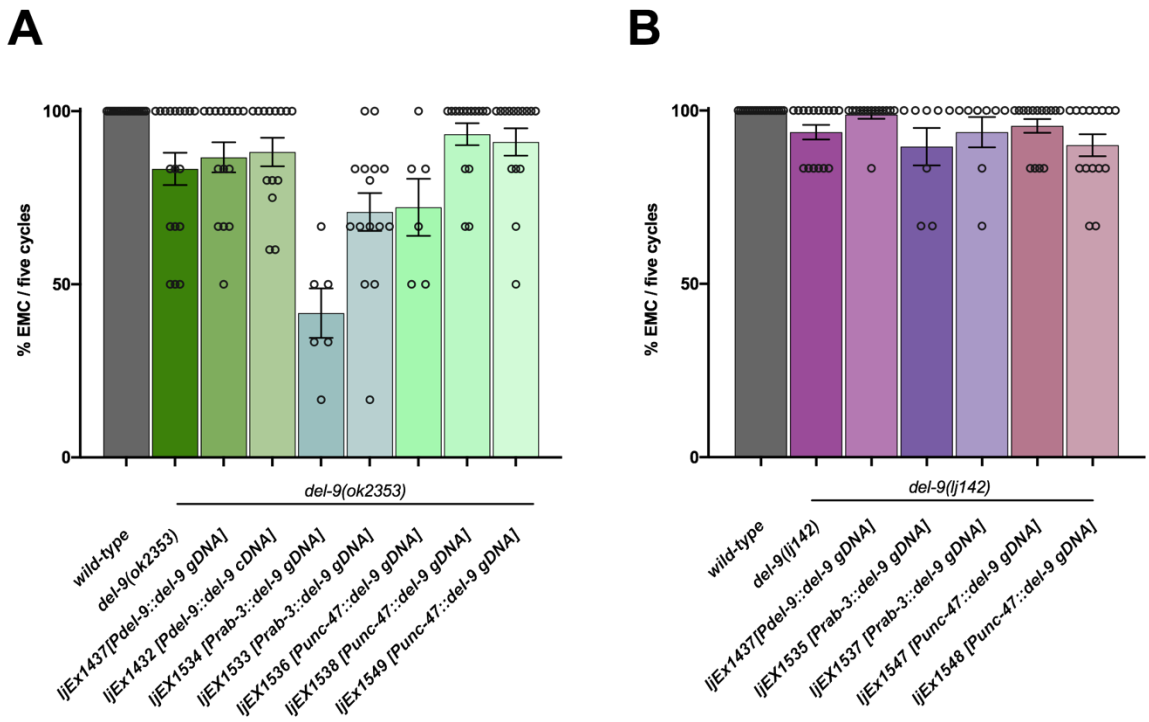

Figure 24: Neuron-specific del-9 expression does not restore missed EMCs.

Overexpression of *del-9* under promoter expressed in GABAergic neurons (*Punc-47*), under its endogenous promoter or under a pan-neuronal promoter (*Prab-3*) exacerbates missed EMCs. Several different transgenic lines were tested. Percentage of EMCs in five consecutive defecation cycles in animals expressing rescue extrachromosomal arrays in an (A) *del-9(ok2363)* and (B) *del-9(lj142)* mutant backgrounds. Mean ± SEM are represented (5>N>20).

4. 2. 5. *del-9* mutations affect timing of egg-laying events

DEL-9 is expressed in both the AVL motoneuron and the vulva muscles (CHAPTER 3, Figure 12), therefore, I wanted to investigate whether *del-9* mutants show defects in egg-laying behaviour by assessing active and inactive states of egg-laying using a three state model previously developed (Figure 25A) (Waggoner et al., 1998). Egg-laying in this model is determined by three parameters; p is the probability of another egg being laid after a given egg-laying event but before the animal enters the inactive phase. This results in short intervals from a single active state governed by the rate constant λ_1. Long intervals in this model result from the inactive state governed by rate constant equal to $p\lambda_2$ (Tong Zhou, 1998, Waggoner et al., 1998). I found that *del-9* mutants' active states were similar to the wild-type with 40 seconds and 38 for the *del-9(lj142)* and 39 seconds for *del-9(ok2353)*. However, intervals for inactive states were significantly prolonged for both mutants, with 40 min for the *del-9(ok2353)* mutant and 32 min for the *del-9(lj142)* mutant, compared to approximately 23 min of inactive phases of the wild-type (Figure 25B). Consistent with these finding, *del-9* mutants also lay on average four eggs per hour which is significantly less eggs than the wild-type with almost six eggs per hour (Figure 25C). This finding that *del-9* mutants show longer inactive states supports the hypothesis that DEL-9 is involved in the regulation of timing of egg-laying events.

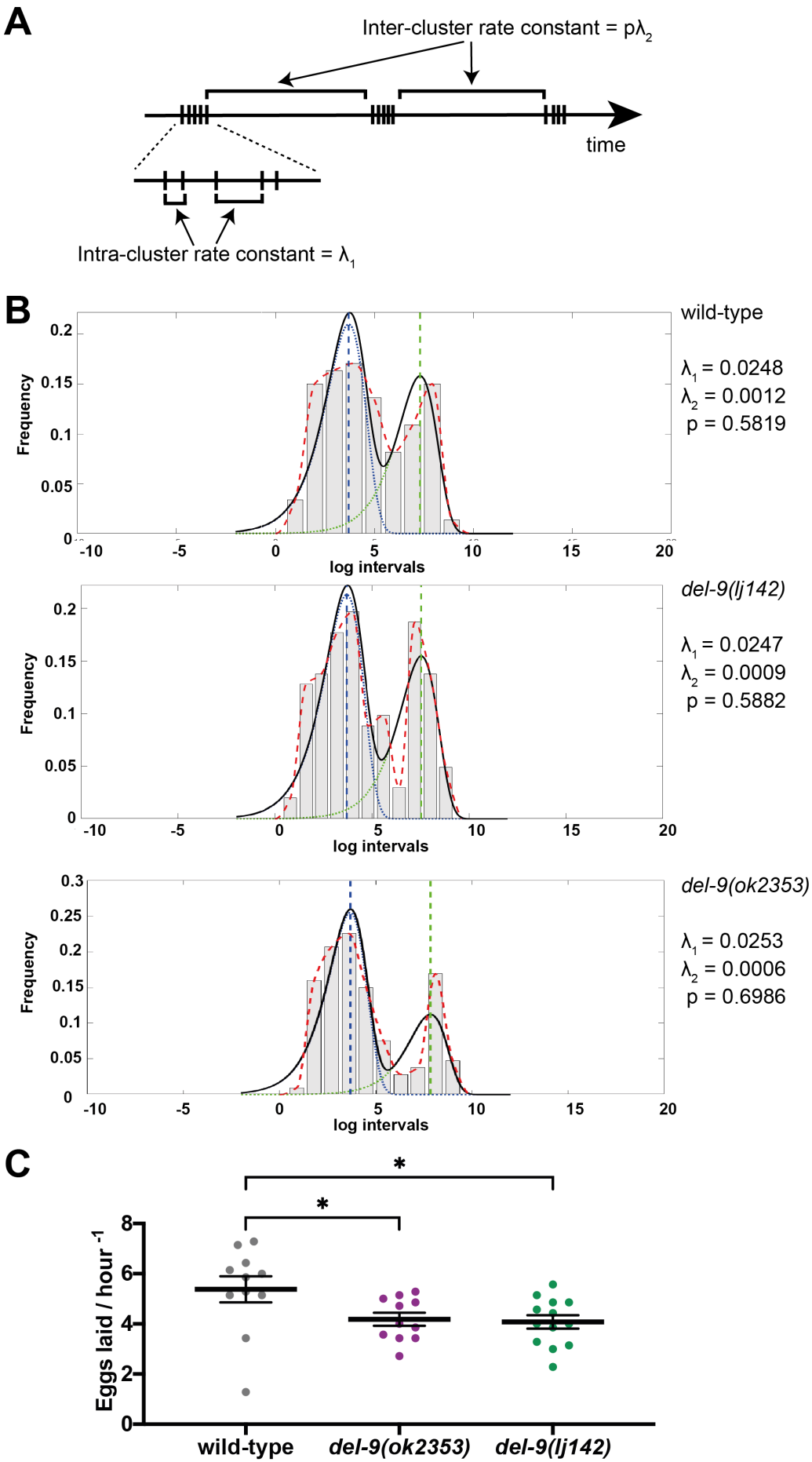
A
Inter-cluster rate constant = pλ2
time
Intra-cluster rate constant = λ1
B
wild-type
λ1 = 0.0248
λ2 = 0.0012
p = 0.5819
del-9(lj142)
λ1 = 0.0247
λ2 = 0.0009
p = 0.5882
del-9(ok2353)
λ1 = 0.0253
λ2 = 0.0006
p = 0.6986
Frequency
log intervals
C
Eggs laid / hour -1
wild-type
del-9(ok2353)
del-9(lj142)

Figure 25: del-9 mutations affect intra-cluster intervals of egg-laying events.

(A) Parameters of egg-laying behaviour (adapted from (Waggoner et al., 1998)). Shown is a representative time line, with egg-laying events indicated by hash marks, for a description see main text. (B) Histograms and parameters of temporal egg-laying data of wild-type in the top graph, the *del-9(lj142)* mutant in the middle graph, and the *del-9(ok2353)* mutant on the bottom graph. Natural log of the interval times on the x-axis, with the relative frequency on the y-axis. The dotted lines indicate the ideal distribution based on maximum likelihood (ML) analysis of the real data. Parameters p, λ_1 and λ_2 are indicated. (C) A non-parametric Kruskal-Wallis test was conducted and showed statistically significant differences between the wild-type and the mutants (H(2) =6.89, *p =0.013). The follow up Dunn's multiple comparisons test indicated that both, the *del-9(lj142)* mutant (Mdn $_{del\text{-}9(lj142)}$ = 4.00, N=12, *p=0.013) and *del-9(ok2353)* mutant (Mdn $_{del\text{-}9(ok2353)}$ = 4.00, N=14, *p=0.035) laid significantly less eggs compared to the wild-type (Mdn $_{wild\text{-}type)}$ = 5.86; N=12). Worms that crawled off the plate were excluded from the analysis. Error bars represent Median and IQR.

4. 2. 6. DEL-9 acts cell-autonomously in the vulva muscles to promote egg-laying

To exclude a deficiency in egg-production, I further investigated egg-retention, a phenotype where eggs are retained in the uterus instead of being laid which could explain the phenotype observed above where *del-9* mutants lay significantly fewer eggs. I found that both *del-9* mutants retain significantly more eggs compared to the wild-type (Figure 26A). This phenotype could be copied by *del-9* RNAi feeding (Appendix D, Supplementary Figure 6). Egg-retention could be rescued by expressing *del-9* cDNA or *del-9* gDNA under its endogenous promoter (Figure 26A). Next, I investigated whether the egg-retention phenotype was due to DEL-9 expression in AVL or the vulva muscles and found that egg-retention could be rescued by overexpressing *del-9* under a vulva muscle specific promoter (*Punc-103e (Collins and Koelle, 2013)*), demonstrating that DEL-9 acts cell-autonomously in the vulva muscles (Figure 26B). A construct containing the *unc-103* promoter only did not affect egg-retention (Figure 26A, B). Overexpression of *del-9* cDNA or gDNA in the wild-type did not cause any phenotype (Figure 26A), however, a small but statistically significant reduction of egg-laying was observed when expressing *del-9* cDNA in AVL (Figure 27A). One hypothesis is that this could be due to a reduction of GABA which might be involved in egg-laying, as mutants deficient for GABA also show a small but significant increase in egg-retention imply a role of GABA in egg-laying behaviours (Figure 27B).

A

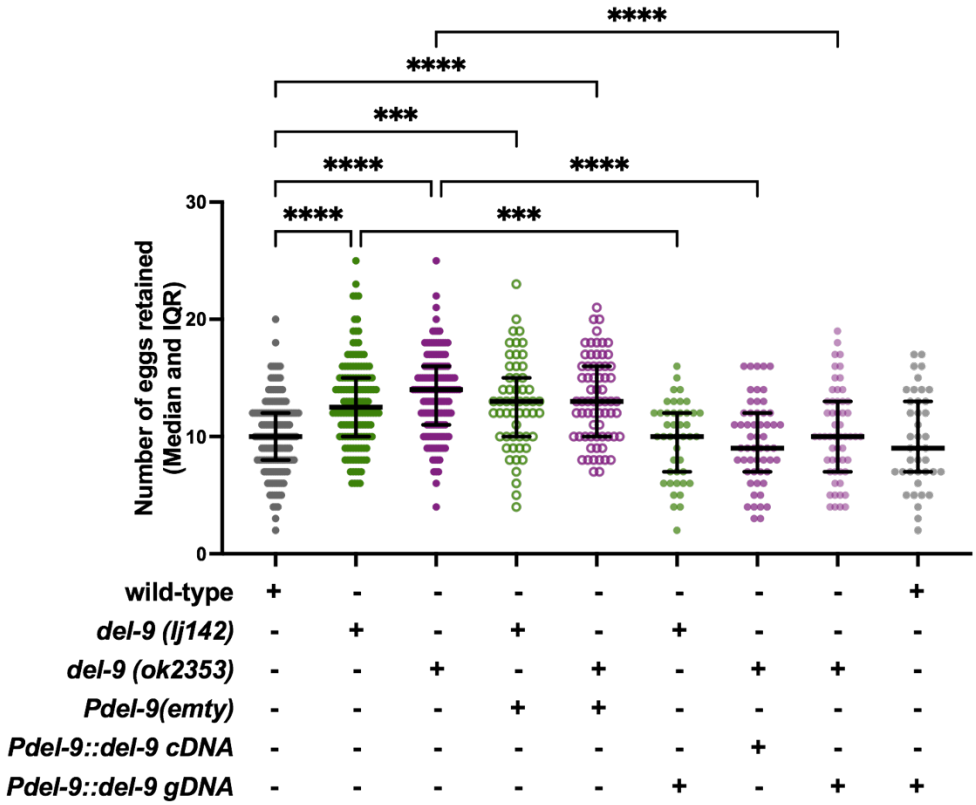
****
****
***
****
****
****
***
Number of eggs retained
(Median and IQR)
30
20
10
0
wild-type + - - - - - - - +
del-9 (lj142) - + - + - + - - -
del-9 (ok2353) - - + - + - + + -
Pdel-9(emty) - - - + + - - - -
Pdel-9::del-9 cDNA - - - - - - + - -
Pdel-9::del-9 gDNA - - - - - + - + +

B

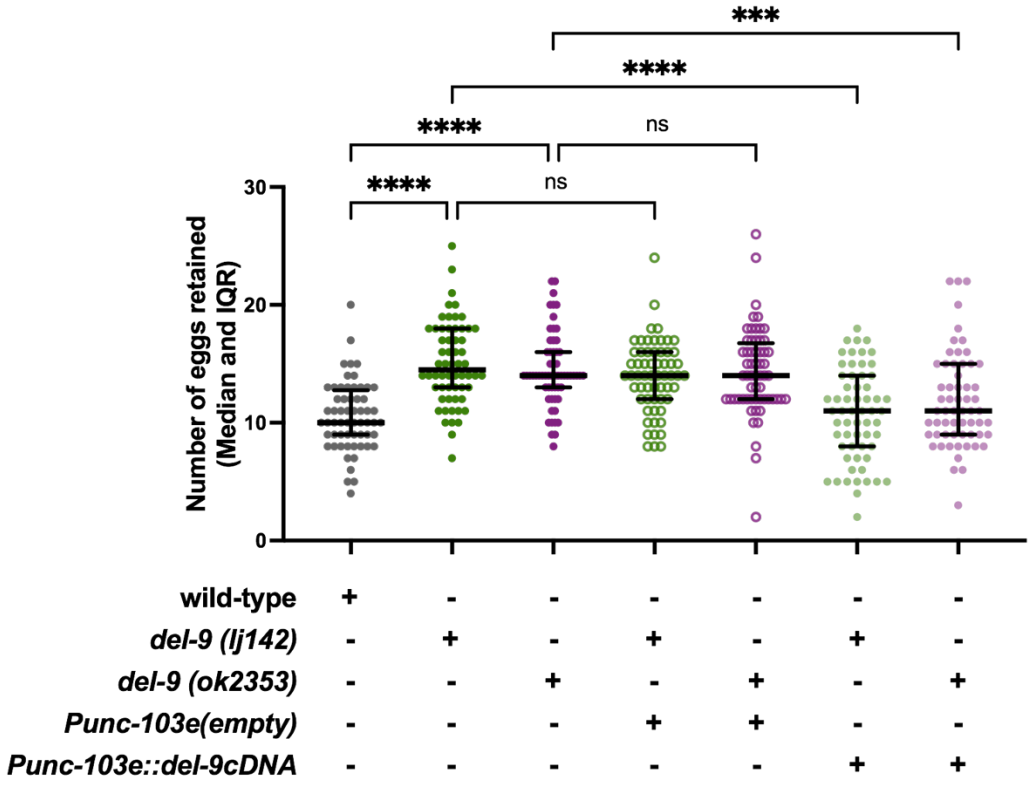
***
****
****
ns
****
ns
Number of eggs retained
(Median and IQR)
30
20
10
0
wild-type + - - - - - -
del-9 (lj142) - + - + - + -
del-9 (ok2353) - - + - + - +
Punc-103e(empty) - - - + + - -
Punc-103e::del-9cDNA - - - - - + +

Figure 26: del-9 expression in the vulva muscles rescues the egg-retention phenotype.

(A) For clarity, only statistically significant differences are indicated in this panel. A Kruskal-Wallis test was highly significant [H(8) = 124.3, ****p <0.0001]. The follow up Dunn's multiple comparisons test indicated that compared to the wild-type (Mdn $_{wild\text{-}type}$ = 10, N=142), the *del-9(lj142)* (Mdn $_{del\text{-}9(lj142)}$ = 12.85, N=140, ****p <0.0001) and *del-9(ok2353)* (Mdn $_{del\text{-}9(ok2353)}$ = 13.57 ± 0.289, N=142, ****p <0.0001) mutants retained significantly more eggs as did the mutants expressing the empty *del-9* promoter (Mdn $_{del\text{-}9(lj140);\ ljEx1583\ [Pdel\text{-}9\ (empty)]}$=13, N=67, ****p <0.0001; Mdn $_{del\text{-}9(ok2353);\ ljEx1582\ [Pdel\text{-}9\ (empty)]}$=13, N=55, ****p <0.0001) . This defect could be rescued by expressing the genomic DNA or the cDNA under the *del-9* transcriptional promoter (Mdn$_{del\text{-}9(lj142);\ ljEx1437[Pdel\text{-}9::del\text{-}9\ genomic\ DNA]}$= 10, N=43, p>0.9999, ns; Mdn $_{del\text{-}9(ok2353)+\ cDNA}$ rescue = 9, N=55; Mdn $_{del\text{-}9(ok2353);\ ljEx1437[Pdel\text{-}9::del\text{-}9\ genomic\ DNA]}$= 10, N=55, p>0.9999, ns). (B) A Kruskal-Wallis test was highly significant [H(6) = 91.70, ****p <0.0001], a follow up Dunn's multiple comparisons test indicated that *del-9(lj142)* (Mdn $_{del\text{-}9(lj142)}$= 14.50, ****p <0.0001) and *del-9(ok2353)* (Mdn $_{del\text{-}9(ok2353)}$ =14, ****p <0.0001) mutants retained significantly more eggs compared to the wild-type (Mdn $_{wild\text{-}type}$= 10.53), so did the *unc-103e* promoter only control (Mdn $_{del\text{-}9(ok2353);\ ljEx1590\ [Punc\text{-}103e\ (empty)]}$= 14, ****p <0.0001; Mdn $_{del\text{-}9(lj140);\ ljEx1589\ [Punc\text{-}103e\ (empty)]}$= 14.00, ***p=0.0003). This defect could be rescued by expressing *del-9* cDNA under the vulva muscle specific transcriptional *unc-103e* promoter (Mdn $_{del\text{-}9(lj142);\ ljEx1591\ [Punc\text{-}103e::del\text{-}9\ cDNA]}$ = 11, p>0.9999, ns; Mdn$_{del\text{-}9(ok2353);\ ljEx1579\ [Punc\text{-}103e::del\text{-}9\ cDNA]}$= 11, p=0.3721, ns). N=60 for all conditions. Error bars are presented as Median and IQR.

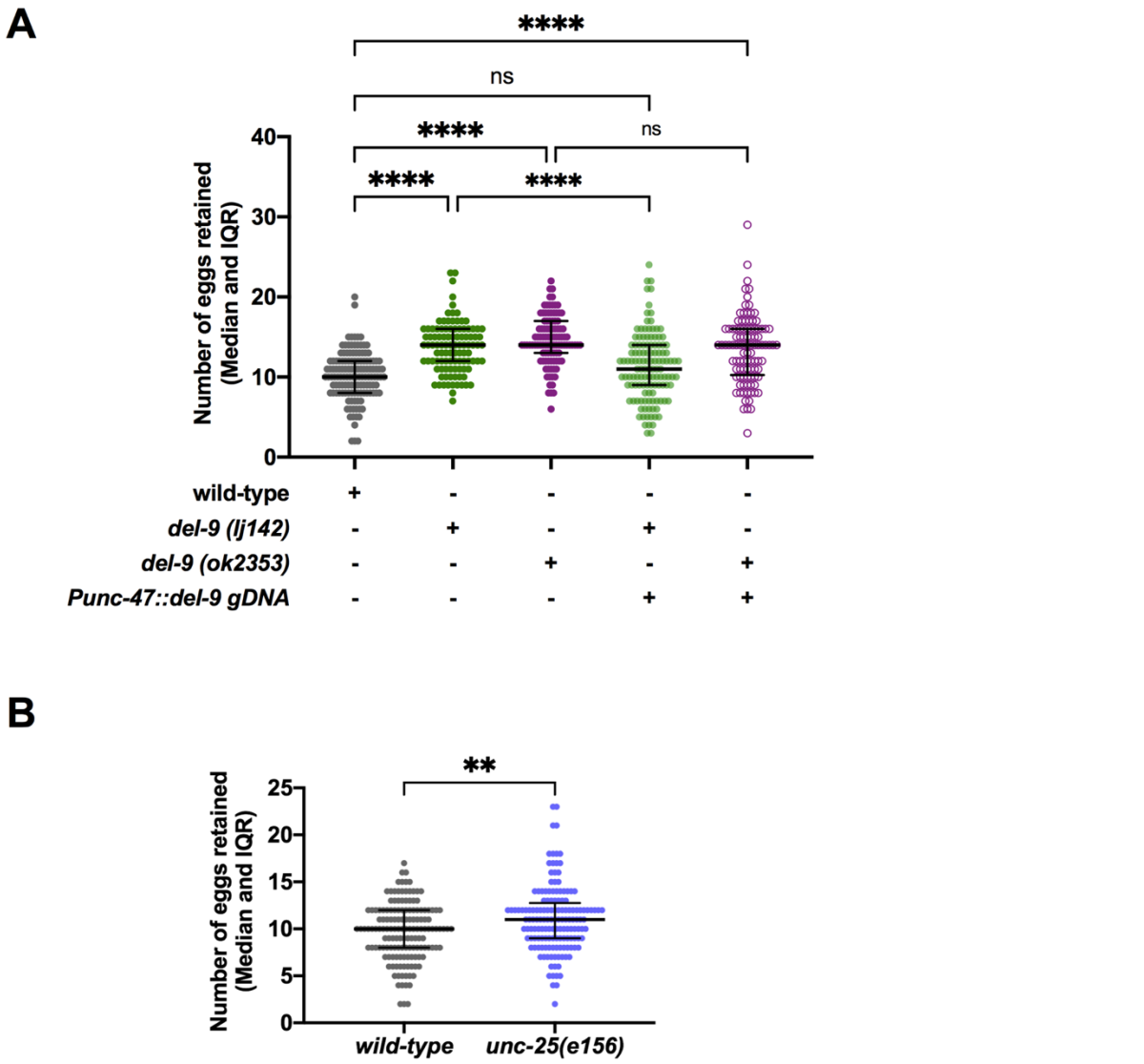

Figure 27: Egg-retention phenotype of del-9(lj142) can be rescued by expression of del-9 in GABAergic neurons.

(A) Mutations that affect AVL functioning results in an increase in egg-retention which can be partially rescued when overexpressing *del-9* in the GABAergic neurons (under the *unc-47* promoter). A non-parametric Kruskal-Wallis test was significant (H(4) = 126.5, ****p<0.0001), and a post-hoc Dunn's multiple comparisons test showed that the *del-9* mutants ($Mdn_{del\text{-}9(lj142)}$= 14,****p<0.0001; $Mdn_{del\text{-}9(ok2353)}$=14,****p<0.0001) retain significantly more eggs than the wild-type (Mdn=10). This could be rescued for the *del-9(lj142)* mutant when overexpressing *del-9* in the GABAergic neurons (Mdn=11, p=0.87, ns) but not for the *del-9(ok2353)* mutant (Mdn=14, ****p<0.0001). (B) GABA mutants also show a small but significant increase in egg-retention. *unc-25(e156)* mutants retained more eggs (Mdn = 11) than the wild-type animals (Mdn = 10). A Mann-Whitney test indicated that this difference was statistically significant, $U(N_{unc\text{-}25(e156)}$ = 148, $N_{wild\text{-}type}$= 149) = 8851, **p=0.0031. Error bars represent Median and IQR.

4. 2. 7. Preliminary genetic evidence supports the hypothesis of proton signalling being involved in egg-laying behaviours

One missing piece of the puzzle is *in vivo* evidence for protons contributing to egg-laying behaviours. In order to provide genetic evidence to address this issue, I tested whether mutants for the intestinal Na^+/H^+ exchanger *pbo-4/nhx-7* displayed similar increased egg-retention behaviours compared to the *del-9* mutants, and whether in double mutants this effect would be even larger. Result from this experiment showed that compared to the wild-type, *pbo-4* mutants retain fewer eggs in the uterus (Figure 28). Double mutants between *del-9* and *pbo-4* have a similar phenotype to the *pbo-4* single mutants (Figure 28). While this is far from being conclusive evidence, it suggests that *pbo-4* might be upstream of the *del-9* signalling cascade. However, further direct evidence is needed to confirm that protons from the intestine might be the source of protons by which *del-9* gets activated (see Discussion).

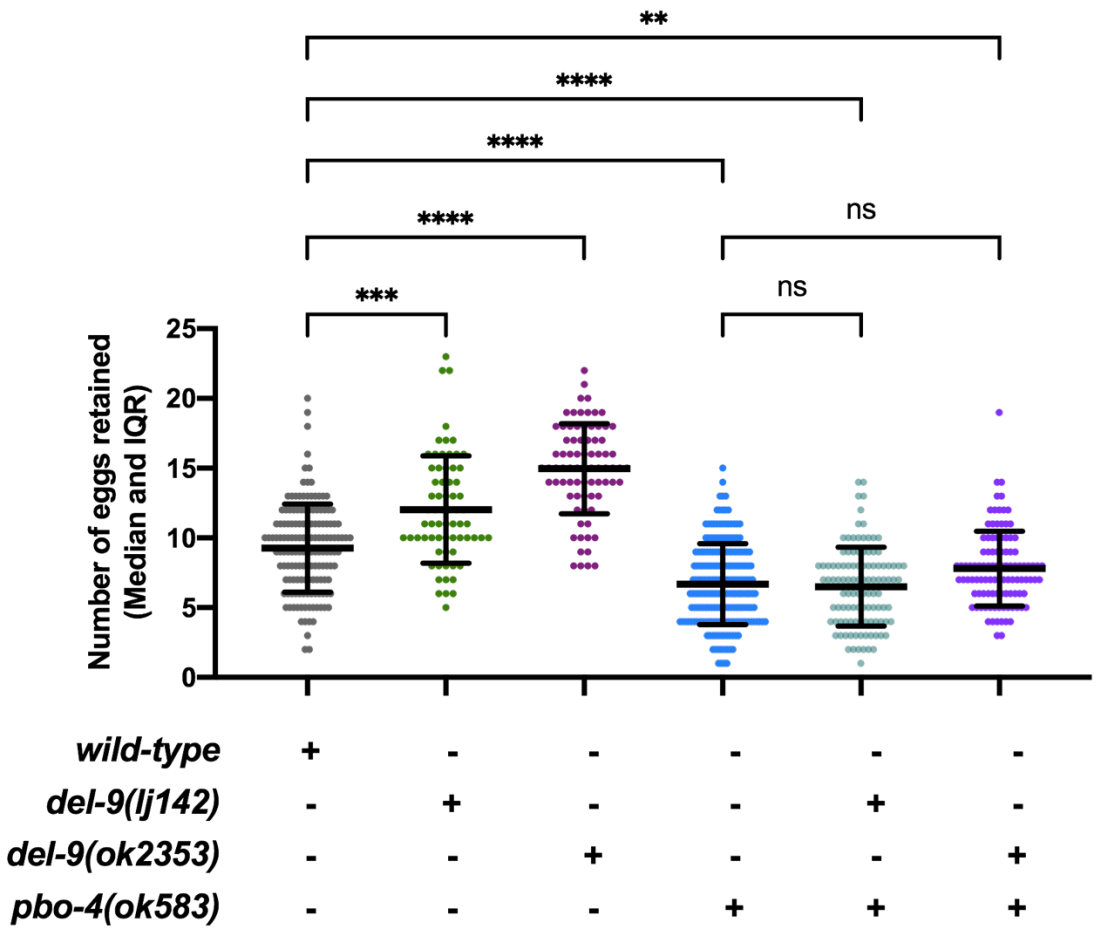

Figure 28: pbo-4 might act genetically upstream of del-9.

Kruskal-Wallis test conducted was statistically significant (H(5) = 273.6, ***p<0.0001). Post-hoc analyses using Dunn's multiple comparisons test indicated that compared to the wild-type ($Mdn_{wild\text{-}type}$= 9 eggs) all mutants tested retained significantly more or fewer eggs ($Mdn_{del\text{-}9(lj142)}$= 11 eggs, z =3.98, ***p=0.0005; $Mdn_{del\text{-}9(ok2353)}$= 15 eggs, z =7.76, ****p<0.0001; $Mdn_{pbo\text{-}4(ok583)}$= 6, ****p<0.0001; $Mdn_{pbo\text{-}4(ok583);del\text{-}9(lj142)}$= 7 eggs, p<0.0001; $Mdn_{pbo\text{-}4(ok583);del\text{-}9(ok2353)}$= 7.5 eggs, **p=0.0055). However, there was no statistically significant change between the pbo-4 single mutants and the *del-9* double mutants ($p_{pbo\text{-}4(ok583);del\text{-}9(lj142)}$>0.99, and $p_{pbo\text{-}4(ok583);del\text{-}9(ok2353)}$=0.94, ns). Error bars represent Median and IQR.

4. 2. 8. *In vivo* localisation of DEL-9

Another issue is that, while I have shown that DEL-9 is expressed in muscles and neurons, the precise localisation has not been described. For formulating hypotheses about its cellular functioning, knowing the subcellular localisation is critical. To address this, I tagged DEL-9 with the red fluorophore mKate2, and expressed it under its endogenous promoter. Results are shown in Figure 29. While there is some diffused fluorophore in the cells, which is likely due to overexpression, DEL-9 localisation can be seen in discrete puncta in the different cell-types. Along axons of what is likely to be PVQ, DEL-9 localisation looks similar to what has previously been reported for the tagged MEC-4 puncta along the touch neurons (Chelur et al., 2002). The tagged DEL-9 can also be seen in puncta on the soma of neurons in the head and in the tail, as well as puncta along the muscles. However, further co-localisation experiments are needed to confirm the precise subcellular localisation within each tissue.

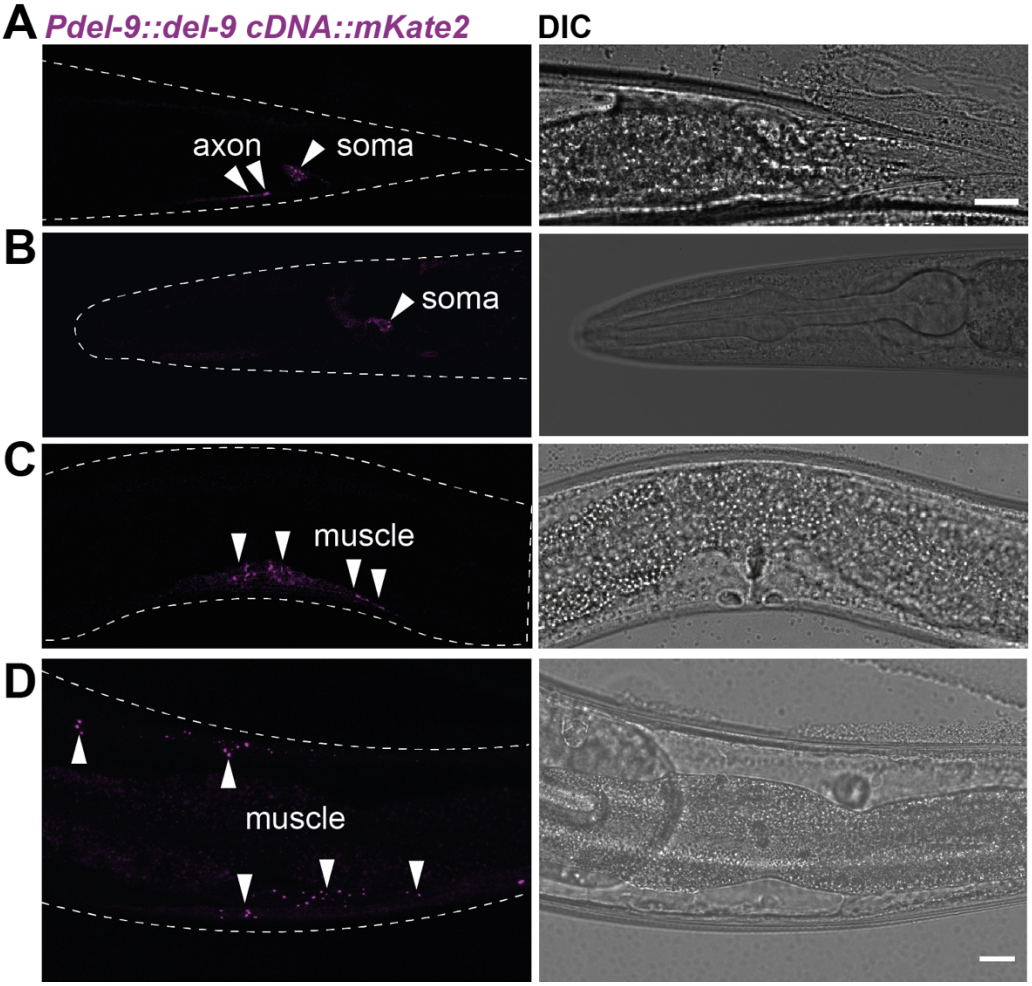

Figure 29: Tagged DEL-9 is expressed in puncta in neurons and muscles.

Localisation of DEL-9::mKate2 expressed under its endogenous promoter *ljEx1546 [Pdel-9::del-9 cDNA::mKate2]* (mixed stages adult worms). (A) DEL-9 expression in the tail on the soma and the axon of a neuron (likely to be PVQ). (B) DEL-9 expression in a head neuron, puncta can be seen on the soma. (C) DEL-9 puncta in the vulva muscles. (D) Puncta along the body of the animal, likely to be body-wall muscles. Puncta are indicated with white arrow heads. Scale bars 10µm.

4. 3. Discussion

In the current chapter, I have expanded on the findings in CHAPTER 3 where I had demonstrated for the first time that there are at least three *C. elegans* acid-sensing DEG/ENaCs, ASIC-1, ACD-2 and DEL-9. All three candidates are cation channels and can be activated in a proton-concentration dependent manner. ACD-2 is a sodium channel selective for Li^+ and Na^+ over K^+. The ion selectivity property is similar to the one previously described for DELM-1 (Han et al., 2013). ASIC-1 has a small preference for Li^+ and K^+ over Na^+ and DEL-9 is unselective for monovalent cations.

This fits in with previous findings that the DEG/ENaCs are a diverse family in their ion selectivity properties (Canessa et al., 1994, Wang et al., 2008, Fechner et al., 2020, Carattino and Della Vecchia, 2012). ASIC-1 and ACD-2 are sensitive to amiloride and acid-evoked currents can be blocked in a dose-dependent manner which is also a common characteristic of the DEG/ENaC super-family (Vullo and Kellenberger, 2020).

Nevertheless, the current findings bear the question of the channels' actual function *in vivo*, especially whether these channels would encounter a prolonged low acidic environment under physiological conditions. Relating the current findings to previous research we can speculate about the *in vivo* function of ASIC-1. For instance, the murine ASIC1 is activated by protonergic neurotransmission which might be comparable with a short increase in acidification due to neurotransmission but could also present a highly variable acidic environment depending on the rate of exocytosis (Du et al., 2014). The electrophysiological properties of the worm ASIC-1 were previously unknown but here I have shown that ASIC-1 can also be activated by external protons in a concentration-dependent manner. Therefore, one can speculate that likewise ASIC-1 might be involved in synaptic transmission. This would fit in well with previous behavioural and genetic research showing that the *C. elegans* ASIC-1 localizes at presynaptic terminals of dopaminergic neurons and enhance dopamine release required for associative learning (Voglis and Tavernarakis, 2008). *C. elegans asic-1* mutants show a lower rate of neurotransmitter release at dopaminergic synapses implicating ASIC-1 in modulating dopamine release. My electrophysiological characterisation of ASIC-1 *in vitro* supports the proposed working model by the Tavernarakis lab. That is, ASIC-1 at the presynaptic terminal is activated by a local drop in pH during the release of dopamine from the pre-synaptic terminal and this activation of ASIC-1 is likely to promote sustained dopaminergic signalling (Voglis and Tavernarakis, 2008).

In contrast to ASIC-1, *in vivo* function of ACD-2 has not yet been investigated. Given its expression pattern expression in head neurons or glia (CHAPTER 3), ACD-2 is likely to be involved in modulating synaptic function similar to what has previously been described for the *C. elegans* ASIC-1 or modulating neuronal function as described for the glial DELM-1, DELM-2 or ACD-1 (Voglis and Tavernarakis, 2008, Han et al., 2013, Wang et al., 2008). However, identification of the tissue, precise channel localisation, and finally subsequent behavioural testing are the necessary next steps before any further hypotheses can be generated.

In this chapter, I focus on DEL-9's role in the GABAergic AVL neuron and the vulva muscles both of which are involved in rhythmic expulsion behaviours. AVL synapses on to the enteric muscle and regulates the expulsion of gut contents as part of the DMP (McIntire et al., 1993). Contraction of the vulva muscles lead to expulsion of eggs during egg-laying (Schafer, 2006). *del-9* mutants show a frequent missing of the EMC during the DMP suggesting a role in AVL, overexpression of *del-9* cDNA could only be rescued in the *del-9(lj142)* mutant under its endogenous promoter, by contrast, overexpression in neuronal tissues exacerbated the mutant defects. Additionally, overexpression in a wild-type induced the same behavioural deficits than in the mutant indicating that level of expression is crucial for proper channel functioning. This might be suggestive that DEL-9 could form a heteromeric channel with other subunits and its lack or overexpression might alter the subunit composition leading to a non-functional channel.

del-9 mutants also show defects in egg-laying behaviour. They retain more eggs in the uterus compared to the wild-type and their inactive phases during egg-laying are prolonged. Egg-retention could be rescued by overexpressing *del-9* under its endogenous promoter as well as under a vulva muscle specific promoter, confirming that it indeed acts cell-autonomous in the vulva muscles. However, I have also seen a rescue for egg-retention for *del-9* expression in GABAergic neurons as well as an increase in egg-retention in GABA mutants. This points to an involvement of GABA in egg-laying behaviours. GABA release is likely to be mediated in an *del-9*-dependent manner from AVL which will discussed further below.

Finally, there is still the unanswered questions about the precise role of *del-9* in both neurons and muscles. Tagging of DEL-9 has shown that DEL-9 localises to puncta on axons, soma and muscle fibres. These puncta pattern suggests synaptic localisation which needs to be confirmed. If they do, one hypothesis is that DEL-9 in the muscle could be activated by co-release of protons from, for instance, the upstream HSN command neuron. Or, DEL-9 in the AVL neuron could function in a similar way to what has been described for ASIC-1 above, but in a feedback loop for GABA release, where activation of DEL-9 could trigger GABA release from AVL which in turn activates the enteric muscle during the DMP. The source of protons in this case might come from the intestine while the worm is on food. If the worm moves off food, defecation and egg-laying stop (Vidal-Gadea et al., 2012) and hence presumably the secretion of protons from the intestine. Genetic evidence from *pbo-4* mutants has

shown that diminishing proton secretion from the intestine did have an effect on egg-retention, however, this might also be a result of overall health of the *pbo-4* mutants which has yet to be assessed.

If DEL-9 does not localise to synapses, an alternative explanation might be that protons binding to DEL-9 might directly activate the vulva muscles. This might be supported by previous research that has observed that animals lacking the command neuron HSN, either through a mutation or though ablation, still engage in active egg-laying states (Collins et al., 2016) suggesting another mechanism that is independent of HSN in initiating egg-laying. This could be tested by directly perfusing low pH over the vulva muscles and assess calcium transients as a measure for activity. Earlier studies suggested a large contribution of regulators for vulva muscle excitability in egg-laying behaviours (Reiner et al., 1995), another hypothesis might therefore be that DEL-9 might function in muscle excitability. Protons secreted from the intestine could hence activate DEL-9 in the vuvla muscles making the muscle more susceptible for other egg-laying cues. A working model of DEL-9 functioning in the vuvla muscle and the AVL neuron are shown below in Figure 30.

While there are still many avenues to explore, I have shown for the first time that there are three members of the *C. elegans* DEG/ENaCs that can form acid-sensing ion channels *in vitro* in Xenopus oocytes. Using DEL-9 as an example, I showed that mutants that lack this channel show abnormalities in rhythmic motor behaviours. Based on this evidence, it can be concluded that the *C. elegans* acid-sensitive ion channels regulate excitability of a wide range of cell types including muscles and neurons.

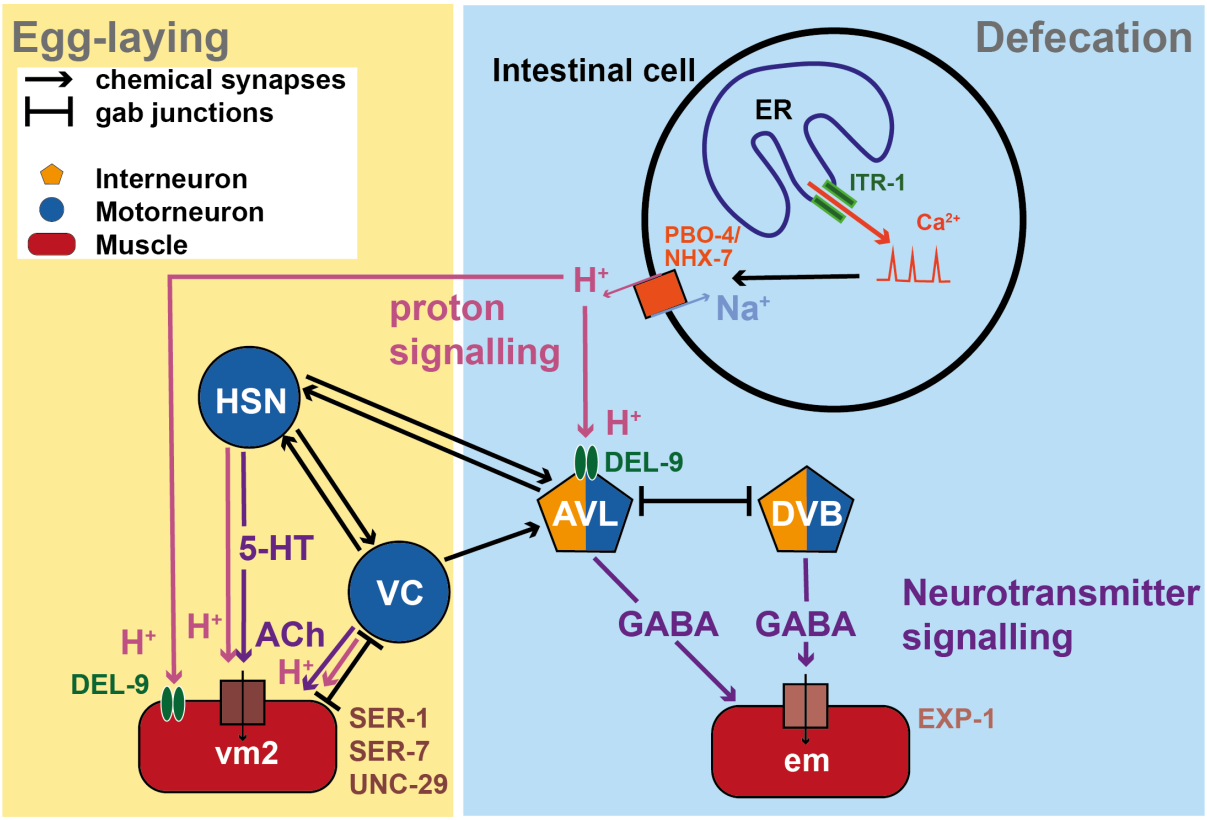

Figure 30: Working model of DEL-9 and proton signalling during egg-laying and defecation.

The rhythmic intestinal Ca^{2+} wave activates PBO-4/NHX-7 leading to secretion of H^+ from the intestine which bind to DEL-9 expressed in the vuvla muscles and AVL. In the vulva muscles DEL-9 might contribute to general cellular excitability, while in AVL activation of DEL-9 might trigger release of GABA which activates the enteric muscle. *Abbreviations:* SER-1 and SER-7 (serotonin GPCRs); UNC-29 (uncordinated (locomotion), acetylcholine-gated cation channel); EXP-1 (Expulsion defective (defecation), GABA-gated cation channel); PBO-4/NHX-7 (pBoc defective (defecation), Na^+/H^+ exchanger); ITR-1 (Inositol Triphosphate Receptor); 5-HT (serotonin); ACh (acetylcholine); ER (Endoplasmic Reticulum); em (enteric muscle); vm2 (vulva muscle). Combined and modified from (Zhao and Schafer, 2013, Schafer, 2006) and (Ravi et al., 2019).

4. 4. Appendix D

4. 4. 1. Introducing mutations and deletions to alter pH sensitivity of ASIC-1

While in *C. elegans*, researchers are concerned with opening DEG/ENaC channels using point mutations (Driscoll and Chalfie, 1991, Wang et al., 2013c, Han et al., 2013, Goodman et al., 2002, Fechner et al., 2020), research on vertebrate ASICs is concerned with altering pH sensitivity of ASIC channels or to diminish them in order to link functional to structural characterisation (Li et al., 2009, Jasti et al., 2007). The DEG/ENaC family shares the same structure with short N- and C-termini, two transmembrane alpha-helices, and a multidomain extracellular loop (Jasti et al., 2007).

From previous research and my current characterisation, it can be concluded that ASIC-1 shares similarities with vertebrate ASICs in terms of electrophysiological and functional characteristics. Firstly, I have demonstrated that the *C. elegans* ASIC-1 is closed at physiological pH and activated by decreasing pH which is similar to the mammalian ASICs (Waldmann et al., 1997). Secondly, like its mammalian homologues, it has shown to be involved in learning and memory (Wemmie et al., 2002, Kreple et al., 2014, Voglis and Tavernarakis, 2008). Therefore, the *C. elegans* ASIC-1 makes a good candidate to study how mutations in the pH sensing domains affect pH sensitivity *in vitro* based on what has previously been described from studying vertebrate ASICs. I used two approaches to disrupt and change pH sensing properties of ASIC-1. The first one is based on small deletions and substitutions in highly conserved regions between the rat ASIC1 (rASIC1, see CHAPTER 3, Appendix C 3. 5. 3., Supplementary Figure 1) and the *C. elegans* DEG/ENaC ASIC-1. The deletions are made in regions that are part of the acidic pocket based on homology to the rat ASIC1 based on previous research (Li et al., 2009, Grunder and Pusch, 2015, Vullo and Kellenberger, 2020) (CHAPTER 3, Appendix C 3. 5. 3., Supplementary Figure 1).

Previous research identified the aromatic residues Tyr-72/Trp-288 at the interface of the extracellular and transmembrane domains of the rat ASIC1 as being responsible for proton-gating (Li et al., 2009). Point mutations from aromatic residues to proline and negatively charged residues eliminated proton-evoked currents. The rat ASIC-1 and the *C. elegans* ASIC-1 share 46.3 % sequence similarity and 28 % sequence identity as determined by the local alignment (Smith-Waterman) (Daily,

2016). The aromatic Tyr-72 residue in rat ASIC1 is not conserved in *C. elegans* ASIC-1. At the position the Trp-288 of the rat ASIC1, the *C. elegans* ASIC-1 has an aromatic residue Tyrosine (Try-601, Y601). Therefore, I designed mutation in this region substituting Tyrosine with hydrophobic residues such as Proline (P) and Glycine (G), as well as with the charged amino acid Lysine (K). This generated the following mutations ASIC-1 (Y601P), ASIC-1 (Y601G) and ASIC-1 (Y601K), respectively. Furthermore, as the region around this area is highly conserved I also generated some single amino acid deletions to investigate if this could produce a shift in pH_{50}. Further deletion mutations were made the predicted the acidic pocket. Previous research has indicated that the acidic pocket is not required for channel function but for activation and desensitisation of ASICs (Vullo and Kellenberger, 2020). Mutations generated are shown below in Supplementary Figure 2.

Results showed that neither *Xenopus* oocytes injected with the deletion mutant cRNA ASIC-1(Δ549-552), ASIC-1(Δ517-522), ASIC-1(495-597), ASIC-1(Δ535-625) based on previous research on the acidic pocket (Vullo and Kellenberger, 2020) nor the ones injected with the substitution mutant cRNA ASIC-1(3xGly549-552) show any currents (Supplementary Figure 3). While this is an interesting result, it gave me little insight into the function of ASIC-1 given that the absence of proton current can have several reasons including functional insensitivity to protons, issues in expression and membrane trafficking and protein misfolding.

The second approach was to generate amino acid substitutions based on a recent paper (Li et al., 2009) in which the authors show functional effects of amino acid substitutions in the putative proton sensor of the rat ASIC1 (rASIC1). They showed that Proline 287 in the loop containing the aromatic residue Trp-288 is essential for rat ASIC1 function. Trp-288 is located at the tip of a loop of the extracellular domain between sites that form the acidic pocket, they also identify a second aromatic residue Tyr-72 immediately after the first transmembrane segment (Li et al., 2009). Introducing point mutations in one or both of these two areas not only changes the kinetics of activation and desensitisation of the channel but also shifts the proton affinity toward a more acidic range (Li et al., 2009). The *C. elegans* ASIC-1 shares 46.3 % similarity with the rat ASIC1 as determined by local aliment (Smith-Waterman) and while the rASIC1 Trp-288 is only similar (Tyrosine 601 in *C. elegans* ASIC-1), the Proline (Y) 287 is highly conserved. Based on amino acid sequence similarity, I introduced several point mutations in the *C. elegans* ASIC-1 changing

Tyrosine (Y) to Proline (P), Lysine (K) or Glysine (G) (Y601P; Y601K; Y601G, respectively).

In order to compare the half-maximal activation pH (pH_{50}) to see a change, each individual oocyte's responses to pH were fitted with the Hill's equation and the individual pH_{50} values were compared. Results showed that all of these amino acid substitution mutants are still functional and that a small deletion of two amino acids did not worsen one of the more complex mutants (ASIC-1 (Y601K(Δ597Δ599))) as quantified by comparison of the actual current (Supplementary Figure 3B). However, the large deletion in the extracellular loop (ASIC-1(Y601K(Δ370-597)) diminishes all currents observed (Supplementary Figure 3A) and was therefore excluded from the analysis as the absence of acid-evoked current cannot be clearly attributed. For instance, the lack of currents of certain constructs may be due to a disruption in the pH sensing function or a lack of expression or general functionality of the channel. Unfortunately, investigating the reason of the lack of currents in these cases poses big challenges in the absence of another readout that show that other channel functions are unaffected. Without another read out it is difficult to know whether the channel is expressed and whether the mutations only alter pH sensitivity or also other functions. Further experiments will be discussed below. Comparing the half-maximal activation pH (pH_{50}), I found that the pH_{50} of the following amino acid substitution mutants ASIC-1(Y601G) and ASIC-1(Y601K) differ statistically significantly from the pH_{50} of the wild-type (WT) ASIC-1 current (Supplementary Figure 3C). While this provides some indication that these amino acids in the *C. elegans* ASICs are responsible for pH-sensing *in vitro*, further experiments are needed to address this further.

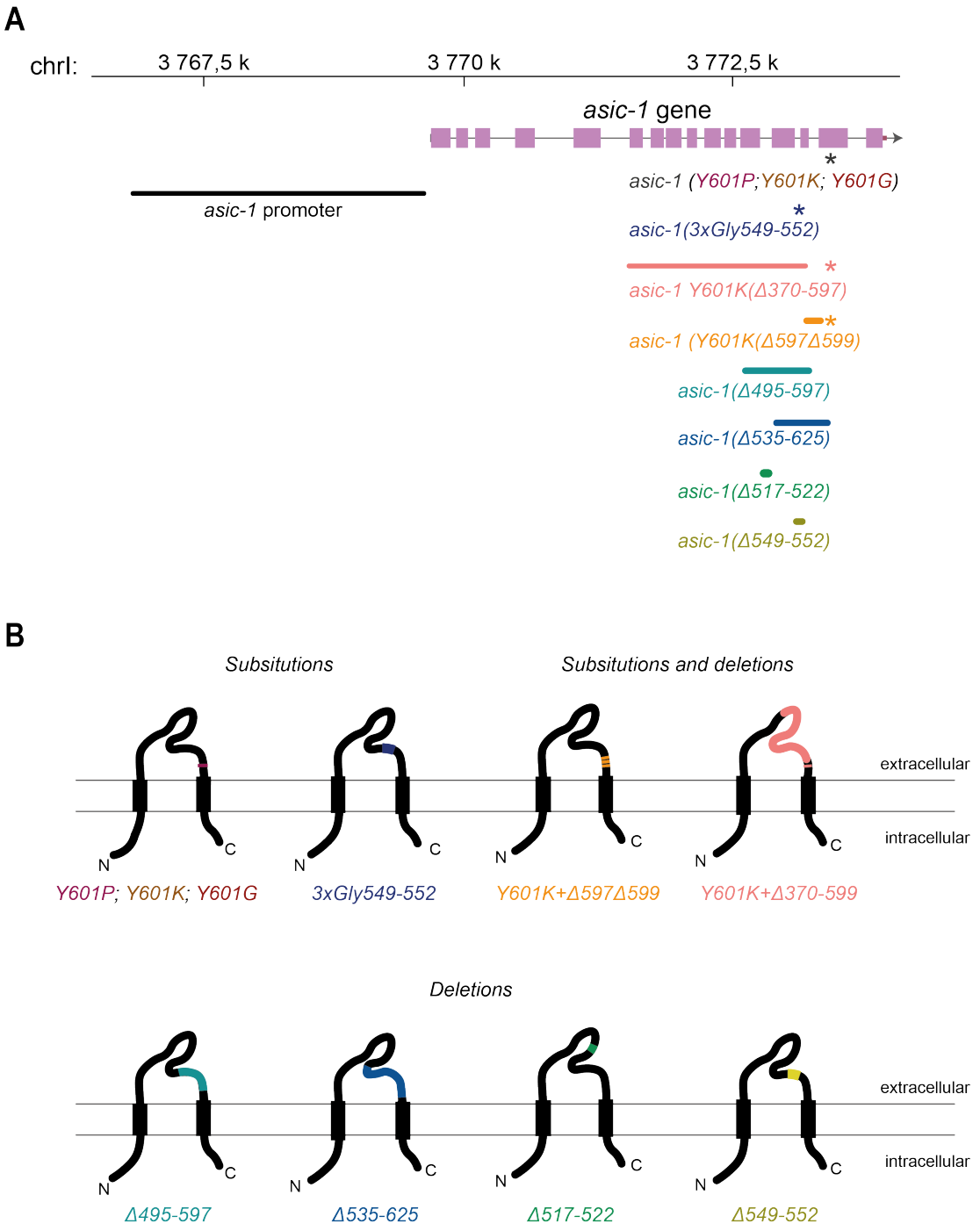

Supplementary Figure 2: Schematic of ASIC-1 point-substitution and deletion mutants.

(A) *asic-1* genomic region on chromosome I (chr I). Pink boxes indicate exons and grey lines indicate introns. Promoter fragment used for reporter line (CHAPTER 3) and mutations used in the study are indicated. (B) Visualisation of ASIC-1 channel subunits containing the following amino acid substitutions ASIC-1 (Y601P), ASIC-1 (Y601K), ASIC-1 (Y601G) and ASIC-1(3xGly549-552). Substitutions and small deletions ASIC-1 (Y601K+ Δ370-597) and ASIC-1 (Y601K+Δ597Δ599). Deletions: ASIC-1(Δ549-552), ASIC-1(Δ517-522), ASIC-1(495-597) or ASIC-1(Δ535-625).

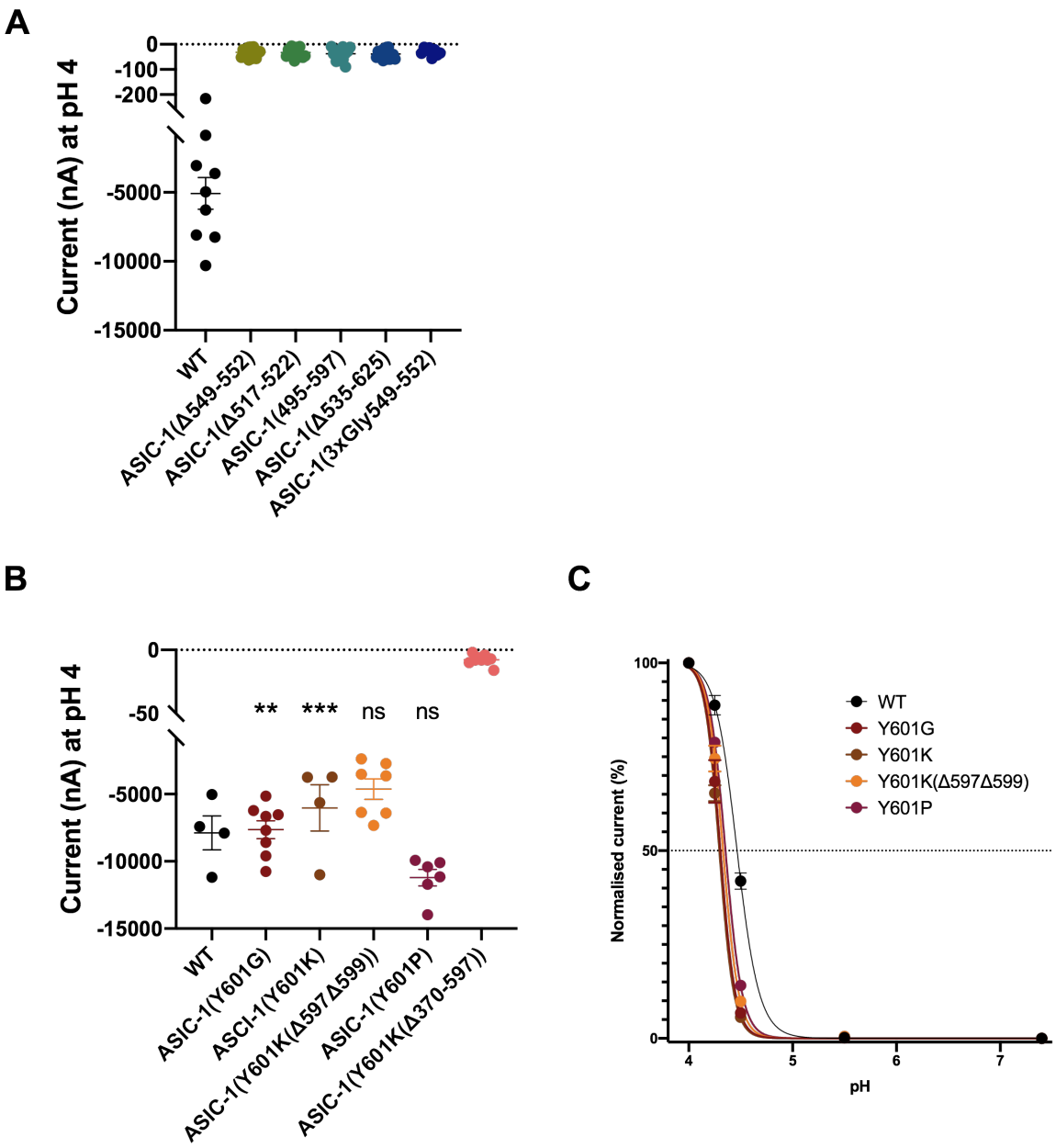

Supplementary Figure 3: Currents recorded from oocytes expressing ASIC-1 point-substitution and deletion mutants.

(A) *Xenopus* oocytes injected with the wild-type (WT) ASIC-1 cRNA show currents compared to the deletion mutants and the mutant where 3 amino acids were replaced by Glycine where no currents could be observed. WT (N=9), ASIC-1(Δ549-552) (N=14), ASIC-1(Δ517-522) (N=15), ASIC-1(495-597) (N=15), ASIC-1(Δ535-625) (N=8), ASIC-1(3xGly549-552) (N=16). (B) *Xenopus* oocytes injected with the wild-type (WT) ASIC-1 cRNA show currents which are comparable to the currents of the point mutation mutants. WT (N=4), ASIC-1(Y601G) (N=8), ASIC-1(Y601K) (N=4), ASIC-1(Y601K(Δ597Δ599)) (N=7), ASIC-1(Y601P) (N= 6), ASIC-1(Y601K(Δ370-597)) (N=9). A Shapiro-Wilk test was conducted to check for normal distribution of the samples confirming normal distribution. A parametric one-way ANOVA test was conducted to compare the currents at pH 4 of the respective point mutations (ASIC-1(Y601K(Δ370-597)) was excluded from the analysis as there was no current

observed). While the ANOVA interaction was highly significant [F (4, 24) = 7.816, p=0.0004], the post-hoc comparisons using the Bonferroni multiple comparison correction indicated that the means of the point mutants (Mean $_{ASIC\text{-}1(Y601G)}$ = -7648 nA, SD = 1882; Mean $_{ASIC\text{-}1(Y601K)}$ = - 6025 nA, SD = 3429; Mean $_{ASIC\text{-}1(Y601K(\Delta597\Delta599))}$ = -4626 nA, SD = -2015; Mean $_{ASIC\text{-}1(Y601P)}$ = -11211 nA, SD = 1511) did not differ significantly from the mean of the wild-type (Mean= -7884, SD =2530). (C) Comparison of half-maximal activation pH (pH_{50}). Assumption for normality assessed by a Shapiro-Wilk test were not met. A non-parametric Kruskal-Wallis test on the pH_{50} was conducted which was highly statistical significant (H = 19.76, ***p >0.0006). A post-hoc Dunn's multiple comparison test revealed that the pH_{50} of the ASIC-1(Y601G) (Mdn = 4.307, z = 3.393, **p=0.0028), ASIC-1(Y601K) (Mdn = 4.297, z= 3.758, ***p=0.0007) mutants differed significantly from the pH_{50} of the wild-type (WT) ASIC-1 (Mdn =4.471). While the pH_{50} of ASIC-1(Y601P) (Mdn= 4.355, z=1.274, p=0.811, ns) and ASIC-1(Y601K(Δ597Δ599)) (Mdn = 4.316, z = 2.369, p=0.713, ns) did not differ statistically significant from eh wild-type ASIC-1. Currents were recorded at a holding potential of – 60mV and normalized to maximal currents (pH 4) and best fitted with the Hill's equation. Error bars represent Mean ± SEM.

4. 4. 2. Co-injection of ASIC-1, DEL-1 and MEC-10 cRNA in *Xenopus* oocytes

While many DEG/ENaC can be expressed as homomeric channels *in vitro*, they tend to form heteromeric channels *in vivo*. Examples include the mammalian ENaCs which comprise three subunits (Canessa et al., 1993, O'Brodovich et al., 1993, Canessa et al., 1994, Palmer and Frindt, 1986), the murine ASIC1a/AIC2b (Sherwood et al., 2011), the Drosophila PPK25/PPK29/PPK23 (Liu et al., 2018) as well as the *C. elegans* MEC-4/MEC-10 mechanotransduction complex (Arnadottir et al., 2011, Brown et al., 2007, Goodman et al., 2002). A recent paper found evidence that the following *C. elegans* DEG/ENaCs *degt-1*, *del-1*, *unc-8*, and *mec-10* are co-expressed in PVD neurons (Tao et al., 2019), two polymodal nociceptive neurons that respond to cold temperature and harsh touch stimuli (Chatzigeorgiou et al., 2010). Evidence from my transcriptional reporter as well as from a previous research (Chatzigeorgiou et al., 2010, Husson et al., 2012) also found that the ASIC-1 is also expressed in the PVD neurons. From the initial screen I had found that ASIC-1 can form a homomer when expressed in *Xenopus* oocytes but DEL-1 or MEC-10 cRNA-injected oocytes did not show a statistically significant acid-sensitive currents on their own (CHAPTER 3). Therefore, I wanted to test whether ASIC-1 could form a heteromeric channel with DEL-1 and/or MEC-10 and whether this could be seen when two (or all three) channels were expressed in a 1:1(:1) ratio in *Xenopus* oocytes.

Results from these co-expression experiments showed that the current amplitude at pH 4 were statistically significantly decreased in *Xenopus* oocytes co-expressing ASIC-1 with other proposed subunits. This was the case when co-injecting ASIC-1 cRNA either only with DEL-1 cRNA or only with MEC-10 cRNA, as well as when all three subunits, ASIC-1, DEL-1 and MEC-10, were injected together. A pH-dose response curve was conducted but did not show a statistically significant shift in the pH_{50} between the homomeric ASIC-1 channel on its own or when co-injected with DEL-1 or MEC-10 RNA or RNA of both.

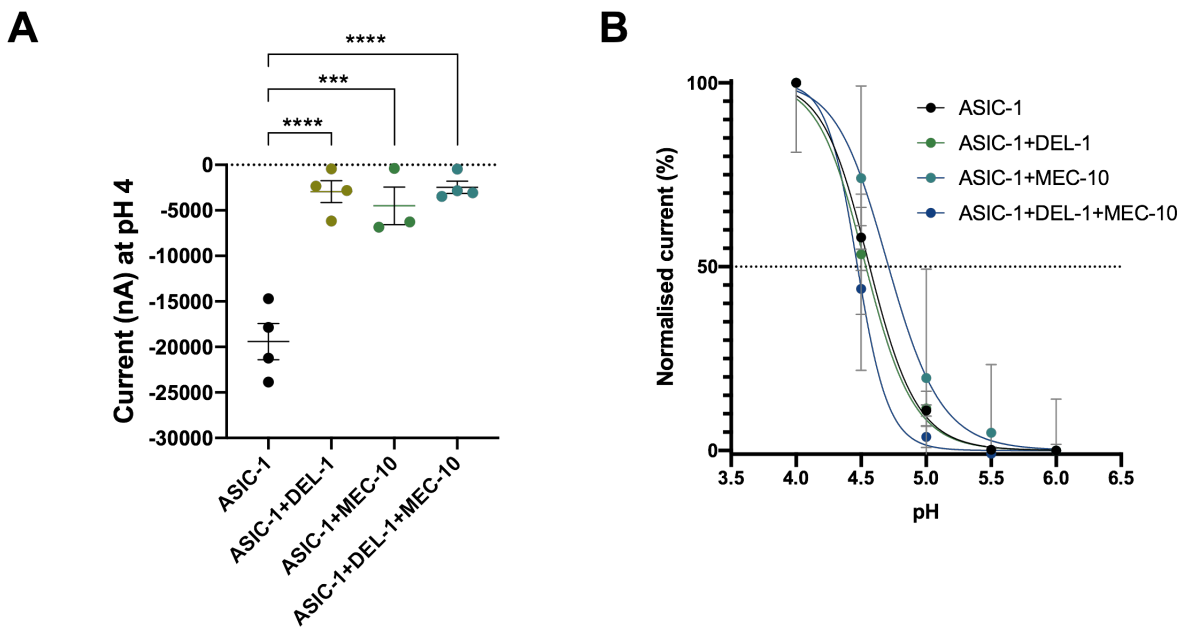

Supplementary Figure 4: Co-expression of ASIC-1 with DEL-1 and MEC-10.

(A) Current amplitude was significantly decreased (ANOVA F (3, 11) = 29.85, ****p<0.0001) in *Xenopus* oocytes co-expressing ASIC-1 cRNA with other proposed subunits. The post-hoc Dunn's multiple comparisons were carried out for all combinations which provided strong evidence that the ASIC-1 homomer (Mean = -19412, SEM =1992) showed significantly increased currents than when co-expressed with other subunits (ASIC-1+DEL-1 (Mean =-2945, SEM = 1193, ****p <0.0001), ASIC-1+MEC-10 (Mean =-4503, SEM =2062, ***p = 0.0001), ASIC-1+DEL-1+MEC-10 (Mean =-2458, SEM =678.6, ****p<0.0001)). (B) Heterologously expressed ASIC-1 channel on its own or in combination with DEL-1 or MEC-10 perfused with solutions of differing pH (pH 4, pH 4.5, pH 5, pH 5.5, pH 6). A Kruskal-Wallis test showed no statistically significant differences pH_{50} between the homomeric ASIC-1 channel and when co-expressed with other potential subunits (H (0) = 2.987, p =0.446, ns). Error bars represent Mean ± SD.

4. 4. 3. ACD-2 currents at pH 4 and pH 3.8

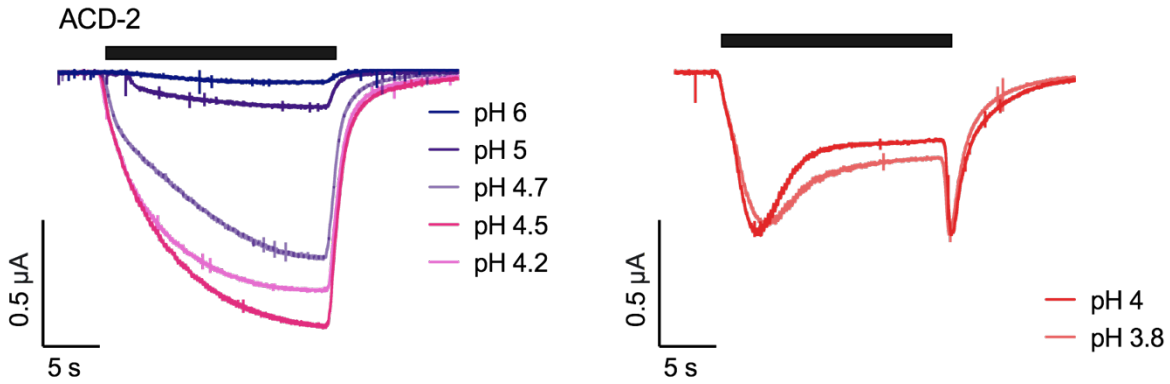

Supplementary Figure 5: ACD-2 currents above and below pH 4.

Representative traces from ACD-2 expressing oocytes (N = 6). Left: perfusion of pH 6 – pH 4.2, show a decrease in current (see main text Figure 20B) while perfusion with <pH 4.2 resulted in a partial desensitisation of the channel. Black bars represent the time of perfusion with low pH from a neutral pH 7.4.

4. 4. 4. *del-9(RNAi)* can mimic egg-retention phenotype

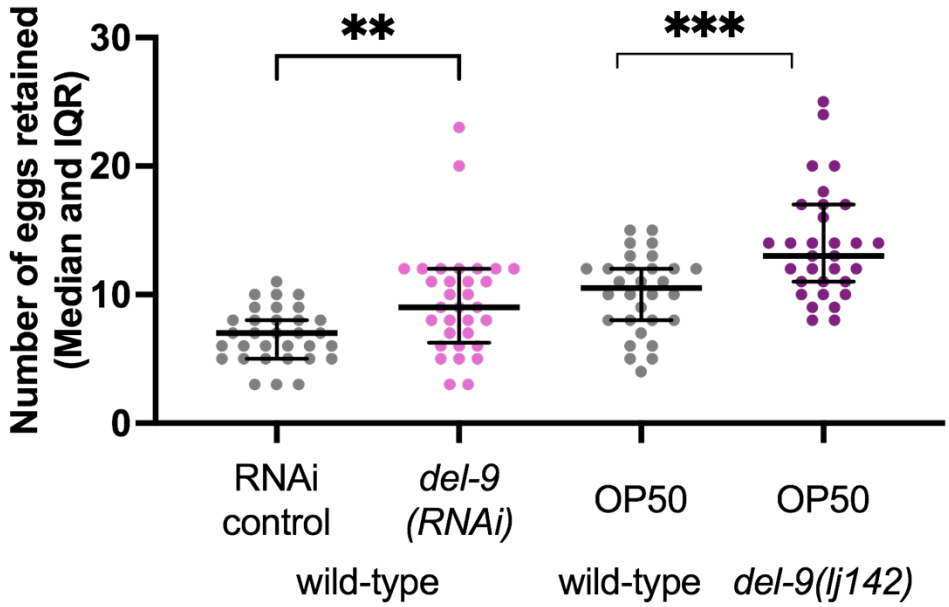

Supplementary Figure 6: del-9(RNAi) can mimic del-9 mutants' egg-retention phenotype.

Wild-type animals on *del-9(RNAi)* bacteria retained more eggs (Mdn = 9) than the ones on the bacteria containing the RNAi control vector (Mdn = 7). A Mann-Whitney test indicated that this difference was statistically significant, $U(N_{RNAi\ control} = 32 , N_{DEL\text{-}9\ RNAi} = 32) = 289.5$, **p=0.0023. On OP50, *del-9(lj142)* mutants retained more eggs (Mdn = 13) than the wild-type animals (Mdn = 10.5). A Mann-Whitney test indicated that this difference was statistically significant, $U(N_{del\text{-}9(lj142)} = 3 , N_{wild\text{-}type} = 32) = 238.5$, ***p=0.0008. However, wild-type animals also retain different amounts of eggs on the RNAi control compared when grown on OP50. Bacterial food sources have previously shown to affect egg-retention (Gardner et al., 2013).

CHAPTER 5 – The acid-sensing DEG/ENaC ACD-5 acts as a timekeeper for rhythmic behaviour by sensing proton fluctuations in the *C. elegans* intestinal lumen

5.1. Abstract

In CHAPTER 3, I identified two groups of *C. elegans* acid-sensing ion channels based on their response to neutral and low pH *in vitro* in *Xenopus* oocytes. In the current chapter I will follow up on the two candidates, ACD-5 and DEL-4, that showed currents at neural pH which are inhibited by low pH. I will then focus on ACD-5 showing that based on its expression pattern and behavioural phenotype, it is involved in the timing rhythmic behaviour initiated by the intestinal cell. Finally, I will explore some candidates that might form a heteromeric channel with ACD-5 in the intestine to regulate rhythmic behaviour *in vivo*.

5.2. Introduction

Central pattern generators are networks of individual cells that produce rhythmic behaviour in the absence of sensory or descending inputs. Well-studied examples include the suprachiasmatic nucleus, a region of the brain in the hypothalamus, which plays a central role in controlling circadian rhythms (Moore and Eichler, 1972, Stephan and Zucker, 1972a, Stephan and Zucker, 1972b). Less attention has been paid to ultradian rhythms with shorter periods. One example of an ultradian rhythm is the defecation motor program (DMP) in *C. elegans* which presents a valuable system for studying the molecular and genetic pathways of short-period cellular oscillators (Avery and Thomas, 1997, Thomas, 1990). The DMP consists of series of body contractions to expel gut contents executed approximately every 50 seconds with very high regularity (Thomas, 1990).

Environmental factors and genetic and molecular mechanism that regulate the DMP have been well described (see CHAPTER 1; (Liu and Thomas, 1994, Branicky and Hekimi, 2006)). Two main oscillatory mechanisms are involved in the DMP generation, firstly, calcium oscillations in the intestinal cell via the inositol 1,4,5-trisphosphate receptor type 1, *itr-1*. Overexpression of *itr-1* decreases the defecation cycle length while loss-of function alleles such as *itr-1(sa73)* slow down the intervals

(Dal Santo et al., 1999). Secondly, as we have seen in CHAPTER 1, proton oscillations, which are an integral part of the DMP inside the intestinal cells, in intestinal lumen as well as outside the intestine where secreted protons signal to proton-receptors on muscles (Beg et al., 2008, Allman et al., 2009, Pfeiffer et al., 2008, Bender et al., 2013, Chauhan et al., 2013). Here, I focus on the intestinal lumen, as previous research has suggested that the luminal wave of protons transitioning from the posterior to the anterior part once a cycle might correspond to sequential activation of proton sensors along the length of the intestine (Bender et al., 2013). This statement is supported by evidence indicating the pH of the intestinal lumen is weakly acidic at around pH 4, but every 50 seconds during the DMP the pH rises to approximately pH 6 (Allman et al., 2009). This of course raises the question of what these proton sensors might be and their role in the DMP. Some of the players that can change the acidity of the intestinal lumen have been identified, these mainly act as pump protons. For instance, loss of the VHA-6 (Vacuolar H ATPase), an enzyme involved in pumping protons across the apical membrane, prevents full acidification of the intestinal lumen and leads to an increased interval between posterior body contractions (pBoc) (Allman et al., 2009). Similarly, the Na^+/H^+ exchangers PBO-4 and PBO-1 show increased and decreased intestinal lumen pH, respectively, and loss of PBO-1 leads to an arrest in the proton wave in the intestinal lumen (Benomar et al., 2020). However, actual proton sensors that directly sense acidity have not yet been identified.

In the current chapter, I present a detailed electrophysiological characterisation on the in CHAPTER 3 identified amiloride-sensitive homomeric channels ADC-5 and DEL-4 that are inhibited at low pH. As the DEL-4 data was generated for a collaboration with the Tavernerakis Lab (Institute of Molecular Biology and Biotechnology, University of Crete), I focus on the role of ACD-5 in the DMP providing genetic and behavioural evidence to demonstrate that the acid-sensing ion channel ACD-5 act as a timekeeper in the *C. elegans* intestine by sensing proton concentrations in the intestinal lumen.

5. 3. Results

5. 3. 1. ACD-5 and DEL-4 can form homomeric amiloride-sensitive cation channels *in vitro* that are inhibited by increasing amount of protons

From the initial screen in CHAPTER 3, we know that ACD-5 and DEL-4 are able to from homomeric channels *in vitro* in *Xenopus* oocytes that can be blocked by both amiloride and increasing proton concentrations. I followed up on this initial finding and demonstrated that both channels could be blocked by amiloride in a dose dependent manner with a half inhibitory concentration IC_{50} of 131 μM for ACD-5 and an IC_{50} of 179 μM for DEL-4 (Figure 30A, B). I further investigated ion selectivity assessing the shift in reversal potential (ΔE_{rev}) by substituting NaCl with either equimolar KCl, LiCl or $CaCl_2$ in the solution (see CHAPTER 4 and Methods). Monovalent ion-substitution experiments were conducted in the absence of Ca^{2+} as Ca^{2+} has shown to block vertebrate ASIC channels (Paukert et al., 2004). Here, I included Ca^{2+} as previous research has suggested that some constitutively open channels are permeable for Ca^{2+} in addition to monovalent cations (Matthewman et al., 2016) the experiments were done as previously described (Wang et al., 2008). Results showed that ACD-5 shows a preference Li^+ over Na^+ and a small preference of K^+ over Na^+ and is impermeable for Ca^{2+}. There was a median positive shift in ΔE_{rev} of 37 mV when shifting from a NaCl solution to a LiCl, and a ΔE_{rev} of 4.4 mV when shifting to a KCl solution (Figure 30C, E). By contrast, the DEL-4 homomeric channel has a high preference for Na^+ and Li^+ over K^+ and is impermeable for Ca^{2+}, with no ΔE_{rev} when shifting from a NaCl solution to a LiCl solution and a median negative shift in ΔE_{rev} of -45 mV when shifting to a KCl solution (Figure 30C, E). One limitation when interpreting the E_{rev} data is that in the Ca^{2+} solution, almost no current was observed (Figure 30), however, it confirms that ACD-5 and DEL-4 channels are impermeable for Ca^{2+}. Furthermore, proton permeability and removal of calcium and cations were assessed for ACD-5 (Figure 32). Results indicated that ACD-5 is not permeable for protons when increasing protons in the extracellular solution, as the ΔE_{rev} did not show a positive shift. Removal of calcium in the extracellular solution also did not alter the ΔE_{rev} further confirming that ACD-5 is unaffected by calcium. By contrast removal of Na^+ from the solution (NMDG) induced a large negative ΔE_{rev} confirming that ACD-5 is a cation channel.

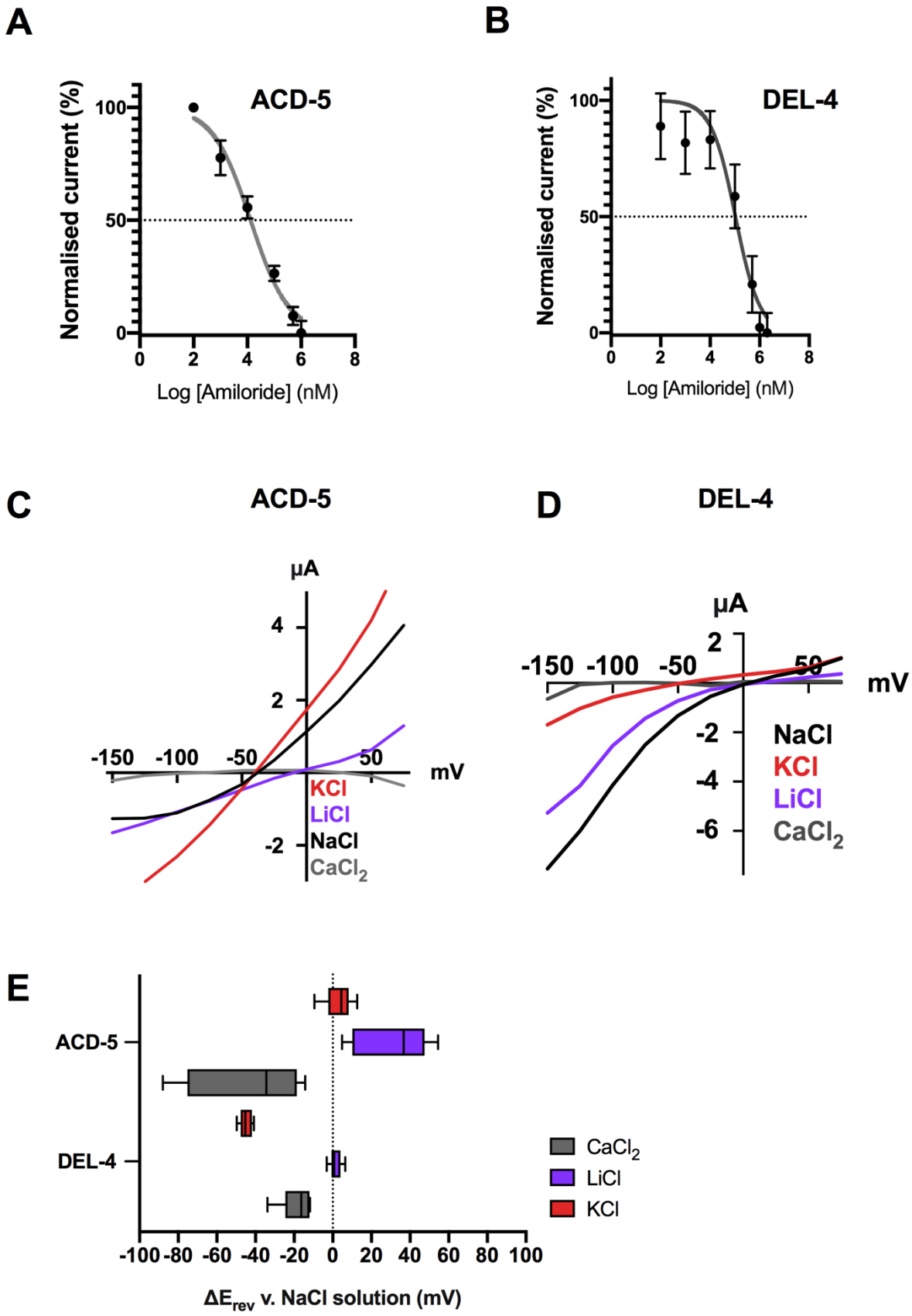

Figure 31: Amiloride-sensitivity and ion selectivity of ACD-5 and DEL-4.

(A) Normalised (I/I_{max}) current of amiloride dose–response curves for the ACD-5 homomer showing a half maximal inhibitory concentration (IC_{50}) of 131 µM ($LogIC_{50}$ = 4.118) (N = 8) indicated by the dashed line. (B) Normalised (I/I_{max}) current of amiloride dose–response curves for the DEL-4 homomer with an IC_{50} of 179 µM for DEL-4 ($LogIC_{50}$ = 5.022) (N = 4) indicated by the dashed line. (C)-(D) Representative current-voltage (IV) relationships for *Xenopus* oocytes expressing ACD-5 and DEL-4. Actual current for each oocyte and leak current is subtracted at pH 7.4. (E) Average calculated from 7<N<9 oocytes for each construct of ΔE_{rev} when shifting from a NaCl solution to $CaCl_2$, KCl or LiCl solution. A negative shift of E_{rev} indicating a preference for Na^+ over the respective ion and a positive shift indicating a preference of the respective ion over Na^+. Data is presented as Median and IQD (inter-quartile distance, as calculated by the Tukey method).

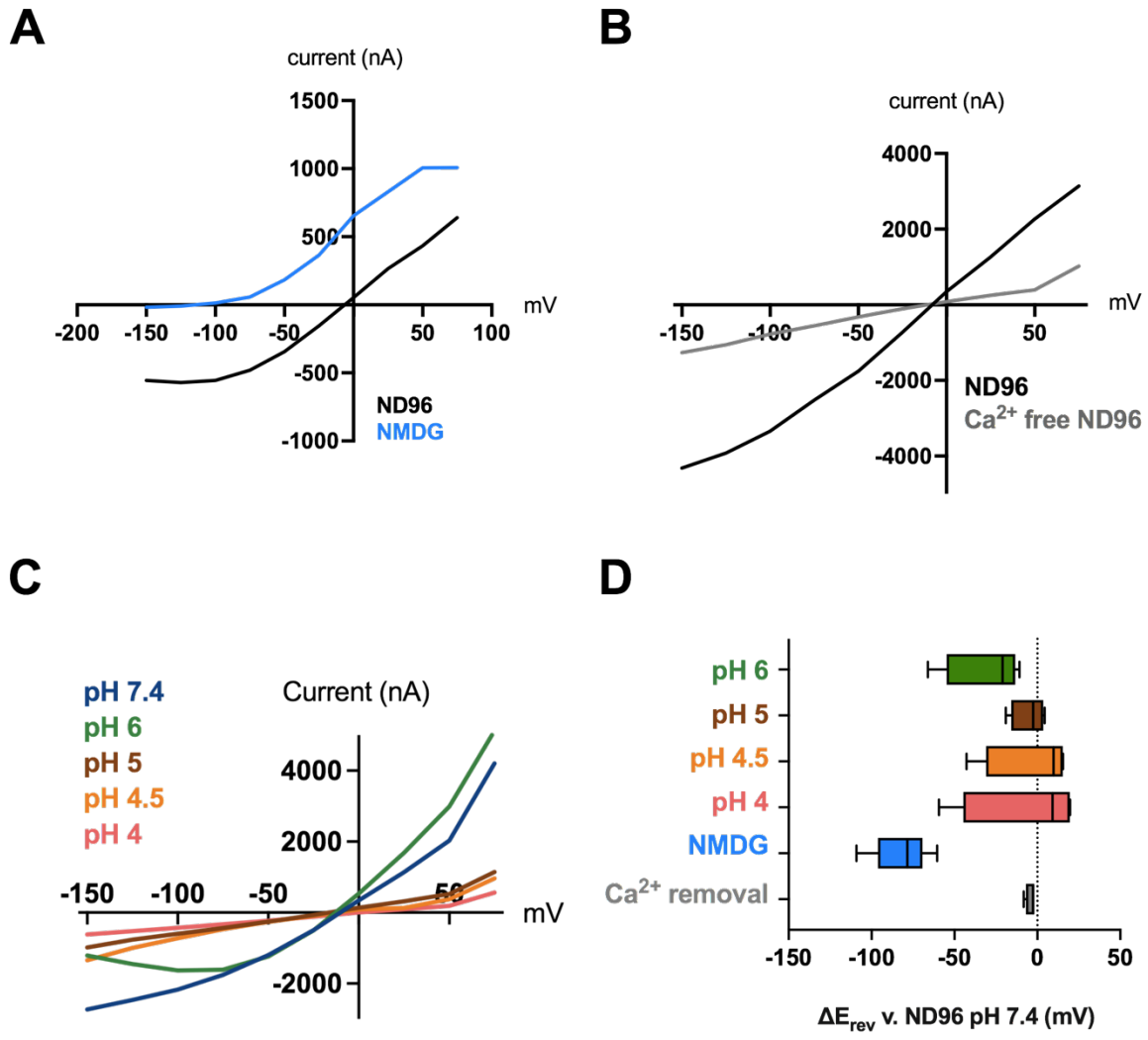

Figure 32: The effect of monovalent cations, Ca^{2+} removal or change in proton concentrations on reversal potential.

Representative current-voltage (IV) relationships for *Xenopus* oocytes expressing ACD-5 under the following conditions: (A) Removal of monovalent cations from the solution. (B) Removal of Calcium in the extracellular solution. (C) Increasing concentrations of protons in the extracellular solution. Actual current for each oocyte and leak current subtracted at pH 7.4. (D) Average calculated from 4<N<8 oocytes for each construct of ΔE_{rev} when shifting from a ND96 solution to the respective condition. A negative shift of E_{rev} indicating a preference for the basal ND96 solution over the respective solution. Error bars represent Median and IQD (inter-quartile distance, as calculated by the Tukey method).

Previous research has shown that the *C. elegans* ACD-1 can form a homomeric channel in *Xenopus* oocytes that is constitutively open at neutral pH and closes rapidly at low pH with a half maximal inhibitory pH (pH_{50}) of 6.4 (Wang et al., 2008). I found that similar to ACD-1, ACD-5 and DEL-4 can also be blocked by decreasing the pH of the extracellular perfusion solution with an inhibitory pH_{50} of 4.87 for ACD-5 (Figure 33C) and a pH_{50} of 5.6 for DEL-4 (Figure 34B). However, ACD-5 currents can be blocked by pH 4 but are enhanced when switching the buffer from basal conditions (pH 7.4) to pH 6 with an excitatory pH_{50} of 6.48 (Figure 33C, D). Similarly, at a pH lower than 5, the DEL-4 channel increases in current again compared to pH 5 with an excitatory pH_{50} of 4.25 (Figure 34B). Raw representative traces of ACD-5 and DEL-4 homomeric channels are shown in Figure 33A, B and Figure 34A, respectively. These observations might indicate the physiological range in which these channels are operating *in vivo*.

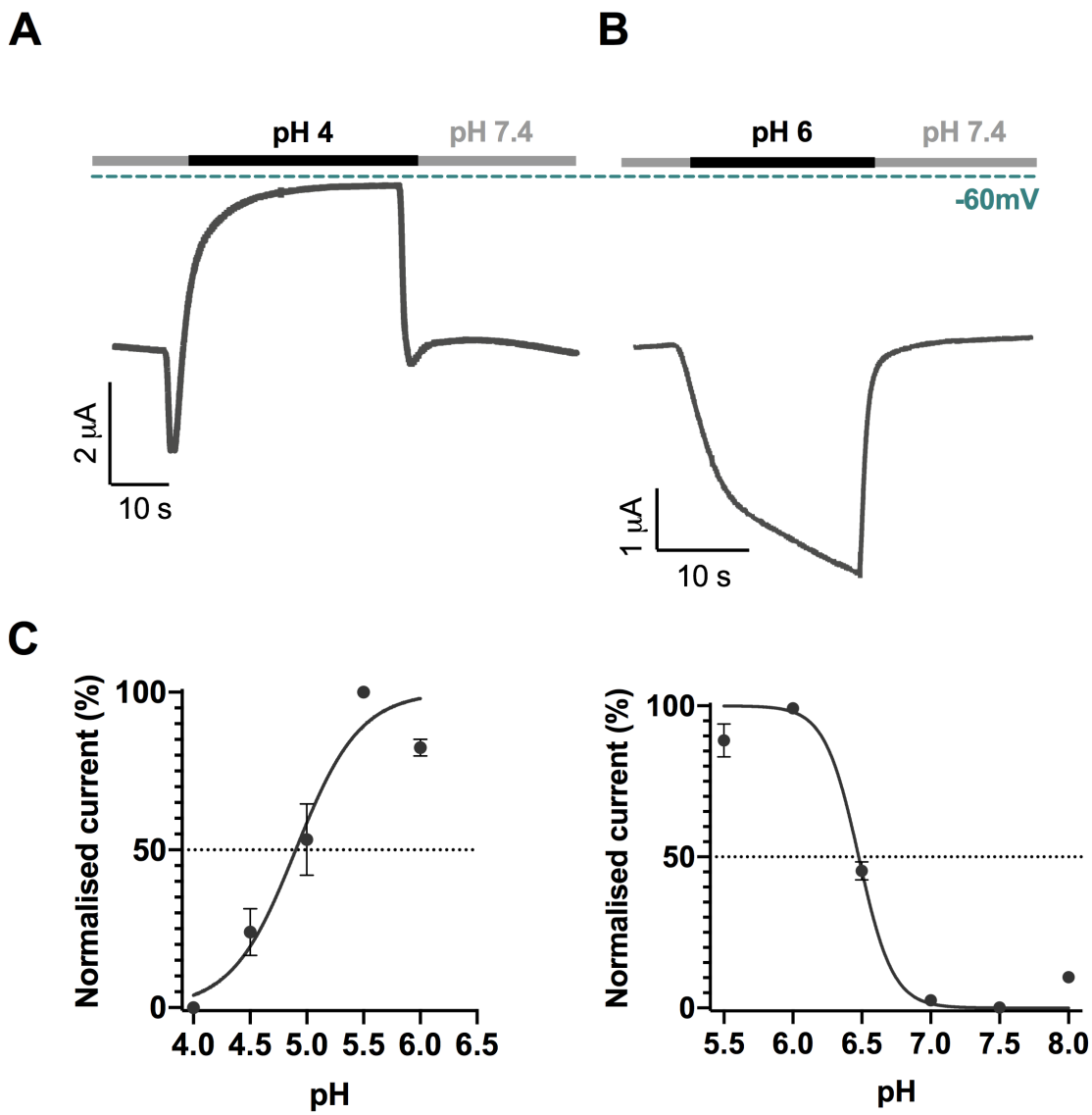

Figure 33:ACD-5 can form a homomeric channel that is inhibited by extracellular protons.

(A) Representative trace of ACD-5 injected *Xenopus* oocytes when perfused with ND96 solution at pH 4. (B) Representative trace of ACD-5 injected Xenopus oocytes when perfused with ND96 solution at pH 6. Currents were recorded at a holding potential of -60mV and traces are baseline-subtracted and drift-corrected using the Roboocyte2^{+} (Multichannels) software. (C) Proton-sensitivity and pH-dose dependence. Heterologously expressed ACD-5 channel perfused with solutions of lowering pH from pH 6 with and inhibitory pH_{50} of 4.90 (N = 5) and when perfused with increasing pH from pH 6 with and excitatory pH_{50} of 6.48 (N = 7). Channel is fully open at 100% current and closed at 0% current. Currents were recorded at a holding potential of -60mV, normalized to maximal currents and best fitted with the Hill's equation (Nonlin fit Log(inhibitor) vs normalized response – variable slope) in GraphPad Prism. Amount of total ACD-5 cRNA (500 ng/µl) injected. Error bars represent Mean ± SEM.

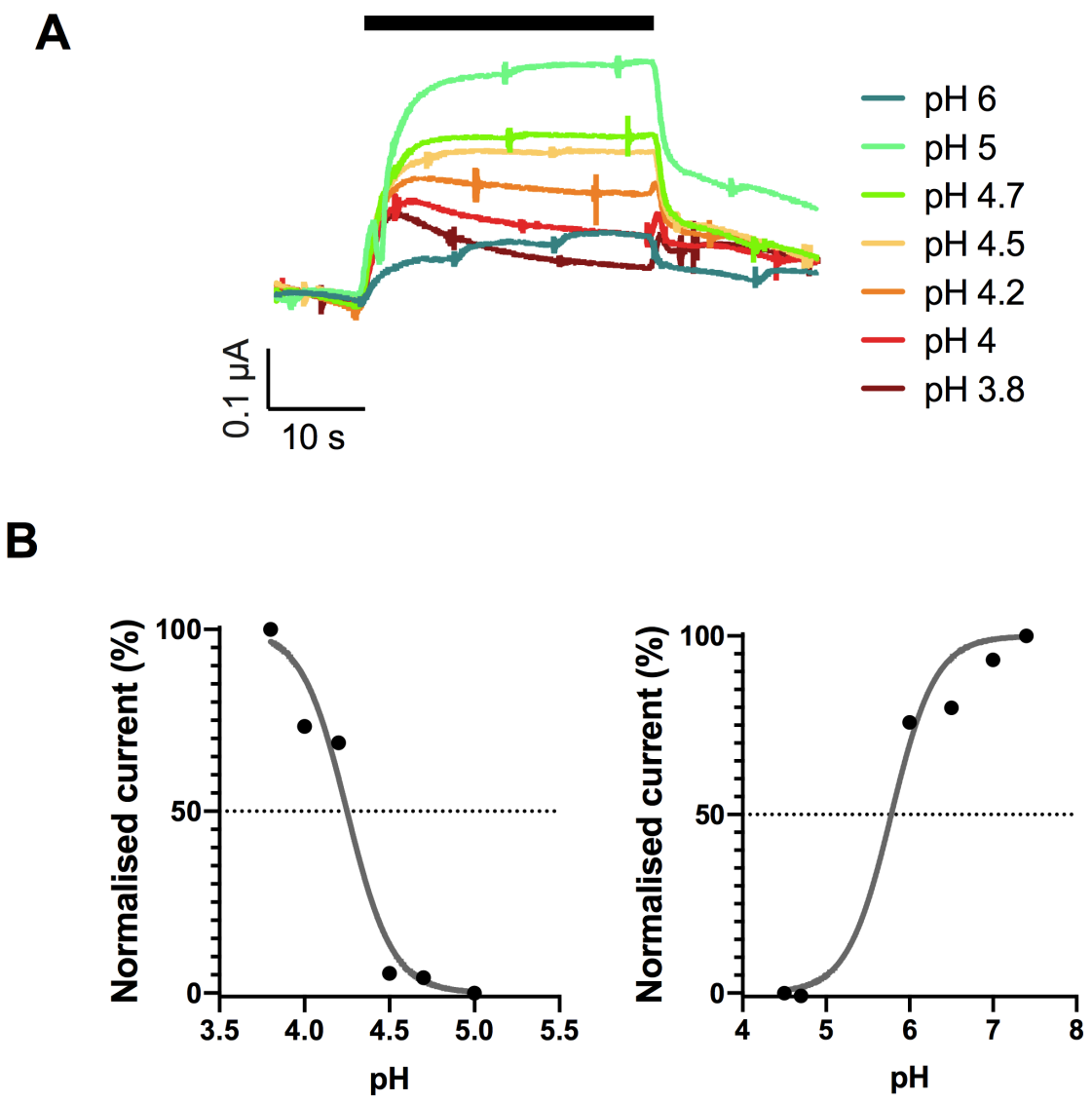

Figure 34: DEL-4 can form a homomeric channel that is inhibited by extracellular protons.

(A) Representative trace of DEL-4 injected *Xenopus* oocytes when perfused with ND96 solution at various proton concentrations from a neutral baseline (pH 7.4). Currents were recorded at a holding potential of -60mV and traces are baseline-subtracted and drift-corrected using the Roboocyte2^{+} (Multichannels) software. (B) Proton-sensitivity and pH-dose dependence. Heterologously expressed DEL-4 channel perfused with solutions of lowering pH from pH 7.4 with and pH_{50} of 5.7 (N = 5) and when perfused with increasing pH from pH 5 with and pH_{50} of 4.25 (N = 5). Channel is fully open at 100% current and closed at 0% current. Currents were recorded at a holding potential of -60mV, normalized to maximal currents and best fitted with the Hill's equation (Nonlin fit Log(inhibitor) vs normalized response – variable slope) in GraphPad Prism. Amount of total DEL-4 cRNA (500 ng/µl) injected. Mean only is shown.

5. 3. 2. ACD-5 is highly expressed in the intestine and localises to the apical membrane

In order to generate hypotheses about ACD-5's potential physiological role, I first investigated its cellular and subcellular expression pattern. For cellular expression, see CHAPTER 3, Figure 10. For exploring subcellular localisation, I firstly tagged the endogenous *acd-5* gene with a GFP using CRISPR/Cas9 (Dokshin et al., 2018), however, the tag was not visible despite the GFP insertion being present in the genomic sequence (see Appendix E 5. 5. 1, Supplementary Figure 7). I then constructed an *acd-5* transcriptional reporter which consists of a 4763bp regulatory sequence upstream of the *acd-5* gene driving the *acd-5* cDNA tagged with the red fluorophore *mKate2*. In this overexpression line, ACD-5 localised to the intestinal apical membrane as confirmed by co-localisation with an apical membrane marker (OPT-2) and markers for the intestinal cytoplasm and the intestinal lumen (Figure 35A, B, C).

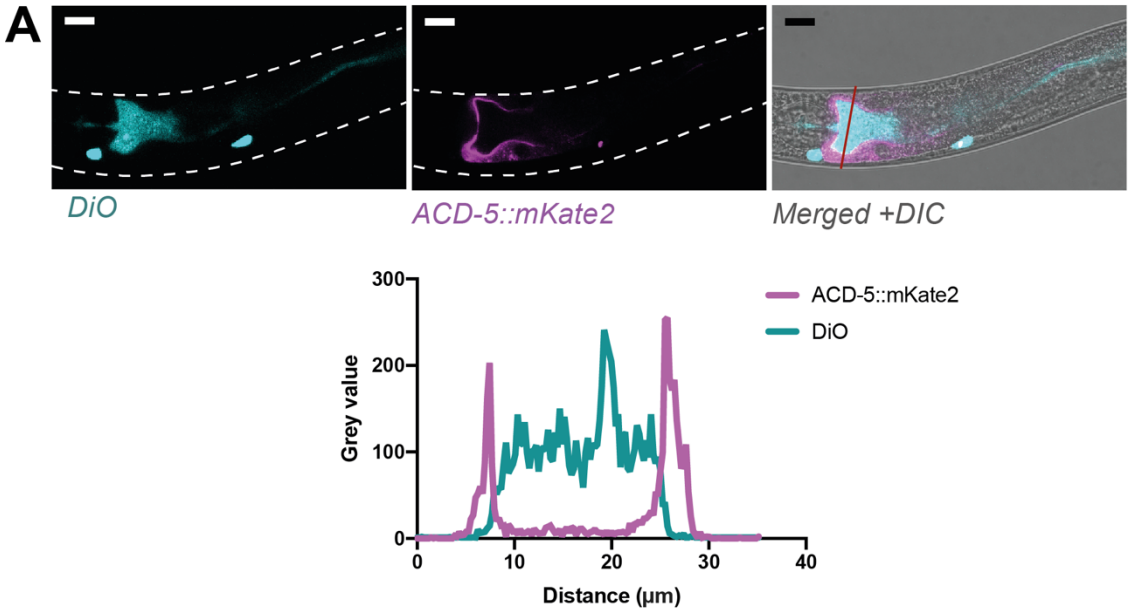
A
DiO
ACD-5::mKate2
Merged +DIC
ACD-5::mKate2
DiO
Grey value
300
200
100
0
0
10
20
30
40
Distance (µm)

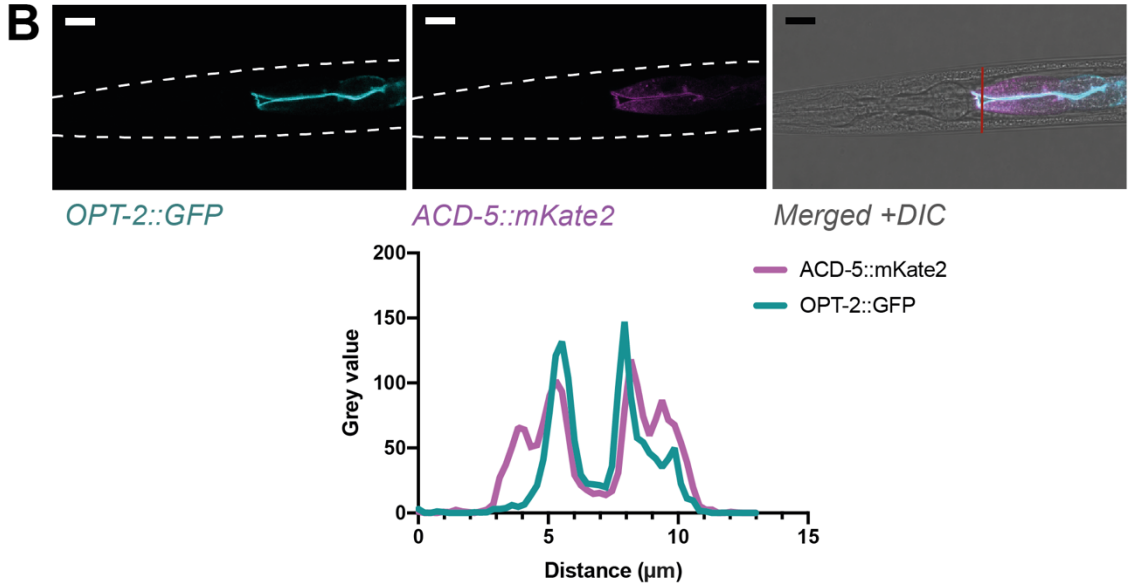
B
OPT-2::GFP
ACD-5::mKate2
Merged +DIC
ACD-5::mKate2
OPT-2::GFP
Grey value
200
150
100
50
0
0
5
10
15
Distance (µm)

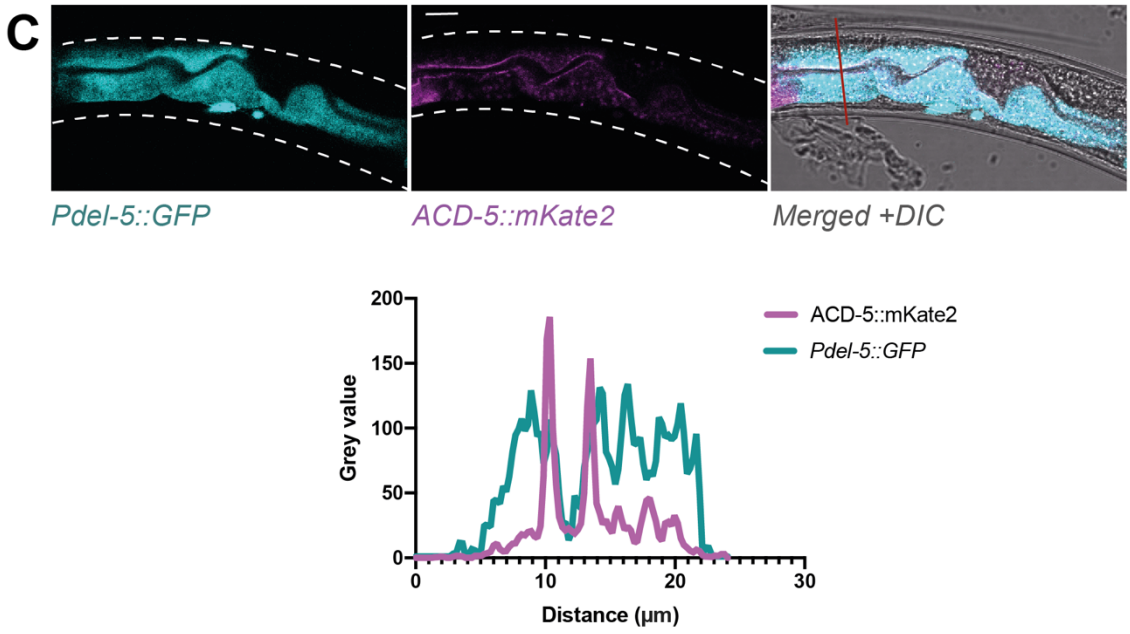
C
Pdel-5::GFP
ACD-5::mKate2
Merged +DIC
ACD-5::mKate2
Pdel-5::GFP
Grey value
200
150
100
50
0
0
10
20
30
Distance (µm)

Figure 35: ACD-5 localised to the intestinal apical membrane.

(A) ACD-5::mKate2 *(ljEx1470)* expression and DiO staining. DiO ingested by the animal marks the intestinal lumen. The intensity profile marks show that ACD-5 is highly enriched at the apical membrane but not the intestinal lumen. (B) Further confirmation of ACD-5 localisation on the apical membrane. Co-labelling of ACD-5::mKate2 with OPT-2::GFP (a proton-coupled OligopePtide Transporter) which has previously shown to be expressed on the apical membrane (Nehrke, 2003). The Intensity profile shows that both fluorophores localise to the apical membrane *in vivo*. Tagged ACD-5 is expressed under its endogenous promoter and the tagged OPT-2 is expressed under its endogenous intestinal promoter. (C) Transcriptional reporter (*Pdel-5*) expressing GFP in the cytoplasm of the intestinal cell. Overlay between the ACD-5::mKate2 shows that ACD-5::mKate2 is strongly expressed on the luminal membrane. The red line represents the location of the intensity prolife taken. Scale bars are 10µm.

5. 3. 3. ACD-5 is involved in regulating timing of rhythmic muscle contractions

My transcriptional reporter in Figure 35 above indicates that ACD-5 localises to the intestinal apical membrane facing the lumen, I tested the possibility that the ACD-5 channel subunit might play a role in the Defecation Motor Program (DMP). I used the *acd-5(ok2657)* mutant previously generated by the *C. elegans* Deletion Mutant Consortium (Consortium, 2012) in which the second transmembrane domain of the *acd-5* channel was truncated but the first transmembrane domain and the extracellular loop stay intact (Figure 36A, B). In addition to this mutant, I generated a complete knock-out of the *acd-5* gene using CRISPR/Cas9 technique adapted to use in *C. elegans* (Dokshin et al., 2018), this allele is *acd-5(lj122)* (Figure 36A, B).

The defecation behaviour was scored by eye using blinded plates containing the wild-type control, the backcrossed *acd-5(ok2657)* mutant and the full knock-out allele *acd-5(lj122)*. Results showed that in accordance with previous findings the wild-type defecation cycle was initiated approximately every 50 seconds at 22 °C room temperature (Avery and Thomas, 1997, Thomas, 1990). The full knock-out *acd-5(lj122)* did not differ from the wild-type control (Figure 36C). The *acd-5(ok2657)* mutants, by contrast, showed longer cycles of 57 seconds (Table 4).

As the phenotype was only observed in the *acd-5(ok2657)* mutants, this led me to hypothesise that this could be a dominant allele. I assessed this by performing two experiments: the first one was to see whether the phenotype of the longer defecation cycles is still observed in heterozygous animals. The second experiment was to express the *acd-5(ok2657)* mutant allele in wild-type animals, under the endogenous promoter (*Pacd-5::acd-5[ok2657]*) or under the intestinal promoter (*Pges-1::acd-*

5[ok2657]), to generate heterozygous mosaic animals (for definition of mosaicism, see CHAPTER 2 – Methods). Results showed that the heterozygous animals and mosaic animals expressing the mutant allele showed prolonged defecation cycles of 55 seconds which were significantly longer than the ones of the wild-type (Figure 36C). These results suggest that *acd-5(ok2657)* is indeed a dominant allele. Variability was also assessed and showed that overexpression of the mutant *acd-5(ok2657)* allele increases variability but so did overexpression of the wild-type *acd-5* (Figure 36D). This suggests that the increased variability is likely to be an effect of overexpression rather than of the *acd-5(ok2657)* mutation itself. An additional observation was an increased fraction of missed EMCs in animals expressing the dominant mutation, which is rarely observed in the wild type (in my control it was never observed but previous studies showed that wild-type animals can miss EMCs in a small fraction of cycles (McIntire et al., 1993, Beg et al., 2008)). Further investigation into this phenotype showed that overexpression of the *acd-5* wild-type cDNA did not show prolonged cycles but showed missed EMCs suggesting that this phenotype is due to overexpression of the subunit (fragment) (Figure 36C, E).

In order to provide physiological evidence that *acd-5(ok2657)* is indeed a dominant mutation that hinders functional channel formation, I expressed the wild-type subunit at a stable concentration in *Xenopus* oocytes with the mutant fragment at varying ratios with the underlying assumption that they would form heteromeric channels *in vitro* (Figure 37B). Oocytes injected with the mutant ACD-5(ok2657) cRNA do not display any currents and are unaffected by amiloride (Figure 37A). Results showed that increasing ratios of ACD-5(ok2657) cRNA co-injected with wild-type ACD-5 cRNA into oocytes decreased currents which is indicative that their co-expression results in non-functional expression.

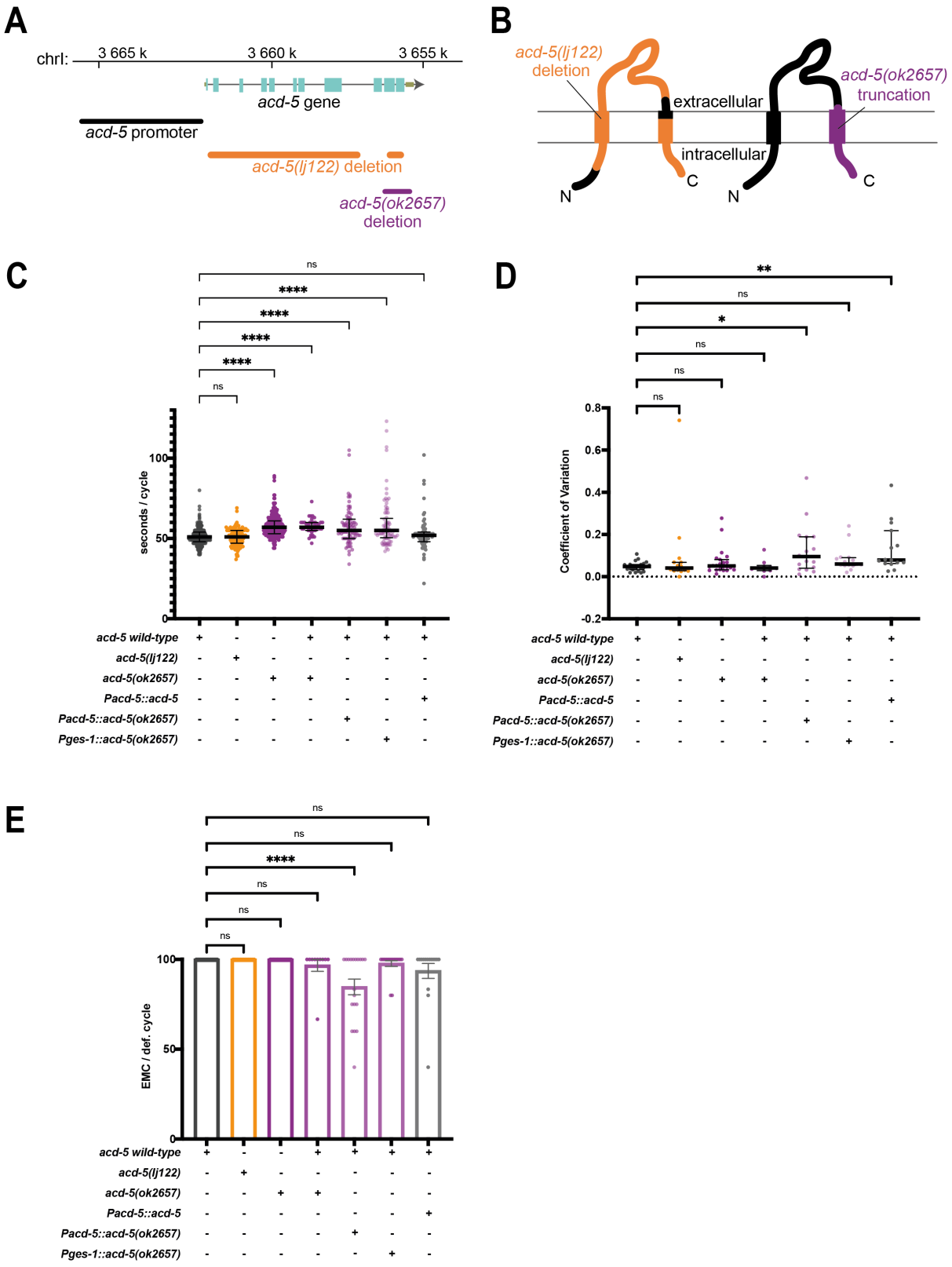

Figure 36: acd-5(ok2657) is a dominant mutation that shows that acd-5 is implicated in maintaining the DMP interval length.

(A) *acd-5* genomic region on chromosome I. Boxes indicate exons and lines indicate introns. Endogenous promoter region and mutations used in the study are shown. (B) Schematic of predicted

ACD-5 protein structure with two transmembrane domains, and cytosolic N and C terminus and an extracellular loop, typical of DEG/ENaC subunits. Mutations used in the study are indicated in orange for the knock-out *acd-5(lj122)* and in purple the truncated *acd-5(ok2657).* (C) *acd-5(ok2657)* is a dominant mutation increasing defecation cycle length. Kruskal-Wallis test was highly significant (H(6) = 249.0, p****<0.0001) for the defecation cycle length of individual cycles. The post-hoc Dunnett's multiple comparisons test found no significant difference between the wild-type and the *acd-5(lj122)* mutant (Z=0.413, p>0.9999, ns) but significant difference between the median cycle length of the *acd-5(ok2657)* mutant (Z=13.37, p****<0.0001), the *acd-5(ok2657)* heterozygous (Z=7.2, p****<0.0001), and animals expressing the extrachromosomal array *ljEx1503 [Pacd-5::acd-5(ok2657)]* (Z=6.488, p****<0.0001), *ljEx1507 [Pges-1::acd-5 (ok2657)]* (Z=6.022, p****<0.0001), but not for the overexpression of *acd-5, ljEx1248* [*Pacd-5::acd-5 cDNA*] in a wild-type background (Z=1.436, p>0.9999, ns). Error bars represent Median and IQR. (D) Variability of the defecation cycles represented as Coefficient of Variation (Standard Deviation (SD) divided by Mean cycle length). Kruskal-Wallis test was significant (H(6)= 20.60, **p=0.0021). A post-hoc Dunn's multiple comparison test indicated that compared to the wild-type controls, only the *ljEx1503 [Pacd-5::acd-5(ok2657)]* (Z=3.17, *p=0.047), and *ljEx1248* [*Pacd-5::acd-5 cDNA]* (Z=2.66, **p=0.0093) in the wild-type had a significantly higher variability between cycles. Error bars represent Median and IQR. (E) Quantification of missed EMC for the indicated genotypes. Kruskal-Wallis test was significant (H(6) = 34.34, ****p<0.0001). A post-hoc Dunn's multiple comparison test indicated that compared to the wild-type controls, only the *ljEx1503 [Pacd-5::acd-5(ok2657)]* expressing animals displayed a statistically significant increase in missed EMCs (Z=4.657, ****p<0.0001). Error bars represent Mean ± SEM.

Table 4: Defecation cycle Intervals of the dominant mutant acd-5(ok2657) and controls.

Cycle length in seconds of five individual cycles per animal. Percentages of EMC and pBoc for each animal (in five cycles).

	N	**Cycle length in seconds (Median (IQR))**	**% of EMC (Mean ± SEM)**	**% of pBoc (Mean ± SEM)**
wild-type	28	51(6)	100	100
acd-5(lj122)	16	51(8)	100	100
acd-5(ok2657)	21	57(8)	100	100
+/acd-5(ok2657)	10	57(5)	96.7 ± 3.33	100
ljEx1500 [Pacd-5::acd-5(ok2657)]	15	55(14)	94.7 ± 2.36	100
ljEx1503 [Pacd-5::acd-5(ok2657)]	17	55(12)	84.6 ± 4.35	100
ljEx1507 [Pges-1::acd-5(ok2657)]	17	55(12)	97.6 ± 1.61	100
ljEx1248 [Pacd-5::acd-5 cDNA] (overexpression)	15	52(6)	93.6 ± 4,17	100

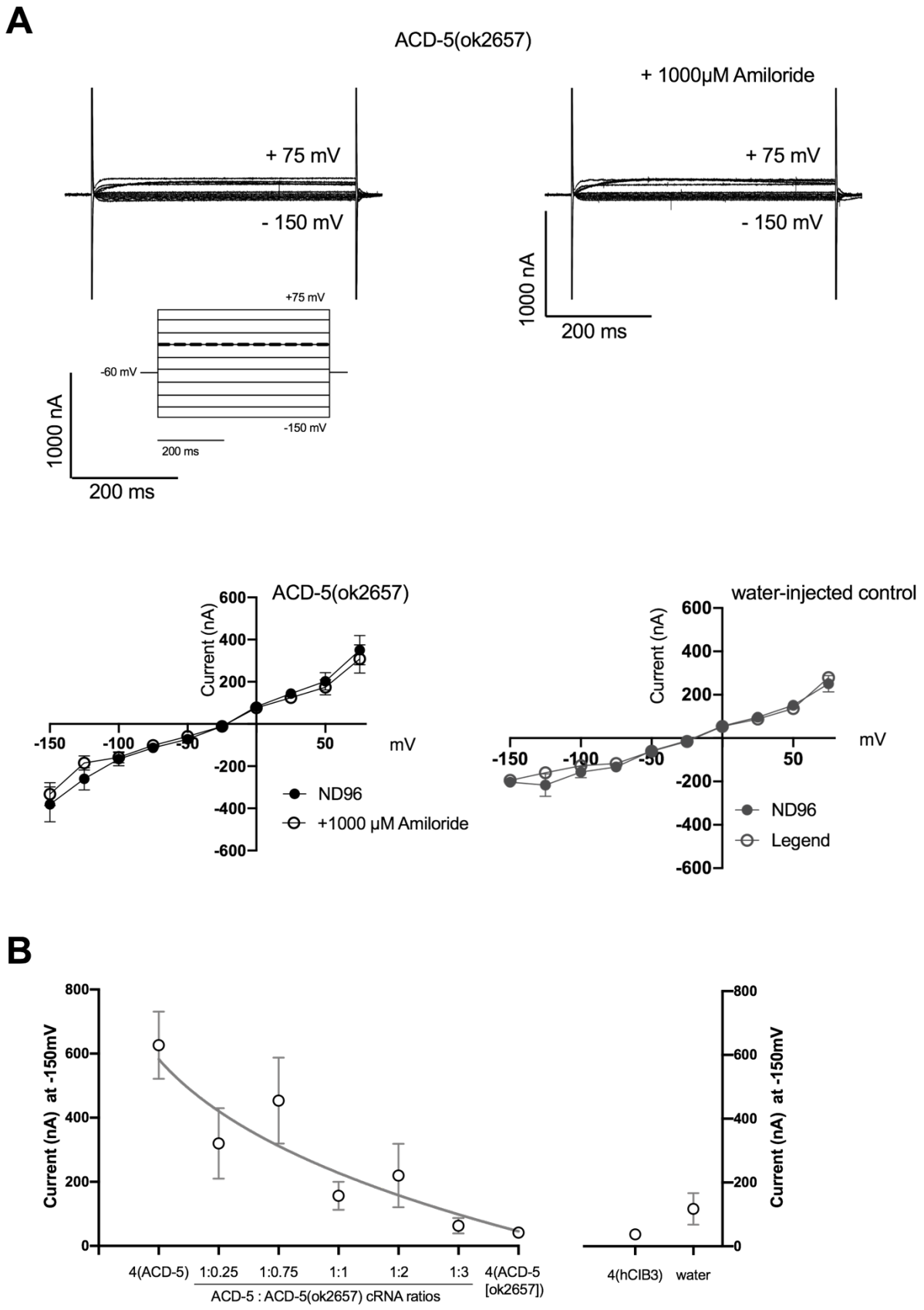

Figure 37: ACD-5(ok2657) disrupts ACD-5 channel functioning in Xenopus oocytes.

(A) Representative currents current–voltage (IV) relationships for *Xenopus* oocytes injected with ACD-5(ok2657) cRNA show no currents and no response to 500μ amiloride (N=10) similar to the water-injected control (N=10). *Xenopus* oocytes are perfused with a basal solution (ND96, pH 7.4) only (black circles), and in presence of the DEG/ENaC channel blocker amiloride (open circles). (B) Altering the ratio of ACD-5 with mutant ACD-5(ok2657) shows that ACD-5(ok2657) inhibits channel-functioning with increasing of its ratio to the wild-type ACD-5. hCiB3 (human Calcium and integrin-binding family member 3, an auxiliary potassium subunit) was used as a "filler" to control for amount of total cRNA (500 ng/μl) injected in each oocyte. Negative controls on the left side: Currents of hCib3 and nuclease-free water injected oocytes. The oocyte membrane was clamped at −60 mV and voltage steps from -150 mV to +75 mV were applied (insert). Currents were normalized to maximal currents. Error bars represent Mean ± SEM.

5. 3. 4. *acd-5* mutants are defective in establishing and maintaining of an appropriate pH in intestinal lumen

My findings from *in vivo* studies indicate that *acd-5* is expressed at the apical membrane facing the intestinal lumen, *acd-5(ok2657)* mutants show a longer defecation cycle period, and the *in vitro* findings from TEVC in oocytes that show *acd-5* can form a constitutively open homomeric channel permeable for monovalent cations that is inhibited by low concentrations of protons. Given the electrophysiological properties, behavioural and localisation data, I wanted to investigate if loss of *acd-5* affects pH of the intestinal lumen. Therefore, we contacted experts that had just developed a novel fluorescent dye (KR35, Figure 38) that accumulates in the *C. elegans* intestine and which can visualise the dynamic wave in intestinal lumen pH (Bender et al., 2013, Benomar et al., 2020). The experiments were done by Brian Ackley (University of Kansas, US) but I analysed the blinded data. Results revealed that mutants carrying the *acd-5*(ok2657) or *acd-5*(lj122) allele showed an overall lower fluorescence, indicative of a less acidic intestinal lumen compared to the wild-type controls (Figure 38 and Figure 39). The results also showed that the mutants displayed a dysregulation of maximum anterior transition (MAT) intensity at much higher rate than in wild-type. Unfortunately, the movies taken were only 2 minutes long and many *acd-5* mutant animals failed to display two MATs in this time which could have biased the results of the timing of between MAT displayed in Figure 39B and Table 5.

While there are always animals displaying a reduced fluorescence in the intestine and therefore cannot be reliably scored, this was much more prominent in *acd-5* mutants. For instance, in the current sample 83% of the wild-type worms could be analysed compared to only 61% and 56% for the *acd-5(lj122)* and *acd-5(ok2657)* mutants, respectively. This could be increased to 80% again by expressing *ljEx1249* (*Pacd-5::acd-5 cDNA*) in either mutant (Table 5). This observation could be explained by a dysregulation of lumen pH or that animals do not feed because of a pharyngeal pumping defect. The latter one was previously assessed by measuring pharyngeal pumping in *acd-5(ok2657)* mutants which was normal (Grundy, 2018). I repeated these experiments with both *acd-5* mutants and confirmed that pumping rate between mutants and wild-type was indeed normal (Appendix E 5. 5. 2., Supplementary Figure 8) confirming that animals indeed present a less acidic overall intestinal pH. However, pharyngeal pumping function does not preclude differenced in ingestion of dye. Brian

Ackely (personal communication) conducted pilot experiments to see if *acd-5* mutants that are longer on KR35 would show higher fluorescence in the intestine but they did not, suggesting that the phenotype observed was indeed due to the less acidic overall intestinal pH. However, additional experiments quantifying the amount of dye taken up using a different type of dye might further strengthen this conclusion.

Another interesting finding was that the acidity of the intestinal lumen could only be rescued in the *acd-5(lj122)* null mutant but not in the *acd-5(ok2657)* mutant. While the expression of *acd-5* in *acd-5(ok2657)* mutants was marginally statistically different from the wild-type, it was not statistically different to the *acd-5(ok2657)* mutant, and hence most likely not a biological rescue. This fits in well with previous findings that this mutation is a dominant mutation that might be able to form a non-functional heteromeric channel with the wild-type ACD-5 or other potential subunits. Taken together all the findings presented above suggest that ACD-5 might indeed be directly involved in maintaining the luminal pH as mutants fail to establish and maintain a normal pH in the intestinal lumen.

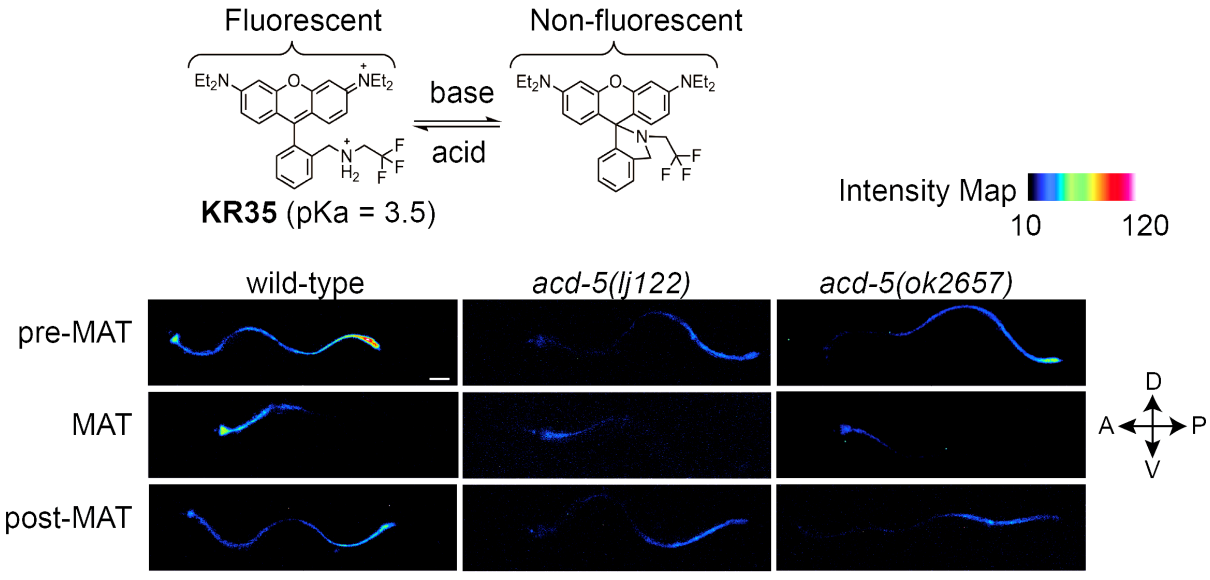

Figure 38: acd-5 mutants show an altered intestinal lumen pH.

Chemical structures of KR35 under acidic and basic conditions. The protonated ring-opened form is highly fluorescent, and the deprotonated spirocyclic form is non-fluorescent (Benomar et al., 2020). Heat map of fluorescence pixel intensity with red representing the most intense fluorescence (high acidity), and black the least intense fluorescence (low acidity). Fluorescence micrographs of wild type

and mutant expressing the *acd-5(lj122)* or *acd-5(ok2657)* allele after feeding on the pH-sensitive probe KR35 for 30 min (10 µM). MAT ± 15 seconds (pre/post-MAT) during the DMP extracted from videos of free moving animals are shown. Scale bar: 50 µm. Imaging experiments were done by Brian Ackley (University of Kansas, US), analysis was conducted by me in ImageJ (Fiji).

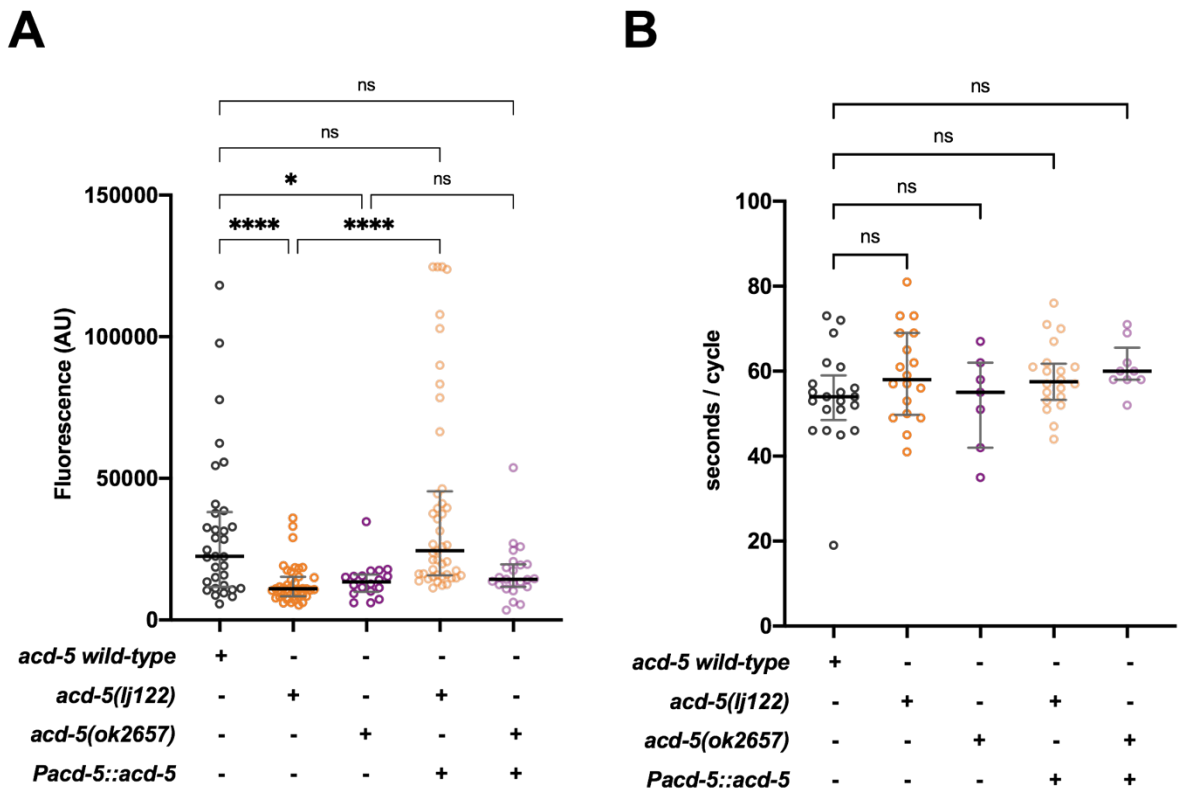

Figure 39: Acidity in the intestinal lumen of acd-5 mutants.

(A) Fluorescence in the maximum anterior transition (MAT). The Kruskal-Wallis test showed a statistically significant difference Fluorescence intensity during the MAT between mutants and wild-type (H(6) = 47.84, ****p<0.0001). Compared to the wild-type, *acd-5(lj122)* mutants (Dunn's test, ****p<0.0001) and *acd-5(ok2657)* mutants (Dunn's test, Z=2.80, *p=0.031) showed a statistically significant decrease in fluorescence in the intestine. **(B)** Interval length between MATs. The Kruskal-Wallis test showed that there was no significant difference cycle length between two MATs between mutants and wild-type with (H(6) = 5.68, p>0.9999, ns) compared to the wild-type, *acd-5(lj122)* mutants and *acd-5(ok2657)* mutants. Error bars represent Median and IQR.

Table 5: MAT analysis using KR35.

Genotype	Animals with MATs [total tested]	MAT interval in seconds (Median (IQR))	MAT Average Fluorescence (AU) (Median (IQR))
wild-type	24 [29]	54(0.5)	22472 (26383)
acd-5(lj122)	19 [31]	58(19.25)	11037(6841)
acd-5(ok2657)	9 [16]	55(20)	13492(6085)
acd-5(lj122); ljEx1249 (Pacd-5::acd-5 cDNA)	20 [25]	57.50(8.5)	24428(29592)
acd-5(ok2657); ljEx1249 (Pacd-5::acd-5 cDNA)	12 [15]	60(7.5)	14362(7933)

5. 3. 5. Genetic interaction between known genetic factors of the DMP and *acd-5*

Next, I used a candidate gene approach to determine the genetic relationship between *acd-5* and known genetic factors of the DMP. Based on the findings above that a dominant mutation of *acd-5* can prolong defecation cycle intervals, I tested *itr-1/acd-5* double mutants, as previous research has found that *itr-1*-dependent signalling act as a timekeeping mechanism (Dal Santo et al., 1999).

Furthermore, the *acd-5* mutants show a similarly high pH in the intestinal lumen than mutants of the Na^+/H^+ exchanger PBO-4 (Benomar et al., 2020). PBO-4 localises to both the basal and apical membrane where it is involved in pumping protons in to the pseudocoelomic space or into the intestinal lumen (Benomar et al., 2020, Beg et al., 2008). As it is likely that ACD-5 senses proton concentration in the intestinal lumen and opens in a particular pH range allowing cations to enter the intestinal cell, I tested whether double mutants between *acd-5* and *itr-1* or *pbo-4* displayed a similar phenotype to single mutants or whether phenotypes could be enhanced or ameliorated.

In line with previous research I found that the *itr-1(sa73)* mutation slows down the defecation cycle significantly and increased variability (Dal Santo et al., 1999, Walker et al., 2002) with 110 seconds compared to the wild-type (49 seconds) or the *acd-5(ok2657)* mutant (55 seconds). Interestingly, compared to *itr-1* single mutants, *acd-5(ok2657)/itr-1* double mutants showed a decrease in interval length with 103

seconds as well as a decrease in variability by half (Figure 40A, B; Table 6). *itr-1* single and double mutants missed EMCs and pBocs at a similar frequency (Figure 40C, D; Table 6). These findings further support a role of *acd-5* in timekeeping of the defecation intervals.

The cycle interval length was not altered in *pbo-4* mutants and the variability was similar to the wild-type and *acd-5* mutants. The *acd-5(ok2657)/pbo-4* double mutant displayed wild-type cycle interval length suggesting that *pbo-4* might act genetically upstream of *acd-5* (Figure 41A). Double mutants displayed a higher variability in cycle length and displayed fewer missed EMCs (6-8%) compared to the single mutant (23%) but they displayed a higher frequency of missed pBoc steps (13%-23%) compared to the *pbo-4* single mutants (5%) (Figure 41B). I was also able to repeat previous research demonstrating that *pbo-4* mutants show no or a weak pBoc and they also frequently miss EMCs (Beg et al., 2008) (Figure 41C, Table 7). These findings are consisted with *pbo-4* acting genetically upstream of *acd-5.*

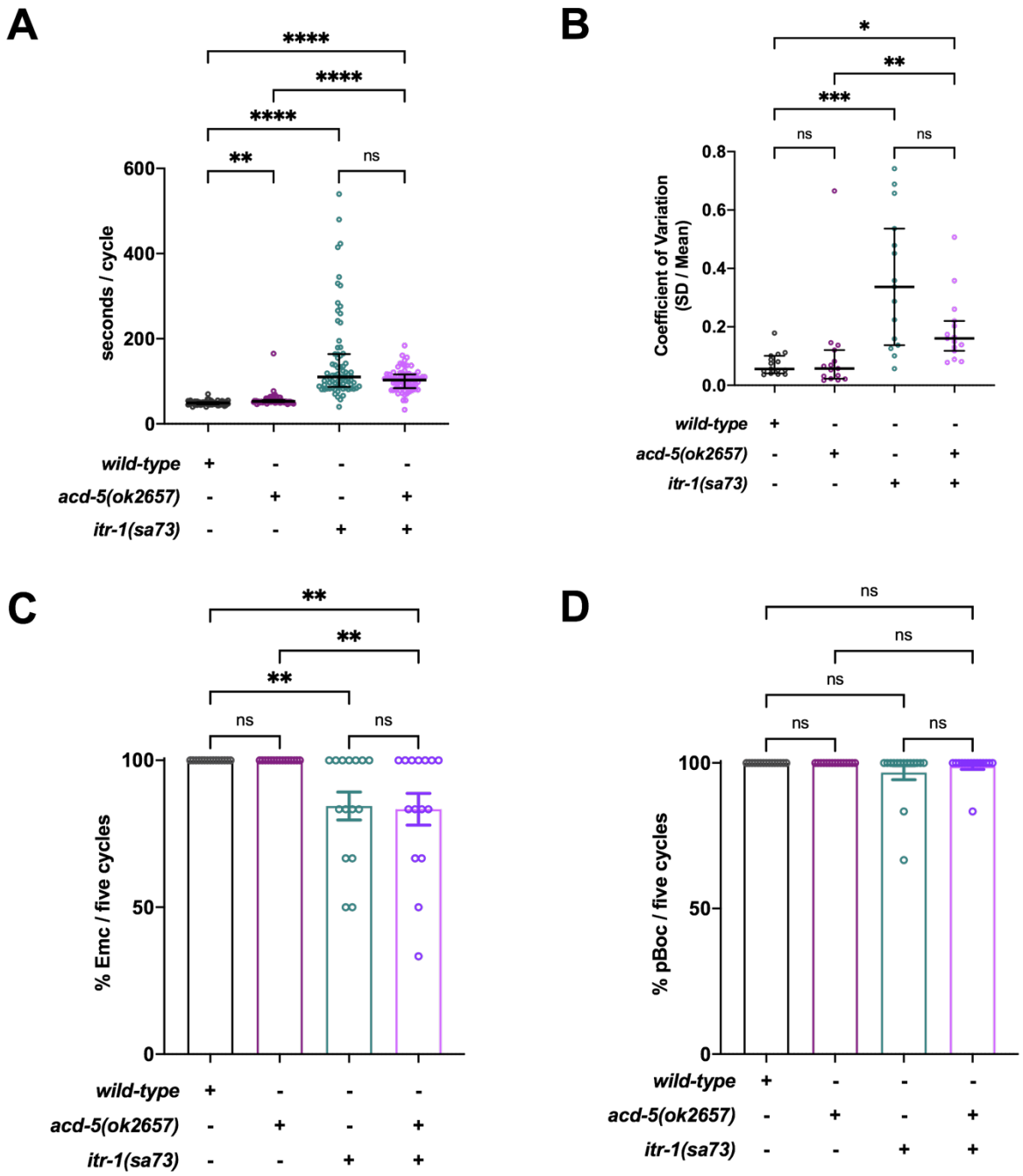

Figure 40: Assessing the genetic relationship between acd-5 and itr-1-dependent calcium signalling in the intestine.

(A) DMP interval length was assessed using a Kruskal-Wallis test which was significant (H(3) = 215.8, ****p<0.0001). A post-hoc Dunn's multiple comparison test indicated that compared to the wild-type (Mdn = 49 sec, N=15), the *acd-5(ok2657)* mutants (Z=3.38, **p=0.0036, N=15) and the *itr-1* single (Z=12.35, ****p<0.0001, N=15) and double mutants (Z=11.12, ****p<0.0001, N=15) showed a statistically significant increase in interval length. Compared to *acd-5(ok2657)* single mutants, double mutants for *acd-5* and *itr-1* also showed an increase in interval length (Z=7.80, ****p<0.0001, N=15) which was similar to *itr-1* single mutants. Error bars represent Median and IQR. **(B) Variability** of the

defecation cycles represented as Coefficient of Variation (Standard Deviation (SD) divided by Mean cycle length). A Kruskal-Wallis test was significant (H(3) = 28.96, ****p<0.0001). A post-hoc Dunn's multiple comparison test indicated *itr-1* single and double mutants show a statistically significantly higher variability compared to the wild-type ($Z_{itr\text{-}1(sa73)}$=4.26, ***p=0.0001; $Z_{itr\text{-}1(sa73)/acd\text{-}5(ok2657)}$=3.14, *p=0.0103), and they also showed significantly more variability than the *acd-5* single mutant ($Z_{itr\text{-}1(sa73)/acd\text{-}5(ok2657)}$=3.19, **p=0.0086). Error bars represent Median and IQR. **(C)** Quantification of missed EMC for the indicated genotypes. Kruskal-Wallis test was significant (H(3) = 20.88, ***p=0.0001). A post-hoc Dunn's multiple comparison test indicated *itr-1* single and double mutants show an increased frequency in missed EMCs ($Z_{itr\text{-}1(sa73)}$= 3.22, **p=0.0078; $Z_{itr\text{-}1(sa73)/acd\text{-}5(ok2657)}$=3.24, **p=0.0071) compared to the wild-type, and they also showed significantly more missed EMCs than the *acd-5* single mutant ($Z_{itr\text{-}1(sa73)/acd\text{-}5(ok2657)}$=3.22, **p=0.0071). Error bars represent Mean ± SEM. **(D)** Quantification of missed pBoc for the indicated genotypes. Kruskal-Wallis test was not significant (H(3) = 3.84, ns). Error bars represent Mean ± SEM.

Table 6: Defecation cycle Intervals of acd-5 and itr-1 mutants.

Cycle length in seconds of five individual cycles per animal. Percentages of EMC and pBoc steps for each animal (in five cycles).

	N	**Cycle length in seconds (Median (IQR))**	**% of EMC (Mean ± SEM)**	**% of pBoc (Mean ± SEM)**
wild-type	15	49(5)	100	100
acd-5(ok2657)	15	55(5.25)	100	100
itr-1(sa73);	15	110(77)	84.4 ± 4.73	96.7 ± 2.41
itr-1(sa73); acd-5(ok2657)	15	103(82)	83.3 ± 5.39	98.9 ±1.11

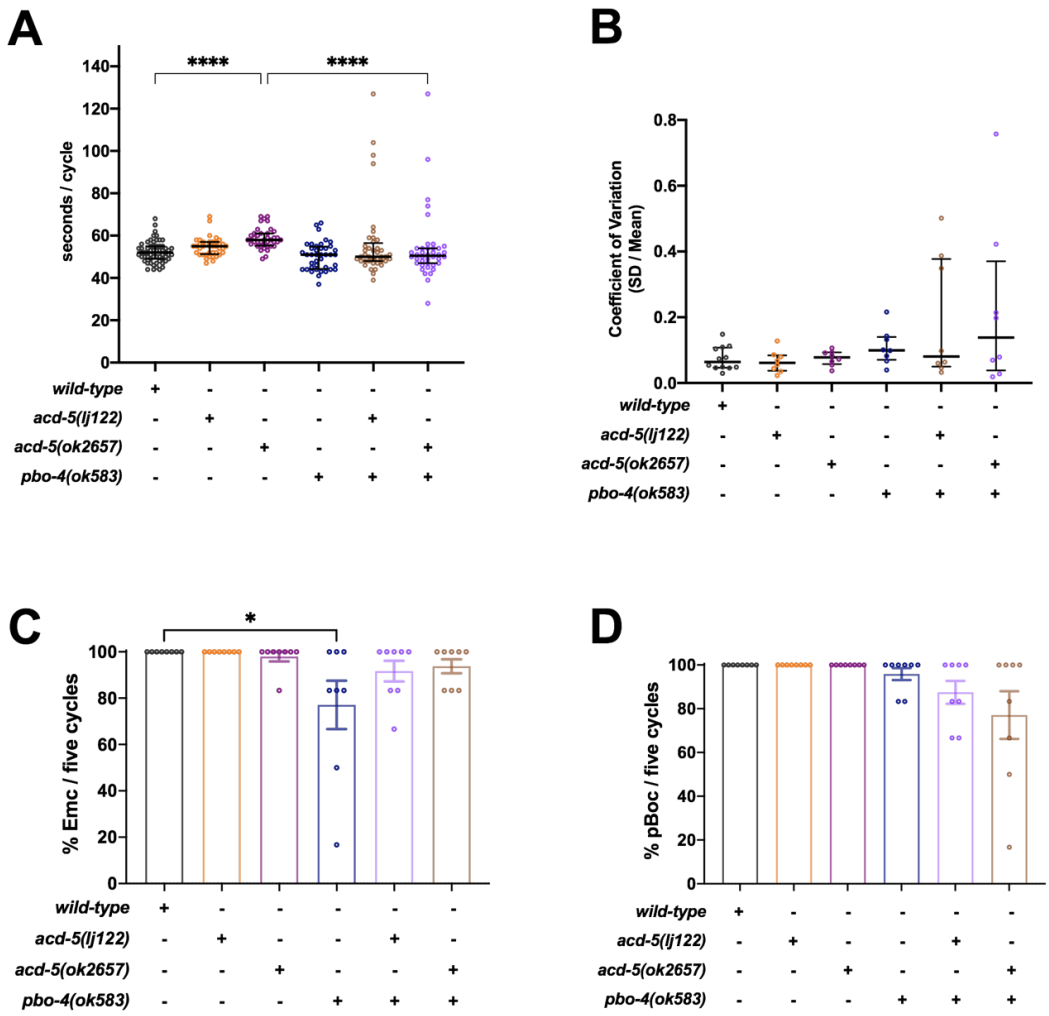

Figure 41: Assessing the genetic relationship between acd-5 and pbo-4-dependent proton-signalling in the intestinal lumen.

For clarity only, statistical significance is indicated by the Asterix. **(A)** DMP interval length was assessed using a Kruskal-Wallis test which was significant (H(5) = 53.22, ****p<0.0001). A post-hoc Dunn's multiple comparison test indicated that compared to the wild-type only the *acd-5(ok2657)* single mutants showed a statistically significant increase in interval length (Z=5.26, ****p<0.0001, N=8) but *acd-5(ok2657)/pbo-4(ok538)* double mutants showed wild-type cycle length. Error bars represent Median and IQR. **(B) Variability** of the defecation cycles represented as Coefficient of Variation (Standard Deviation (SD) divided by Mean cycle length). Kruskal-Wallis test was not significant (H(5) = 4.653, p=0.460, ns). Error bars represent Median and IQR. **(C)** Quantification of missed EMCs for the indicated genotypes. Kruskal-Wallis test was significant (H(5) = 13.66, *p=0.018). A post-hoc Dunn's multiple comparison test indicated that compared to the wild-type only the *pbo-4(ok538)* single mutants showed a statistically significant increase in interval length (Z=2.96, *p=0.46). Error bars represent Mean ± SEM. **(D)** Quantification of missed pBoc steps for the indicated genotypes. Kruskal-Wallis test was significant (H(5) = 14.84, *p=0.0111). A post-hoc Dunn's multiple comparison test indicated that none of the groups tested differed statistically significantly form another. Error bars represent Mean ± SEM.

Table 7: Defecation cycle Intervals of acd-5 and pbo-4 mutants.

Cycle length in seconds of five individual cycles per animal. Percentages of EMC and pBoc steps for each animal (in five cycles).

	N	**Cycle length in seconds (Median (IQR))**	**% of EMC (Mean ± SEM)**	**% of pBoc (Mean ± SEM)**
wild-type	12	52(6)	100	100
acd-5(lj122)	8	55(5.75)	100	100
acd-5(ok2657)	8	58(5.75)	97.9 ± 2.08	100
pbo-4(ok583)	8	51(10.5)	77.1 ± 10.4	95.8 ±2.73
pbo-4(ok583); acd-5(lj122)	8	50(8.5)	91.7 ± 4.45	87.5 ± 5.22
pbo-4(ok583);acd-5(ok2657)	8	50.5(7)	93.7 ± 3.05	77.1 ± 10.9

5. 3. 6. *In vitro* evidence for interactions between DEG/ENaC subunits

As mentioned in CHAPTER 1, DEG/ENaCs can form heteromeric as well as homomeric channels. In CHAPTER 3 and from previous research, we have evidence that in addition to *acd-5*, there are at least three more DEG/ENaC subunits expressed in the intestine, these are *acd-3*, *del-5* and *flr-1*. While there is no data on *acd-3* and *del-5*, *flr-1* has previously shown to regulate defecation and, like ACD-5, FLR-1::GFP accumulates at the apical membrane of the intestinal cells (Take-Uchi et al., 1998). To assess whether ACD-5 as well as the dominant mutant fragment ACD-5(ok2657) interacts with one of the candidates directly, a post-doc in the lab Yi-Quan Tang carried out a co-immunoprecipitation (CoIP) and pull-down assay. ACD-5 and its mutant fragment coimmunoprecipitated with all candidates, FLR-1, ACD-3 and DEL-5, in extracts from HEK293T cells heterologously expressing V5-tagged ACD-5 or mutant fragment and the 3xFLAG-tagged candidate (Figure 42). This finding provided further evidence that ACD-5 could form a heteromeric channel *in vivo*.

Some mammalian heteromeric ASIC channels differ in their proton-sensing properties from homomeric channels (Hesselager et al., 2004). Therefore, I tested whether proton responses were altered when co-injecting oocytes with ACD-3, DEL-5 or FLR-1 cRNA in addition to ACD-5 in *Xenopus* oocytes. As shown in CHAPTER 2, ACD-3, DEL-5 and FLR-1 are insensitive to low pH when expressed in *Xenopus* oocytes and only DEL-5 is amiloride sensitive showing enhanced currents in the presence of the blocker. Results of co-expression are shown in Figure 43, however, there was no shift in pH_{50} for decreasing or increasing pH responses suggesting that ACD-5 might be the main pH-sensing subunit of a potential heteromeric channel. Interpreting the results of co-expression experiments is quite complex as besides forming homomeric or heteromeric complexes, subunits could also form a mixed population of channels which might mask or dilute effects of heteromeric assemblies (Hesselager et al., 2004).

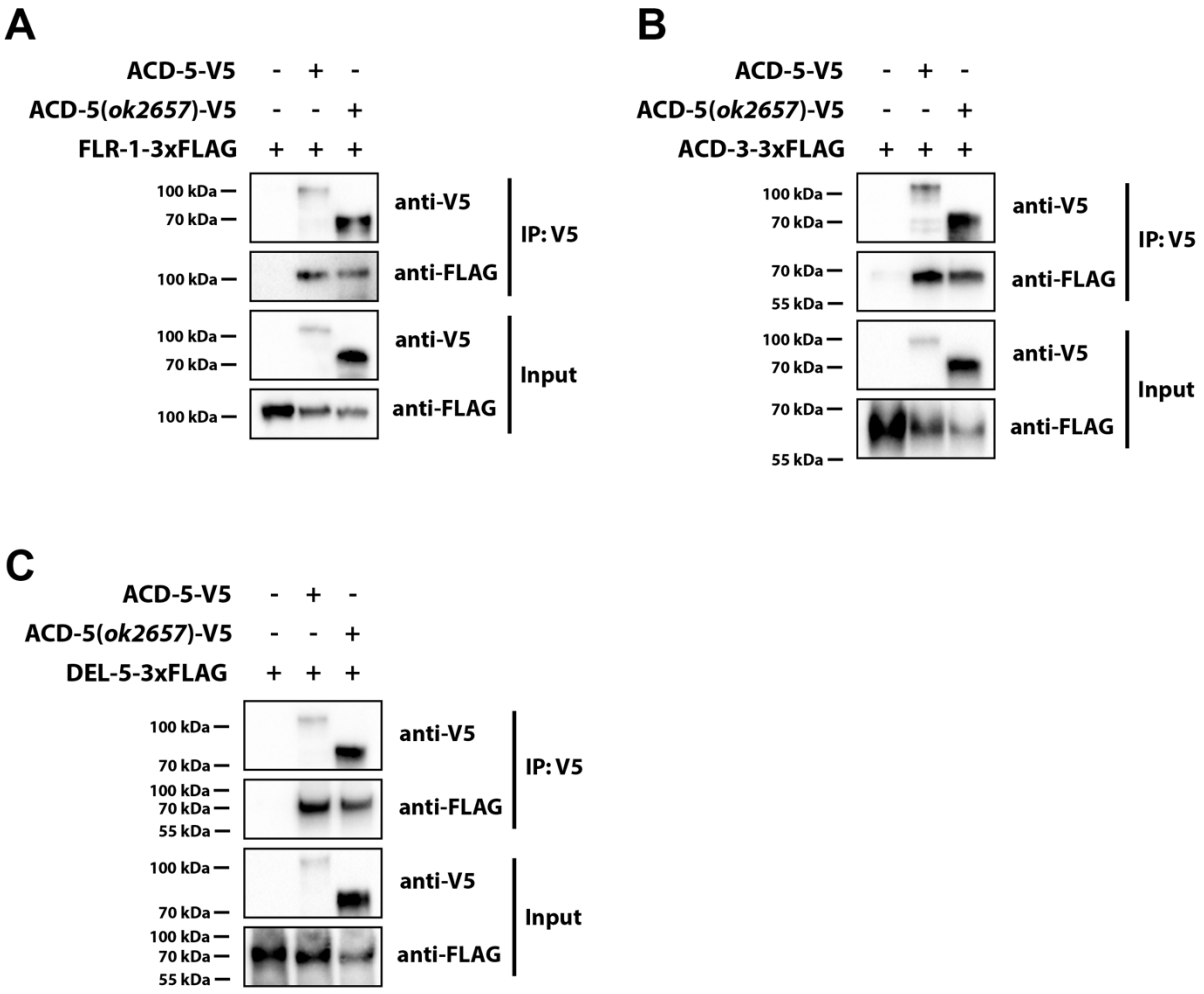

***Figure 42: ACD-5 interacts with FLR-1, ACD-3 and DEL-5* in vitro.**

CoIP of ACD-5 and ACD-5(ok2657) with (A) FLR-1 (B) ACD-3 and (C) DEL-5 in HEK293T cells. Pull-down analysis of purified V5-tagged ACD-5 constructs and 3xFLAG-tagged candidate subunits. Proteins are visualized by western blot. Experiment and analysis done by Yi-Quan Tang.

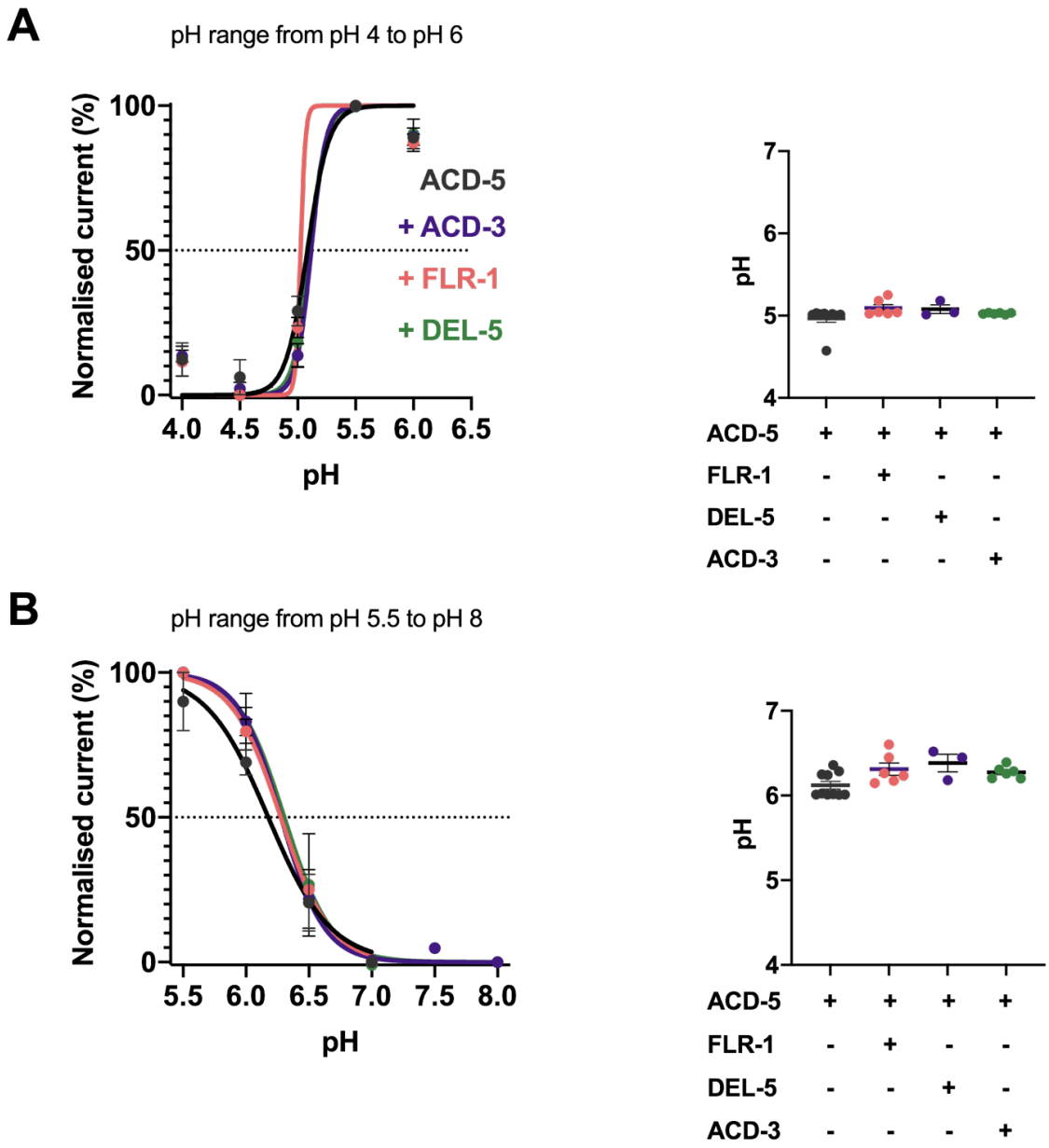

Figure 43: Co-injection of ACD-5 with other potential subunits into Xenopus oocytes.

pH response curves covering a rage from pH 8 – pH 4. ACD-5 cRNA (dark grey)-injected only and co-injected with FLR-1 cRNA (light red), ACD-3 cRNA (purple) or DEL-5 cRNA (green) perfused with solutions within the (A) range pH 4 – pH 6. *Left*: pH_{50} of 5.08 (N = 9) for ACD-5 and co-expression with FLR-1 (pH_{50} of 5.03, N = 6), ACD-3 (pH_{50} of 5.12, N = 6) and DEL-5 (pH_{50} of 5.11, N = 3). *Right*: Quantification of pH_{50} for each oocyte. (B) Range pH 5.5 – pH 8. *Left*: pH_{50} of 6.18 (N = 10) for ACD-5 and co-expression with FLR-1 (pH_{50} of 6.28, N = 5), ACD-3 (pH_{50} of 6.28, N = 5) and DEL-5 (pH_{50} of 6.31, N = 3). *Right*: Quantification of pH_{50} for each oocyte. Channel is fully open at 100% current and closed at 0% current. Currents were recorded at a holding potential of -60mV, normalized to maximal currents and best fitted with the Hill's equation (Nonlin fit Log(inhibitor) vs normalized response – variable slope) in GraphPad Prism. hCIB3 cRNA was used as a filler to account for the same amount of total cRNA (500 ng/µl) injected into the oocyte. Error bars represent Mean ± SEM.

5. 3. 7. Behavioural and gene expression data further supports and interaction between *acd-5* and *flr-1*

Based on the expression pattern and evidence from the CoIP experiments described above, I now wanted to test whether I can find evidence using behavioural experiments that these subunits can form a heteromeric channel *in vivo*. From other *C. elegans* DEG/ENaCs we know that double mutants can display enhanced phenotypes for instance in the case of *delm-1/delm-2* double mutant responses to nose touch is statistically smaller than those of single mutants suggesting that they may act independently (Han et al., 2013). Others, such as *del-1, mec-10*, and *unc-8* function in the same genetic pathway to regulate movements as double and triple mutants show movement phenotypes indistinguishable from single mutants (Tao et al., 2019).

We already have evidence that *flr-1* mutants show aberrant DMP and localised to the apical membrane (Take-Uchi et al., 1998, Kwan et al., 2008, Katsura et al., 1994). *flr-1(ut11)* mutants are unhealthy, they are small and thin, develop very slowly and lay few eggs and are therefore hard to cross and to maintain. As mentioned in CHAPTER 1, another way to target knock-down of particular genes apart from using mutants is to use RNA interference (RNAi) by feeding (Kamath et al., 2001). The RNAi knock-down of *flr-1* resulted in a similar phenotype of thin, small worms with few eggs and showed similar defecation defects to the *flr-1(ut11)* mutants previously described (Take-Uchi et al., 1998). *flr-1(ut11)* mutants have previously been described as having shorter defecation cycles with few longer than 300 seconds but with high variability (Take-Uchi et al., 1998, Kwan et al., 2008). By contrast, *flr-1(RNAi)* animals showed a singly increased median defecation cycles of 54 seconds which was not significantly different to the wild-type, however, this was halved in the *acd-5* mutant backgrounds with median cycle length of 33-37 seconds (Figure 44A; Table 8). Another striking phenotype was the increase in variability of *flr-1(RNAi)* animals which decreased slightly but was also present in *acd-5* mutants on *flr-1(RNAi)* (Figure 44A; Table 8). This difference in cycle length and variability compared to previous publications is most likely due to the knock-down of *flr-1* while in the *flr-1(ut11)* is a point mutation that might change channel functioning. Similar to previous observations (Take-Uchi et al., 1998), animals on *flr-1(RNAi)* also displayed missed pBoc and EMC steps in 16% and 29% of average defecation cycles, respectively (Figure 44C; Table 8). The

frequency of missed pBoc steps were rescued in the *acd-5(ok2657)* mutants on *flr-1(RNAi)* but the frequency of missed EMCs increased slightly to over 30% in both mutant backgrounds (Figure 44C; Table 8). Missed EMCs were also observed in animals on *acd-3(RNAi)* but at a lower frequency to the ones on *flr-1(RNAi)*.

flr-1(RNAi) gave reliable convincing results similar to what had been described for animals carrying the *flr-1(ut11)* allele, suggesting that *flr-1(ut11)* might be a null-mutant. The effect of loss of *acd-3* and *del-5* had not been tested before and in the RNAi feeding experiments, they do not display strong phenotypes. This could be due to ineffective RNAi, so I tested mutants of both genes and double mutants between *acd-3* or *del-5* and *acd-5*. For *acd-3*, I used a mutation that was already available from the CGC, the *acd-3(ok1335)* mutation is a truncation of most of the extracellular loop and the second transmembrane domain. For *del-5,* I used CRISPR/Cas9 to create a deletion that removes the predicted N-terminal fragment, with the remainder of the gene being out of frame, so no protein is generated, this allele is called *del-5(lj138)* (Figure 45A, B). *acd-5(ok2657)/acd-3* double mutants could rescue the phenotype of the prolonged intervals in *acd-5(ok2657)* single mutants (Figure 45C). By contrast, *del-5* double mutant with either *acd-5* allele displayed significantly longer defecation cycles compared to the *del-5* single mutant or wild-type, which were similar to those of the *acd-5(ok2657)* single mutants. (Figure 45D, Table 9). *acd-3* single and double mutants with *acd-5(ok2657)* as well as *acd-5(ok2657)/del-5* double mutants also showed a significant increase in missed EMCs compared to the wild-type and *acd-5(ok2657)* single mutants (Figure 45E, Table 9). *acd-3* single and *acd-5(ok2657)/acd-3* double mutants show a higher variability compared to the wild-type (Figure 45D). Taken together these experiments suggest that *acd-5* genetically interact with *flr-1*, *acd-3* and *del-5*.

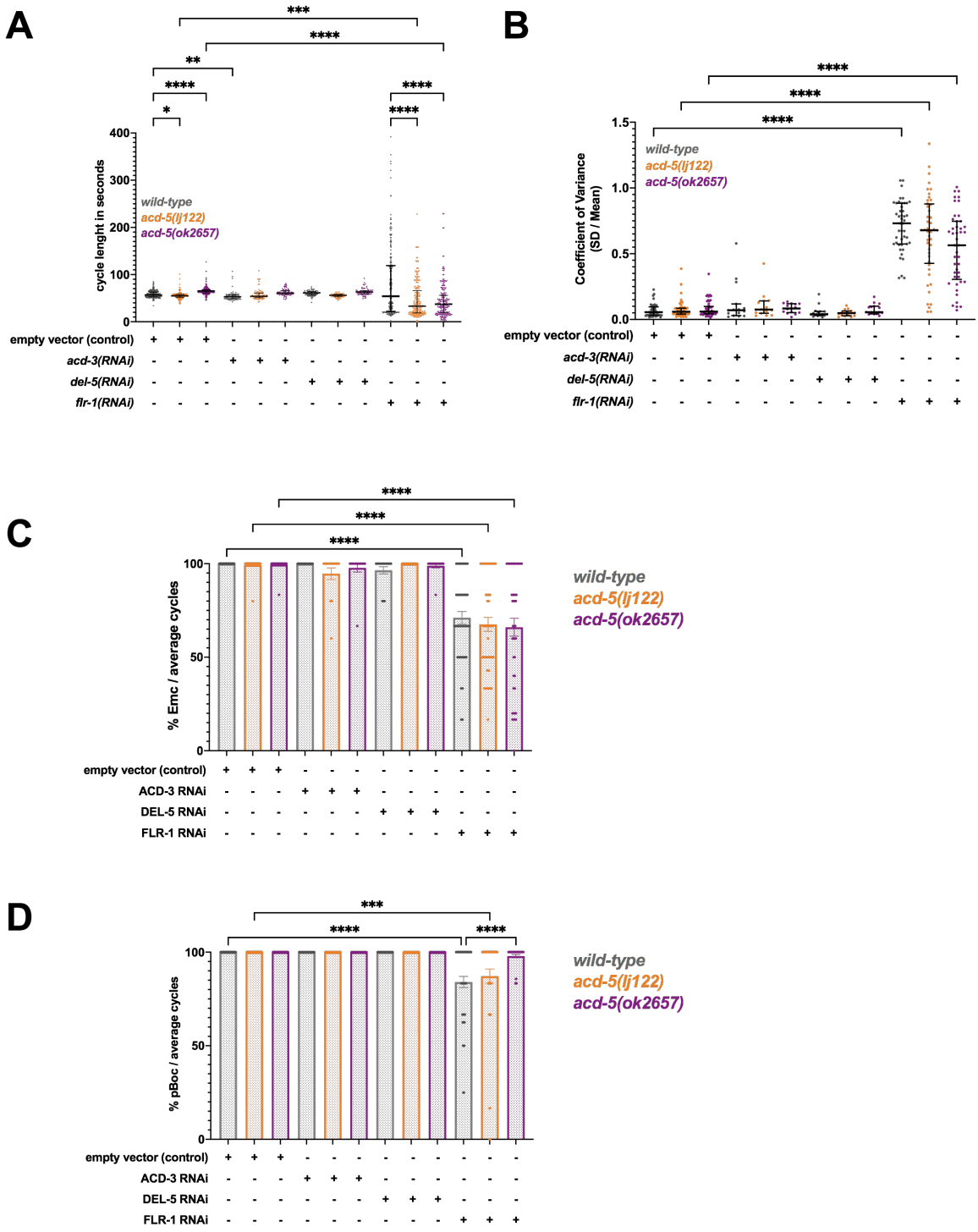

Figure 44: RNAi knock-down of acd-3, del-5 and flr-1 in sensitised acd-5 mutant backgrounds.

For clarity, only statistically significant results are indicated. (A) DMP interval length was assessed using a Kruskal-Wallis test which was significant (H(11) = 385.9, ****p<0.0001). A post-hoc Dunn's multiple comparison test indicated that compared to the wild-type the *acd-5(lj122)* (Z= *3.297*, *p=0.0127), *acd-5(ok2657)* mutants (Z=*7.162*, ****p<0.0001), and the wild-type on *acd-3(RNAi)* showed a statistically significant difference interval length (Z=3.387, **p=0.0092), while on *flr-1(RNAi), acd-5(lj122)* mutants

(Z=*3.961*, ***p=0.001) and *acd-5(ok2657)* mutants (Z=*15.15*, ****p<0.0001) show a statistically significant decrease in cycle length. This was also statistically significant shorter than the wild-type on *flr-1(RNAi),* i.e. *acd-5(lj122)* mutants (Z=*6.945*, ****p<0.0001) and *acd-5(ok2657)* mutants (Z=*7.888*, ****p<0.0001). Error bars represent Median and IQR. (B) Variability of the defecation cycles represented as Coefficient of Variation (Standard Deviation (SD) divided by Mean cycle length). A Kruskal-Wallis test was significant (H(11) = 241.9, ****p<0.0001). A post-hoc Dunn's multiple comparison test indicated that only the *flr-1(RNAi)* strongly affected variability ($Z_{wt[flr\text{-}1(RNAi)]}$=9.262, ****p<0.0001; $Z_{acd\text{-}5(lj122)[flr\text{-}1(RNAi)]}$=7.827, ****p<0.0001; $Z_{acd\text{-}5(lok2657)[flr\text{-}1(RNAi)]}$= 7.012, ****p<0.0001). Error bars represent Median and IQR. (C) Quantification of missed EMCs. A Kruskal-Wallis test which was significant (H(11) = 191.2, ****p<0.0001). A post-hoc Dunn's multiple comparison test indicated that compared to the wild-type controls, the wild-type and both mutants on *flr-1(RNAi)* displayed a statistically significant increase in missed EMCs ($Z_{wt[flr\text{-}1(RNAi)]}$=6.32, ****p<0.0001; $Z_{acd\text{-}5(lj122)[flr\text{-}1(RNAi)]}$=6.37, ****p<0.0001; $Z_{acd\text{-}5(lok2657)[flr\text{-}1(RNAi)]}$= 6.14, ****p<0.0001). Error bars represent Mean ± SEM. (D) Quantification of missed pBoc steps. A Kruskal-Wallis test which was significant (H(11) = 101.2, ****p<0.0001). A post-hoc Dunn's multiple comparison test indicated that compared to the wild-type controls, the wild-type and both mutants on *flr-1(RNAi)* displayed a statistical significant increase in missed pBocs ($Z_{wt[flr\text{-}1(RNAi)]}$=6.385, ****p<0.0001; $Z_{acd\text{-}5(lj122)[flr\text{-}1(RNAi)]}$=4.153, ***p=0.0004) but not the acd-5(ok2657) mutant which was statistically different to the *wild-type[flr-1(RNAi)]* ($Z_{acd\text{-}5(lok2657)[flr\text{-}1(RNAi)]}$= 5.25, ****p<0.0001). Error bars represent Mean ± SEM.

Table 8: Defecation cycle Intervals for RNAi feeding experiments

Cycle length in seconds of five individual cycles per animal. Percentages of EMC and pBoc steps for each animal (in five cycles).

Genotype	RNAi	N	Cycle length in seconds (Median (IQR))	% pBoc/five cycles (Mean ± SEM)	% EMC/five cycles (Mean ± SEM)
wild-type		32	57(10)	100	100
acd-5(lj122)		32	55(6)	100	99.39 ± 0.61
acd-5(ok2657)		33	65(7)	100	99.49 ± 0.05
wild-type	DEL-5	17	61(7)	100	96.50 ± 1.91
acd-5(lj122)	DEL-5	15	56(5)	100	100
acd-5(ok2657)	DEL-5	15	63(7)	100	98.90 ± 1.11
wild-type	ACD-3	15	53(8)	100	100
acd-5(lj122)	ACD-3	15	54(10)	100	94.70 ± 3.07
acd-5(ok2657)	ACD-3	15	61(8)	100	97.80 ± 2.22

wild-type	FLR-1	48	54(97)	84.00 ± 2.99	71.11 ± 3.37
acd-5(lj122)		48	33(47.5)	87.20 ± 3.79	67.53 ± 3.73
acd-5(ok2657)		45	37(37)	97.90 ± 0.82	66.00 ± 4.78

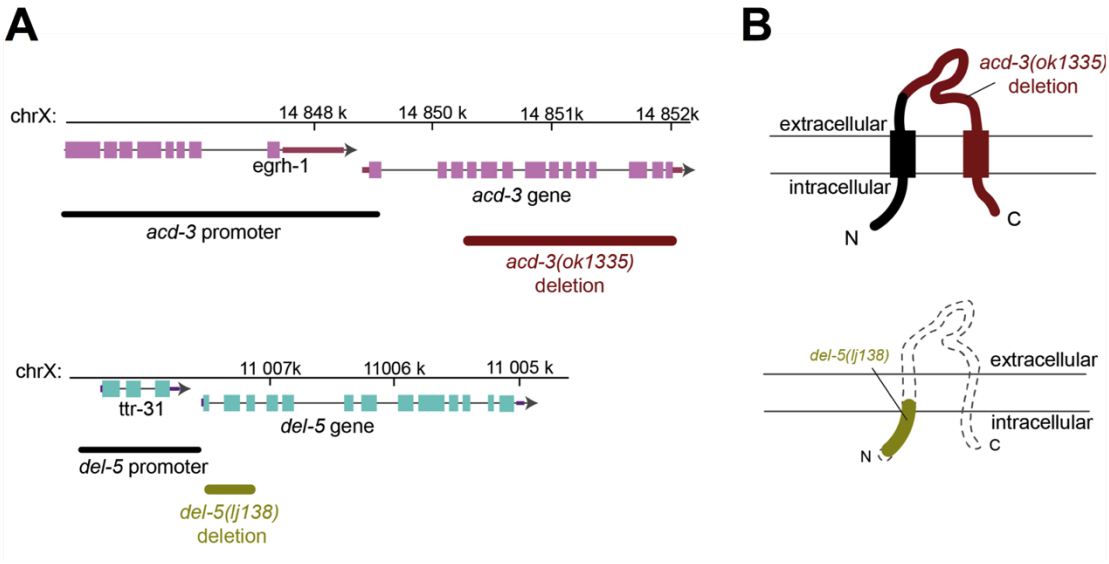
A
chrX:
14 848 k
14 850 k
14 851k
14 852k
egrh-1
acd-3 gene
acd-3 promoter
acd-3(ok1335)
deletion
chrX:
11 007k
11006 k
11 005 k
ttr-31
del-5 gene
del-5 promoter
del-5(lj138)
deletion
B
acd-3(ok1335)
deletion
extracellular
intracellular
N
C
del-5(lj138)
extracellular
intracellular
N
C

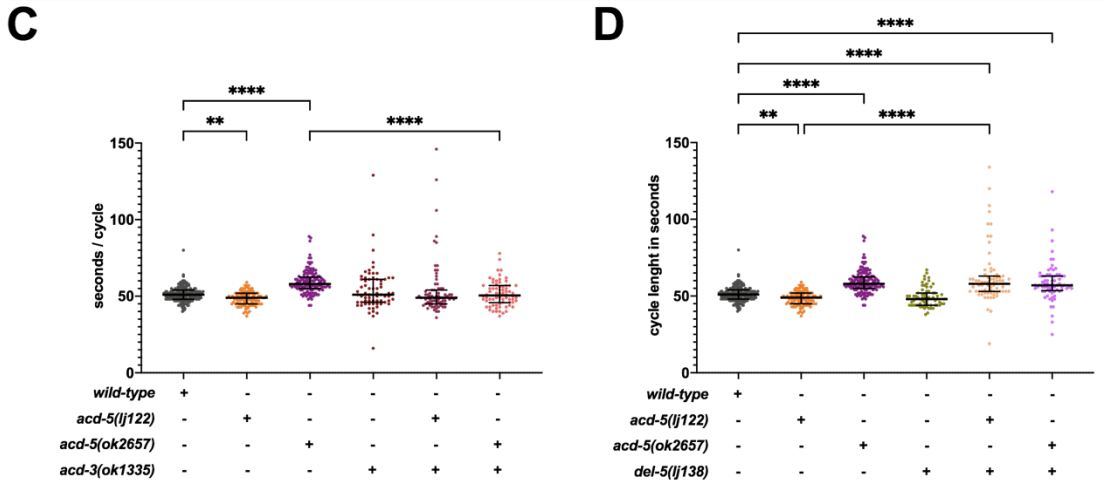
C
seconds / cycle
wild-type
acd-5(lj122)
acd-5(ok2657)
acd-3(ok1335)
D
cycle lenght in seconds
wild-type
acd-5(lj122)
acd-5(ok2657)
del-5(lj138)

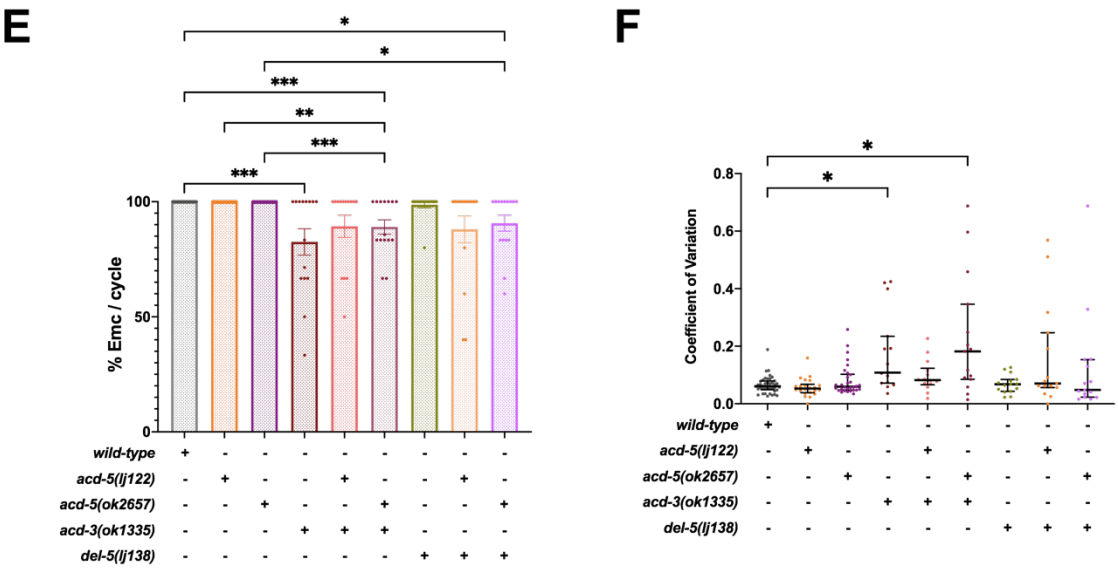
E
% Emc / cycle
wild-type
acd-5(lj122)
acd-5(ok2657)
acd-3(ok1335)
del-5(lj138)
F
Coefficient of Variation
wild-type
acd-5(lj122)
acd-5(ok2657)
acd-3(ok1335)
del-5(lj138)

Figure 45: Assessment of DMP for double mutants of acd-5 and acd-3 or del-5.

(A) *acd-3 and del-5* genomic region on chromosome X. Boxes indicate exons and lines indicate introns. Endogenous promoter region and mutations used in the study are shown. (B) Schematic of predicted ACD-3 and DEL-5 protein structure with two transmembrane domains, and cytosolic N and C terminus and an extracellular loop, typical of DEG/ENaC subunits. Mutations used in the study are indicated in brown for the *acd-3(ok1335)* and in olive green the *del-5(lj138).* (C) DMP interval length was assessed using a Kruskal-Wallis test which was significant (H(5) = 168.0, ****p<0.0001). *acd-3(ok1335)* mutants have a normal DMP interval length. A post-hoc Dunn's multiple comparison test indicated that compared to the wild-type both *acd-5* mutants, *acd-5(ok2657)* (Z=3.65, ****p<0.0001) and *acd-5(lj122)* (Z=9.68, ****p<0.0001) showed a statistically significant increase in interval length. But double-mutants had a wild-type cycle length which was significantly lower than the *acd-5(ok2657)* single mutant ($Z_{acd\text{-}5(ok2657)/acd\text{-}3(ok1335)}$= 7.39, ****p<0.0001). Error bars represent Median and IQR. (D) DMP interval length was assessed using a Kruskal-Wallis test which was significant (H(5) = 257.8, ****p<0.0001). A post-hoc Dunn's multiple comparison test indicated that compared to the wild-type not only the two *acd-5* mutants (see (C)) but also the *del-5/acd-5* double mutants showed an statistically significant increase in cycle length ($Z_{acd\text{-}5(ok2657)/del\text{-}5(lj138)}$ =7.46, ****p<0.0001; ($Z_{acd\text{-}5(lj122)/del\text{-}5(lj138)}$=6.78, ****p<0.0001). Error bars represent Median and IQR. (E) Quantification of missed EMCs. A Kruskal-Wallis test which was significant (H(8) = 50.10, ****p<0.0001). A post-hoc Dunn's multiple comparison test indicated that compared to the wild-type, the *acd-3* single and double mutants showed a significant increase in missed EMCs ($Z_{acd\text{-}3(ok1335)}$= 4.278, ***p=0.0003; $Z_{acd\text{-}3(ok1335)/acd\text{-}5(ok2657)}$= 4.36, ***p=0.0002). *acd-3* double mutants showed a significant increase in missed EMCs compared to the *acd-5(ok2657)* single mutants ($Z_{acd\text{-}3(ok1335)/acd\text{-}5(ok2657)}$= 4.174, ***p=0.0005). Similarly, *acd-5(ok2657)/del-5(lj138)* double mutants showed a significantly higher frequency of missed EMCs compared to the wild-type ($Z_{del\text{-}5(lj138)/acd\text{-}5(ok2657)}$= 3.37, *p=0.0127) or the *acd-5(ok2657)* single mutants ($Z_{del\text{-}5(lj138)/acd\text{-}5(ok2657)}$= 3.23, *p=0.0211). Error bars represent Mean ± SEM. (F) Variability of the defecation cycles represented as Coefficient of Variation (Standard Deviation (SD) divided by Mean cycle length). A Kruskal-Wallis test was not significant (H(8) = 29.59, ***p=0.0002). A post-hoc Dunn's multiple comparison test indicated *acd-3* single and *acd-3(ok1335)/acd-5(ok2657)* double mutants show a statistically significant higher variability compared to the wild-type ($Z_{acd\text{-}3(ok1335)}$=3.36, *p=0.0123; $Z_{acd\text{-}3(ok1335))/acd\text{-}5(ok2657)}$=3.41, *p=0.0102). All mutants were all scored together. For clarity, only statistically significant results are indicated in the Figure. Error bars represent Median and IQR.

Table 9: Defecation cycle Intervals for acd-5 double mutants with acd-3 or del-5.

Cycle length in seconds of five individual cycles per animal. Percentages of EMC and pBoc steps for each animal (in five cycles).

	N	**Cycle length in seconds (Median (IQR))**	**% EMC/five cycles (Mean ± SEM)**
wild-type	40	51(6)	100
acd-5(lj122)	22	49(7)	100
acd-5(ok2657)	30	58(7.5)	100
acd-3(ok1335)	15	51(15)	82.5 ± 5.69
del-5(lj138)	15	48(8)	98.7 ± 1.33
acd-5(ok2657); acd-3 (ok1335)	15	49(9)	89 ± 3.1
acd-5(lj122); acd-3 (ok1335)	15	50.5(11.2)	89.3 ± 4.82
acd-5(lj122) I; del-5 (lj138)	15	58(10)	88 ± 5.79
acd-5(ok2657) I; del-5 (lj138)	14	57(9.5)	90.7 ± 3.46

5.4. Discussion

In the current chapter, I presented the work on two proton-sensitive DEG/ENaCs, ACD-5 and DEL-4 that are inhibited by low pH. Both channels can form amiloride-sensitive homomeric channels *in vitro* in *Xenopus* oocytes that are permeable for monovalent cations, but not Ca^{2+}. DEL-4 forms a Na^+ channel that is also permeable for Li^+, ACD-5 is permeable for both Na^+ and K^+ similar to what has been previously proposed for other DEG/ENaCs (Fechner et al., 2020). Both show responses to a particular range of pH which might reflect their physiological function *in vivo.* Outside this range such as when ectopic expressed in *Xenopus* oocytes and perfused with pH above pH 6.5 for ACD-5 or below pH 4.5 responses seen might be due to an non-physiological environment for these channels. Support for this hypothesis comes from imaging of the luminal pH in the *C. elegans* intestine which ranges from 5.96 ± 0.31 in the anterior pharynx to 3.59 ± 0.09 in the posterior intestine (Chauhan et al., 2013). Similarly, responding to a particular range of pH has also previously been described for human ENaC currents which are regulated by pH within the range found in epithelia where they are expressed (Collier and Snyder, 2009). I further explored this hypothesis that the pH range reflect their physiological function by focussing on ACD-5 in the intestinal cells. I provided evidence for the hypothesis that ACD-5 functions in intestine where it senses fluctuation in proton concentrations and contributes to acidification of the intestinal lumen and rhythmic behaviour.

ACD-5 is highly expressed in the intestine where it localises to the apical membrane facing the intestinal lumen. By investigating rhythmic muscle contractions of the DMP, I have shown that the dominant *acd-5(ok2657)* mutant allele can prolong the defecation cycle intervals. Experiments done in collaboration with the Ackerly lab at the University of Kansas provided evidence for a direct proton-sensing role of ACD-5, as *acd-5* mutants are defective in establishing and maintaining an appropriate acidic pH in the intestinal lumen. This could be rescued only for the *acd-5*(lj122) mutant allele. The most likely explanation for longer cycles and inability to rescue cycle length and intestinal pH, might be that *acd-5(ok2657)* can still form a heteromeric channel with itself or other potential subunits, or otherwise disrupts their function, by preventing their trafficking or sequestering a factor required for proper channel functioning. This hypothesis is supported by the finding that similar to homozygous *acd-5(ok2657)* mutants, heterozygous mutants also display the same prolonged defecation cycle length. In addition, heterologous expression of the mutant fragment and the wild-type

in oocytes indicated that heteromeric channels are not functional. I also assessed if the other DEG/ENaC subunits, ACD-3, FLR-1 and DEL-5, expressed in the intestine, can form a heteromeric channel with ACD-5 or its mutant fragment ACD-5(ok2657). The *in vitro* assay in HEK cells by Yi-Quan Tang showed that all of them can interact with both fragments *in vitro*. Follow-up behavioural experiments showed that *flr-1(RNAi)* had the strongest phenotype on muscle contraction, individual cycle length and variability of all potential subunits, while only a small effect of the others on behaviour could be observed. The observation that *acd-5* mutants suppress several aspects of the *flr-1* phenotype does nevertheless indicate that these phenotypes are dependent on *acd-5*, and further, that an ACD-5-containing (pH-dependent) channel plays a central role in the aberrant signalling pathways that result from the absence of FLR-1. Furthermore, both ACD-5 and FLR-1 are expressed on the apical membrane of the intestinal lumen which further supports that they are likely to interact *in vivo*. However, one experiment that might test the interaction of FLR-1 and ACD-5 further is to perform RNAi feeding experiment on *flr-1* mutants on *acd-5(RNAi)*.

acd-5(ok2657)/acd-3(ok1335) double mutants rescued the phenotype of the prolonged intervals in *acd-5(ok2657)* single mutants. This suppression of the *acd-5*(ok2657) phenotype by an *acd-3* mutation suggests that *acd-3* is required for the aberrant signalling resulting from *acd-5(ok2657)*. *del-5* double mutant with either *acd-5* allele displayed significantly longer defecation cycles comparable to those of the *acd-5(ok2657)* single mutants which indicates that both play an important role in maintaining DMP. Phenotypes observed are not very strong, therefore is likely that subunits are to some degree redundant and can compensate for each other, or they could reflect a different channel composition or failure of some components to localise. *In vivo* co-localisation of tagged subunits as well as additional intestinal lumen pH imaging might provide further evidence that they indeed interact *in vivo*.

In order to explore potential mechanism underlying *acd-5* functioning, I acquired genetic evidence crossing the *acd-5* mutants into genetic pathways of known DMP regulators, the intestinal calcium wave (dependent on *itr-1*) and the protons secreted from the intestinal cells (dependent on *pbo-4/nhx-7*). *acd-5(ok2657)/itr-1* double mutants displayed a decreased in cycle length as well as a decreased variability compared to the *itr-1* single mutants. This effect was similar to the *flr-1(RNAi)* mutants, and more generally there is a certain degree of similarity between *itr-1* and *flr-1* mutant phenotypes suggesting that they might be in the same genetic

pathway. The *acd-5(ok2657)/pbo-4* double mutant displayed wild-type/*pbo-4* cycle length but with higher variability, double mutants also displayed fewer missed EMCs but higher missed pBocs compared to the single *pbo-4* mutants. Consequently, genetic evidence has provided some insight that ACD-5 might interact with genetic pathways regulating the intestinal calcium oscillations and intestinal proton-secretion.

While at this point we can only speculate on how this can be explained at a physiological level, it might be that further dysregulation of pH in the intestinal lumen of single mutants can explain the observed phenotypes. For instance, previous studies have demonstrated a relationship between the acidification of the intestinal lumen and the physical movement of the proton wave (Maximum Anterior Transition, MAT). They showed this by using two mutants with opposite phenotypes, *pbo-4* mutants which have a more neutral intestinal lumen pH and a wild-type MAT, and *pbo-1* mutants which have a highly acidic intestinal lumen pH and do not display any MAT (Benomar et al., 2020, Wagner et al., 2011). *pbo-1/pbo-4* double mutant, by contrast, had more neutral intestinal lumen pH compared with *pbo-1* single mutants and exhibited MAT (Benomar et al., 2020). Single mutants of either gene also display observable EMCs and pBocs but at reduced frequency and reduced strength (Wagner et al., 2011, Beg et al., 2008) suggesting intestinal lumen acidity might translate to motor outputs. Additionally, loss of another proton pump, VHA-6, prevents full acidification of the intestinal lumen and leads to increased defecation cycle intervals (Allman et al., 2009), providing further evidence for this this hypothesis.

Coming back to the current findings, as the pH of *pbo-4* mutants is already more neutral, an additive decrease in acidification might not further disrupt signals related to lumen pH. However, it might disrupt functions related to ACD-5 channel activity which in turn might disrupt regularity of the calcium oscillations, hence we might see the increase in variability between the cycles in double mutants. If indeed MAT and cycle length are linked, *itr-1(sa73)* phenotypes might be a milder version of phenotypes observed in *pbo-1* mutants with respect to luminal pH. Loss of *acd-5* in *itr-1* mutants might make the pH less acidic and hence decrease the variability between the cycles as pH is now closer to wild-type conditions. This would also explain the decrease in average cycle length observed in double mutants. However, further evidence is needed to support these claims.

Taken together the evidence presented here, I propose the following working model for a role of ACD-5 in maintenance of acidification of the intestinal lumen (Figure

46): Homomeric or heteromeric ACD-5 channels are expressed on the apical membrane where they directly sense proton fluctuations in the intestinal lumen. *In vivo* characterisation has shown that the ACD-5 channel is closed at low pH and opens at around pH 6. This range of pH is interesting because the intestinal lumen maintains a pH around pH 4, but every 45-50 seconds during the DMP the pH rises to approximately pH 6 (Allman et al., 2009). Consequent opening of the ACD-5 channel could change the membrane potential by an influx of cations, especially Na^+ and K^+, which might directly interact with the Ca^{2+} signalling in the intestinal cell. Another possibility is that the ACD-5-mediated cation influx directly or indirectly (via interaction with Ca^{2+} signalling), triggers a feedback cascade that activates PBO-4 and other proton pumps which then pump protons into the intestinal lumen and the pseudocoelom which in turn initiates the pBoc. Mutations of the homomeric or heteromeric ACD-5 channel, for instance in the case of ACD-5(ok2657), might interfere with this signalling leading to a delay in PBO-4 activation and hence longer intervals. Likewise, inability to sense proton concentration in the intestinal lumen might lead to disruption of the command to pump protons back into the intestinal lumen, and these mutants thus display a lower degree of acidification of the intestinal lumen.

One common observation was that *acd-5* double mutants had an ameliorating effect on variability and an effect on cycle length with the strongest evidence coming from double mutants between *acd-5* and *itr-1(sa73)* or *flr-1(RNAi)* and the implication of this observation will be discussed here. Previous research has provided evidence that variability and cycle length can be changed independently suggesting that there might be an underlying pacemaker which functions independently of the observable rhythm of the DMP and is unaffected by cycle variability (Kwan et al., 2008). The behavioural experiment presented above further support this hypothesis, for instance, *acd-5(ok2657)/itr-1* double mutants showed only a small decrease in defecation interval length but a strong decrease in variability by more than half. By contrast, the cycle variability of wild-type worms on *flr-1(RNAi)* is increased to 73.1% compared to 5.5% on the control RNAi, similarly, for *acd-5(ok2657)* and *acd-5(lj122)* mutants on *flr-1(RNAi)*, the variability increased to 56.4% and 67.8%, respectively, compared to 5.8% and 5.9% on the control RNAi. Consequently, in all conditions, variability is approximately an elevenfold higher in animals on *flr-1(RNAi)*. This fits in with previous research suggesting that *flr-1* being involved in maintaining rhythmicity either with or in parallel to the TRPM (Transient Receptor Potential Melastatin) encoding genes *gon-*

2 and *gtl-1* (Kwan et al., 2008). Our RNAi experiments support this conclusion as *flr-1(RNAi)* significantly increases variability. By contrast, the cycle length of animals on *flr-1(RNAi)* decreased from a median of 54s in the wild-type background to 33-37s in the two *acd-5* mutant backgrounds suggesting an involvement of *acd-5* in the regulation of defecation cycles length. However, double mutants between the dominant *acd-5(ok2657)* mutation and *itr-1(sa73)* showed defecation cycles similar to *itr-1* single mutants but variability decreased in double mutants suggesting that *acd-5* also plays a role in maintaining rhythmicity. These experiments nevertheless support the hypothesis that there are different factors that are independently responsible for maintaining rhythmicity and cycle length (Kwan et al., 2008). ACD-5 and FLR-1 are both membrane proteins on the apical membrane which suggests they are likely to contribute to membrane excitability of the intestinal cell.

As discussed above, the *acd-5(ok2657)* mutation is likely to be a dominant mutation because it leads to a mutant phenotype in the presence of a wild-type copy of the gene. This has been shown by unsuccessful attempts to rescue of any of the *acd-5(ok2657)* mutant phenotypes by overexpressing the wild-type copy, heterozygous animals also display the mutant phenotype and overexpression of the mutant fragment under the *acd-5* promoter or an intestinal promoter can phenocopy the mutant phenotype of prolonged defecation cycles. However, there are some caveats when using dominant mutations such as *acd-5(ok2657)* to study and infer gene function (Fay and Spencer, 2006). For instance, dominant mutations can be expressed in normal amount but the generated protein might be much more active than its wild-type counterpart. Similarly, there might be issues at the level of transcription of the dominant allele as it might be present in unusually large numbers of mRNA molecules in the cell but not being translated. This in turn could interfere with normal expression of the wild-type transcripts leading to their degradation. However, one argument against this hypothesis is, that when expressed in HEK cells, the mutant ACD-5(ok2657) protein can be detected and can even be pulled-down with other potential subunits. This suggests that the protein is made and that it can still assemble with the other candidate subunits. However, it is possible that the dominant allele might be present in larger amounts of mRNA molecules and therefore the expression level of the mutant protein is higher. This is supported by the observation by Yi-Quan Tang who conducted the Co-IP experiments and found that in HEK cells the mutant band visualised on a western blot was larger than the ACD-5 wild-type band.

The experiment in *Xenopus* oocytes provided evidence that with increasing mutant ratios (while maintaining stable wild-type subunit concentrations), channel activity is reduced. While it suggests that the dominant mutation interferes with the wild-type function, this is also a difficult readout. In contrast to the dominant gain-of-function *mec-4d* mutation where channel function has shown to be altered by measuring currents *in vitro* (Brown et al., 2007), the ACD-5(ok2657) fragment expressed in oocytes does not show any currents or any response to amiloride or pH which makes it difficult to interpret its function in the absence of another functional readout. Furthermore, both *in vivo* in the worm as well as *in vitro* in *Xenopus* oocytes, it is not apparent if ACD-5(ok2657) directly inhibits the activity of the wild-type subunit though, for instance, dimerization, or whether it inhibits the activity of another protein that is required for the normal function or expression of the wild-type protein which could include auxiliary subunits. One way to test the hypothesis of disruptions by ACD-5(ok2657) could be to express the tagged wild-type ACD-5 or FLR-1 which we know to be expressed at the apical membrane (Take-Uchi et al., 1998) in an *acd-5(ok2657)* mutant background to investigate whether the dominant *acd-5* mutation would change or disrupt their subcellular localisation.

Focussing ACD-5, I have provided electrophysiological, genetic and behavioural evidence that ion channels act as timekeepers by maintaining luminal pH though sensing proton concentrations in the intestinal lumen. This has generated new insights into how the rhythmic behaviours, such as the DMP, are controlled and has provided some insight for potential other candidates that are activated and influence the wave of protons along the length of the intestine. Finally, in support of previous research (Beg et al., 2008), it shows that protons can act as transmitters that control behaviour that is independent of the nervous system.

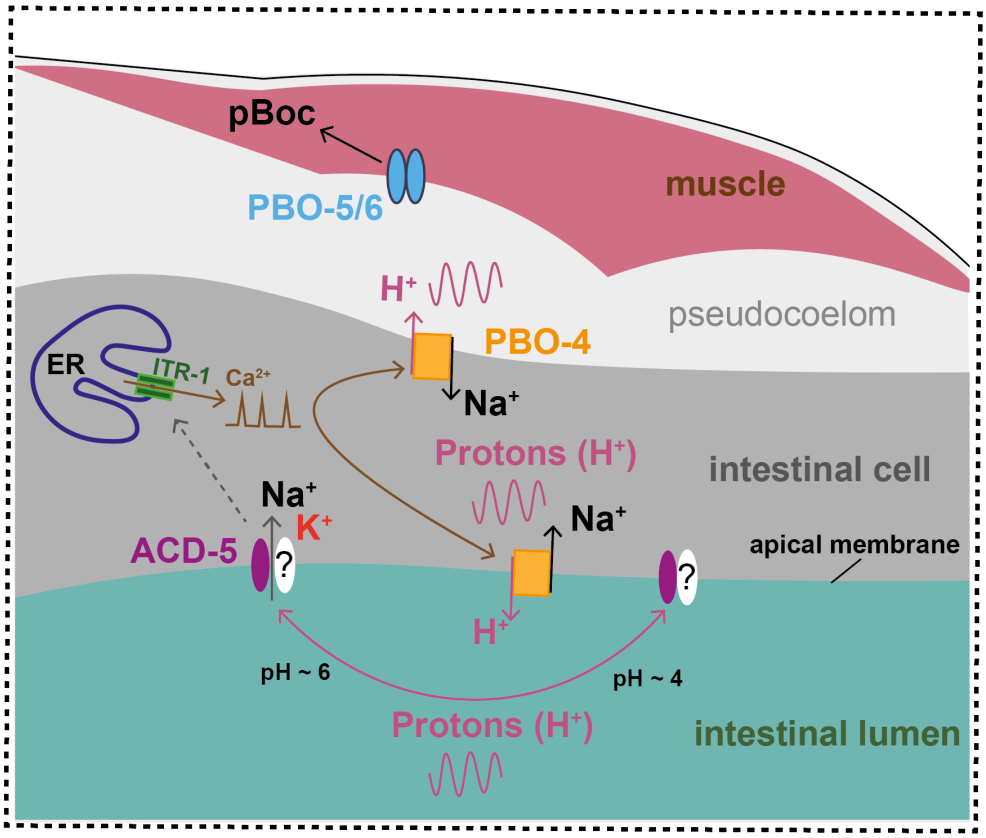

Figure 46: Working model of ACD-5 in the intestine.

ACD-5 heteromeric channels are expressed on the apical membrane facing the intestinal lumen. Other subunits could be FLR-1, ACD-3 or DEL-5 (indicated with a question mark). Intestinal lumen pH and pseudocoelomic pH oscillates due to the activity of proton pumps such as PBO-4. ACD-5 is closed at pH 4. If the pH in the intestinal lumen reaches pH 6, ACD-5 opens, resulting in an influx of cations, Na^+ and K^+, which might directly interact with the ITR-1-dependent Ca^{2+} oscillations (dotted arrows). Calcium release in turn triggers the activation of POB-4 (and other proton pumps) to pump protons into the intestinal lumen and the pseudocoelom (body cavity) initiating the pBoc via activation of PBO-5/6, a heteromeric “cys-loop” proton-gated cation channel. ER: Endoplasmic reticulum.

5. 5. Appendix E

5. 5. 1. Single copy GFP tagged ACD-5 CRISPR insertion mutants

In order to visualise ACD-5's endogenous localisation, I constructed a single copy GFP tag at the C-terminus of the endogenous *acd-5* gene taking advantages of the recent advances in *C. elegans* gene editing using CRISPR/Cas9 (Dokshin et al., 2018). However, even though the copy was inserted as verified by PCR (Supplementary Figure 7B) and Sanger sequencing, the tagged endogenous ACD-5 was not visible by confocal microscopy (Supplementary Figure 7A). Starvation or dauer entry did not enhance the expression of ACD-5 visibly. The most likely reason is that ACD-5 is not highly expressed in the intestine and therefore hard to detect using a single copy GFP. There are multiple ways to increase signal amplification of tagged ACD-5 including multiple GFP tags or using a tandem split GFP system (Chen et al., 2018). However, the most convenient and widely used technique is using extrachromosomal arrays (Mello et al., 1991), and therefore I turned to this technique which is shown above.

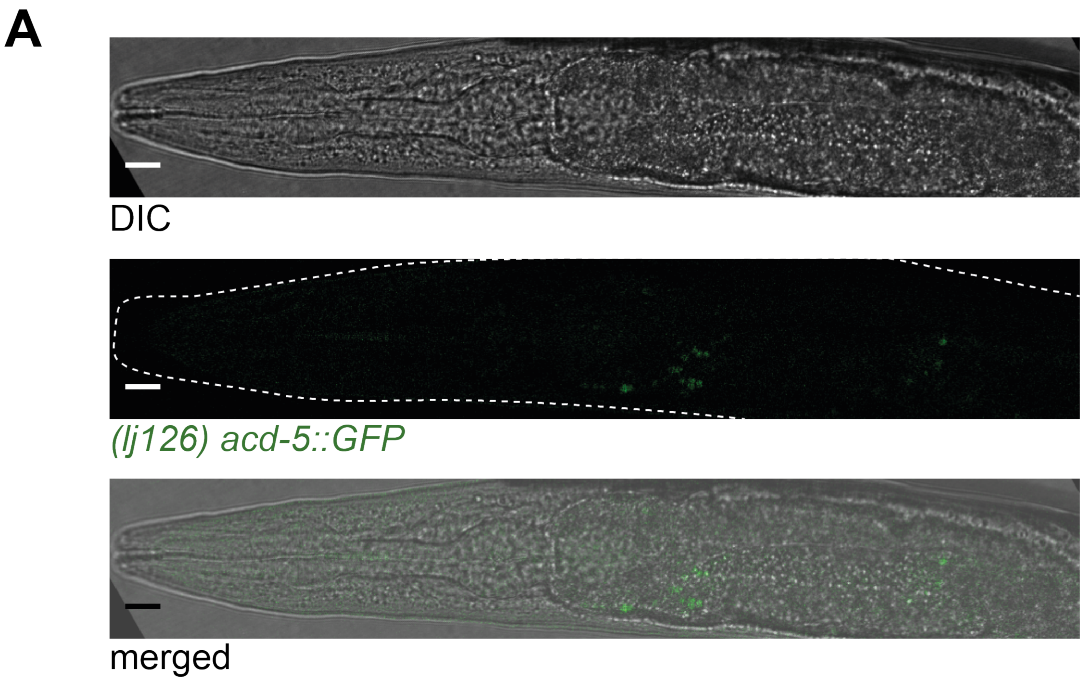

Supplementary Figure 7: Endogenous acd-5 C-terminally tagged with GFP.

(A) Confocal picture of animals expressing an endogenous GFP-tag at the C-terminus of the acd-5 gene. GFP is not visible, only autofluorescence of granule. Scale bars are 10 µm. (B) Genotyping of *acd-5* C-terminally tagged with GFP. Agarose gel-electrophorese picture of the AQ4723 [*lj126(acd-5::GFP)* I] stain and the N2 wild-type. The following primers were used for amplification Forward primer 3' cgcagctagagtttcacagc 5'; Revers primer 3' cagagctttaacattgagatgcc 5'. Predicted band length: GFP inserted: 2066 bp and wild-type (GFP not inserted) 1202 bp. Ladder used is GeneRuler Express DNA ladder (5kb). GFP insertion was also confirmed by Sanger Sequencing.

5. 5. 2. Pharyngeal pumping in acd-5 mutants is normal

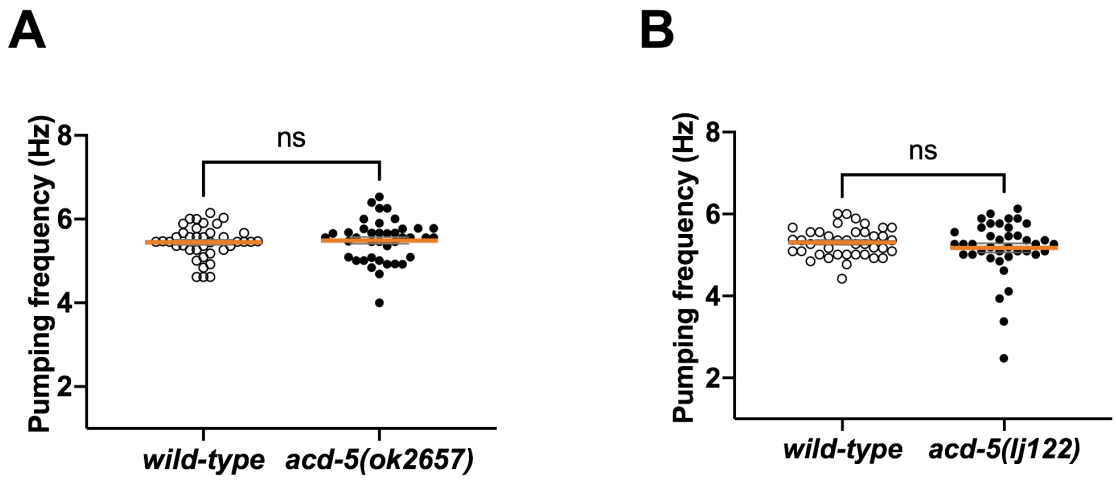

Supplementary Figure 8: Assessing pharyngeal pumping in the acd-5 mutants.

(A) Wild-type (Mdn=5.46 Hz) and *acd-5(ok2657)* mutants (Mdn=5.56 Hz) show similar pumping rates. A Mann-Whitney test confirmed that there was no statistically significant difference between the pharyngeal pumping rate in *acd-5(ok2657)* mutants compared to the wild-type, $U(N_{acd\text{-}5(ok2657)}= 39, N_{wild\text{-}type}= 40) = 713.5$, $p = 0.517$, ns). (B) Wild-type (Mdn=5.31 Hz) and *acd-5(lj122)* mutants (Mdn=5.27 Hz) show similar pumping rates. A Mann-Whitney test confirmed that there was no statistically significant difference between the pharyngeal pumping rate in *acd-5(lj122)* mutants compared to the wild-type, $U(N_{acd\text{-}5(lj122)}=40, N_{wild\text{-}type}= 40) = 773$, $p = 0.80$, ns). Replicates from four independent samples on four independent days. Error bars represent Mean ± SEM.

CHAPTER 6 – Global and neuronal expression of the DEG/ENaC *acd-5* is regulated by *daf-7*/TGFβ-like signalling

6. 1. Introduction

6. 1. 1. Genetic pathways that regulate dauer formation

Regulation of gene expression as a response to developmental or environmental cues is a mechanism by which organisms can alter their behaviour. The dauer larva, described in CHAPTER 1, presents a suitable model to study the effect of developmental stress on gene expression. Besides dauer-specific behaviours and morphology, dauer gene expression patterns are also uniquely altered (Cassada and Russell, 1975, Golden and Riddle, 1984, Jeong et al., 2009) suggesting a major contribution of genetic regulation in this process. Forward genetic screening has allowed to dissect and classify genetic pathways that affect dauer formation in the absence of environmental cues (see Figure 47, Table 10) and has led to the identification of mutants that are unable to form dauer larvae (dauer formation defective, daf-d) and those which form dauer larvae even under favourable conditions (dauer formation constitutive, daf-c) (Golden and Riddle, 1984, Albert and Riddle, 1988, Vowels and Thomas, 1992). Unsurprisingly, genetic dauer pathways have been implicated in tissue remodelling during dauer formation (see review (Androwski et al., 2017)). One example are four of the six inner-labial (IL2) neurons that undergo extensive dendritic arborisation in dauer which is regulated by the RFX-type transcription factor *daf-19* (Schroeder et al., 2013).

In the light of the findings below, I will now focus on *daf-7/TGFβ-like* signalling which is one of the major pathways that regulate dauer formation in addition to *daf-2/insulin-like* signalling. The TGFβ superfamily is a conserved family that mediates many developmental cell–cell interaction processes including cell identity, function, and survival (Klass and Hirsh, 1976). In *C. elegans*, there are two different TGFβ receptors DAF-1 (Type I Receptor) and DAF-4 (Type II Receptor), both of which are widely expressed, and their TGFβ ligand is DAF-7 (Georgi et al., 1990, Estevez et al., 1993, Ren et al., 1996). DAF-7 is expressed and released from ASI sensory head neurons in the presence of food promoting reproductive development (meaning

attainment of adult morphology and onset of egg laying) both in L1 larvae and when recovering from dauer. Dauer pheromones inhibit *daf-7* expression and thus promote dauer formation, consequently *daf-7* mutants are daf-c (Ren et al., 1996). Well-established conserved downstream targets of *daf-7/TGFβ* are the SMAD proteins DAF-8 and DAF-14 (mammalian orthologues are Smad8 and Smad2/3, respectively) and DAF-5 and DAF-3 (mammalian orthologues are Snox/Ski and Smad4, respectively) (Park et al., 2010). In addition, downstream targets of the *daf-7*/TGFβ-like signalling pathway also include *C. elegans* chemosensory receptor genes (Nolan et al., 2002). While in wild-type animals these genes are expressed in ASI neurons, in *daf-7/TGFβ* pathway mutants' expression is abolished (Nolan et al., 2002). Behavioural implication of changes in expression of these chemoreceptors in dauers or post-dauers have not been investigated.

This brings us to an even more interesting question: What changes in animals that have undergone dauer after they resume development? While when exiting from dauer, IL2 dendritic arbours retract returning to a similar morphology to non-dauers, there is evidence that there are long-lasting changes in post-dauers IL2, as after retracting dendritic arbours some visible remnant branches are left behind (Schroeder et al., 2013). Similarly, PVD neurons of post-dauers grow a higher number of quaternary branches compared to animals that had not undergone dauers (Richardson et al., 2019). There is little known about post-dauer genetic and morphological changes and on how these changes manifest in post-dauer animals in terms of physiology and behaviour.

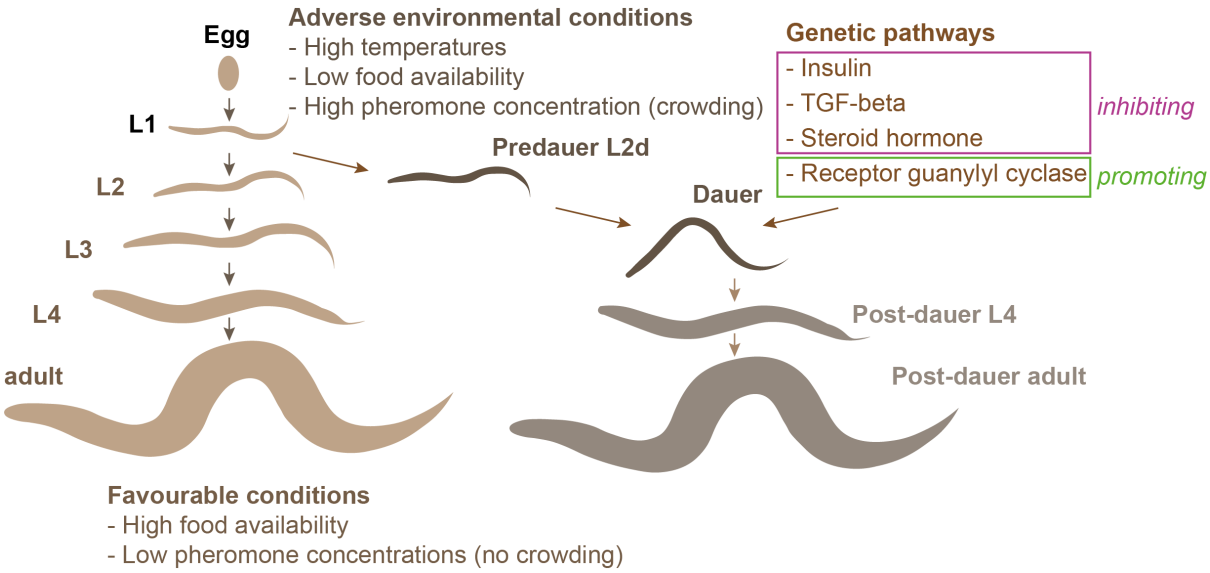

Figure 47: Dauer and post-dauer development.

Environmental conditions and genetic pathways influence the decision of the worm to go into dauer diapause. If favourable conditions return, the dauer larvae can excite the dauer diapause and resume development via a post-dauer L4 into an egg-laying post-dauer adult. Schematic modified from (Androwski et al., 2017).

Table 10: Overview of genetic pathways that are involved in dauer formation.

Genetic pathway	*Example gene*	External cues	Dauer regulation	References
Receptor guanylyl cyclase	*daf-11*	chemotaxis, sensing pheromones	promoting	(Riddle et al., 1981, Thomas et al., 1993, Birnby et al., 2000)
Insulin	*daf-2*	food-related cues	inhibiting	(Riddle et al., 1981, Kenyon et al., 1993, Kimura et al., 1997)
Transforming Growth Factor-β (TGFβ)	*daf-7*	food-related cues		(Estevez et al., 1993, Riddle and Albert, 1997, Albert and Riddle, 1988)
Steroid hormone	*daf-9*	dauer development vs. reproductive development		(Jia et al., 2002, Gerisch and Antebi, 2004, Mak and Ruvkun, 2004)

6. 1. 2. Genetic regulation of DEG/ENaC channels

Finally, in the light of the current research, I will briefly give an overview of the literature surrounding the genetic evidence of *C. elegans* DEG/ENaCs regulation which is related to cell-death signalling cues and dauer pathways. For instance, *unc-8*-dependent developmental synaptic remodelling is regulated by calcium and shares a common pathway with the pro-apoptotic cell death gene CED-4 (Miller-Fleming et al., 2016). Forward genetic screens have identified that gain-of-function mutations in *unc-8* and two other DEG/ENaC-encoding genes, *mec-4* and *deg-1* promote neuronal cell death (Shreffler et al., 1995, Driscoll and Chalfie, 1991, Chalfie and Wolinsky, 1990). Dauer entry or downregulation of insulin/IGF-1-like signalling using mutants of the insulin receptor (*daf-2*) or transcription factor *daf-16*/FOXO prevents neuronal degeneration triggered by cell death-causing mutation in *mec-4* and *deg-1* (Calixto et al., 2012). This in turn suggests some degree of genetic relationship between dauer and the DEG/ENaCs *mec-4* and *deg-1.* There is further evidence for transcriptional regulation of DEG/ENaCs by genes involved in dauer formation. For instance, the transcription factor DAF-19 activates gene expression in a variety of ciliated neurons, amongst them the IL2s (De Stasio et al., 2018). *daf-19* mutants are daf-c. Expression of transcriptional reporters in *daf-19* null and wild-type genetic backgrounds determined that the expression of the worm DEG/ENaCs *asic-2* and *del-4* depend on neuronally expressed DAF-19 (De Stasio et al., 2018). In this chapter, I am investigating regulatory pathways of *acd-5* in dauer and post-dauers. My results show that *acd-5* neuronal and global upregulation in dauers and post-dauers is controlled by the *daf-7/TGFβ-like* signalling pathway. Given this finding, I further explore the genetic relationship of *daf-7/TGFβ-like* signalling and *acd-5* as well as its role in sensory neurons.

6. 2. Results

6. 2. 1. The *acd-5* reporter expression pattern is altered during dauer arrest and after dauer recovery

In order to investigate the expression pattern of *acd-5*, I constructed an *acd-5* transcriptional reporter which consists of a 4763 bp regulatory sequence upstream of the start codon of the *acd-5* gene (Figure 48A) which is the distance to the next gene.

Expression of an *acd-5* promoter was previously described in the lab (Grundy, 2018) using a promoter consisting of a regulatory sequence 1501 bp upstream of the *acd-5* gene start codon. The promoter showed strong expression in the intestine and faint expression in head neurons which were suggested to be ASI (Grundy, 2018). However, for subsequent experiments I used the longer promoter that I had constructed. I verified that in well-fed animals that had not undergone dauer, the *acd-5* promoter was highly expressed throughout the intestine (Figure 48B), while in starved worms that had entered the dauer larvae stage, additional expression was observed in two head neurons (Figure 48C). I re-analysed the expression pattern of the shorter promoter (1501 bp) from (Grundy, 2018) and I could confirm the expression observed in my long promoter in intestine and in dauer larva head neurons (Appendix F, Supplementary Figure 9). Change of expression during dauer can also be observed for the DEG/ENaCs ACD-2 and DEL-9 (Appendix F, Supplementary Figure 10). My results suggest that the neuronal upregulation of expression of the *acd-5* promoter is specific to dauer larvae because it cannot be detected in any other larval stage in both well-fed or staved conditions including the L1 arrested larvae (Figure 48D). Interestingly, I also observed that the upregulation of the *acd-5* reporter persisted in post-dauers (Figure 48E) for at least for 86 hours after recovery (Figure 48F) suggesting that the upregulation is due to a permanent change after the animal has undergone dauer.

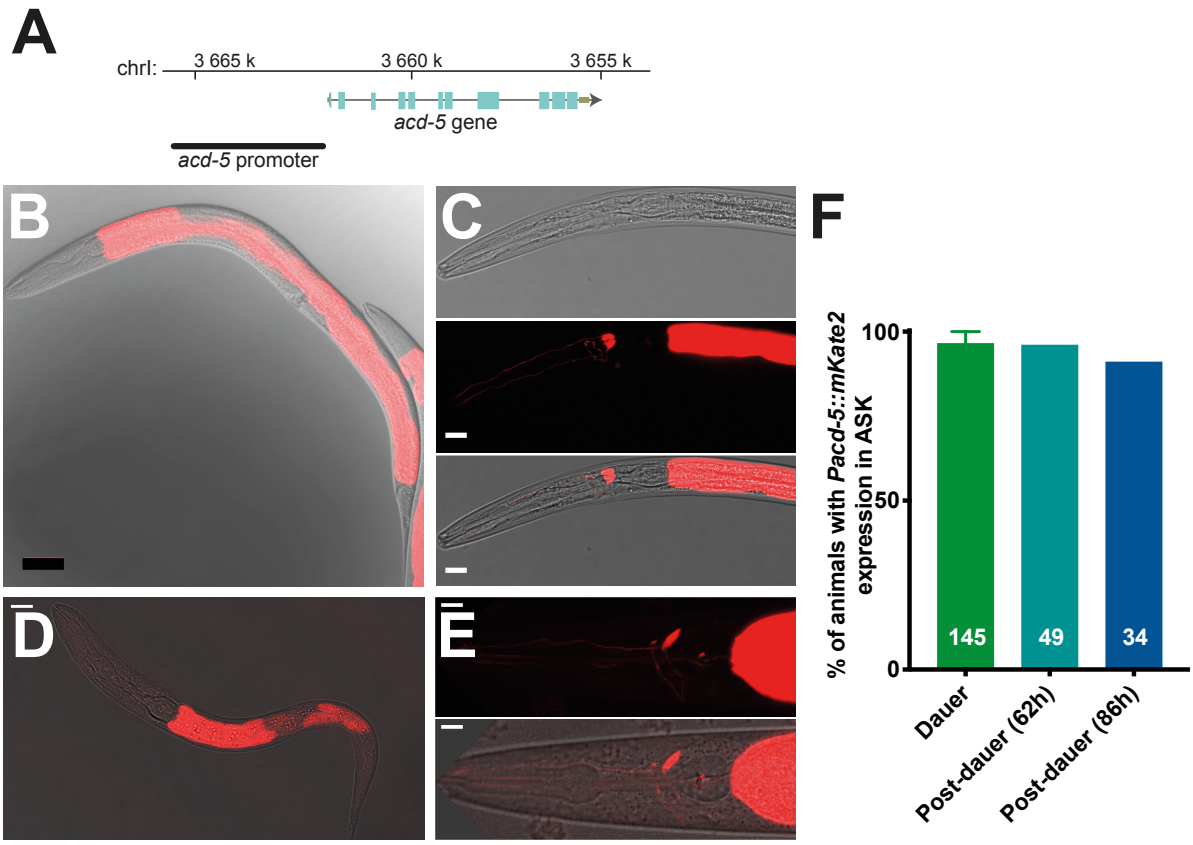

Figure 48: Expression pattern of the acd-5 promoter driving the red fluorophore mKate2.

(A) *acd-5* genomic region on chromosome I. Boxes indicate exons and lines indicate introns. Transgenic animals expressing *ljEx1225 [Pacd-5::mKate2]* under (B) normal food conditions (L4 larvae) where mKate2 is highly expressed in the intestine and during the (C) dauer larvae stage, where it becomes upregulated in two head neurons. (D) Developmentally arrested L1 larvae starved for five days expressing *ljEx1225 [Pacd-5::mKate2]* show only expression in the intestine. (E) Post-dauer animals after 24 hours recovering from dauer still show upregulation of the *acd-5* promoter in the head neurons. (E) Quantification of the percentage of animals with visible mKate2 expression in head neurons in dauer and post-dauer after 62 hours and 86 hours after dauer recovery on food. Mean ± SEM are shown. White scale bars are 10 µm, black scalebar in (A) is 100 µm.

6. 2. 2. The *acd-5* becomes upregulated in the polymodal sensory ASK neurons during dauer

In order to determine the identity of the head neurons which showed upregulation of the *acd-5* promoter in dauer, I used a cell-specific promoter *Psra-9::YC3.60* to identify the neurons as the ASK neurons (Figure 49A), as promoters can change in dauer, I also used DiO filling (Figure 49B) to confirm the expression pattern. Functions of the ASK neurons include sensing pheromones, and chemotaxis to the amino acid lysine

(Macosko et al., 2009, Kim et al., 2009a, Bargmann and Horvitz, 1991, Wakabayashi et al., 2009).

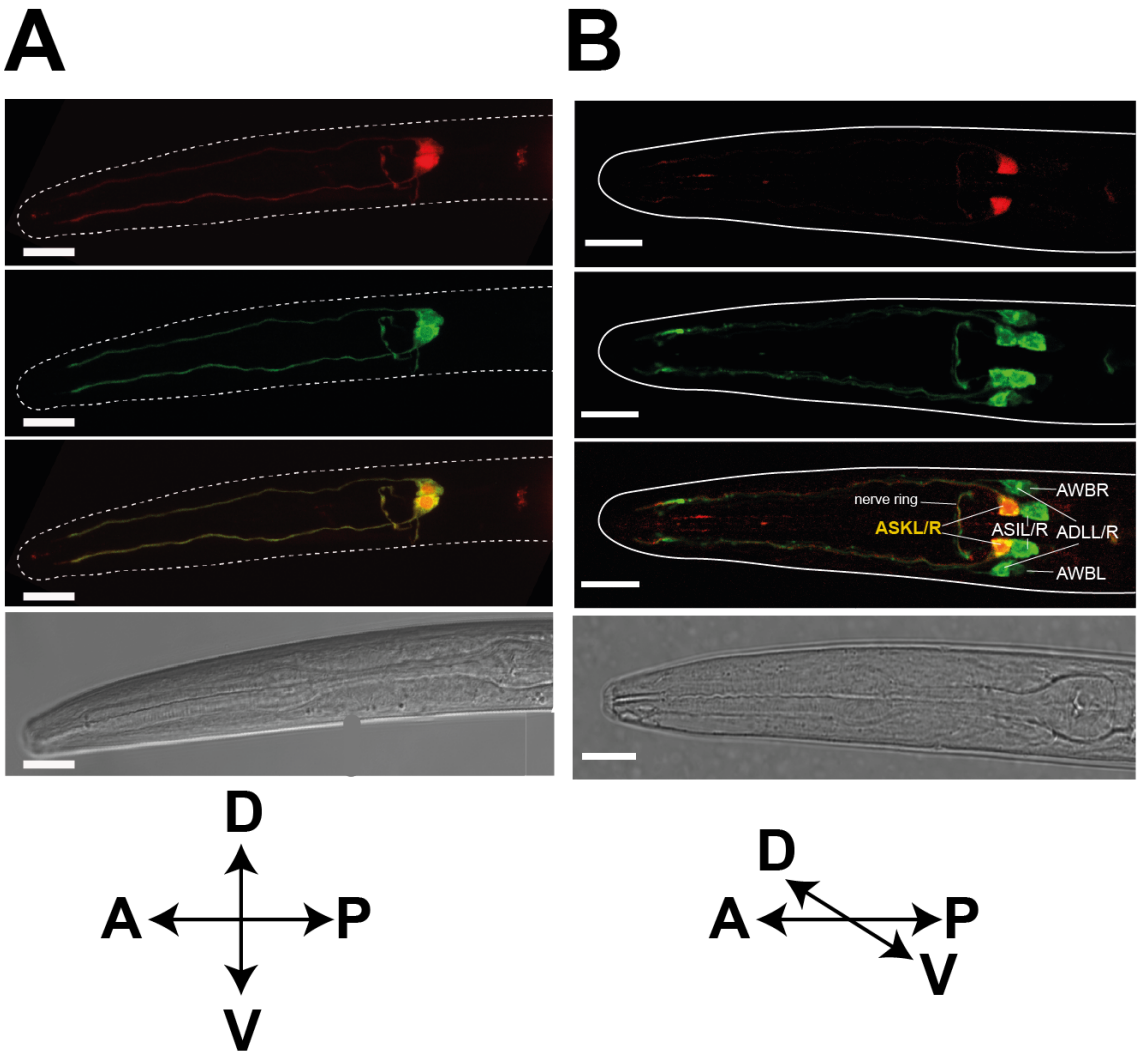

Figure 49: The acd-5 promoter is upregulated in ASK neurons in dauers.

(A) The head neurons in the dauer stage were identified as ASK neurons using the ASK-specific promoter *sra-9* driving the cyan chimeric fluorophore Cameleon (*ljEx543 [Psra-9::YC3.60)*. (B) DiO fill of amphid neurons and expression of *ljEx1225 [Pacd-5::mKate2]* in wild-type dauer in ASK neurons. Dorsal-ventral view, dorsal level. L/R=Left and Right. Scale bars are 10 µm.

6. 2. 3. Neuronal upregulation of *acd-5* is specific to the dauer stage and is regulated by the *daf-7/TGFβ-like* signalling pathway

In order to explore the underlying signalling pathway for *acd-5* expression in the ASK neurons and to confirm that it is specific to dauers, I tested environmental factors and candidate *daf*-genes implicated in dauer formation.

First, I tested environmental factors facilitating dauer entry to explore whether they would induce expression of *acd-5* in ASK. These environmental factors were high temperatures (growing the worms at 25°C or heat shock for 6 hours at 30°C), starvation (of non-dauers) and exposure to crude pheromones on the plate (previously made by Laura Grundy in the lab according to the following protocol (Zhang et al., 2013)) or C9 pheromone (previously obtained from Rebecca Butcher's lab). However, as shown in Table 11, temperature, starvation or pheromones were insufficient to induce high *acd-5* expression in ASK. Nevertheless, 24 hours exposure to C9 induced faint expression in two head neurons of some animals screened which could be the ASK neurons (Table 11). More detailed analysis is required to confirm these results; however, this suggests that that pathways related to sensing concentrations of pheromone in the environment could be implicated in up-regulation of *acd-5* in ASK.

I then assessed genetic factors that could lead to neuronal *acd-5* expression. I crossed the *acd-5* transcriptional reporter into mutants of different *daf*-pathways to determine which genetic pathway might regulate ASK expression of *acd-5*. My results showed that dauer larvae in all dauer-constitutive genetic backgrounds express the *acd-5* promoter in ASK neurons in dauers. These dauers have formed on plates with plenty of food and space (Table 12), which in turn suggest that neither starvation nor overcrowding are the main factors for ACD-5 expression in ASK, which is also supported by the previous findings shown above. However, it shows that *acd-5* expression in ASK is specific to the dauer larvae and is likely to be modulated by genes responsible for dauer formation or maintenance.

However, the most convincing genetic evidence was a visible upregulation in head neurons, presumably ASK neurons, in mutants of the *daf-7/TGFβ-like* signalling pathway. These were *daf-1*, *daf-4* and *daf-7* mutants (Figure 50) which had not undergone dauer but were raised at the permissive temperature of 15°C. There are two additional known TGFβ pathways to *daf-7*, one that regulates body size involving DBL-1 (DPP/BMP-Like), and the other one is dependent on UNC-129 involved in axon guidance (Morita et al., 1999, Suzuki et al., 1999, Nash et al., 2000). Dendrite morphology of ASK neurons did not differ from the wild-type in *acd-5(ok2567)* mutants (Figure 51A, B), suggesting that ACD-5 is not involved in axon guidance that depend on UNC-129. However, interestingly, preliminary data showed that most *dbl-1* mutants showed expression of the *acd-5* promoter in only one ASK head neuron. Unilateral

expression is also occasionally observed in the wild-type dauer where it is likely to be due to mosaic expression of the promoter.

I further tested mutants with structural abnormalities in the chemosensory cilia which are unable to physically sense and respond to pheromones or water-soluble attractants. Preliminary results in Table 12 showed that cilia defective *osm-6(p811)* mutants show occasionally a weak expression of *Pacd-5::mKate2* in head neurons which might be indicative of genetic pathways. Additional quantification might be needed to draw a conclusion from these observations.

Table 11: Assessment of environmental conditions as cues for neuronal acd-5 expression.

Summary of expression patterns of non-dauer mosaic animals expressing the *acd-5* transcriptional promoter driving *mKate2 (ljEx1225 [Pacd-5::mKate2])* under different environmental conditions.

Condition	***mKate2* expression in ASK**
starvation (6 or 24 hours)	*OFF*
30 °C heat-shock	*OFF*
high temperatures 25 °C	*OFF*
crude pheromones	*OFF*
C9 pheromones	*weak/ON*

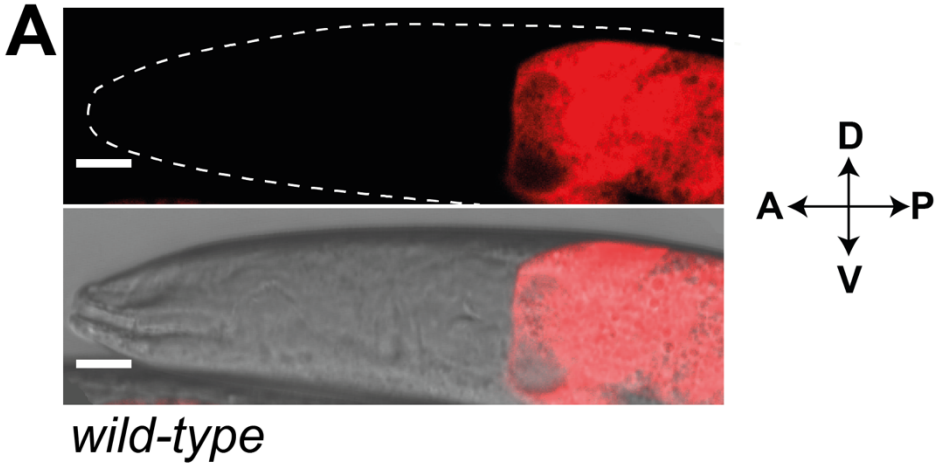
A
D
A
P
V
wild-type
B
D
A
P
V
daf-1(m40)
C
D
A
P
V
daf-4(e1364ts)
D
D
A
P
V
daf-7(e1372)

Figure 50: Upregulation of acd-5 in ASK in mutants of the daf-7/TGFβ-like signalling pathway.

Compared to the (A) wild-type where no expression of the *acd-5* promoter (*ljEx1225 [Pacd-5::mKate2])* can be observed in the head neurons, (B) *daf-1,* (C) *daf-4* and (D) *daf-7* mutants show upregulation of the *acd-5* promoter in ASK head neurons (white arrow head) in all developmental stages (here presented are young adults grown at the permissive temperature 15°C for the *daf-7/TGFβ* mutants). Scale bars are 10 µm.

Table 12: Assessment of genetic pathways involved in neuronal acd-5 expression.

Summary of expression of patterns of mosaic mutants expressing the *acd-5* transcriptional promoter driving *mKate2 (ljEx1225[Pacd-5::mKate2])*.

	genetic pathway	***mKate2* expression in ASK**	
		non-dauer adults	**long-term dauer**
WT	-	OFF	ON
acd-5(ok2657)	-	OFF	ON
daf-1(m40)	TGFβ-like pathway	ON	ON
daf-2(e1370)	Insulin-like pathway	OFF	ON
daf-4(e1364ts)	TGFβ-like pathway	ON	ON
daf-7(e1372)	TGFβ-like pathway	ON	ON
daf-9(m540)	Steroid hormone pathway	weak/OFF	ON
daf-11(ks67)	Receptor guanylyl cyclase pathway	OFF	weak/OFF
daf-16(mu86)	Insulin-like pathway	*-not tested yet-*	ON
dbl-1(ok3749)	TGFβ-like pathway	One ON/one OFF	ON
osm-6(p811)	Cilia mutant	weak/inconclusive	N/A*
unc-129(ev554)	TGFβ-like pathway	*-not tested yet-*	

*due to deformed cilia, these mutants do not go into dauer (Vowels and Thomas, 1992)

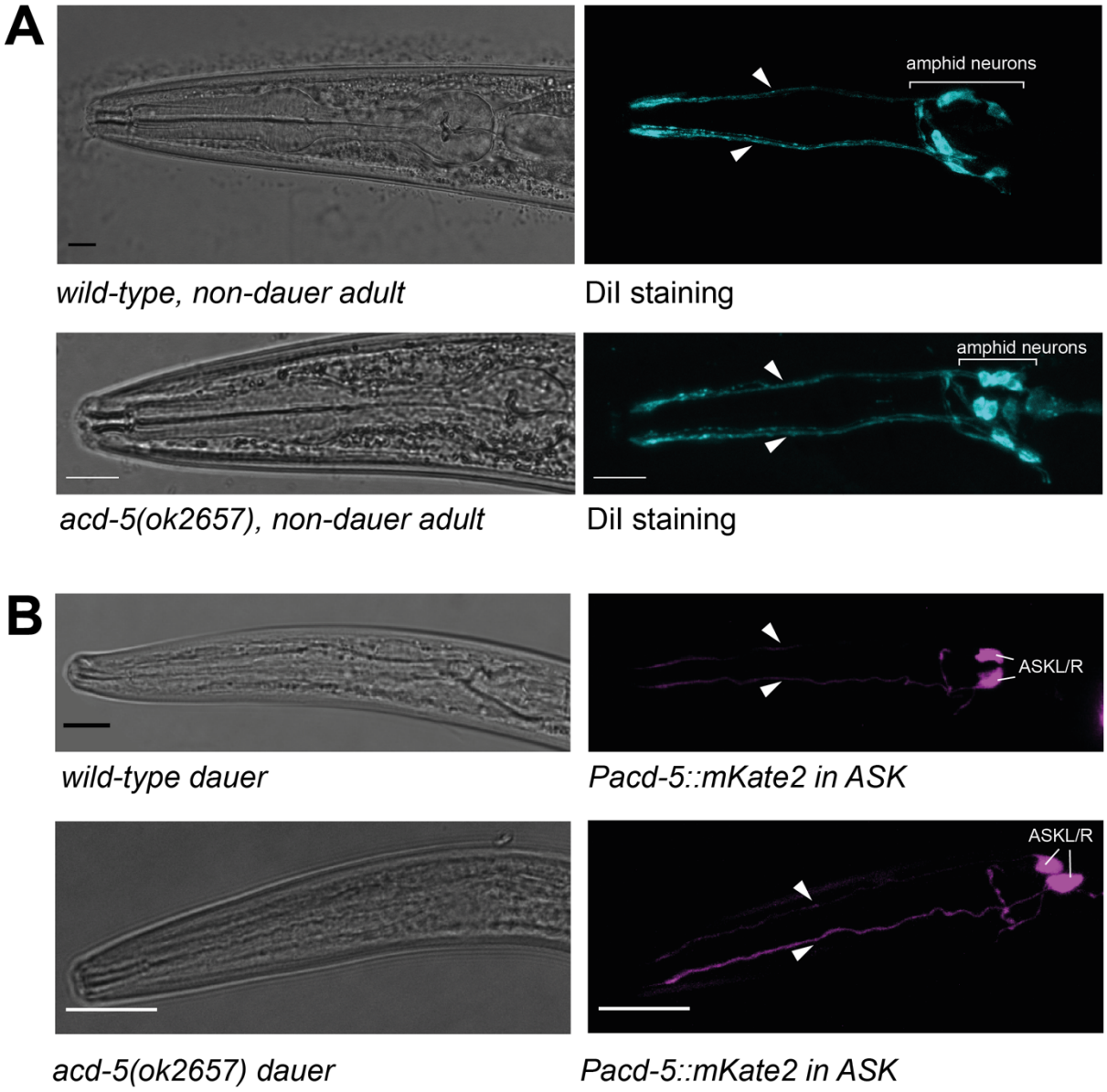

Figure 51: Dendrite morphology of ASK in wild-type worms and acd-5(ok2567) mutants.

(A) DiI-fill in non-dauer adults showing morphology of all amphid dendrites. (B) Wild-type dauers and *acd-5(ok2657)* mutants dauers expressing *ljEx1225 [Pacd-5::mKate2]* in ASK neurons. Dendrites are marked with a white arrow head. Scale bars are 10 µm.

6. 2. 4. Global upregulation of *acd-5* in dauers, post-dauers and *daf-7* mutants

Promoter-fluorophore-fusions are suitable for determining gene expression in a particular tissue or neuron, but are unsuitable for quantifying expression of genes because their intensity and expression can vary between animals, furthermore mosaicism is an issue. Therefore, I used qPCR to quantify upregulation of *acd-5* in dauers. The web-based dauer metabolic database for *C. elegans* (www.DauerDB.org) provided evidence that *acd-5* relative expression is higher at the dauer stage

compared to other larvae stages with an approximately 150 fold-increase compared to the relative expression of the reference gene, *act-1* (actin) (Jeong et al., 2009). However, several accounts have indicated that actin expression can vary under different experimental conditions (Thellin et al., 1999, Dheda et al., 2004, Banda et al., 2008) and might therefore not be an ideal control. Therefore, in the current assay I compared relative *acd-5* expression to the following housekeeping genes used as controls: *pmp-3* ((Peroxisomal Membrane Protein related) which encodes a putative ABC), *cdc-42* ((Cell Division Cycle related) which encodes an RHO GTPase), and *Y45F10D.4* (which encodes a putative iron-sulphur cluster assembly enzyme). These housekeeping genes' expression levels are remarkably stable, with relatively little variation between different larval stages and conditions (Hoogewijs et al., 2008). As dauers are a specialised form of L3 larvae, I compared relative expression of *acd-5* between long term dauers and L3 non-dauer wild-type animals, between wild-type L3 and L3 *daf-7(e1372)* non-dauers (grown at 15°C), as well as L4 post-dauer larvae that had recovered from dauer and L4 non-dauers that had never undergone dauer.

qRT-PCR analysis of *acd-5* confirmed its relative upregulation in dauer, post-dauers and *daf-7(e1372)* mutants showing that *acd-5* expression is indeed highly upregulated ($>10^{14}$) in all three conditions (dauer, post-dauers and *daf-7* mutants) (Figure 52A, B, C). This high upregulation is unlikely to be due to upregulation of *acd-5* in ASK neurons only, but might rather reflect a global upregulation of *acd-5* expression as quantitatively, the vast majority of *acd-5* expression is in the intestine, which would mask any change in ASK neurons.

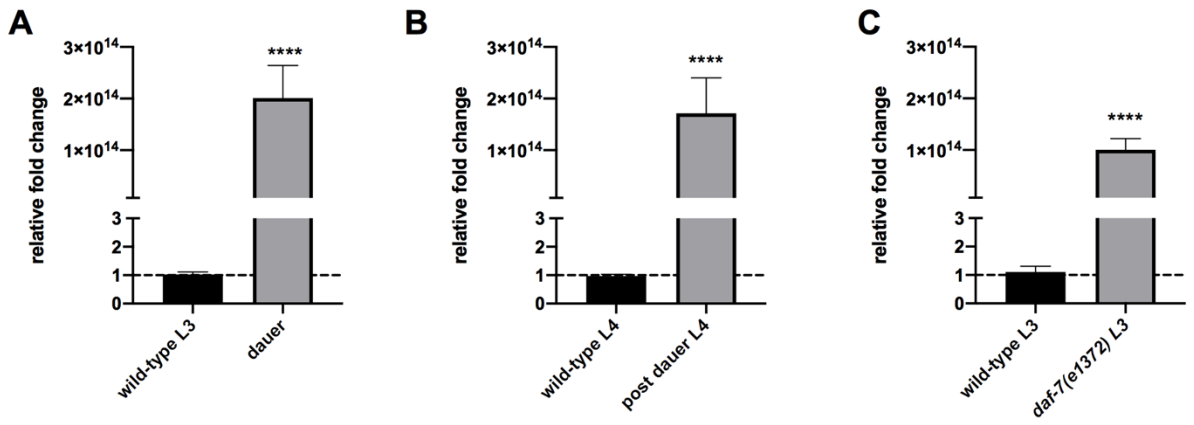

Figure 52: RT-qPCR analysis of the acd-5 gene.

(A) wild-type L3 and dauer, (B) wild-type L4 and post-dauer (24 hours after dauer recovery) and (C) wild-type L3 and *daf-7(e1372)* L3s. Bar graphs represent mean transcript levels normalized to control transcripts (*cdc-42; Y45F10D.4, pmp-3*), from 3 independent biological replicates. Error bars represent Mean ± SEM. Significance was assessed by a Mann-Whitney U test, ****p< 0.0001.

6. 2. 5. Relationship between *acd-5* and dauer entry and exit

6. 2. 5. 1. acd-5 null mutation does not rescue the dauer-formation phenotype of daf-7 mutants

While ASK has been implicated in sensing pheromones in a sensitised *npr-1* mutant background (Macosko et al., 2009, Kim et al., 2009a, Fenk and de Bono, 2017), I was unable to see a response for crude pheromones in our current settings (see Appendix F 6. 4. 2., Supplementary Figure 11). The concentrations of pheromones in their environment are a crucial cue for worms to make the decision to go into dauer, I could not find any evidence that *acd-5* is involved in dauer formation or that the upregulation of the *acd-5* promoter in ASK occurs prior to dauer entry. However, due to the observation that it might act downstream of *daf-7*, and *daf-7* mutants form dauers at restrictive temperatures (25°C) with a 100% penetrance even on food (Riddle et al., 1981), I tested whether the *acd-5(lj122)* mutation had an effect on this phenotype using double mutations between *acd-5(lj122)* and *daf-7(e1372)*. As expected, after raising the animals for two days at 25°C, 100% of wild-type and *acd-5(lj122)* mutants were at the L4 stage while 100% *of daf-7(e1372)* mutants went into dauer (Figure 53). Double mutants exhibited dauer formation phenotypes similar to those of *daf-7* single mutants

(99.45 %). This suggests that although *acd-5* expression is upregulated in dauer, and controlled by *daf-7*, it is unlikely that *acd-5* is involved in *daf-7*-dependent dauer entry.

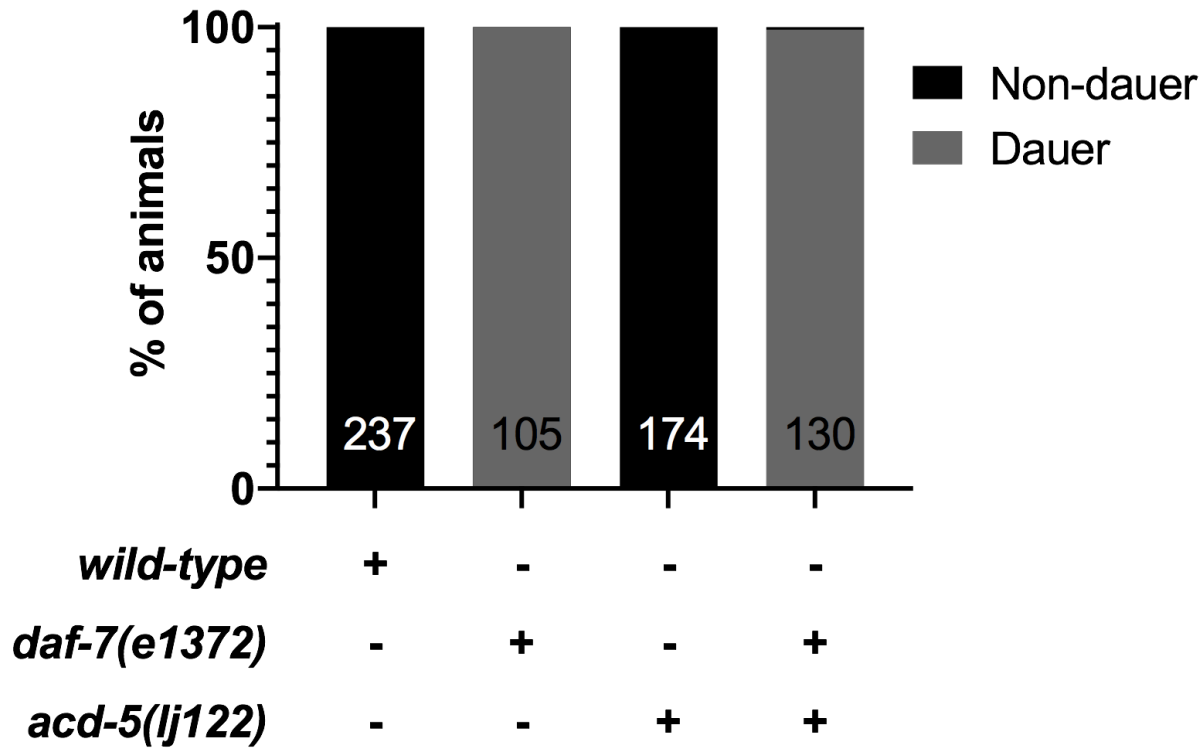

Figure 53: Percentage of dauers of animals raised at 25°C.

Numbers of animals tested are indicated in the bargraphs. Experiment was replicated 4 times.

6. 2. 5. 2. acd-5 mutants recover more slowly from dauer

While I have not found evidence that *acd-5* is involved in dauer entry, I observed that the *acd-5* promoter continued to be activated in ASK in post-dauers after the worm has resumed development which might imply a function in dauer exit. Therefore, I quantified the timeline of *acd-5(ok2657)* mutants exiting dauer and found that they do so more slowly than the wild-type (Figure 54). This supports the hypothesis that *acd-5* might function in dauer exit. However, I cannot exclude the possibility that this slower development is due to a general developmental delay in *acd-5(ok2657)* mutants (Figure 56 below).

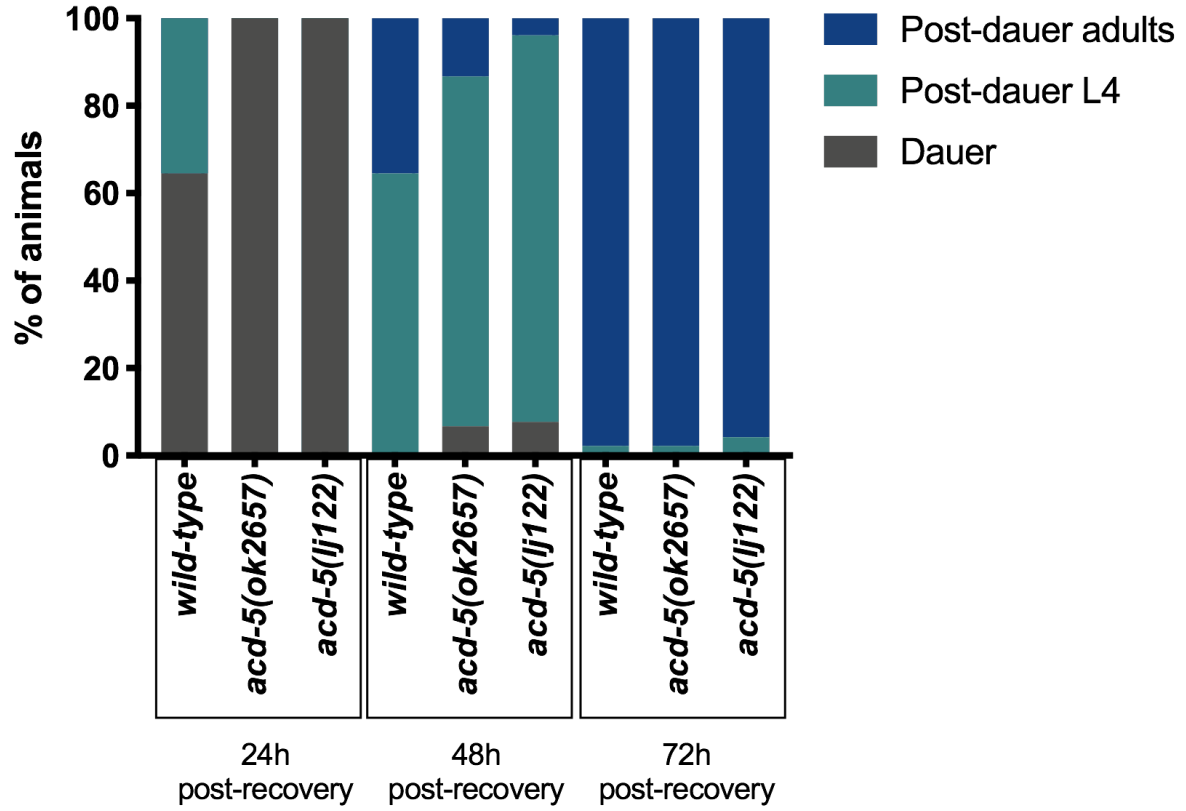

Figure 54: acd-5 mutants recover more slowly from dauer.

Percentages of wild-type and animals and acd-5 mutants at each stage after recovery from dauer. $N_{wild\text{-}type}$ = 31; $N_{acd\text{-}5(ok2657)}$ = 45; $N_{acd\text{-}5(lj122)}$ = 26.

6. 2. 6. Effect of *acd-5* mutations on other *daf-7*/TGFβ mutant phenotypes

As shown, upregulation of the *acd-5* promoter in the ASK neurons was highest in *daf-7*/TGFβ pathway signalling mutants and relative expression data of *acd-5* in *daf-7(e1372)* mutants further supports a genetic relationship between the two genes. Therefore, in order to gain an understanding of this relationship, I investigated whether *acd-5* could suppress phenotypes that are associated with mutations in the *daf-7*/TGFβ signalling pathway. These include the longer lifespan and reduced brood size at permissive temperatures and increased inactive phases during egg-laying of *daf-7* mutants (Shaw et al., 2007, Dalfo et al., 2012, Waggoner et al., 1998). Furthermore, mutants of the *daf-7*/TGFβ signalling pathway can display a small body size, this is the case for *daf-4* mutants (Wang et al., 2002, Estevez et al., 1993). The effects of the *acd-5* mutations on those phenotypes are described below.

6. 2. 6. 1. acd-5 null-mutation exacerbate body size of daf-4 mutants

I first investigated whether the *acd-5(lj122)* null mutation had an effect on the phenotypes of TGFβ mutants. Unlike *daf-7* which acts from ASI neurons to produce non-autonomous effects in the rest of the organism including promoting dauer formation, *daf-4* has been proposed to regulate body size cell-autonomous in multiple tissues including the intestine and *daf-4(e1364)* mutants have a characteristic small body size (Inoue and Thomas, 2000, Wang et al., 2002, Estevez et al., 1993). I generated double mutants by crossing *acd-5(lj122)* with the temperature-sensitive *daf-4(e1364)* mutant. Raising them to L4 stage at permissive temperature, the small body size characteristic of the *daf-4(e1364)* mutants was exacerbated in double mutants between *daf-4(e1364)* and *acd-5(lj122)* as they were visible smaller than *daf-4* single mutant (Figure 55). However, differences in developmental timing cannot be excluded.

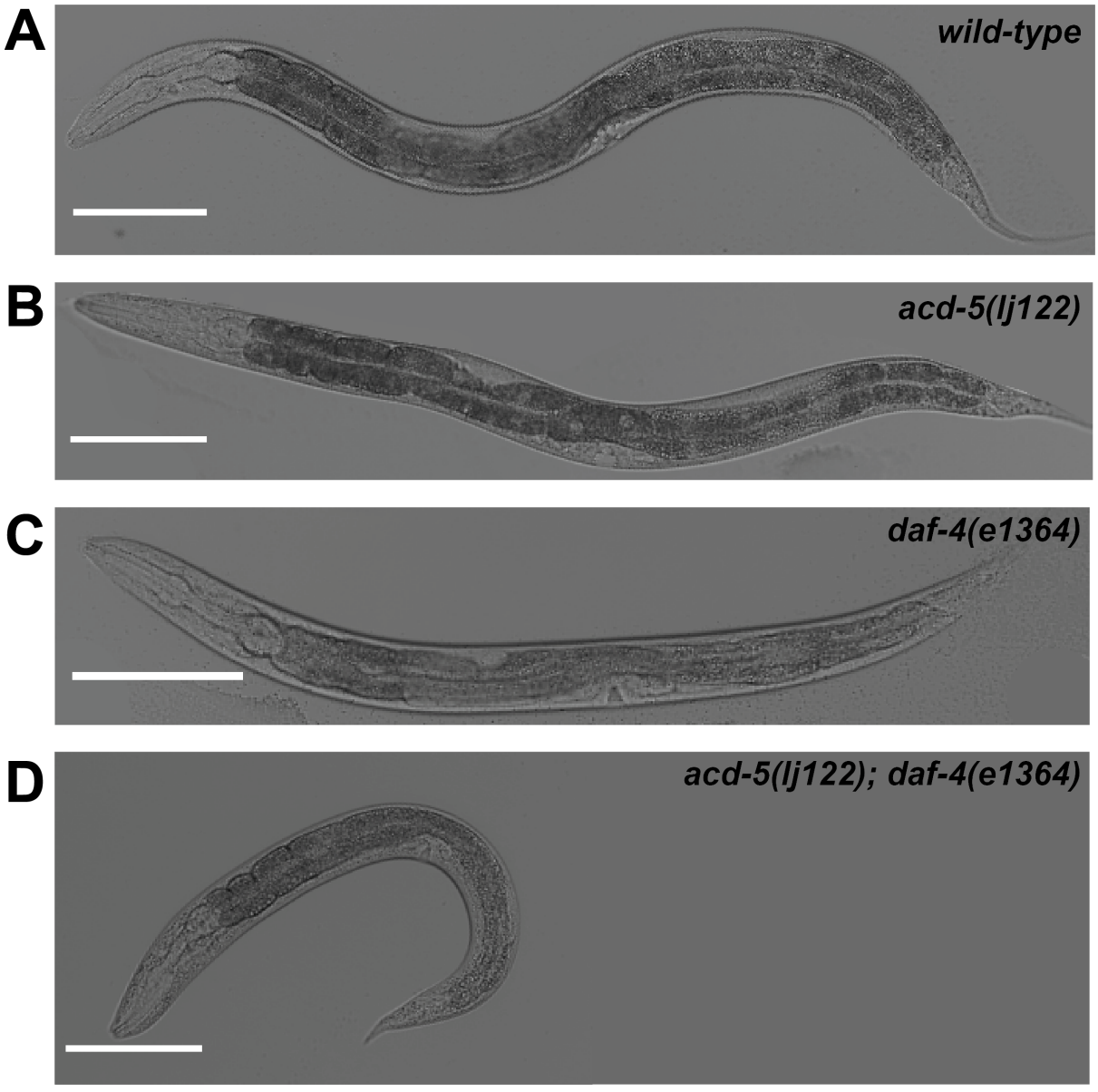

Figure 55: Body morphology of L4 larvae raised at permissive temperatures 15°C.

(A) Wild-type L4 larvae. (B) *acd-5(lj122)* mutant L4 larvae. (C) *daf-4(e1364)* mutant L4 larvae. (D) *acd-5(lj122)/daf-4(e1364)* double mutant L4 larvae. Scale bars are 100 µm.

6. 2. 6. 2. acd-5 mutants show a normal lifespan but a developmental delay and reduced brood size

Given the genetic relationship of *daf-7* and *acd-5*, I quantified the generation time for each strain to develop from an egg to an egg-laying adult. The developmental timing (measured by the onset of egg-laying) in *acd-5(ok2657)* mutants was delayed by seven hours compared to the wild-type (Figure 56A). Furthermore, reproductive health was assessed by counting hatched progeny on individual days as well as the total brood size during the whole egg laying period. There was no difference between mutants and wild-type in hatched progeny with a median of 205 and 210 hatched offspring per animal indicating that the *acd-5(ok2657)* mutants are healthy (Figure 56B). However, *acd-5(ok2657)* mutants showed a significant decreased overall amount of egg laid per animal with a median of 236 total eggs laid counted over the five days compared to the wild-type with a median of 282 (Figure 56C). The pattern of egg-laying activity also differed from the wild-type showing a significantly decrease in eggs laid on day 2 and 5 suggesting that they also show an altered timing of maximal egg-laying (Figure 56C). The lifespan assayed (starting from day one of adulthood) showed no significant difference between the wild-type and the mutant, nor did the rescues, which were included because I had obtained preliminary data of a small effect on lifespan of the *acd-5(ok2657)* mutation (Figure 56D). These results point towards a role of ACD-5 in developmental timing but lifespan is unaffected in *acd-5(ok2657)* mutants.

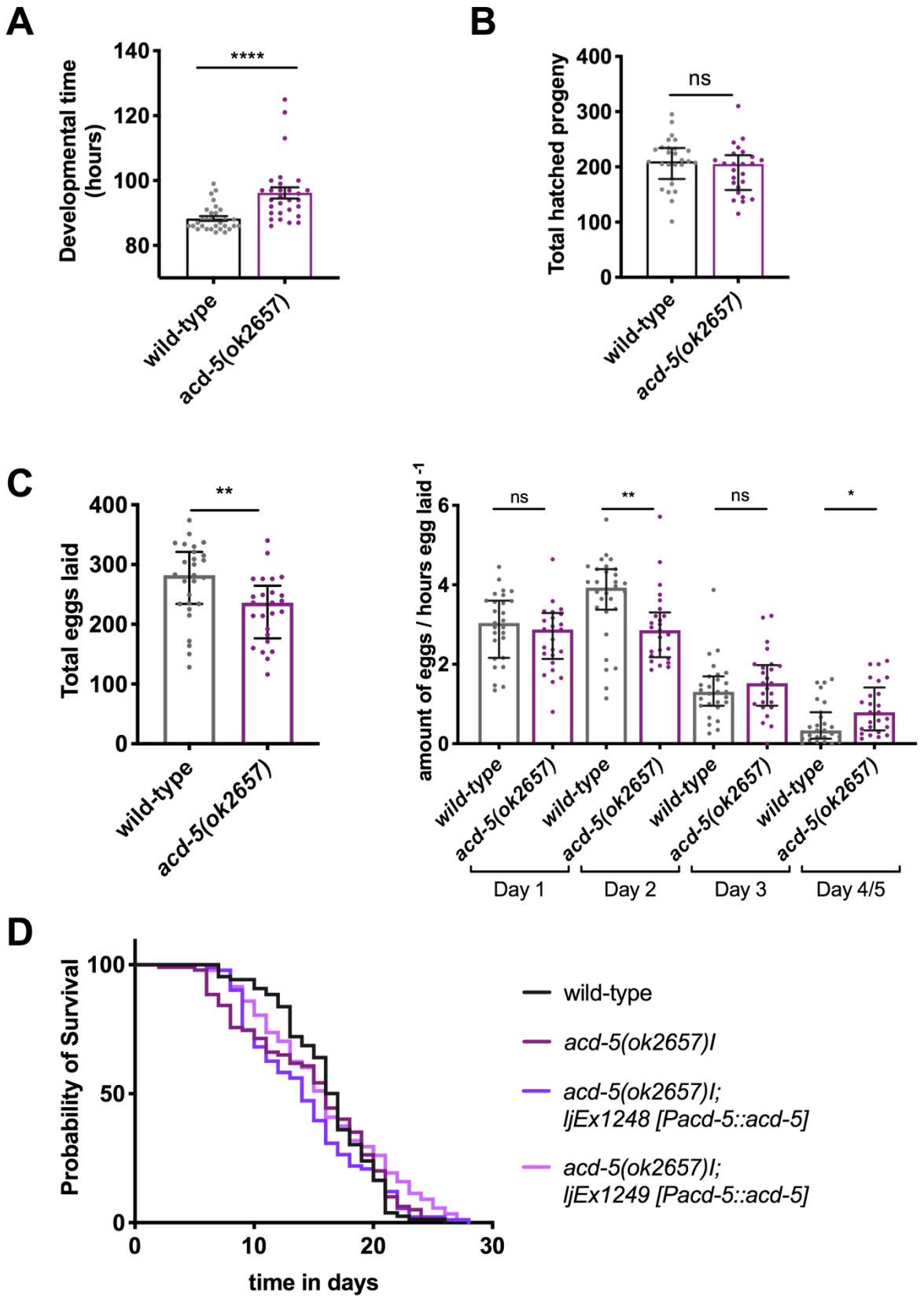

Figure 56: Developmental timing and lifespan of acd-5(ok2657) mutants.

(A) Generation time (in hours) of individual worms was assessed showing that *acd-5(ok2657)* mutants develop slower (Mdn $_{\text{wild-type}}$ =87, Mdn$_{\textit{acd-5}(\text{ok2657})}$ =94). A Mann-Whitney test showed that this difference

was statistically significant $U(N_{wild\text{-}type}=30, N_{acd\text{-}5(ok2657)}=29) = 140.5$, ****p<0.0001. (B) Total number of hatched progeny over the egg-laying period is similar in mutants and wild-type ($Mdn_{wild\text{-}type}=210$, $Mdn_{acd\text{-}5(ok2657)}=205$) as determined by a Mann-Whitney test $U(N_{wild\text{-}type}=27, N_{acd\text{-}5(ok2657)}=25) = 262$, p=0.17, ns. Total hatched progeny. (C) Total number of eggs laid over the egg-laying period is smaller in mutants and wild-type ($Mdn_{wild\text{-}type}=282$, $Mdn_{acd\text{-}5(ok2657)}=236$) as determined by a Mann-Whitney test $U(N_{wild\text{-}type}=27, N_{acd\text{-}5(ok2657)}=25) = 194.5$, **p=0.008. Distribution of eggs laid per day. Because the *acd-5(ok2657)* mutants started egg-laying later, the number of eggs was normalised: T=0 is the time at which the first egg was laid. Day 1: Mann-Whitney test $U(N_{wild\text{-}type}=30, N_{acd\text{-}5(ok2657)}=25) = 311.5$, p=0.38, ns. Day 2: Mann-Whitney test $U(N_{wild\text{-}type}=30, N_{acd\text{-}5(ok2657)}=25) = 195.5$, **p=0.002. Day 3: Mann-Whitney test $U(N_{wild\text{-}type}=27, N_{acd\text{-}5(ok2657)}=25) = 286.5$, p=0.036, ns. Day 4/5: Mann-Whitney test $U(N_{wild\text{-}type}=27, N_{acd\text{-}5(ok2657)}=25) = 199.5$, *p=0.011. (C) Lifespan of wild-type (black), *acd-5(ok2657)* mutants (purple) and rescues (light purple). Log-Rank (Mantel-Cox) test was not significant p=0.129. Median survival for the wild-type as 17 days, for the *acd-5(ok2657)* mutants was 16 days and for the rescues 14 and 16. Error bars represent Median and IQR.

6. 2. 6. 3. The acd-5 null-mutation changes egg-laying behaviour in a sensitised daf-7 mutant background

In order to investigate whether *acd-5* could suppress *daf-7* mutation-phenotypes, I chose to investigated the pattern of egg-laying events in both single mutants and double mutants of *acd-5(lj122)* and *daf-7(e1372)*. Egg-laying events can be modelled as discrete behavioural states; an active state during which egg-laying occurs and inactive states during which eggs are retained (Waggoner et al., 1998). I hypothesised that *acd-5/daf-7* double mutants might be able to ameliorate or rescue *daf-7* egg-laying phenotypes which manifest themselves in long inactive phases (Waggoner et al., 1998).

For this experiment, all animals were grown to L4 larval stage at 15°C (the permissive temperature for the temperature-sensitive *daf-7(e1372)* mutants) and then shifted to 22°C room temperature the night prior to the day of the experiment. Results of the egg-laying experiment showed wild-type inactive states of approximately 26 min (Figure 57A) and the *acd-5(lj122)* mutants had similar inactive states with approximately 25 min (Figure 57B), while the *daf-7(e1372)* mutants showed a decrease in inactive states with about 19 min (Figure 57C) and the double mutants showed increased inactive states of 29 minutes (Figure 57D). Within the active states, egg-laying intervals were 37 seconds for the wild-type, 52 seconds for the *acd-5(lj122)*, 28 seconds for the *daf-7(e1372)* and 33 seconds for the *acd-5(lj122)*/*daf-7(e1372)* double mutants. Showing that both inter-cluster (inactive states) and intra-cluster

(active states) events show a decrease in the *daf-7(e1372)* mutant and these are unaffected by *acd-5(lj122)*.

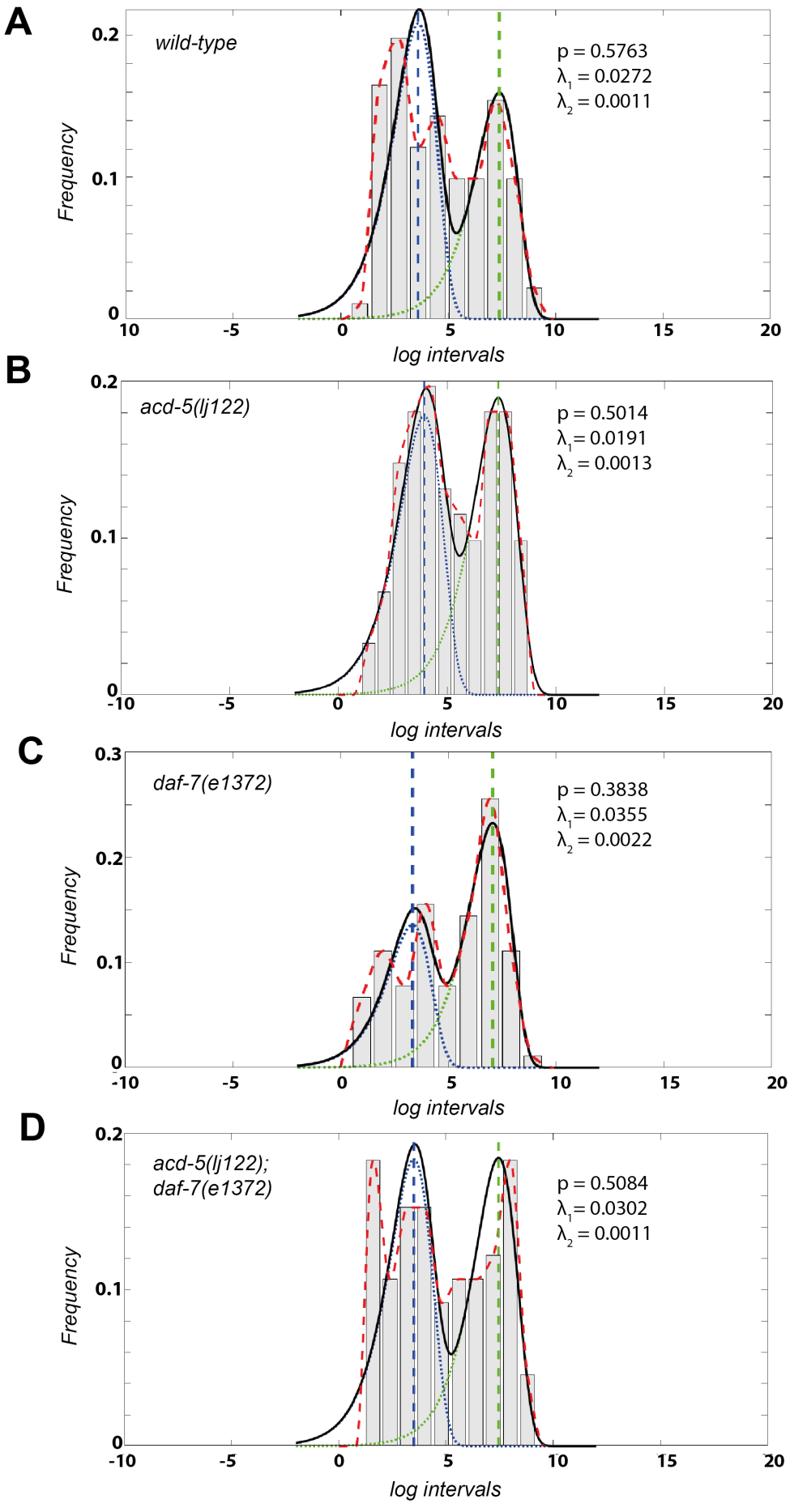
A
wild-type
p = 0.5763
λ1 = 0.0272
λ2 = 0.0011
Frequency
log intervals
B
acd-5(lj122)
p = 0.5014
λ1 = 0.0191
λ2 = 0.0013
Frequency
log intervals
C
daf-7(e1372)
p = 0.3838
λ1 = 0.0355
λ2 = 0.0022
Frequency
log intervals
D
acd-5(lj122);
daf-7(e1372)
p = 0.5084
λ1 = 0.0302
λ2 = 0.0011
Frequency
log intervals

Figure 57: Egg-laying intervals of acd-5(lj122) and daf-7 mutants.

(A) wild-type N=12 (parameters: p = 0.5763, λ_1 = 0.0272 and λ_2 = 0.0011). (B) *acd-5(lj122)* mutant N=12 (parameters: p = 0.5014, λ_1 = 0.0191 and λ_2 = 0.0013). (C) *daf-7(e1372)* N=12 (parameters: p = 0.3838, λ_1 = 0.0355 and λ_2 = 0.0022). (D) Double mutants between *acd-5(lj122)* and *daf-7(e1372)* N=11 (parameters: p = 0.5084, λ_1 = 0.0302 and λ_2 = 0.0011). Intra-cluster time constant $1/\lambda_1$ (blue dotted line). Inter-cluster time constant $1/p\lambda_2$ (green dotted line).

6. 2. 7. *acd-5* mutants show chemosensory deficits in sensing food and lysine

6. 2. 7. 1. acd-5 mutants perform poor on the food racing assay

In the large-scale screen of locomotor micro-behaviours conducted in the Schafer lab, *acd-5(ok2657)* mutants show increased time spent dwelling (rather than foraging) compared with controls (Yemini et al., 2013). This behaviour is usually observed at high food concentrations, suggesting a defect in distinguishing the absence from the presence of food in *acd-5* mutants. Therefore, I tested whether the *acd-5(ok2657)* mutants show any defects in their general food-sensing ability using the food-racing assay (see CHAPTER 2 – Methods). The results showed that within 2 hours, 98 % of wild-type worms had reached the food-patch, compared to 73 % and 68 % of *acd-5(ok2657)* and *acd-5(lj122)* mutants, respectively. Post-dauer adults were tested alongside and performed worse for each phenotype with 81 % of wild-type post-dauer reaching the food patch after 2 hours and 28 % and 30 % of *acd-5(ok2657)* and *acd-5(lj122)* mutants, respectively (Figure 58). The phenotype could not be rescued in the *acd-5(ok2657)* mutant (see Appendix F, Supplementary Figure 12), that is not surprising, since it appears to be dominant mutation (see CHAPTER 5 – The acid-sensing DEG/ENaC ACD-5 acts as a timekeeper for rhythmic behaviour by sensing proton fluctuations in the C. *elegans intestinal* lumen). The rescue for the *acd-5(lj122)* mutant needs to be tested.

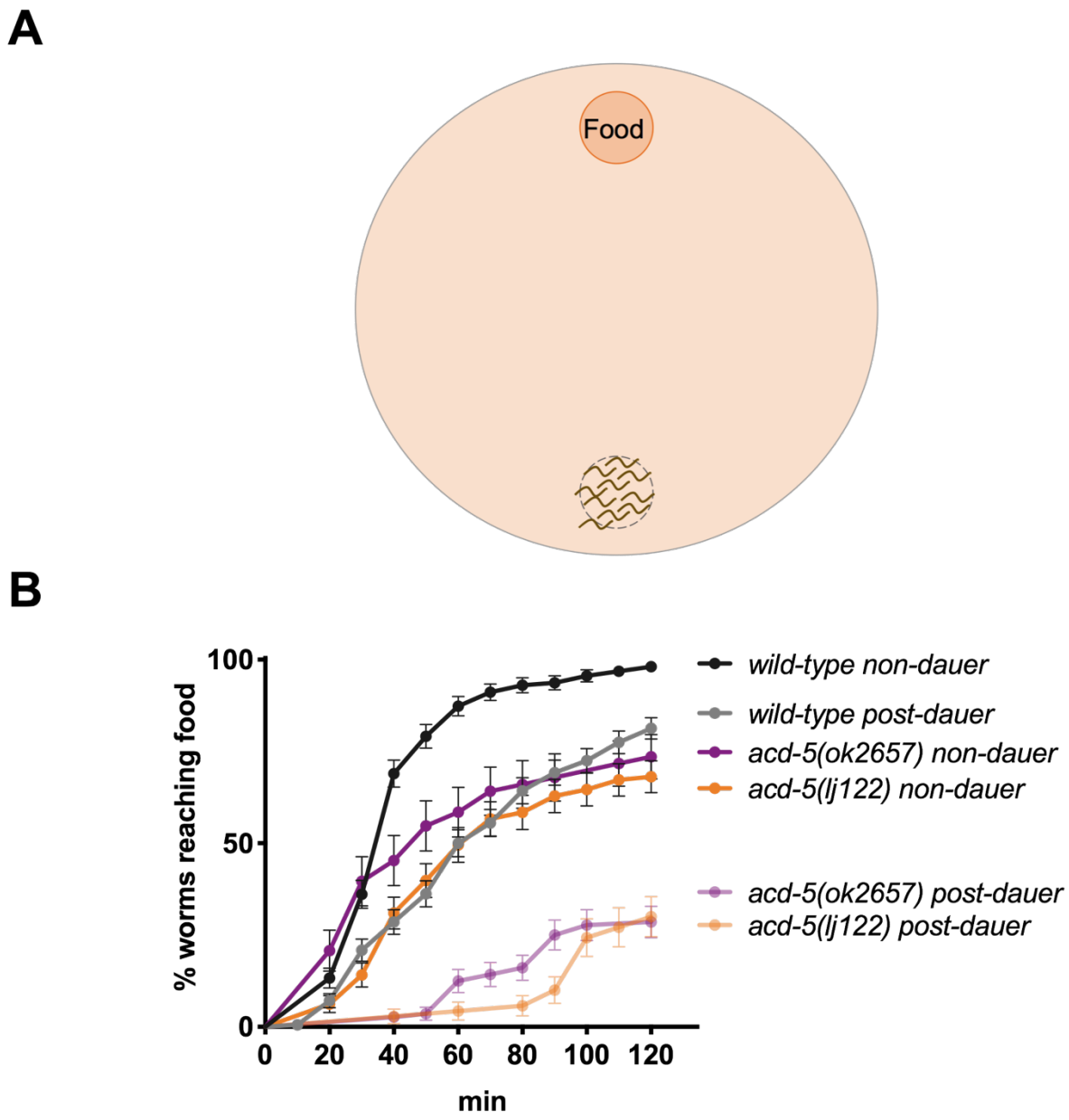

Figure 58: acd-5 mutants perform poorly on the food-racing assay.

(A) Assay plate (90mm NGM plate): On one side of the plate is a small food patch of OP50, opposite to the food patch worms are placed. The number of animals reaching food was recorded every 10 min for of time of 2 h. (B) The cumulative number that reached the food spot is displayed. Post-dauer animals reach the food patch less frequent compared to non-dauer animals. *acd-5* mutants also show lower success in reaching the food patch compared to the wild-type in both conditions. Log-Rank (Mantel-Cox) test was significant ***p>0.0001 with a Chi-square value of 28.1. Median time reaching the food patch for non-dauer wild-type was 40min, for the *acd-5(ok2657)* mutants was 50 min and for *acd-5(lj122)* 70 min. Median time reaching the food patch for post-dauer wild-type was 65 min but could not be determined for post-dauer *acd-5(ok2657)* and acd-5(lj122). Error bars represent Percentages ± Standard Error (SE).

6. 2. 7. 2. acd-5(ok2657) mutants show deficits in lysine sensing

Given the phenotype in food sensing above, the upregulation of ACD-5 in the sensory ASK neurons in dauers, and that DEG/ENaC channels (e.g. DEG-1 (Wang et al., 2012)) in these neurons are known to affect chemotaxis towards lysine, I decided to assay for defects in chemotaxis towards lysine which is known to be sensed by the ASK neurons (Bargmann and Horvitz, 1991, Wakabayashi et al., 2009). The results showed that *acd-5(ok2657)* mutants are impaired for lysine sensing as only 55% were attracted to lysine compared to 100% of wild-type animals and 60% of *deg-1(u38u421)* mutants which were used as controls (Figure 59B). To exclude movement defects relating to reaching the lysine patch, I tested attraction and repulsion to benzaldehyde, which is a chemoattractant at low concentrations but a repellent at high concentrations. It is a much more potent attractant than lysine, therefore populations of animals were tested which allows for the calculation of a chemotaxis index. In this assay, *acd-5(ok2657)* mutants were not defective for neither attraction nor repulsion to different concentrations of benzaldehyde (Appendix F, Supplementary Figure 13) suggesting that firstly, that the animals did not display a general defect on movement towards an attractant, and secondly that they did not display a general chemosensory defect. This supports the hypothesis that ACD-5 is indeed involved in sensing specific food cues associated with ASK function.

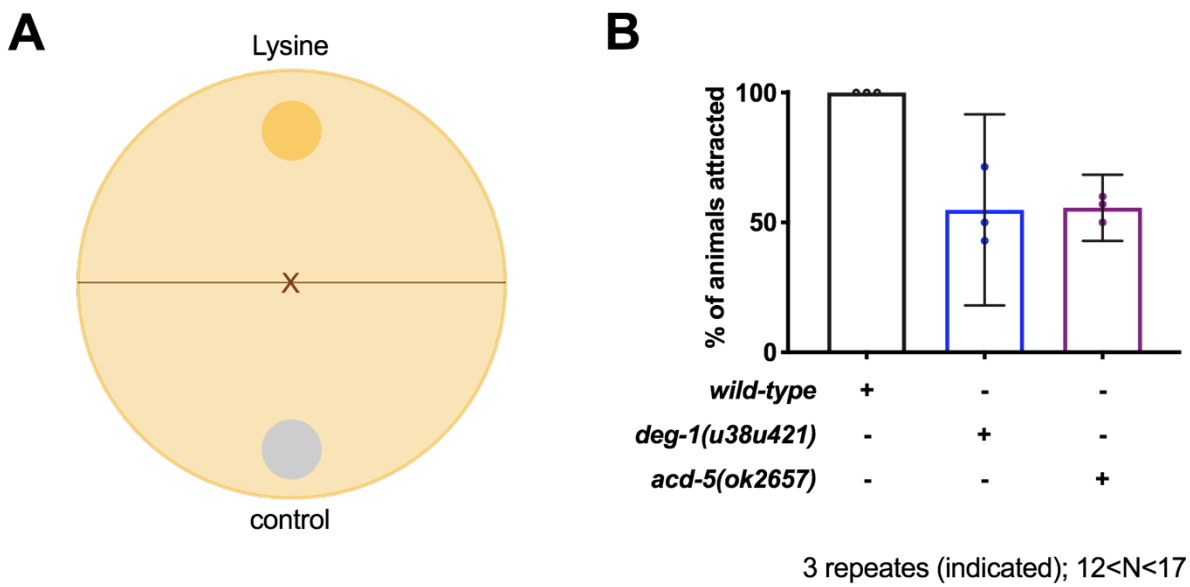

Figure 59: Lysine chemotaxis assay.

(A) Lysine gradient single worms assay plate (90mm NGM plate). Protocol modified from (Bargmann and Horvitz, 1991). Single worms were put on the middle line. The plugs soaked in lysine or water were previously removed (circles) and create a gradient of lysine (peak gradient 0.5M lysine). (B) Percentage of individual animals that are attracted to the amino acid lysine. *deg-1(u38u421)* (blue) mutants are chosen as a negative control as they show lysine sensing deficits(Wang et al., 2008). Similar to the *deg-1* mutants, *acd-5* mutants (purple) show a reduced attraction to lysine compared to the wild-type (black). Mean and 95% Confidence Intervals are indicated. N=3 independent replicates with 5 worms for each condition.

6. 3. Discussion

In the current chapter, I have identified *daf-7/TGFβ-like* signalling as a new regulatory pathway for neuronal and global upregulation of the DEG/ENaC *acd-5* in dauers and post-dauers. *acd-5* upregulation persists in post-dauers and therefore represents a permanent change after dauer recovery. This also implies that there might be some lasting-changes in *daf-7/TGFβ-like* signalling in post-dauers. Further exploration of their genetic relationship has shown that *acd-5* mutations can supress *daf-7* phenotypes in egg-laying and exacerbate small body size morphology of *daf-4* mutants. Taken together with the finding of *acd-5* conditional upregulation in dauer ASK in *daf-7* mutants suggests that *acd-5* is downstream of *daf-7*.

While my research agrees with previous findings that *daf-7* mutants show an altered egg-lying pattern, they are in contrast with what has previously been reported. Previous research has shown that *daf-7* mutants show clustered egg laying with long inactive phases compared to the wild-type (Waggoner et al., 1998). However, in my experiments, *daf-7* mutants show shorter inactive phases than the wild-type. There are several possible explanations for the difference in inactive states (Waggoner et al., 1998). Firstly, all animals were grown at 15°C until L4 before shifted to room temperature (22°C) overnight. Previous reported results from *daf-7* mutants shifted the animals to room temperature just prior to the experiment (Waggoner et al., 1998). While in laboratory conditions, temperatures between 15°C–25°C is considered physiological, temperature fluctuations have a major effect on parameters that reflect the physiology including longevity and developmental timing, both of which are prolonged at low temperatures (Klass, 1977, Gomez-Orte et al., 2018, Brenner, 1974). Consequently, growing the worms at 15°C might have impacted on the worms themselves (or bacterial food growth or health). It is also possible that raising the worms at 15°C has slowed general physiological processes which might explain the observed prolonged inactive states of approximately 26 min in the wild-type compared to about 20min what was shown in experiments where the wild-type was grown at 22°C (see CHAPTER 3 – Systematic *in vivo* and in vitro *characterisation of* C. elegans DEG/*ENaCs*) and what has previously been reported (Waggoner et al., 1998). A second explanation might be that the temperature fluctuation of shifting 15°C to 22°C might have caused some disruption of physiology and had an impact on this phenotype, as even fluctuation within the physiological range can change *C. elegans* metabolic response which can alter the worm transcriptome (Gomez-Orte et al., 2018).

A third explanation is the presence of a background mutation. The *daf-7(e1372)* allele was created using a treatment with the mutagen Ethyl methanesulfonate (EMS) by Jonathan Hodgkin, which has likely to have introduced mutations other than in *daf-7*. I backcrossed the *daf-7(e1372)* strain 6x with the wild-type. Backcrossing is a common practice to place the mutations of interest in a wild-type genetic background and to remove unwanted background mutations that arise by using mutagens to generate mutations. Nevertheless, the current findings support a role in egg-laying of *daf-7* which is affected by *acd-5*.

However, the genetic relationship of *acd-5* with *daf-7* at this point is speculative. The key question here is where ACD-5 is acting: Whether there are low levels of ACD-5 expressed in ASK neurons in non-dauers or whether ACD-5 acts solely the intestine or in both tissues to sense food-related cues. Presence of food the environment inhibits dauer larva formation and stimulates egg-laying via the sensory neuron ASI which releases DAF-7 (Cassada and Russell, 1975, Ren et al., 1996). Release of DAF-7 from ASI promotes reproductive development as well as recovering from dauer, however, dauer pheromones inhibit *daf-7* expression and thus promote dauer formation (Ren et al., 1996). Non-dauer *daf-7* mutants show an altered egg-laying behaviour with altered inactive phases compared to the wild-type which could be related to food sensing. However, the intestine has also shown to be involved in modulating behaviour in response to food cues (Lee and Mylonakis, 2017). As explored in CHAPTER 5, *acd-5(ok2657)* is a is likely to be a dominant mutation which brings its own limitations (see CHAPTER 5 for a detailed discussion) but also makes rescue more complicated. However, having the *acd-5(lj122)* putative null mutation makes it easier to address this question by using tissue-specific knock-outs or tissue-specific rescues.

A related open question is what is the role of ACD-5 in ASK during dauer? Genetic mechanisms regulating DEG/ENaC expression have previously been linked to tissue remodelling during development, for instance, UNC-8 plays a role in activation-dependent synapse removal in remodelling GABAergic neurons during post-embryonic development (Miller-Fleming et al., 2016). Therefore, upregulation of ACD-5 in ASK during dauer might change neuronal excitability by (increasing) expression in synapses, thereby strengthening previous synapses or, remodelling new synapses. As expression data of the tagged endogenous ACD-5 protein is difficult to obtain (see CHAPTER 5 – 5. 5. Appendix E, Supplementary Figure 7), I have not

verified precise localisation of ACD-5 in ASK, however, potential synaptic localisation could be confirmed by verifying whether it colocalises with a synaptic marker. Behavioural consequences of ACD-5 upregulation could make the neuron more sensitive to input from other neurons, for instance in response to food cues. This could be addressed with using calcium imaging setup (described in 6. 4. Appendix F, Supplementary Figure 11). Decreased sensitivity to food cues might be supported by my data shows that *acd-5* mutants show a slower recovery from dauer and resuming development as speed of dauer recovery is dependent on food-availability (Kaul et al., 2014, Golden and Riddle, 1984). While this could be related to sensing food as a marker for favourable conditions and a cue to exit dauer, an alternative explanation could be that this slower development is linked with the general slower developmental timing observed in the mutant even during reproductive development when animals had not undergone dauer which is unrelated to the ASK expression. However, in support of an involvement of food-sensing role, post-dauers perform poorer in the food racing assay compared to their non-dauer counterparts, and *acd-5* mutants also show lower success in reaching the food patch compared to the wild-type in both conditions. However, this provides limited evidence for the hypothesis that ACD-5 in ASK is directly involved in food sensing. Nevertheless, ASI does synapse directly onto ASK, so a direct effect is possible. Therefore, the role of *acd-5* upregulation could be to change the nature of those ASI-ASK synapses. Another factor that makes it difficult to dissect the relationship between food-sensing and *acd-5* functions is its global upregulation in dauer, post-dauer and *daf-7* mutant, indicating that intestinal expression (the dominant site of expression) is also upregulated.

ASK is a “supporting neuron” which has shown to further enhance phenotypes when ablated in addition to other amphid sensory neurons. For instance, SDS avoidance is significantly lower in animals in which ASH and ASK neurons had been ablated than when only the ASH neurons had been ablated (Hilliard et al., 2002). Similarly, genetic evidence showed that *daf-11* dauer-constitutive (daf-c) phenotype depends mainly on the ASJ neuron with ASK playing a minor role (Schackwitz et al., 1996). There is strong evidence that ASK is involved in dauer formation via the pheromone receptors SRBC-64 and SRBC-66 which localise to its sensory cilia (Kim et al., 2009b). Genetic evidence also suggests that these receptors act genetically upstream of the of *daf-7/TGFβ-like* signalling in dauer formation as they cannot rescue the *daf-7* daf-c phenotype (Kim et al., 2009b). However, based on the genetic data

that *daf-7/TGFβ-like* signalling supresses *acd-5* expression in ASK and an *acd-5* mutation does not have an effect on daf-c phenotype of *daf-7* mutants, it is unlikely that ACD-5 in ASK is directly involved in dauer formation.

6. 4. Appendix F

6. 4. 1. Dauer expression pattern of DEG/ENaCs

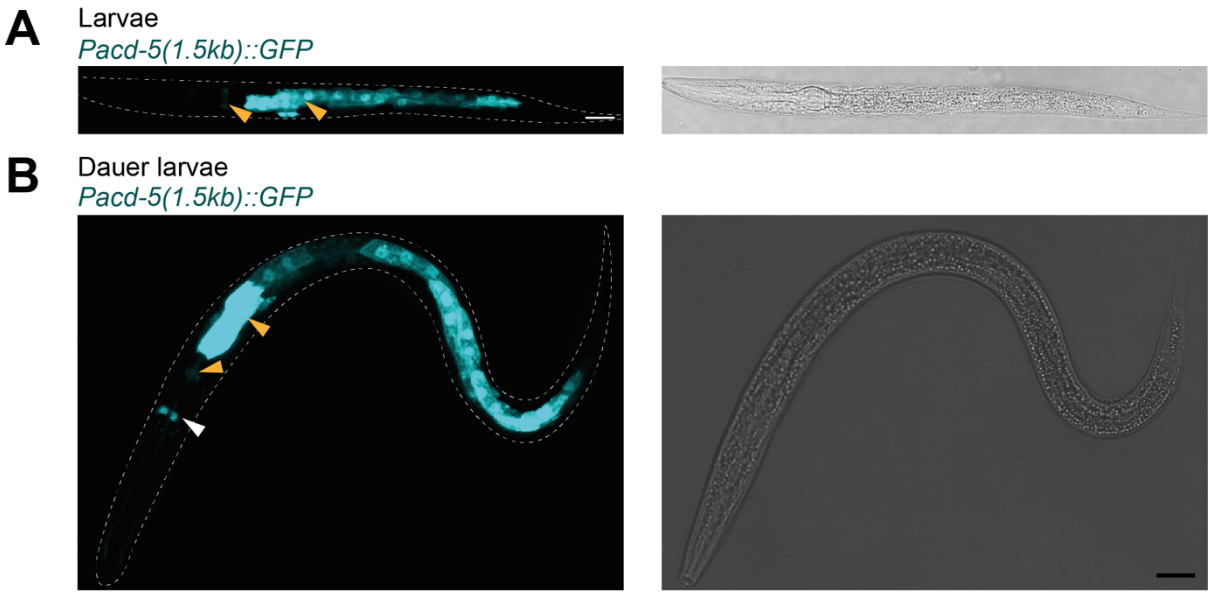

Supplementary Figure 9: Expression pattern of the short acd-5 promoter.

Expression pattern of the *acd-5* promoter driving a green fluorescent protein (GFP) used in (Grundy, 2018). Transgenic animals expressing *ljEx879 [Pacd-5::GFP]* (1502 bp upstream of the *acd-5* start codon) under (A) normal food conditions (young larvae) where GFP is highly expressed in the intestine (yellow arrow) and faint expression in what could be the pharyngeal valve (yellow arrow in the head). (B) Additional upregulation of *Pacd-5::GFP* in the dauer larvae stage in two head neurons (white arrow). Scale bars: 10 µm.

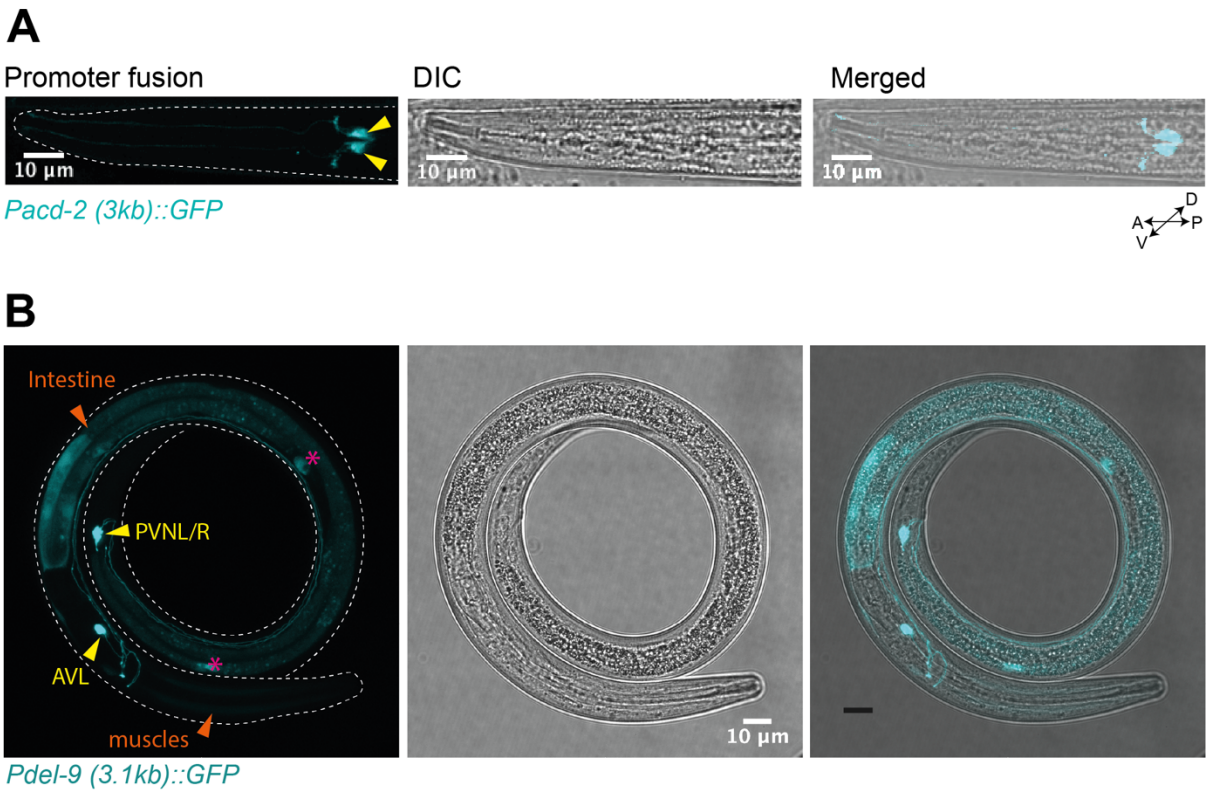

Supplementary Figure 10: Transcriptional promoter-GFP fusion patterns of del-9 and acd-2 change during dauer.

(A) *ljEX1344 [Pacd-2::GFP]* during dauer is enhanced in two head neurons (yellow arrows). (B) *ljEx1361 [Pdel-9::GFP]* expression pattern changes in dauer, it becomes upregulated in the intestine and downregulated in muscles and neurons, apart from AVL and the PVN neurons where it is still heavily expressed.

6. 4. 2. Calcium imaging in response to crude pheromones

One open question is still the precise role of acd-5 in chemosensation. Given the temporal and spatial expression of acd-5 promoter in ASK neurons specifically in dauer larvae, I hypothesised that ACD-5 might be involved in pheromone sensing. In order to test whether ACD-5 is directly involved in chemosensation such as sensing the food cue Lysine or sensing pheromones, I assessed calcium responses in the ASK of first in well-fed wild-type animals and acd-5 mutants to crude pheromones (previously made by Laura Grundy in the lab according to the following protocol (Zhang et al., 2013)) in a microfluidic chip (Supplementary Figure 11). Microfluidic devices present many advantages as they provide a system for delivering temporal and spatial controlled stimuli und controlled environmental conditions. In this experiment the worm is immobilised in a chamber and only the nose is exposed to the chemical stimulus, in this case Pheromones or Lysine solution. As shown in Supplementary Figure 12, despite previous evidence for an involvement in sensing pheromones (in a sensitised npr-1 mutant background) or lysine (Fenk and de Bono, 2017, Wakabayashi et al., 2009), I could not detect any response to either stimulus. I further tried to optimise a response to lysine, OP50 and Pheromones in different buffers (Extracellular solution, M9, CTX in addition to S-Basal) at multiple different concentrations, however, I could not see any calcium transients in ASK (Data not shown).

There were many experimental issues, for instance the expression of GCaMP3 in ASK was very dim therefore, only 3/>20 wild-type animals and 6/>20 *acd-5(ok2657)* mutants showed bright enough GCaMP signal to be able to be analysed. Selection for animals expressing a bright transgene resulted in complete loss of the transgene after 2-3 generations. Several attempts to integrate the transgene using UV irradiation (Mariol et al., 2013) were unsuccessful suggesting some degree of toxicity of GCaMP3 in ASK.

Regarding a lack of a response, it might be the case that ACD-5 expression in the ASK neurons is triggered by pheromones and does not sense them directly. This might be partially supported by preliminary evidence that animals grown in the presence of C9 show a faint expression of the *acd-5* promoter expression in ASK.

Furthermore, chemosensory properties of ACD-5 could also be non-neuronal. While ACD-5 in the intestine is not responsible for expression of ACD-5 in ASK as *acd-5(ok2657)* mutants still express the *Pacd-5::mKate2* in ASK in dauer and post-

dauers, it could be that ACD-5 has a role in the intestine to modulate chemotaxis by, for instance, signalling a “satiety” or a “starvation” signal to the sensory neurons. Recent research has shown that starvation increases avoidance behaviour to dauer pheromones in adult worms (Ryu et al., 2018) via secretion of the insulin-like peptide INS-18 from the intestine. Therefore, one possibility could be that signalling from the intestine could trigger ACD-5 expression in ASK for instance by insulin-like peptides.

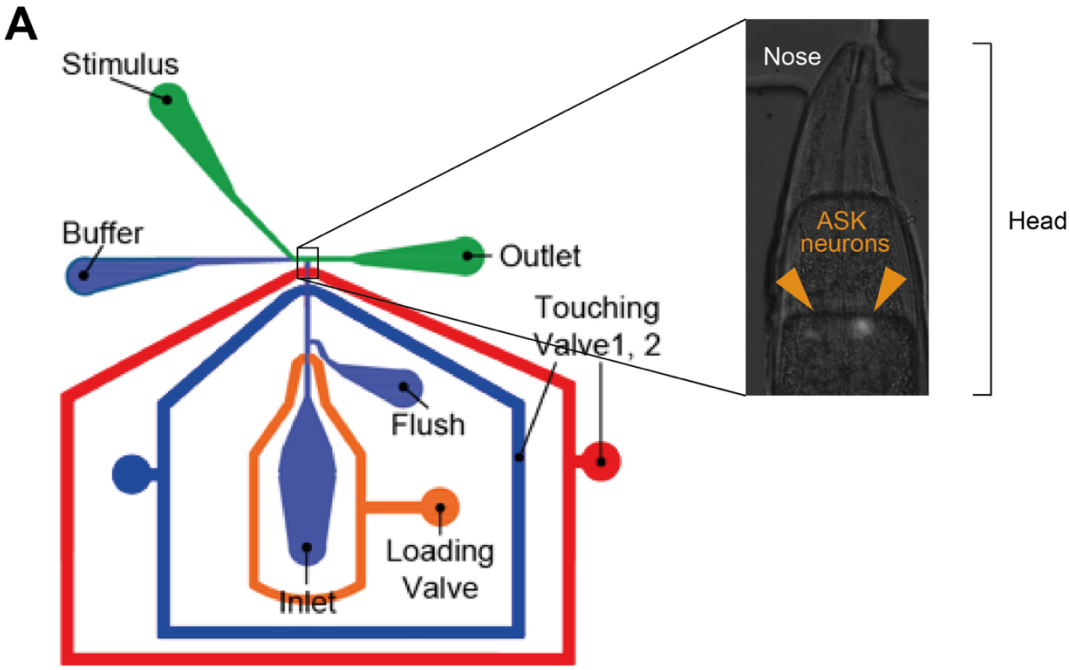

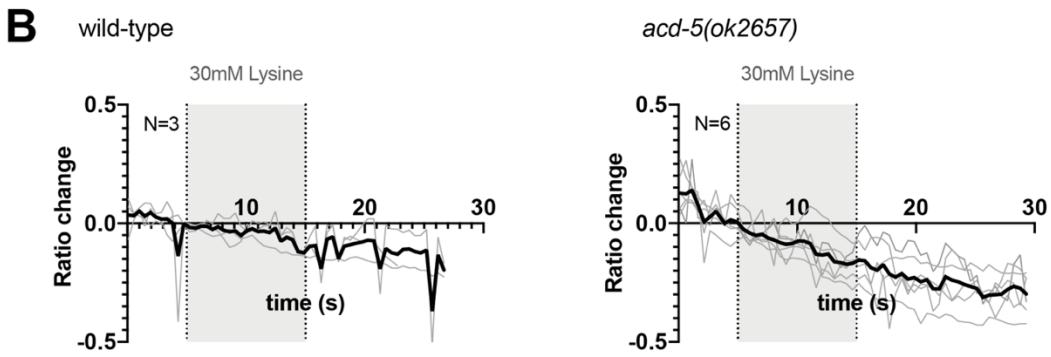

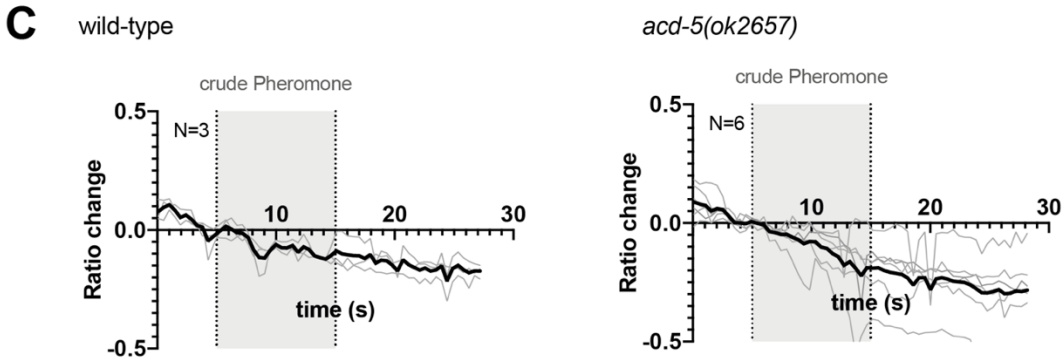

Supplementary Figure 11: Exploring Calcium transients in the ASK neurons in a microfluidic chip.

(A) Dual Stimulation Chip design. Schemata adapted from Yongmin Cho (Dual Chip as used in (Chew et al., 2018)). (B) Calcium transients in ASK neurons in response to 30mM Lysine stimulation for 10 seconds. (C) Calcium transients in ASK neurons in response to crude Pheromones stimulation for 10 seconds.

6. 4. 3. Additional chemotaxis experiments

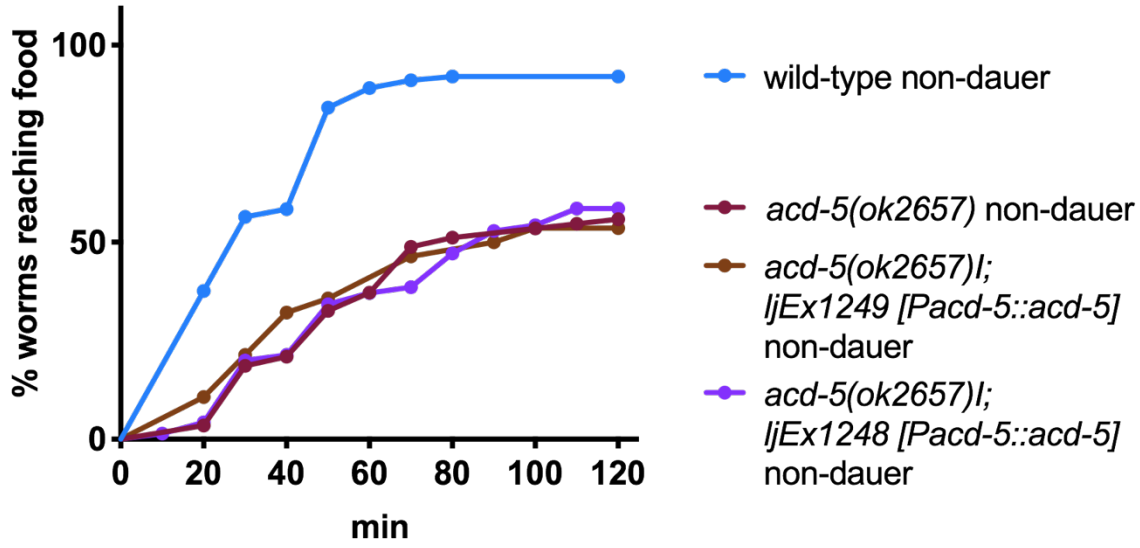

Supplementary Figure 12: Food-racing assay: Rescue experiment.

The cumulative number that reached the food spot is displayed in the following panels. Rescue of *acd-5* under its endogenous promoter could not rescue the deficit in food-sensing in the *acd-5(ok2657)* mutant, that this is not surprising, since it appears to be dominant-negative, and that the *acd-5(lj122)* mutant needs to be tested

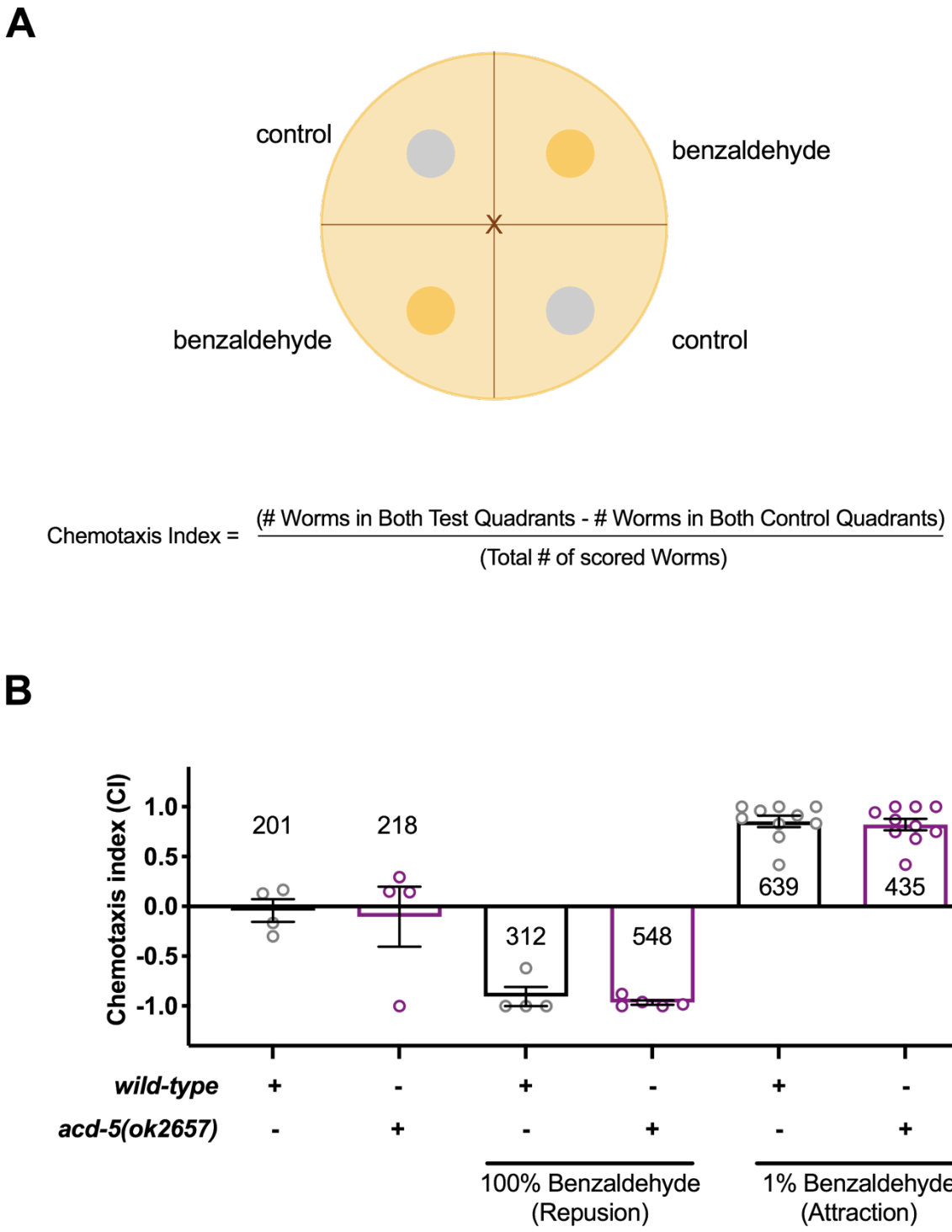

Supplementary Figure 13: Chemotaxis experiments with acd-5 mutants.

(A) A schematic of the assay plates used in the benzaldehyde assay (using the protocol by (Margie et al., 2013). Plates are divided into quadrants two test and two controls. Worms were put in the inner circle and were only scored if they had crossed the circle into the quadrants. (B) Chemotaxis index for *acd-5* mutants (purple) and WT (grey) in response to Benzaldehyde which acts as a repellent at 100% and an attractant at 1%. Each data point represents one trial. Both, the *acd-5* mutant and the wild-type are attracted and repelled by benzaldehyde, respectively (N=4-10 trials with 50-250 worms; Mann-

Whitney U test). (C) Chemotaxis index for *acd-5* mutants and WT in response to benzaldehyde under both well-fed conditions (N=4-10 trials with 50-250 worms; Mann-Whitney U test).

CHAPTER 7 – General conclusion and further directions

7. 1. General conclusion

The research conducted as part of this thesis has added to the current field of proton signalling taking advantage of the model system *C. elegans* in combination with using TEVC. *C. elegans* are amenable to a variety of genetic and behavioural tools which allows to address the question of how protons are implicated in the generation of behaviour. By contrast, using TEVC, I was able to test individual subunits in isolation *in vitro* in *Xenopus* oocytes to further dissect their function.

Building on previous research across species showing that ASIC channels are proton-receptors, there are three main contributions to the field. The first one is that I have described for the first time that there are at least three *C. elegans* DEG/ENaCs that can be activated by protons: ASIC-1, ACD-2 and DEL-9. Here I focus on DEL-9 which is expressed in neurons and muscle where it contributes to the execution of rhythmic muscle contractions during egg-laying and defecation, implicating proton signalling in these behaviours. I have also identified two subunits that are inhibited at low pH, ACD-5 and DEL-4 in addition to the previously characterised ACD-1 subunit (Wang et al., 2008). The second contribution is that for the first time, I have demonstrated that the intestinal proton wave is maintained by acid-sensing ion channels in addition to Na^+/H^+ exchangers, and that proton sensing can directly translate to behavioural outputs independent of the nervous system. And finally, I have identified *daf-7*/TGF-β signalling as a new regulatory genetic pathway for neuronal and global upregulation of ACD-5 in dauers and post-dauers.

7. 2. Further directions

Many of the observations in this thesis warrant further investigation and specific examples have been discussed in previous chapters. However, the current thesis raised some important general questions about protonergic transmission, proton-sensing ion channels, their regulation and their role in behaviour. While I have solved some pieces of the puzzle relating to subunit functioning *in vitro* and genetic role *in vivo*, for DEL-9, one piece is still missing which is the direct evidence that these channel subunits sense protons *in vivo*. The former could be addressed using caged protons or perfusion of low pH over exposed vulva muscles of mutant and wild-type expressing a calcium indicator as a measure of activity. A related question is the question where the protons that activate DEL-9 channels originate. While it is likely that protons activating the vulva muscles or AVL are secreted from the intestine, it might equally be likely that they are released from synaptic vesicles in synapses from upstream neurons. This could be addressed by determining the precise subcellular localisation of the channel. By contrast, for ACD-5, I have shown a direct role in sensing protons in the intestine and its involvement in maintaining acidity in the intestinal lumen. Previous evidence has shown that Na^+/H^+ exchanger and proton pumps are responsible for acidification of the intestinal lumen, which are in this instance the source of protons (Allman et al., 2009, Bender et al., 2013, Benomar et al., 2020).

Another avenue for further investigation is if protons are the sole activators for the identified subunits. While for ACD-5 it is very likely that protons could be the sole ligand for the homomeric or heteromeric channel, this is more difficult to determine for DEL-9. Its localisation suggests that DEL-9 might be exposed to neurotransmitters, neuropeptides and other diffusible messengers that could stimulate or change the response of the DEL-9 channel. Mammalian ASICs have previously described as ‘coincidence detectors’ as they are modulated by a variety of ligands including serotonin (Wang et al., 2013b). Serotonin is a potent activator of egg-laying and is also secreted from HSN neurons that synapse onto the vulva muscles expressing DEL-9. Therefore, other ligands that modulate the *C. elegans* DEG/ENaCs might be an interesting avenue to explore.

Other further sets of experiments could be the identification of heteromeric channels and their implication in behaviour. As shown previously, there are few DEG/ENaCs that show the same expression pattern but there is a lot of overlap in

some neurons including PVD and IL2s as well as in the intestine (see CHAPTER 3). While it is possible that subunits co-expressed in these neurons form heteromeric channels, it is equally likely that they are expressed in different synapses or along different parts of the neuron or intestine. In CHAPTER 5, I showed evidence that the subunits in the intestine interact *in vitro* which provides some evidence that they could interact *in vivo*. As mentioned, the expression pattern of subunits does not always overlap in the same tissue or cell indicating that they might form heteromeric channels with other subunits depending on the tissue in which they are expressed. This of course opens up another huge field for further investigation about the function of different heteromeric channels. *C. elegans* have stereotypic nervous system and stereotypic synaptic connections but with a high degree of structural plasticity underlying their establishment and maintenance at different life stages and in dauer (Jin and Qi, 2018). Combination of different ion channel such as DEG/ENaCs might be mean to remodel synapses and hence modulate cellular functioning throughout development. Conditional upregulation of ACD-5 in ASK, for instance, might contribute to the structural plasticity of the dauer nervous system. Other support from this hypothesis comes from another DEG/ENaC, *unc-8,* which is involved in activity-dependent developmental remodelling of GABAergic synapses between different larval stages (Miller-Fleming et al., 2016). Further characterisation of DEG/ENaC expression patterns during development and under environmental stress in dauer larvae, combined with investigation of development-specific behaviours, might shed some light on to the underlying mechanisms of neural- and behavioural plasticity.

Bibliography

ADAMS, C. M., PRICE, M. P., SNYDER, P. M. & WELSH, M. J. 1999a. Tetraethylammonium block of the BNC1 channel. *Biophys J,* 76**,** 1377-83.

ADAMS, C. M., SNYDER, P. M. & WELSH, M. J. 1999b. Paradoxical stimulation of a DEG/ENaC channel by amiloride. *J Biol Chem,* 274**,** 15500-4.

AHRENS, M. B., ORGER, M. B., ROBSON, D. N., LI, J. M. & KELLER, P. J. 2013. Whole-brain functional imaging at cellular resolution using light-sheet microscopy. *Nat Methods,* 10**,** 413-20.

ALBERT, P. S. & RIDDLE, D. L. 1988. Mutants of Caenorhabditis elegans that form dauer-like larvae. *Dev Biol,* 126**,** 270-93.

ALLMAN, E., JOHNSON, D. & NEHRKE, K. 2009. Loss of the apical V-ATPase a-subunit VHA-6 prevents acidification of the intestinal lumen during a rhythmic behavior in C. elegans. *Am J Physiol Cell Physiol,* 297**,** C1071-81.

ANDROWSKI, R. J., FLATT, K. M. & SCHROEDER, N. E. 2017. Phenotypic plasticity and remodeling in the stress-induced Caenorhabditis elegans dauer. *Wiley Interdiscip Rev Dev Biol,* 6.

ARNADOTTIR, J., O'HAGAN, R., CHEN, Y., GOODMAN, M. B. & CHALFIE, M. 2011. The DEG/ENaC protein MEC-10 regulates the transduction channel complex in Caenorhabditis elegans touch receptor neurons. *J Neurosci,* 31**,** 12695-704.

ATKINSON, H. J., MORRIS, J. H., FERRIN, T. E. & BABBITT, P. C. 2009. Using sequence similarity networks for visualization of relationships across diverse protein superfamilies. *PLoS One,* 4**,** e4345.

AVERY, L. & THOMAS, J. H. 1997. Feeding and Defecation *C. elegans II, edited by Riddle, D. L., Blumenthal, T., Meyer, B. J.,Priess, J. R., in Cold Spring Harbor Laboratory Press,* 2nd edition**,** 679-716.

AWAYDA, M. S. & SUBRAMANYAM, M. 1998. Regulation of the epithelial Na+ channel by membrane tension. *J Gen Physiol,* 112**,** 97-111.

BABINI, E., PAUKERT, M., GEISLER, H. S. & GRUNDER, S. 2002. Alternative splicing and interaction with di- and polyvalent cations control the dynamic range of acid-sensing ion channel 1 (ASIC1). *J Biol Chem,* 277**,** 41597-603.

BACONGUIS, I., BOHLEN, C. J., GOEHRING, A., JULIUS, D. & GOUAUX, E. 2014. X-ray structure of acid-sensing ion channel 1-snake toxin complex reveals open state of a Na(+)-selective channel. *Cell,* 156**,** 717-29.

BANDA, M., BOMMINENI, A., THOMAS, R. A., LUCKINBILL, L. S. & TUCKER, J. D. 2008. Evaluation and validation of housekeeping genes in response to ionizing radiation and chemical exposure for normalizing RNA expression in real-time PCR. *Mutat Res,* 649**,** 126-34.

BARGMANN, C. I., HARTWIEG, E. & HORVITZ, H. R. 1993. Odorant-selective genes and neurons mediate olfaction in C. elegans. *Cell,* 74**,** 515-27.

BARGMANN, C. I. & HORVITZ, H. R. 1991. Chemosensory neurons with overlapping functions direct chemotaxis to multiple chemicals in C. elegans. *Neuron,* 7**,** 729-42.

BARGMANN, C. I. & MARDER, E. 2013. From the connectome to brain function. *Nat Methods,* 10**,** 483-90.

BARON, A., SCHAEFER, L., LINGUEGLIA, E., CHAMPIGNY, G. & LAZDUNSKI, M. 2001. Zn2+ and H+ are coactivators of acid-sensing ion channels. *J Biol Chem,* 276**,** 35361-7.

BARON, A., WALDMANN, R. & LAZDUNSKI, M. 2002. ASIC-like, proton-activated currents in rat hippocampal neurons. *J Physiol,* 539**,** 485-94.
BÄSSLER, E. L., NGO-ANH, T. J., GEISLER, H. S., RUPPERSBERG, J. P. & GRUNDER, S. 2001. Molecular and functional characterization of acid-sensing ion channel (ASIC) 1b. *J Biol Chem,* 276**,** 33782-7.
BEG, A. A., ERNSTROM, G. G., NIX, P., DAVIS, M. W. & JORGENSEN, E. M. 2008. Protons act as a transmitter for muscle contraction in C. elegans. *Cell,* 132**,** 149-160.
BEG, A. A. & JORGENSEN, E. M. 2003. EXP-1 is an excitatory GABA-gated cation channel. *Nat Neurosci,* 6**,** 1145-52.
BENDER, A., WOYDZIAK, Z. R., FU, L., BRANDEN, M., ZHOU, Z., ACKLEY, B. D. & PETERSON, B. R. 2013. Novel acid-activated fluorophores reveal a dynamic wave of protons in the intestine of Caenorhabditis elegans. *ACS Chem Biol,* 8**,** 636-42.
BENOMAR, S., LANSDON, P., BENDER, A. M., PETERSON, B. R., CHANDLER, J. R. & ACKLEY, B. D. 2020. The C. elegans CHP1 homolog, pbo-1, functions in innate immunity by regulating the pH of the intestinal lumen. *PLoS Pathog,* 16**,** e1008134.
BENTLEY, B., BRANICKY, R., BARNES, C. L., CHEW, Y. L., YEMINI, E., BULLMORE, E. T., VERTES, P. E. & SCHAFER, W. R. 2016. The Multilayer Connectome of Caenorhabditis elegans. *PLoS Comput Biol,* 12**,** e1005283.
BENTLEY, P. J. 1968. Amiloride: a potent inhibitor of sodium transport across the toad bladder. *J Physiol,* 195**,** 317-30.
BESSON, T., LINGUEGLIA, E. & SALINAS, M. 2017. Pharmacological modulation of Acid-Sensing Ion Channels 1a and 3 by amiloride and 2-guanidine-4-methylquinazoline (GMQ). *Neuropharmacology,* 125**,** 429-440.
BHAGATWALA, J., HARRIS, R. A., PARIKH, S. J., ZHU, H., HUANG, Y., KOTAK, I., SEIGLER, N., PIERCE, G. L., EGAN, B. M. & DONG, Y. 2014. Epithelial sodium channel inhibition by amiloride on blood pressure and cardiovascular disease risk in young prehypertensives. *J Clin Hypertens (Greenwich),* 16**,** 47-53.
BIANCHI, L., GERSTBREIN, B., FROKJAER-JENSEN, C., ROYAL, D. C., MUKHERJEE, G., ROYAL, M. A., XUE, J., SCHAFER, W. R. & DRISCOLL, M. 2004. The neurotoxic MEC-4(d) DEG/ENaC sodium channel conducts calcium: implications for necrosis initiation. *Nat Neurosci,* 7**,** 1337-44.
BIRNBY, D. A., LINK, E. M., VOWELS, J. J., TIAN, H., COLACURCIO, P. L. & THOMAS, J. H. 2000. A transmembrane guanylyl cyclase (DAF-11) and Hsp90 (DAF-21) regulate a common set of chemosensory behaviors in caenorhabditis elegans. *Genetics,* 155**,** 85-104.
BOHLEN, C. J., CHESLER, A. T., SHARIF-NAEINI, R., MEDZIHRADSZKY, K. F., ZHOU, S., KING, D., SANCHEZ, E. E., BURLINGAME, A. L., BASBAUM, A. I. & JULIUS, D. 2011. A heteromeric Texas coral snake toxin targets acid-sensing ion channels to produce pain. *Nature,* 479**,** 410-4.
BOIKO, N., KUCHER, V., STOCKAND, J. D. & EATON, B. A. 2012. Pickpocket1 Is an Ionotropic Molecular Sensory Transducer. *J. Biol. Chem.,* 287**,** 39878–39886.
BRANICKY, R. & HEKIMI, S. 2006. What keeps C. elegans regular: the genetics of defecation. *Trends Genet,* 22**,** 571-9.
BRANON, T. C., BOSCH, J. A., SANCHEZ, A. D., UDESHI, N. D., SVINKINA, T., CARR, S. A., FELDMAN, J. L., PERRIMON, N. & TING, A. Y. 2018. Efficient

proximity labeling in living cells and organisms with TurboID. *Nat Biotechnol,* 36**,** 880-887.
BRENNER, S. 1974. The genetics of Caenorhabditis elegans. *Genetics,* 77**,** 71-94.
BROWN, A. E., YEMINI, E. I., GRUNDY, L. J., JUCIKAS, T. & SCHAFER, W. R. 2013. A dictionary of behavioral motifs reveals clusters of genes affecting Caenorhabditis elegans locomotion. *Proc Natl Acad Sci U S A,* 110**,** 791-6.
BROWN, A. L., FERNANDEZ-ILLESCAS, S. M., LIAO, Z. & GOODMAN, M. B. 2007. Gain-of-function mutations in the MEC-4 DEG/ENaC sensory mechanotransduction channel alter gating and drug blockade. *J Gen Physiol,* 129**,** 161-73.
BRUNDAGE, L., AVERY, L., KATZ, A., KIM, U. J., MENDEL, J. E., STERNBERG, P. W. & SIMON, M. I. 1996. Mutations in a C. elegans Gqalpha gene disrupt movement, egg laying, and viability. *Neuron,* 16**,** 999-1009.
BYERLY, L., CASSADA, R. C. & RUSSELL, R. L. 1976. The life cycle of the nematode Caenorhabditis elegans. I. Wild-type growth and reproduction. *Dev Biol,* 51**,** 23-33.
C. ELEGANS SEQUENCING CONSORTIUM 1998. Genome sequence of the nematode C. elegans: a platform for investigating biology. *Science,* 282**,** 2012-8.
CALAHORRO, F., KEEFE, F., DILLON, J., HOLDEN-DYE, L. & O'CONNOR, V. 2019. Neuroligin tuning of pharyngeal pumping reveals extrapharyngeal modulation of feeding in Caenorhabditis elegans. *J Exp Biol,* 222.
CALIXTO, A., JARA, J. S. & COURT, F. A. 2012. Diapause formation and downregulation of insulin-like signaling via DAF-16/FOXO delays axonal degeneration and neuronal loss. *PLoS Genet,* 8**,** e1003141.
CAMERON, P., HIROI, M., NGAI, J. & SCOTT, K. 2010. The molecular basis for water taste in Drosophila. *Nature,* 465**,** 91-5.
CANESSA, C. M., HORISBERGER, J. D. & ROSSIER, B. C. 1993. Epithelial sodium channel related to proteins involved in neurodegeneration. *Nature,* 361**,** 467-70.
CANESSA, C. M., SCHILD, L., BUELL, G., THORENS, B., GAUTSCHI, I., HORISBERGER, J. D. & ROSSIER, B. C. 1994. Amiloride-sensitive epithelial Na+ channel is made of three homologous subunits. *Nature,* 367**,** 463-7.
CAO, J., PACKER, J. S., RAMANI, V., CUSANOVICH, D. A., HUYNH, C., DAZA, R., QIU, X., LEE, C., FURLAN, S. N., STEEMERS, F. J., ADEY, A., WATERSTON, R. H., TRAPNELL, C. & SHENDURE, J. 2017. Comprehensive single-cell transcriptional profiling of a multicellular organism. *Science,* 357**,** 661-667.
CARATTINO, M. D. & DELLA VECCHIA, M. C. 2012. Contribution of residues in second transmembrane domain of ASIC1a protein to ion selectivity. *J Biol Chem,* 287**,** 12927-34.
CARATTINO, M. D., SHENG, S. & KLEYMAN, T. R. 2004. Epithelial Na+ channels are activated by laminar shear stress. *J Biol Chem,* 279**,** 4120-6.
CASEY, J. R., GRINSTEIN, S. & ORLOWSKI, J. 2010. Sensors and regulators of intracellular pH. *Nat Rev Mol Cell Biol,* 11**,** 50-61.
CASSADA, R. C. & RUSSELL, R. L. 1975. The dauerlarva, a post-embryonic developmental variant of the nematode Caenorhabditis elegans. *Dev Biol,* 46**,** 326-42.
CHALFIE, M. & SULSTON, J. 1981. Developmental genetics of the mechanosensory neurons of Caenorhabditis elegans. *Dev Biol,* 82**,** 358-70.

CHALFIE, M., SULSTON, J. E., WHITE, J. G., SOUTHGATE, E., THOMSON, J. N. & BRENNER, S. 1985. The neural circuit for touch sensitivity in Caenorhabditis elegans. *J Neurosci,* 5**,** 956-64.
CHALFIE, M. & WOLINSKY, E. 1990. The identification and suppression of inherited neurodegeneration in Caenorhabditis elegans. *Nature,* 345**,** 410-6.
CHARPENTIER, E., RICHTER, H., VAN DER OOST, J. & WHITE, M. F. 2015. Biogenesis pathways of RNA guides in archaeal and bacterial CRISPR-Cas adaptive immunity. *FEMS Microbiol Rev,* 39**,** 428-41.
CHATZIGEORGIOU, M., YOO, S., WATSON, J. D., LEE, W. H., SPENCER, W. C., KINDT, K. S., HWANG, S. W., MILLER, D. M., 3RD, TREININ, M., DRISCOLL, M. & SCHAFER, W. R. 2010. Specific roles for DEG/ENaC and TRP channels in touch and thermosensation in C. elegans nociceptors. *Nat Neurosci,* 13**,** 861-8.
CHAUHAN, V. M., ORSI, G., BROWN, A., PRITCHARD, D. I. & AYLOTT, J. W. 2013. Mapping the pharyngeal and intestinal pH of Caenorhabditis elegans and real-time luminal pH oscillations using extended dynamic range pH-sensitive nanosensors. *ACS Nano,* 7**,** 5577-87.
CHELUR, D. S., ERNSTROM, G. G., GOODMAN, M. B., YAO, C. A., CHEN, L., R, O. H. & CHALFIE, M. 2002. The mechanosensory protein MEC-6 is a subunit of the C. elegans touch-cell degenerin channel. *Nature,* 420**,** 669-73.
CHEN, B., ZOU, W., XU, H., LIANG, Y. & HUANG, B. 2018. Efficient labeling and imaging of protein-coding genes in living cells using CRISPR-Tag. *Nat Commun,* 9**,** 5065.
CHEN, X. & GRUNDER, S. 2007. Permeating protons contribute to tachyphylaxis of the acid-sensing ion channel (ASIC) 1a. *J Physiol,* 579**,** 657-70.
CHEN, X., POLLEICHTNER, G., KADURIN, I. & GRUNDER, S. 2007. Zebrafish acid-sensing ion channel (ASIC) 4, characterization of homo- and heteromeric channels, and identification of regions important for activation by H+. *J Biol Chem,* 282**,** 30406-13.
CHESLER, M. & KAILA, K. 1992. Modulation of pH by neuronal activity. *Trends Neurosci,* 15**,** 396-402.
CHEW, Y. L., TANIZAWA, Y., CHO, Y., ZHAO, B., YU, A. J., ARDIEL, E. L., RABINOWITCH, I., BAI, J., RANKIN, C. H., LU, H., BEETS, I. & SCHAFER, W. R. 2018. An Afferent Neuropeptide System Transmits Mechanosensory Signals Triggering Sensitization and Arousal in C. elegans. *Neuron,* 99**,** 1233-1246 e6.
CHEW, Y. L., WALKER, D. S., TOWLSON, E. K., VERTES, P. E., YAN, G., BARABASI, A. L. & SCHAFER, W. R. 2017. Recordings of Caenorhabditis elegans locomotor behaviour following targeted ablation of single motorneurons. *Sci Data,* 4**,** 170156.
CHO, Y., OAKLAND, D. N., LEE, S. A., SCHAFER, W. R. & LU, H. 2018. On-chip functional neuroimaging with mechanical stimulation in Caenorhabditis elegans larvae for studying development and neural circuits. *Lab Chip,* 18**,** 601-609.
CHO, Y., PORTO, D. A., HWANG, H., GRUNDY, L. J., SCHAFER, W. R. & LU, H. 2017. Automated and controlled mechanical stimulation and functional imaging in vivo in C. elegans. *Lab Chip,* 17**,** 2609-2618.
CICCARELLI, F. D., DOERKS, T., VON MERING, C., CREEVEY, C. J., SNEL, B. & BORK, P. 2006. Toward automatic reconstruction of a highly resolved tree of life. *Science,* 311**,** 1283-7.
COLLIER, D. M. & SNYDER, P. M. 2009. Extracellular protons regulate human ENaC by modulating Na+ self-inhibition. *J Biol Chem,* 284**,** 792-8.

COLLINS, K. M., BODE, A., FERNANDEZ, R. W., TANIS, J. E., BREWER, J. C., CREAMER, M. S. & KOELLE, M. R. 2016. Activity of the C. elegans egg-laying behavior circuit is controlled by competing activation and feedback inhibition. *Elife,* 5.

COLLINS, K. M. & KOELLE, M. R. 2013. Postsynaptic ERG potassium channels limit muscle excitability to allow distinct egg-laying behavior states in Caenorhabditis elegans. *J Neurosci,* 33**,** 761-75.

CONG, L., WANG, Z., CHAI, Y., HANG, W., SHANG, C., YANG, W., BAI, L., DU, J., WANG, K. & WEN, Q. 2017. Rapid whole brain imaging of neural activity in freely behaving larval zebrafish (Danio rerio). *Elife,* 6.

CONSORTIUM, C. E. D. M. 2012. large-scale screening for targeted knockouts in the Caenorhabditis elegans genome. *G3 (Bethesda),* 2**,** 1415-25.

COOK, S. J., JARRELL, T. A., BRITTIN, C. A., WANG, Y., BLONIARZ, A. E., YAKOVLEV, M. A., NGUYEN, K. C. Q., TANG, L. T., BAYER, E. A., DUERR, J. S., BULOW, H. E., HOBERT, O., HALL, D. H. & EMMONS, S. W. 2019. Whole-animal connectomes of both Caenorhabditis elegans sexes. *Nature,* 571**,** 63-71.

DAILY, J. 2016. Parasail: SIMD C library for global, semi-global, and local pairwise sequence alignments. *BMC Bioinformatics,* 17**,** 81.

DAL SANTO, P., LOGAN, M. A., CHISHOLM, A. D. & JORGENSEN, E. M. 1999. The inositol trisphosphate receptor regulates a 50-second behavioral rhythm in C. elegans. *Cell,* 98**,** 757-67.

DALFO, D., MICHAELSON, D. & HUBBARD, E. J. 2012. Sensory regulation of the C. elegans germline through TGF-beta-dependent signaling in the niche. *Curr Biol,* 22**,** 712-9.

DE STASIO, E. A., MUELLER, K. P., BAUER, R. J., HURLBURT, A. J., BICE, S. A., SCHOLTZ, S. L., PHIRKE, P., SUGIAMAN-TRAPMAN, D., STINSON, L. A., OLSON, H. B., VOGEL, S. L., EK-VAZQUEZ, Z., ESEMEN, Y., KORZYNSKI, J., WOLFE, K., ARBUCKLE, B. N., ZHANG, H., LOMBARD-KNAPP, G., PIASECKI, B. P. & SWOBODA, P. 2018. An Expanded Role for the RFX Transcription Factor DAF-19, with Dual Functions in Ciliated and Nonciliated Neurons. *Genetics,* 208**,** 1083-1097.

DEITMER, J. W. 2007. Acid–Base Transport and pH Regulation. *Handbook of Neurochemistry and Molecular Neurobiology- Brain Energetics. Integration of Molecular and Cellular Processes (Springer, Boston, MA)***,** 469-486.

DEITMER, J. W. & ROSE, C. R. 1996. pH regulation and proton signalling by glial cells. *Prog Neurobiol,* 48**,** 73-103.

DEREEPER, A., AUDIC, S., CLAVERIE, J. M. & BLANC, G. 2010. BLAST-EXPLORER helps you building datasets for phylogenetic analysis. *BMC Evol Biol,* 10**,** 8.

DEREEPER, A., GUIGNON, V., BLANC, G., AUDIC, S., BUFFET, S., CHEVENET, F., DUFAYARD, J. F., GUINDON, S., LEFORT, V., LESCOT, M., CLAVERIE, J. M. & GASCUEL, O. 2008. Phylogeny.fr: robust phylogenetic analysis for the non-specialist. *Nucleic Acids Res,* 36**,** W465-9.

DHEDA, K., HUGGETT, J. F., BUSTIN, S. A., JOHNSON, M. A., ROOK, G. & ZUMLA, A. 2004. Validation of housekeeping genes for normalizing RNA expression in real-time PCR. *Biotechniques,* 37**,** 112-4, 116, 118-9.

DIOCHOT, S., BARON, A., RASH, L. D., DEVAL, E., ESCOUBAS, P., SCARZELLO, S., SALINAS, M. & LAZDUNSKI, M. 2004. A new sea anemone peptide,

APETx2, inhibits ASIC3, a major acid-sensitive channel in sensory neurons. *EMBO J,* 23**,** 1516-25.
DIOCHOT, S., BARON, A., SALINAS, M., DOUGUET, D., SCARZELLO, S., DABERT-GAY, A. S., DEBAYLE, D., FRIEND, V., ALLOUI, A., LAZDUNSKI, M. & LINGUEGLIA, E. 2012. Black mamba venom peptides target acid-sensing ion channels to abolish pain. *Nature,* 490**,** 552-5.
DOKSHIN, G. A., GHANTA, K. S., PISCOPO, K. M. & MELLO, C. C. 2018. Robust Genome Editing with Short Single-Stranded and Long, Partially Single-Stranded DNA Donors in Caenorhabditis elegans. *Genetics,* 210**,** 781-787.
DRISCOLL, M. & CHALFIE, M. 1991. The mec-4 gene is a member of a family of Caenorhabditis elegans genes that can mutate to induce neuronal degeneration. *Nature,* 349**,** 588-93.
DU, J., HOSSAIN, Z. & MANDAL, J. 2017. Protons: A neurotransmitter in the brain. *Edorium J Cell Biol* 3**,** 1–3.
DU, J., REZNIKOV, L. R., PRICE, M. P., ZHA, X. M., LU, Y., MONINGER, T. O., WEMMIE, J. A. & WELSH, M. J. 2014. Protons are a neurotransmitter that regulates synaptic plasticity in the lateral amygdala. *Proc Natl Acad Sci U S A,* 111**,** 8961-6.
DULAI, J. S., SMITH, E. S. J. & RAHMAN, T. 2021. Acid-sensing ion channel 3: An analgesic target. *Channels (Austin),* 15**,** 94-127.
DURRNAGEL, S., FALKENBURGER, B. H. & GRUNDER, S. 2012. High Ca(2+) permeability of a peptide-gated DEG/ENaC from Hydra. *J Gen Physiol,* 140**,** 391-402.
ELIAS, I. & LAGERGREN, J. 2007. Fast computation of distance estimators. *BMC Bioinformatics,* 8**,** 89.
ELKHATIB, W., SMITH, C. L. & SENATORE, A. 2019. A Na(+) leak channel cloned from Trichoplax adhaerens extends extracellular pH and Ca(2+) sensing for the DEG/ENaC family close to the base of Metazoa. *J Biol Chem,* 294**,** 16320-16336.
ESCOUBAS, P., DE WEILLE, J. R., LECOQ, A., DIOCHOT, S., WALDMANN, R., CHAMPIGNY, G., MOINIER, D., MENEZ, A. & LAZDUNSKI, M. 2000. Isolation of a tarantula toxin specific for a class of proton-gated Na+ channels. *J Biol Chem,* 275**,** 25116-21.
ESPELT, M. V., ESTEVEZ, A. Y., YIN, X. & STRANGE, K. 2005. Oscillatory Ca2+ signaling in the isolated Caenorhabditis elegans intestine: role of the inositol-1,4,5-trisphosphate receptor and phospholipases C beta and gamma. *J Gen Physiol,* 126**,** 379-92.
ESTEVEZ, M., ATTISANO, L., WRANA, J. L., ALBERT, P. S., MASSAGUE, J. & RIDDLE, D. L. 1993. The daf-4 gene encodes a bone morphogenetic protein receptor controlling C. elegans dauer larva development. *Nature,* 365**,** 644-9.
FAY, D. & SPENCER, A. 2006. Genetic mapping and manipulation: chapter 8--Dominant mutations. *WormBook***,** 1-6.
FAZIA, T., PASTORINO, R., NOTARTOMASO, S., BUSCETI, C., IMBRIGLIO, T., CANNELLA, M., GENTILINI, D., MORANI, G., TICCA, A., BITTI, P., BERZUINI, C., DALMAY, T., BATTAGLIA, G. & BERNARDINELLI, L. 2019. Acid sensing ion channel 2: A new potential player in the pathophysiology of multiple sclerosis. *Eur J Neurosci,* 49**,** 1233-1243.
FECHNER, S., D'ALESSANDRO, I., WANG, L., TOWER, C., TAO, L. & GOODMAN, M. 2020. Divergent ion selectivity and sensitivity to anti-hypertensive and non-

steroidal anti-inflammatory drugs of DEG/ENaC/ASIC channels in C. elegans. *bioRxiv*.
FELSENSTEIN, J. 1989. PHYLIP - Phylogeny Inference Package (Version 3.2). *Cladistics,* 5**,** 164-166.
FENK, L. A. & DE BONO, M. 2017. Memory of recent oxygen experience switches pheromone valence in Caenorhabditis elegans. *Proc Natl Acad Sci U S A,* 114**,** 4195-4200.
FERNANDEZ, N. F., GUNDERSEN, G. W., RAHMAN, A., GRIMES, M. L., RIKOVA, K., HORNBECK, P. & MA'AYAN, A. 2017. Clustergrammer, a web-based heatmap visualization and analysis tool for high-dimensional biological data. *Sci Data,* 4**,** 170151.
FINKEL, A. S., GAGE, P. W., 1985. Conventional Voltage Clamping With Two Intracellular Microelectrodes.
FIRE, A., XU, S., MONTGOMERY, M. K., KOSTAS, S. A., DRIVER, S. E. & MELLO, C. C. 1998. Potent and specific genetic interference by double-stranded RNA in Caenorhabditis elegans. *Nature,* 391**,** 806-11.
FRASER, A. G., KAMATH, R. S., ZIPPERLEN, P., MARTINEZ-CAMPOS, M., SOHRMANN, M. & AHRINGER, J. 2000. Functional genomic analysis of C. elegans chromosome I by systematic RNA interference. *Nature,* 408**,** 325-30.
FRIESE, M. A., CRANER, M. J., ETZENSPERGER, R., VERGO, S., WEMMIE, J. A., WELSH, M. J., VINCENT, A. & FUGGER, L. 2007. Acid-sensing ion channel-1 contributes to axonal degeneration in autoimmune inflammation of the central nervous system. *Nat Med,* 13**,** 1483-9.
FROKJAER-JENSEN, C., DAVIS, M. W., HOPKINS, C. E., NEWMAN, B. J., THUMMEL, J. M., OLESEN, S. P., GRUNNET, M. & JORGENSEN, E. M. 2008. Single-copy insertion of transgenes in Caenorhabditis elegans. *Nat Genet,* 40**,** 1375-83.
FRONIUS, M. & CLAUSS, W. G. 2008. Mechano-sensitivity of ENaC: may the (shear) force be with you. *Pflugers Arch,* 455**,** 775-85.
GARCIA-ANOVEROS, J., GARCIA, J. A., LIU, J. D. & COREY, D. P. 1998. The nematode degenerin UNC-105 forms ion channels that are activated by degeneration- or hypercontraction-causing mutations. *Neuron,* 20**,** 1231-41.
GARDNER, M., ROSELL, M. & MYERS, E. M. 2013. Measuring the effects of bacteria on C. elegans behavior using an egg retention assay. *J Vis Exp***,** e51203.
GARTY, H., ASHER, C. & YEGER, O. 1987. Direct inhibition of epithelial Na+ channels by a pH-dependent interaction with calcium, and by other divalent ions. *J Membr Biol,* 95**,** 151-62.
GASCUEL, O. 1997. BIONJ: an improved version of the NJ algorithm based on a simple model of sequence data. *Mol Biol Evol,* 14**,** 685-95.
GEFFENEY, S. L., CUEVA, J. G., GLAUSER, D. A., DOLL, J. C., LEE, T. H., MONTOYA, M., KARANIA, S., GARAKANI, A. M., PRUITT, B. L. & GOODMAN, M. B. 2011. DEG/ENaC but not TRP channels are the major mechanoelectrical transduction channels in a C. elegans nociceptor. *Neuron,* 71**,** 845-57.
GEORGI, L. L., ALBERT, P. S. & RIDDLE, D. L. 1990. daf-1, a C. elegans gene controlling dauer larva development, encodes a novel receptor protein kinase. *Cell,* 61**,** 635-45.
GERISCH, B. & ANTEBI, A. 2004. Hormonal signals produced by DAF-9/cytochrome P450 regulate C. elegans dauer diapause in response to environmental cues. *Development,* 131**,** 1765-76.

GERLT, J. A. 2017. Genomic Enzymology: Web Tools for Leveraging Protein Family Sequence-Function Space and Genome Context to Discover Novel Functions. *Biochemistry,* 56**,** 4293-4308.
GERLT, J. A., BOUVIER, J. T., DAVIDSON, D. B., IMKER, H. J., SADKHIN, B., SLATER, D. R. & WHALEN, K. L. 2015. Enzyme Function Initiative-Enzyme Similarity Tool (EFI-EST): A web tool for generating protein sequence similarity networks. *Biochim Biophys Acta,* 1854**,** 1019-37.
GOLDEN, J. W. & RIDDLE, D. L. 1984. The Caenorhabditis elegans dauer larva: developmental effects of pheromone, food, and temperature. *Dev Biol,* 102**,** 368-78.
GOLUBOVIC, A., KUHN, A., WILLIAMSON, M., KALBACHER, H., HOLSTEIN, T. W., GRIMMELIKHUIJZEN, C. J. & GRUNDER, S. 2007. A peptide-gated ion channel from the freshwater polyp Hydra. *J Biol Chem,* 282**,** 35098-103.
GOMEZ-ORTE, E., CORNES, E., ZHELEVA, A., SAENZ-NARCISO, B., DE TORO, M., INIGUEZ, M., LOPEZ, R., SAN-JUAN, J. F., EZCURRA, B., SACRISTAN, B., SANCHEZ-BLANCO, A., CERON, J. & CABELLO, J. 2018. Effect of the diet type and temperature on the C. elegans transcriptome. *Oncotarget,* 9**,** 9556-9571.
GOODMAN, M. B., ERNSTROM, G. G., CHELUR, D. S., O'HAGAN, R., YAO, C. A. & CHALFIE, M. 2002. MEC-2 regulates C. elegans DEG/ENaC channels needed for mechanosensation. *Nature,* 415**,** 1039-42.
GOWRISANKARAN, S. & MILOSEVIC, I. 2020. Regulation of synaptic vesicle acidification at the neuronal synapse. *IUBMB Life,* 72**,** 568-576.
GRUNDER, S. & ASSMANN, M. 2015. Peptide-gated ion channels and the simple nervous system of Hydra. *J Exp Biol,* 218**,** 551-61.
GRUNDER, S. & CHEN, X. 2010. Structure, function, and pharmacology of acid-sensing ion channels (ASICs): focus on ASIC1a. *Int J Physiol Pathophysiol Pharmacol,* 2**,** 73-94.
GRUNDER, S. & PUSCH, M. 2015. Biophysical properties of acid-sensing ion channels (ASICs). *Neuropharmacology,* 94**,** 9-18.
GRUNDY, L. J. 2018. The Automatic Tracking Of Caenorhabditis elegans And Its Use In Determining Genetic Function. *PhD thesis. Open Reserach Online. The Open University.* .
GRUOL, D. L., BARKER, J. L., HUANG, L. Y., MACDONALD, J. F. & SMITH, T. G. J. 1980. Hydrogen ions have multiple effects on the excitability of cultured mammalian neurons. *Brain Res,* 183**,** 247-252.
HAMM, L. L., FENG, Z. & HERING-SMITH, K. S. 2010. Regulation of sodium transport by ENaC in the kidney. *Curr Opin Nephrol Hypertens,* 19**,** 98-105.
HAMMARLUND, M., HOBERT, O., MILLER, D. M., 3RD & SESTAN, N. 2018. The CeNGEN Project: The Complete Gene Expression Map of an Entire Nervous System. *Neuron,* 99**,** 430-433.
HAN, L., WANG, Y., SANGALETTI, R., D'URSO, G., LU, Y., SHAHAM, S. & BIANCHI, L. 2013. Two novel DEG/ENaC channel subunits expressed in glia are needed for nose-touch sensitivity in Caenorhabditis elegans. *J Neurosci,* 33**,** 936-49.
HARDEGE, I., XU, S., GORDON, R. D., THOMPSON, A. J., FIGG, N., STOWASSER, M., MURRELL-LAGNADO, R. & O'SHAUGHNESSY, K. M. 2015. Novel Insertion Mutation in KCNJ5 Channel Produces Constitutive Aldosterone Release From H295R Cells. *Mol Endocrinol,* 29**,** 1522-30.

HESSELAGER, M., TIMMERMANN, D. B. & AHRING, P. K. 2004. pH Dependency and desensitization kinetics of heterologously expressed combinations of acid-sensing ion channel subunits. *J Biol Chem,* 279**,** 11006-15.
HIGHSTEIN, S. M., HOLSTEIN, G. R., MANN, M. A. & RABBITT, R. D. 2014. Evidence that protons act as neurotransmitters at vestibular hair cell-calyx afferent synapses. *Proc Natl Acad Sci U S A,* 111**,** 5421-6.
HILL, A., ZHENG, X., LI, X., MCKINNEY, R., DICKMAN, D. & BEN-SHAHAR, Y. 2017. The Drosophila Postsynaptic DEG/ENaC Channel ppk29 Contributes to Excitatory Neurotransmission. *J Neurosci,* 37**,** 3171-3180.
HILL, A. S. & BEN-SHAHAR, Y. 2018. The synaptic action of Degenerin/Epithelial sodium channels. *Channels (Austin),* 12**,** 262-275.
HILLIARD, M. A., BARGMANN, C. I. & BAZZICALUPO, P. 2002. C. elegans responds to chemical repellents by integrating sensory inputs from the head and the tail. *Curr Biol,* 12**,** 730-4.
HOAGLAND, E. N., SHERWOOD, T. W., LEE, K. G., WALKER, C. J. & ASKWITH, C. C. 2010. Identification of a calcium permeable human acid-sensing ion channel 1 transcript variant. *J Biol Chem,* 285**,** 41852-62.
HOBERT, O. 2013. The neuronal genome of Caenorhabditis elegans. *WormBook***,** 1-106.
HOLZER, P. 2009. Acid-sensitive ion channels and receptors. *Handb Exp Pharmacol***,** 283-332.
HOOGEWIJS, D., HOUTHOOFD, K., MATTHIJSSENS, F., VANDESOMPELE, J. & VANFLETEREN, J. R. 2008. Selection and validation of a set of reliable reference genes for quantitative sod gene expression analysis in C. elegans. *BMC Mol Biol,* 9**,** 9.
HORVITZ, H. R., CHALFIE, M., TRENT, C., SULSTON, J. E. & EVANS, P. D. 1982. Serotonin and octopamine in the nematode Caenorhabditis elegans. *Science,* 216**,** 1012-4.
HUANG, M. & CHALFIE, M. 1994. Gene interactions affecting mechanosensory transduction in Caenorhabditis elegans. *Nature,* 367**,** 467-70.
HUANG, M., GU, G., FERGUSON, E. L. & CHALFIE, M. 1995. A stomatin-like protein necessary for mechanosensation in C. elegans. *Nature,* 378**,** 292-5.
HUSSON, S. J., COSTA, W. S., WABNIG, S., STIRMAN, J. N., WATSON, J. D., SPENCER, W. C., AKERBOOM, J., LOOGER, L. L., TREININ, M., MILLER, D. M., 3RD, LU, H. & GOTTSCHALK, A. 2012. Optogenetic analysis of a nociceptor neuron and network reveals ion channels acting downstream of primary sensors. *Curr Biol,* 22**,** 743-52.
IMANIKIA, S., OZBEY, N. P., KRUEGER, C., CASANUEVA, M. O. & TAYLOR, R. C. 2019. Neuronal XBP-1 Activates Intestinal Lysosomes to Improve Proteostasis in C. elegans. *Curr Biol,* 29**,** 2322-2338 e7.
IMMKE, D. C. & MCCLESKEY, E. W. 2001. Lactate enhances the acid-sensing Na+ channel on ischemia-sensing neurons. *Nat Neurosci,* 4**,** 869-70.
IMMKE, D. C. & MCCLESKEY, E. W. 2003. Protons open acid-sensing ion channels by catalyzing relief of Ca2+ blockade. *Neuron,* 37**,** 75-84.
INOUE, T. & THOMAS, J. H. 2000. Targets of TGF-beta Signaling inCaenorhabditis elegans Dauer Formation. *Developmental Biology,* 217**,** 192–204.
JAEGER, A. H., STANLEY, M., WEISS, Z. F., MUSSO, P. Y., CHAN, R. C., ZHANG, H., FELDMAN-KISS, D. & GORDON, M. D. 2018. A complex peripheral code for salt taste in Drosophila. *Elife,* 7.

JANG, M. S., TOYOSHIMA, Y., TOMIOKA, M., KUNITOMO, H. & IINO, Y. 2019. Multiple sensory neurons mediate starvation-dependent aversive navigation in Caenorhabditis elegans. *Proc Natl Acad Sci U S A,* 116**,** 18673-18683.
JASTI, J., FURUKAWA, H., GONZALES, E. B. & GOUAUX, E. 2007. Structure of acid-sensing ion channel 1 at 1.9 A resolution and low pH. *Nature,* 449**,** 316-23.
JEONG, P., KWON, M., JOO, H. & PAIK, Y. 2009. Molecular Time-Course and the Metabolic Basis of Entry into Dauer in Caenorhabditis elegans. *PLoS One,* 4**,** e4162.
JIA, K., ALBERT, P. S. & RIDDLE, D. L. 2002. DAF-9, a cytochrome P450 regulating C. elegans larval development and adult longevity. *Development,* 129**,** 221-31.
JIN, Y. & QI, Y. B. 2018. Building stereotypic connectivity: mechanistic insights into structural plasticity from C. elegans. *Curr Opin Neurobiol,* 48**,** 97-105.
JINEK, M., CHYLINSKI, K., FONFARA, I., HAUER, M., DOUDNA, J. A. & CHARPENTIER, E. 2012. A programmable dual-RNA-guided DNA endonuclease in adaptive bacterial immunity. *Science,* 337**,** 816-21.
JOSE, A. M., BANY, I. A., CHASE, D. L. & KOELLE, M. R. 2007. A specific subset of transient receptor potential vanilloid-type channel subunits in Caenorhabditis elegans endocrine cells function as mixed heteromers to promote neurotransmitter release. *Genetics,* 175**,** 93-105.
JOSPIN, M. & ALLARD, B. 2004. An amiloride-sensitive H+-gated Na+ channel in Caenorhabditis elegans body wall muscle cells. *J Physiol,* 559**,** 715-20.
KAMATH, R. S. & AHRINGER, J. 2003. Genome-wide RNAi screening in Caenorhabditis elegans. *Methods,* 30**,** 313-21.
KAMATH, R. S., FRASER, A. G., DONG, Y., POULIN, G., DURBIN, R., GOTTA, M., KANAPIN, A., LE BOT, N., MORENO, S., SOHRMANN, M., WELCHMAN, D. P., ZIPPERLEN, P. & AHRINGER, J. 2003. Systematic functional analysis of the Caenorhabditis elegans genome using RNAi. *Nature,* 421**,** 231-7.
KAMATH, R. S., MARTINEZ-CAMPOS, M., ZIPPERLEN, P., FRASER, A. G. & AHRINGER, J. 2001. Effectiveness of specific RNA-mediated interference through ingested double-stranded RNA in Caenorhabditis elegans. *Genome Biol,* 2**,** RESEARCH0002.
KARP, X. 2018. Working with dauer larvae. *WormBook,* 2018**,** 1-19.
KARPUSHEV, A. V., ILATOVSKAYA, D. V. & STARUSCHENKO, A. 2010. The actin cytoskeleton and small G protein RhoA are not involved in flow-dependent activation of ENaC. *BMC Res Notes,* 3**,** 210.
KASHLAN, O. B. & KLEYMAN, T. R. 2011. ENaC structure and function in the wake of a resolved structure of a family member. *Am J Physiol Renal Physiol,* 301**,** F684-96.
KATOH, K., MISAWA, K., KUMA, K. & MIYATA, T. 2002. MAFFT: a novel method for rapid multiple sequence alignment based on fast Fourier transform. *Nucleic Acids Res,* 30**,** 3059-66.
KATOH, K. & STANDLEY, D. M. 2013. MAFFT multiple sequence alignment software version 7: improvements in performance and usability. *Mol Biol Evol,* 30**,** 772-80.
KATSURA, I., KONDO, K., AMANO, T., ISHIHARA, T. & KAWAKAMI, M. 1994. Isolation, characterization and epistasis of fluoride-resistant mutants of Caenorhabditis elegans. *Genetics,* 136**,** 145-54.
KAUL, T. K., REIS RODRIGUES, P., OGUNGBE, I. V., KAPAHI, P. & GILL, M. S. 2014. Bacterial fatty acids enhance recovery from the dauer larva in Caenorhabditis elegans. *PLoS One,* 9**,** e86979.

KAULICH, E., GRUNDY, L. J., SCHAFER, W. R. & WALKER, D. S. unpublished. Genetic insights into the diverse functions of the DEG/ENaC family.
KELLENBERGER, S., GAUTSCHI, I. & SCHILD, L. 2003. Mutations in the epithelial Na+ channel ENaC outer pore disrupt amiloride block by increasing its dissociation rate. *Mol Pharmacol,* 64**,** 848-56.
KELLENBERGER, S. & SCHILD, L. 2002. Epithelial sodium channel/degenerin family of ion channels: a variety of functions for a shared structure. *Physiol Rev,* 82**,** 735-67.
KENYON, C., CHANG, J., GENSCH, E., RUDNER, A. & TABTIANG, R. 1993. A C-Elegans Mutant That Lives Twice as Long as Wild-Type. *Nature,* 366**,** 461-464.
KERR, R., LEV-RAM, V., BAIRD, G., VINCENT, P., TSIEN, R. Y. & SCHAFER, W. R. 2000. Optical imaging of calcium transients in neurons and pharyngeal muscle of C. elegans. *Neuron,* 26**,** 583-94.
KIM, K., SATO, K., SHIBUYA, M., ZEIGER, D. M., BUTCHER, R. A., RAGAINS, J. R., CLARDY, J., TOUHARA, K. & SENGUPTA, P. 2009a. Two Chemoreceptors Mediate Developmental Effects of Dauer Pheromone in C-elegans. *Science,* 326**,** 994-998.
KIM, K., SATO, K., SHIBUYA, M., ZEIGER, D. M., BUTCHER, R. A., RAGAINS, J. R., CLARDY, J., TOUHARA, K. & SENGUPTA, P. 2009b. Two chemoreceptors mediate developmental effects of dauer pheromone in C. elegans. *Science,* 326**,** 994-8.
KIMURA, K. D., TISSENBAUM, H. A., LIU, Y. & RUVKUN, G. 1997. daf-2, an insulin receptor-like gene that regulates longevity and diapause in Caenorhabditis elegans. *Science,* 277**,** 942-6.
KLASS, M. & HIRSH, D. 1976. Non-ageing developmental variant of Caenorhabditis elegans. *Nature,* 260**,** 523-5.
KLASS, M. R. 1977. Aging in the nematode Caenorhabditis elegans: major biological and environmental factors influencing life span. *Mech Ageing Dev,* 6**,** 413-29.
KREPLE, C. J., LU, Y., TAUGHER, R. J., SCHWAGER-GUTMAN, A. L., DU, J., STUMP, M., WANG, Y., GHOBBEH, A., FAN, R., COSME, C. V., SOWERS, L. P., WELSH, M. J., RADLEY, J. J., LALUMIERE, R. T. & WEMMIE, J. A. 2014. Acid-sensing ion channels contribute to synaptic transmission and inhibit cocaine-evoked plasticity. *Nat Neurosci,* 17**,** 1083-91.
KRISHTAL, O. A. & PIDOPLICHKO, V. I. 1980. A receptor for protons in the nerve cell membrane. *Neuroscience,* 5**,** 2325-7.
KURAKU, S., ZMASEK, C. M., NISHIMURA, O. & KATOH, K. 2013. aLeaves facilitates on-demand exploration of metazoan gene family trees on MAFFT sequence alignment server with enhanced interactivity. *Nucleic Acids Res,* 41**,** W22-8.
KWAN, C. S., VAZQUEZ-MANRIQUE, R. P., LY, S., GOYAL, K. & BAYLIS, H. A. 2008. TRPM channels are required for rhythmicity in the ultradian defecation rhythm of C. elegans. *BMC Physiol,* 8**,** 11.
KWEON, H. J. & SUH, B. C. 2013. Acid-sensing ion channels (ASICs): therapeutic targets for neurological diseases and their regulation. *BMB Rep,* 46**,** 295-304.
LARKIN, M. A., BLACKSHIELDS, G., BROWN, N. P., CHENNA, R., MCGETTIGAN, P. A., MCWILLIAM, H., VALENTIN, F., WALLACE, I. M., WILM, A., LOPEZ, R., THOMPSON, J. D., GIBSON, T. J. & HIGGINS, D. G. 2007. Clustal W and Clustal X version 2.0. *Bioinformatics,* 23**,** 2947-8.
LEE, K. & MYLONAKIS, E. 2017. An Intestine-Derived Neuropeptide Controls Avoidance Behavior in Caenorhabditis elegans. *Cell Rep,* 20**,** 2501-2512.

LETUNIC, I. & BORK, P. 2019. Interactive Tree Of Life (iTOL) v4: recent updates and new developments. *Nucleic Acids Res,* 47**,** W256-W259.
LI, T., YANG, Y. & CANESSA, C. M. 2009. Interaction of the aromatics Tyr-72/Trp-288 in the interface of the extracellular and transmembrane domains is essential for proton gating of acid-sensing ion channels. *J Biol Chem,* 284**,** 4689-94.
LI, W. G., YU, Y., HUANG, C., CAO, H. & XU , T. L. 2011. Nonproton ligand sensing domain is required for paradoxical stimulation of acid-sensing ion channel 3 (ASIC3) channels by amiloride. *J Biol Chem,* 286**,** 42635-42646.
LIN, H. P., MANN, K. J., STAROSTINA, E., KINSER, R. D. & PIKIELNY, C. W. 2005. A Drosophila DEG/ENaC channel subunit is required for male response to female pheromones. *Proceedings of the National Academy of Sciences of the United States of America,* 102**,** 12831-12836.
LINGUEGLIA, E., VOILLEY, N., WALDMANN, R., LAZDUNSKI, M. & BARBRY, P. 1993. Expression cloning of an epithelial amiloride-sensitive Na+ channel. A new channel type with homologies to Caenorhabditis elegans degenerins. *FEBS Lett,* 318**,** 95-9.
LIU, D. W. & THOMAS, J. H. 1994. Regulation of a periodic motor program in C. elegans. *J Neurosci,* 14**,** 1953-62.
LIU, L., LEONARD, A. S., MOTTO, D. G., FELLER, M. A., PRICE, M. P., JOHNSON, W. A. & WELSH, M. J. 2003. Contribution of Drosophila DEG/ENaC genes to salt taste. *Neuron,* 39**,** 133-46.
LIU, T., WANG, Y., TIAN, Y., ZHANG, J., ZHAO, J. & GUO, A. 2018. The receptor channel formed by ppk25, ppk29 and ppk23 can sense the Drosophila female pheromone 7,11-heptacosadiene. *Genes Brain Behav***,** e12529.
LO, C. C. & CHIANG, A. S. 2016. Toward Whole-Body Connectomics. *J Neurosci,* 36**,** 11375-11383.
LOYTYNOJA, A. & GOLDMAN, N. 2010. webPRANK: a phylogeny-aware multiple sequence aligner with interactive alignment browser. *BMC Bioinformatics,* 11**,** 579.
MACOSKO, E. Z., POKALA, N., FEINBERG, E. H., CHALASANI, S. H., BUTCHER, R. A., CLARDY, J. & BARGMANN, C. I. 2009. A hub-and-spoke circuit drives pheromone attraction and social behaviour in C-elegans. *Nature,* 458**,** 1171-U110.
MAK, H. Y. & RUVKUN, G. 2004. Intercellular signaling of reproductive development by the C. elegans DAF-9 cytochrome P450. *Development,* 131**,** 1777-86.
MARGIE, O., PALMER, C. & CHIN-SANG, I. 2013. C. elegans Chemotaxis Assay. *Jove-Journal of Visualized Experiments*.
MARIOL, M. C., WALTER, L., BELLEMIN, S. & GIESELER, K. 2013. A rapid protocol for integrating extrachromosomal arrays with high transmission rate into the C. elegans genome. *J Vis Exp***,** e50773.
MATHEW, N. D., MATHEW, M. D. & SURAWSKI, P. P. 2014. Nanoparticle imaging and diagnostic of Caenorhabditis elegans intracellular pH. *Anal Biochem,* 450**,** 52-6.
MATTHEWMAN, C., MILLER-FLEMING, T. W., MILLER, D. M. R. & BIANCHI, L. 2016. Ca2+ permeability and Na+ conductance in cellular toxicity caused by hyperactive DEG/ENaC channels. *Am J Physiol Cell Physiol,* 311**,** C920-C930.
MCINTIRE, S. L., JORGENSEN, E., KAPLAN, J. & HORVITZ, H. R. 1993. The GABAergic nervous system of Caenorhabditis elegans. *Nature,* 364**,** 337-41.
MELLO, C. & FIRE, A. 1995. DNA transformation. *Methods Cell Biol,* 48**,** 451-82.

MELLO, C. C., KRAMER, J. M., STINCHCOMB, D. & AMBROS, V. 1991. Efficient gene transfer in C.elegans: extrachromosomal maintenance and integration of transforming sequences. *EMBO J,* 10**,** 3959-70.

MIESENBOCK, G., DE ANGELIS, D. A. & ROTHMAN, J. E. 1998. Visualizing secretion and synaptic transmission with pH-sensitive green fluorescent proteins. *Nature,* 394**,** 192-5.

MILLER-FLEMING, T. W., PETERSEN, S. C., MANNING, L., MATTHEWMAN, C., GORNET, M., BEERS, A., HORI, S., MITANI, S., BIANCHI, L., RICHMOND, J. & MILLER, D. M. 2016. The DEG/ENaC cation channel protein UNC-8 drives activity-dependent synapse removal in remodeling GABAergic neurons. *Elife,* 5.

MIYAWAKI, A., GRIESBECK, O., HEIM, R. & TSIEN, R. Y. 1999. Dynamic and quantitative Ca2+ measurements using improved cameleons. *Proc Natl Acad Sci U S A,* 96**,** 2135-40.

MOLECULARDEVICES 2012. The Axon Guide: Electrophysiology and Biophysics Laboratory Techniques. . p.72.

MOORE, R. Y. & EICHLER, V. B. 1972. Loss of a circadian adrenal corticosterone rhythm following suprachiasmatic lesions in the rat. *Brain Res,* 42**,** 201-6.

MORITA, K., CHOW, K. L. & UENO, N. 1999. Regulation of body length and male tail ray pattern formation of Caenorhabditis elegans by a member of TGF-beta family. *Development,* 126**,** 1337-47.

NAKAI, J., OHKURA, M. & IMOTO, K. 2001. A high signal-to-noise Ca(2+) probe composed of a single green fluorescent protein. *Nat Biotechnol,* 19**,** 137-41.

NASH, B., COLAVITA, A., ZHENG, H., ROY, P. J. & CULOTTI, J., G. 2000. The forkhead transcription factor UNC-130 is required for the graded spatial expression of the UNC-129 TGF-beta guidance factor in C. elegans. *Genes Dev,* 14**,** 2486-2500.

NEHRKE, K. 2003. A reduction in intestinal cell pHi due to loss of the Caenorhabditis elegans Na+/H+ exchanger NHX-2 increases life span. *J Biol Chem,* 278**,** 44657-66.

NEHRKE, K. & MELVIN, J. E. 2002. The NHX family of Na+-H+ exchangers in Caenorhabditis elegans. *J Biol Chem,* 277**,** 29036-44.

NGUYEN, J. P., SHIPLEY, F. B., LINDER, A. N., PLUMMER, G. S., LIU, M., SETRU, S. U., SHAEVITZ, J. W. & LEIFER, A. M. 2016. Whole-brain calcium imaging with cellular resolution in freely behaving Caenorhabditis elegans. *Proc Natl Acad Sci U S A,* 113**,** E1074-81.

NICHOLS, A. L. A., EICHLER, T., LATHAM, R. & ZIMMER, M. 2017. A global brain state underlies C. elegans sleep behavior. *Science,* 356.

NOLAN, K. M., SARAFI-REINACH, T. R., HORNE, J. G., SAFFER, A. M. & SENGUPTA, P. 2002. The DAF-7 TGF-beta signaling pathway regulates chemosensory receptor gene expression in C-elegans. *Genes & Development,* 16**,** 3061-3073.

O'BRODOVICH, H., CANESSA, C., UEDA, J., RAFII, B., ROSSIER, B. C. & EDELSON, J. 1993. Expression of the epithelial Na+ channel in the developing rat lung. *Am J Physiol,* 265**,** C491-6.

ORTEGA-RAMIREZ, A., VEGA, R. & SOTO, E. 2017. Acid-Sensing Ion Channels as Potential Therapeutic Targets in Neurodegeneration and Neuroinflammation. *Mediators Inflamm,* 2017**,** 3728096.

PALMER, L. G. & ANDERSEN, O. S. 1989. Interactions of amiloride and small monovalent cations with the epithelial sodium channel. Inferences about the nature of the channel pore. *Biophys J,* 55**,** 779-87.
PALMER, L. G. & FRINDT, G. 1986. Amiloride-sensitive Na channels from the apical membrane of the rat cortical collecting tubule. *Proc Natl Acad Sci U S A,* 83**,** 2767-70.
PARK, D., ESTEVEZ, A. & RIDDLE, D. L. 2010. Antagonistic Smad transcription factors control the dauer/non-dauer switch in C. elegans. *Development,* 137**,** 477-85.
PARK, E. C. & HORVITZ, H. R. 1986. C. elegans unc-105 mutations affect muscle and are suppressed by other mutations that affect muscle. *Genetics,* 113**,** 853-67.
PATTISON, L. A., CALLEJO, G. & ST JOHN SMITH, E. 2019. Evolution of acid nociception: ion channels and receptors for detecting acid. *Philos Trans R Soc Lond B Biol Sci,* 374**,** 20190291.
PAUKERT, M., BABINI, E., PUSCH, M. & GRUNDER, S. 2004. Identification of the Ca2+ blocking site of acid-sensing ion channel (ASIC) 1: implications for channel gating. *J Gen Physiol,* 124**,** 383-94.
PAUKERT, M., CHEN, X., POLLEICHTNER, G., SCHINDELIN, H. & GRUNDER, S. 2008. Candidate amino acids involved in H+ gating of acid-sensing ion channel 1a. *J Biol Chem,* 283**,** 572-81.
PFEIFFER, J., JOHNSON, D. & NEHRKE, K. 2008. Oscillatory transepithelial H(+) flux regulates a rhythmic behavior in C. elegans. *Curr Biol,* 18**,** 297-302.
QADRI, Y. J., SONG, Y., FULLER, C. M. & BENOS, D. J. 2010. Amiloride docking to acid-sensing ion channel-1. *J Biol Chem,* 285**,** 9627-35.
RABINOWITCH, I., CHATZIGEORGIOU, M. & SCHAFER, W. R. 2013. A gap junction circuit enhances processing of coincident mechanosensory inputs. *Curr Biol,* 23**,** 963-7.
RABINOWITCH, I., CHATZIGEORGIOU, M., ZHAO, B., TREININ, M. & SCHAFER, W. R. 2014. Rewiring neural circuits by the insertion of ectopic electrical synapses in transgenic C. elegans. *Nat Commun,* 5**,** 4442.
RABINOWITCH, I. & SCHAFER, W. R. 2015. Engineering new synaptic connections in the C. elegans connectome. *Worm,* 4**,** e992668.
RAMBAUT, A. 2010. FigTree v1.3.1. . *Institute of Evolutionary Biology, University of Edinburgh, Edinburgh.* http://tree.bio.ed.ac.uk/software/figtree/.
RAVI, B., GARCIA, J. & COLLINS, K. 2019. The HSN egg-laying command neurons regulate the defecation motor program in Caenorhabditis elegans: Integration. *MicroPubl Biol,* 2019.
REINER, D. J., WEINSHENKER, D. & THOMAS, J. H. 1995. Analysis of dominant mutations affecting muscle excitation in Caenorhabditis elegans. *Genetics,* 141**,** 961-76.
REN, P., LIM, C. S., JOHNSEN, R., ALBERT, P. S., PILGRIM, D. & RIDDLE, D. L. 1996. Control of C. elegans larval development by neuronal expression of a TGF-beta homolog. *Science,* 274**,** 1389-91.
RHOADES, J. L., NELSON, J. C., NWABUDIKE, I., YU, S. K., MCLACHLAN, I. G., MADAN, G. K., ABEBE, E., POWERS, J. R., COLON-RAMOS, D. A. & FLAVELL, S. W. 2019. ASICs Mediate Food Responses in an Enteric Serotonergic Neuron that Controls Foraging Behaviors. *Cell,* 176**,** 85-97 e14.

RICHARDSON, C. E., YEE, C. & SHEN, K. 2019. A hormone receptor pathway cell-autonomously delays neuron morphological aging by suppressing endocytosis. *PLoS Biol,* 17**,** e3000452.
RIDDLE, D. L. & ALBERT, P. S. 1997. Genetic and Environmental Regulation of Dauer Larva Development. *In:* ND, RIDDLE, D. L., BLUMENTHAL, T., MEYER, B. J. & PRIESS, J. R. (eds.) *C. elegans II.* Cold Spring Harbor (NY).
RIDDLE, D. L., SWANSON, M. M. & ALBERT, P. S. 1981. Interacting genes in nematode dauer larva formation. *Nature,* 290**,** 668-71.
RIEMANN, A., IHLING, A., THOMAS, J., SCHNEIDER, B., THEWS, O. & GEKLE, M. 2015. Acidic environment activates inflammatory programs in fibroblasts via a cAMP-MAPK pathway. *Biochim Biophys Acta,* 1853**,** 299-307.
ROLLINS, J. A., HOWARD, A. C., DOBBINS, S. K., WASHBURN, E. H. & ROGERS, A. N. 2017. Assessing Health Span in Caenorhabditis elegans: Lessons From Short-Lived Mutants. *J Gerontol A Biol Sci Med Sci,* 72**,** 473-480.
RUFFIN, V. A., SALAMEH, A. I., BORON, W. F. & PARKER, M. D. 2014. Intracellular pH regulation by acid-base transporters in mammalian neurons. *Front Physiol,* 5**,** 43.
RYU, L., CHEON, Y., HUH, Y. H., PYO, S., CHINTA, S., CHOI, H., BUTCHER, R. A. & KIM, K. 2018. Feeding state regulates pheromone-mediated avoidance behavior via the insulin signaling pathway in Caenorhabditis elegans. *EMBO J*.
SAEKI, S., YAMAMOTO, M. & IINO, Y. 2001. Plasticity of chemotaxis revealed by paired presentation of a chemoattractant and starvation in the nematode Caenorhabditis elegans. *J Exp Biol,* 204**,** 1757-64.
SATLIN, L. M., SHENG, S., WODA, C. B. & KLEYMAN, T. R. 2001. Epithelial Na(+) channels are regulated by flow. *Am J Physiol Renal Physiol,* 280**,** F1010-8.
SCHACKWITZ, W. S., INOUE, T. & THOMAS, J. H. 1996. Chemosensory neurons function in parallel to mediate a pheromone response in C. elegans. *Neuron,* 17**,** 719-28.
SCHAFER, W. F. 2006. Genetics of egg-laying in worms. *Annu Rev Genet,* 40**,** 487-509.
SCHEFFER, L. K., XU, C. S., JANUSZEWSKI, M., LU, Z., TAKEMURA, S. Y., HAYWORTH, K. J., HUANG, G. B., SHINOMIYA, K., MAITLIN-SHEPARD, J., BERG, S., CLEMENTS, J., HUBBARD, P. M., KATZ, W. T., UMAYAM, L., ZHAO, T., ACKERMAN, D., BLAKELY, T., BOGOVIC, J., DOLAFI, T., KAINMUELLER, D., KAWASE, T., KHAIRY, K. A., LEAVITT, L., LI, P. H., LINDSEY, L., NEUBARTH, N., OLBRIS, D. J., OTSUNA, H., TRAUTMAN, E. T., ITO, M., BATES, A. S., GOLDAMMER, J., WOLFF, T., SVIRSKAS, R., SCHLEGEL, P., NEACE, E., KNECHT, C. J., ALVARADO, C. X., BAILEY, D. A., BALLINGER, S., BORYCZ, J. A., CANINO, B. S., CHEATHAM, N., COOK, M., DREHER, M., DUCLOS, O., EUBANKS, B., FAIRBANKS, K., FINLEY, S., FORKNALL, N., FRANCIS, A., HOPKINS, G. P., JOYCE, E. M., KIM, S., KIRK, N. A., KOVALYAK, J., LAUCHIE, S. A., LOHFF, A., MALDONADO, C., MANLEY, E. A., MCLIN, S., MOONEY, C., NDAMA, M., OGUNDEYI, O., OKEOMA, N., ORDISH, C., PADILLA, N., PATRICK, C. M., PATERSON, T., PHILLIPS, E. E., PHILLIPS, E. M., RAMPALLY, N., RIBEIRO, C., ROBERTSON, M. K., RYMER, J. T., RYAN, S. M., SAMMONS, M., SCOTT, A. K., SCOTT, A. L., SHINOMIYA, A., SMITH, C., SMITH, K., SMITH, N. L., SOBESKI, M. A., SULEIMAN, A., SWIFT, J., TAKEMURA, S., TALEBI, I., TARNOGORSKA, D., TENSHAW, E., TOKHI, T., WALSH, J. J., YANG, T., HORNE, J. A., LI, F., PAREKH, R., RIVLIN, P. K., JAYARAMAN, V., COSTA,

M., JEFFERIS, G. S., et al. 2020. A connectome and analysis of the adult Drosophila central brain. *Elife,* 9.
SCHILD, L., SCHNEEBERGER, E., GAUTSCHI, I. & FIRSOV, D. 1997. Identification of amino acid residues in the alpha, beta, and gamma subunits of the epithelial sodium channel (ENaC) involved in amiloride block and ion permeation. *J Gen Physiol,* 109**,** 15-26.
SCHMIDT, A., BAUKNECHT, P., WILLIAMS, E. A., AUGUSTINOWSKI, K., GRÜNDER, S. & JÉKELY, G. 2018. Dual signaling of Wamide myoinhibitory peptides through a peptide-gated channel and a GPCR in Platynereis. *The FASEB Journal***,** 5338-5349.
SCHROEDER, N. E., ANDROWSKI, R. J., RASHID, A., LEE, H., LEE, J. & BARR, M. M. 2013. Dauer-specific dendrite arborization in C. elegans is regulated by KPC-1/Furin. *Curr Biol,* 23**,** 1527-35.
SCHULTZ, R. D. & GUMIENNY, T. L. 2012. Visualization of Caenorhabditis elegans cuticular structures using the lipophilic vital dye DiI. *J Vis Exp***,** e3362.
SELA, I., ASHKENAZY, H., KATOH, K. & PUPKO, T. 2015. GUIDANCE2: accurate detection of unreliable alignment regions accounting for the uncertainty of multiple parameters. *Nucleic Acids Res,* 43**,** W7-14.
SHAIKH, S. A. & TAJKHORSHID, E. 2008. Potential cation and H+ binding sites in acid sensing ion channel-1. *Biophys J,* 95**,** 5153-64.
SHANNON, P., MARKIEL, A., OZIER, O., BALIGA, N. S., WANG, J. T., RAMAGE, D., AMIN, N., SCHWIKOWSKI, B. & IDEKER, T. 2003. Cytoscape: a software environment for integrated models of biomolecular interaction networks. *Genome Res,* 13**,** 2498-504.
SHAW, W. M., LUO, S., LANDIS, J., ASHRAF, J. & MURPHY, C. T. 2007. The C. elegans TGF-beta Dauer pathway regulates longevity via insulin signaling. *Curr Biol,* 17**,** 1635-45.
SHERMAN, T., CHERNOVA, M. N., CLARK, J. S., JIANG, L., ALPER, S. L. & NEHRKE, K. 2005. The abts and sulp families of anion transporters from Caenorhabditis elegans. *Am J Physiol Cell Physiol,* 289**,** C341-51.
SHERWOOD, T. W., LEE, K. G., GORMLEY, M. G. & ASKWITH, C. C. 2011. Heteromeric acid-sensing ion channels (ASICs) composed of ASIC2b and ASIC1a display novel channel properties and contribute to acidosis-induced neuronal death. *J Neurosci,* 31**,** 9723-34.
SHI, S., LUKE, C. J., MIEDEL, M. T., SILVERMAN, G. A. & KLEYMAN, T. R. 2016. Activation of the Caenorhabditis elegans Degenerin Channel by Shear Stress Requires the MEC-10 Subunit. *J Biol Chem,* 291**,** 14012-22.
SHIMIZU, K., ASHIDA, K., HOTTA, K. & OKA, K. 2019. Food deprivation changes chemotaxis behavior in Caenorhabditis elegans. *Biophys Physicobiol,* 16**,** 167-172.
SHREFFLER, W., MAGARDINO, T., SHEKDAR, K. & WOLINSKY, E. 1995. The unc-8 and sup-40 genes regulate ion channel function in Caenorhabditis elegans motorneurons. *Genetics,* 139**,** 1261-72.
SMITH, C. J., WATSON, J. D., SPENCER, W. C., O'BRIEN, T., CHA, B., ALBEG, A., TREININ, M. & MILLER, D. M., 3RD 2010. Time-lapse imaging and cell-specific expression profiling reveal dynamic branching and molecular determinants of a multi-dendritic nociceptor in C. elegans. *Dev Biol,* 345**,** 18-33.
SOTO, E., ORTEGA-RAMIREZ, A. & VEGA, R. 2018. Protons as Messengers of Intercellular Communication in the Nervous System. *Frontiers in Cellular Neuroscience,* 12.

SPECTOR, A. C., GUAGLIARDO, N. A. & ST JOHN, S. J. 1996. Amiloride disrupts NaCl versus KCl discrimination performance: implications for salt taste coding in rats. *J Neurosci,* 16**,** 8115-22.
STEPHAN, F. K. & ZUCKER, I. 1972a. Circadian rhythms in drinking behavior and locomotor activity of rats are eliminated by hypothalamic lesions. *Proc Natl Acad Sci U S A,* 69**,** 1583-6.
STEPHAN, F. K. & ZUCKER, I. 1972b. Rat drinking rhythms: central visual pathways and endocrine factors mediating responsiveness to environmental illumination. *Physiol Behav,* 8**,** 315-26.
STINCHCOMB, D. T., SHAW, J. E., CARR, S. H. & HIRSH, D. 1985. Extrachromosomal DNA transformation of Caenorhabditis elegans. *Mol Cell Biol,* 5**,** 3484-96.
SÜDHOF, T. C. 2017. Molecular Neuroscience in the 21(st) Century: A Personal Perspective. *Neuron,* 96**,** 536-541.
SULSTON, J. E. & HORVITZ, H. R. 1977. Post-embryonic cell lineages of the nematode, Caenorhabditis elegans. *Dev Biol,* 56**,** 110-56.
SULSTON, J. E., SCHIERENBERG, E., WHITE, J. G. & THOMSON, J. N. 1983. The embryonic cell lineage of the nematode Caenorhabditis elegans. *Dev Biol,* 100**,** 64-119.
SUTHERLAND, S. P., BENSON, C. J., ADELMAN, J. P. & MCCLESKEY, E. W. 2001. Acid-sensing ion channel 3 matches the acid-gated current in cardiac ischemia-sensing neurons. *Proc Natl Acad Sci U S A,* 98**,** 711-6.
SUZUKI, H., KERR, R., BIANCHI, L., FROKJAER-JENSEN, C., SLONE, D., XUE, J., GERSTBREIN, B., DRISCOLL, M. & SCHAFER, W. R. 2003. In vivo imaging of C. elegans mechanosensory neurons demonstrates a specific role for the MEC-4 channel in the process of gentle touch sensation. *Neuron,* 39**,** 1005-17.
SUZUKI, Y., YANDELL, M. D., ROY, P. J., KRISHNA, S., SAVAGE-DUNN, C., ROSS, R., M.,, PADGETT, R. W. & WOOD, W. B. 1999. A BMP homolog acts as a dose-dependent regulator of body size and male tail patterning in Caenorhabditis elegans. *Development,* 126**,** 241-250.
TAKAGAKI, N., OHTA, A., OHNISHI, K., KAWANABE, A., MINAKUCHI, Y., TOYODA, A., FUJIWARA, Y. & KUHARA, A. 2020. The mechanoreceptor DEG-1 regulates cold tolerance in Caenorhabditis elegans. *EMBO Rep,* 21**,** e48671.
TAKE-UCHI, M., KAWAKAMI, M., ISHIHARA, T., AMANO, T., KONDO, K. & KATSURA, I. 1998. An ion channel of the degenerin/epithelial sodium channel superfamily controls the defecation rhythm in Caenorhabditis elegans. *Proc Natl Acad Sci U S A,* 95**,** 11775-80.
TAN, G., MUFFATO, M., LEDERGERBER, C., HERRERO, J., GOLDMAN, N., GIL, M. & DESSIMOZ, C. 2015. Current Methods for Automated Filtering of Multiple Sequence Alignments Frequently Worsen Single-Gene Phylogenetic Inference. *Syst Biol,* 64**,** 778-91.
TANG, Y. Q., LEE, S. A., RAHMAN, M., VANAPALLI, S. A., LU, H. & SCHAFER, W. R. 2020. Ankyrin Is An Intracellular Tether for TMC Mechanotransduction Channels. *Neuron,* 107**,** 112-125 e10.
TAO, L., PORTO, D., LI, Z., FECHNER, S., LEE, S. A., GOODMAN, M. B., XU, X. Z. S., LU, H. & SHEN, K. 2019. Parallel Processing of Two Mechanosensory Modalities by a Single Neuron in C. elegans. *Dev Cell,* 51**,** 617-631 e3.
TAVERNARAKIS, N., SHREFFLER, W., WANG, S. & DRISCOLL, M. 1997. unc-8, a DEG/ENaC family member, encodes a subunit of a candidate mechanically gated channel that modulates C. elegans locomotion. *Neuron,* 18**,** 107-19.

TAYLOR, S. R., SANTPERE, G., WEINREB, A., BARRETT, A., REILLY, M. B., XU, C., VAROL, E., OIKONOMOU, P., GLENWINKEL, L., MCWHIRTER, R., POFF, A., BASAVARAJU, M., RAFI, I., YEMINI, E., COOK, S. J., ABRAMS, A., VIDAL, B., CROS, C., TAVAZOIE, S., SESTAN, N., HAMMARLUND, M., HOBERT, O. & MILLER, D. M. 2020. Molecular topography of an entire nervous system. *Bioarchive*.

TEIWES, J. & TOTO, R. D. 2007. Epithelial sodium channel inhibition in cardiovascular disease. A potential role for amiloride. *Am J Hypertens,* 20**,** 109-17.

THELLIN, O., ZORZI, W., LAKAYE, B., DE BORMAN, B., COUMANS, B., HENNEN, G., GRISAR, T., IGOUT, A. & HEINEN, E. 1999. Housekeeping genes as internal standards: use and limits. *Biotechnol,* 75**,** 291-295.

THOMAS, J. H. 1990. Genetic analysis of defecation in Caenorhabditis elegans. *Genetics,* 124**,** 855-72.

THOMAS, J. H., BIRNBY, D. A. & VOWELS, J. J. 1993. Evidence for Parallel Processing of Sensory Information Controlling Dauer Formation in Caenorhabditis Elegans. *Genetics,* 134**,** 1105–1117.

TONG, Y. G. & BURGLIN, T. R. 2010. Conditions for dye-filling of sensory neurons in Caenorhabditis elegans. *J Neurosci Methods,* 188**,** 58-61.

TONG ZHOU, G., SCHAFER, W. R., SCHAFER, R. W. 1998. A three-state biological point process model and its parameter estimation. *IEEE Transactions on Signal Processing,* 46**,** 2698-2707.

TRENT, C., TSUING, N. & HORVITZ, H. R. 1983. Egg-laying defective mutants of the nematode Caenorhabditis elegans. *Genetics,* 104**,** 619-47.

UCHITEL, O. D., GONZALEZ INCHAUSPE, C. & WEISSMANN, C. 2019. Synaptic signals mediated by protons and acid-sensing ion channels. *Synapse,* 73**,** e22120.

UPPALURI, S. & BRANGWYNNE, C. P. 2015. A size threshold governs Caenorhabditis elegans developmental progression. *Proc Biol Sci,* 282**,** 20151283.

VAN BEMMELEN, M. X., HUSER, D., GAUTSCHI, I. & SCHILD, L. 2015. The Human Acid-Sensing Ion Channel ASIC1a: Evidence for a Homotetrameric Assembly State at the Cell Surface. *PLoS One,* 10**,** e0135191.

VIDAL-GADEA, A. G., DAVIS, S., BECKER, L. & PIERCE-SHIMOMURA, J. T. 2012. Coordination of behavioral hierarchies during environmental transitions in Caenorhabditis elegans. *Worm,* 1**,** 5-11.

VINA, E., PARISI, V., CABO, R., LAURA, R., LOPEZ-VELASCO, S., LOPEZ-MUNIZ, A., GARCIA-SUAREZ, O., GERMANA, A. & VEGA, J. A. 2013. Acid-sensing ion channels (ASICs) in the taste buds of adult zebrafish. *Neurosci Lett,* 536**,** 35-40.

VOGLIS, G. & TAVERNARAKIS, N. 2008. A synaptic DEG/ENaC ion channel mediates learning in C. elegans by facilitating dopamine signalling. *EMBO J,* 27**,** 3288-99.

VOILLEY, N. 2004. Acid-sensing ion channels (ASICs): new targets for the analgesic effects of non-steroid anti-inflammatory drugs (NSAIDs). *Curr Drug Targets Inflamm Allergy,* 3**,** 71-9.

VOILLEY, N., DE WEILLE, J., MAMET, J. & LAZDUNSKI, M. 2001. Nonsteroid Anti-Inflammatory Drugs Inhibit Both the Activity and the Inflammation-Induced Expression of Acid-Sensing Ion Channels in Nociceptors. *J Neurosci,* 21**,** 8026–8033.

VOWELS, J. J. & THOMAS, J. H. 1992. Genetic analysis of chemosensory control of dauer formation in Caenorhabditis elegans. *Genetics,* 130**,** 105-23.
VULLO, S. & KELLENBERGER, S. 2020. A molecular view of the function and pharmacology of acid-sensing ion channels. *Pharmacol Res,* 154**,** 104166.
VYVERS, A., SCHMIDT, A., WIEMUTH, D. & GRUNDER, S. 2018. Screening of 109 neuropeptides on ASICs reveals no direct agonists and dynorphin A, YFMRFamide and endomorphin-1 as modulators. *Sci Rep,* 8**,** 18000.
WAGGONER, L. E., ZHOU, G. T., SCHAFER, R. W. & SCHAFER, W. R. 1998. Control of alternative behavioral states by serotonin in Caenorhabditis elegans. *Neuron,* 21**,** 203-14.
WAGNER, J., ALLMAN, E., TAYLOR, A., ULMSCHNEIDER, K., KOVANDA, T., ULMSCHNEIDER, B., NEHRKE, K. & PETERS, M. A. 2011. A calcineurin homologous protein is required for sodium-proton exchange events in the C. elegans intestine. *Am J Physiol Cell Physiol,* 301**,** C1389-403.
WAKABAYASHI, T., KIMURA, Y., OHBA, Y., ADACHI, R., SATOH, Y. & SHINGAI, R. 2009. In vivo calcium imaging of OFF-responding ASK chemosensory neurons in C. elegans. *Biochimica Et Biophysica Acta-General Subjects,* 1790**,** 765-769.
WALDMANN, R., CHAMPIGNY, G., BASSILANA, F., HEURTEAUX, C. & LAZDUNSKI, M. 1997. A proton-gated cation channel involved in acid-sensing. *Nature,* 386**,** 173-177.
WALDMANN, R., CHAMPIGNY, G., VOILLEY, N., LAURITZEN, I. & LAZDUNSKI, M. 1996. The mammalian degenerin MDEG, an amiloride-sensitive cation channel activated by mutations causing neurodegeneration in Caenorhabditis elegans. *J Biol Chem,* 271**,** 10433-6.
WALKER, D. S., GOWER, N. J., LY, S., BRADLEY, G. L. & BAYLIS, H. A. 2002. Regulated disruption of inositol 1,4,5-trisphosphate signaling in Caenorhabditis elegans reveals new functions in feeding and embryogenesis. *Mol Biol Cell,* 13**,** 1329-37.
WALKER, D. S. & SCHAFER, W. R. 2020. Distinct roles for innexin gap junctions and hemichannels in mechanosensation. *Elife,* 9.
WANG, H., GIRSKIS, K., JANSSEN, T., CHAN, J. P., DASGUPTA, K., KNOWLES, J. A., SCHOOFS, L. & SIEBURTH, D. 2013a. Neuropeptide secreted from a pacemaker activates neurons to control a rhythmic behavior. *Curr Biol,* 23**,** 746-54.
WANG, J., KALETSKY, R., SILVA, M., WILLIAMS, A., HAAS, L. A., ANDROWSKI, R. J., LANDIS, J. N., PATRICK, C., RASHID, A., SANTIAGO-MARTINEZ, D., GRAVATO-NOBRE, M., HODGKIN, J., HALL, D. H., MURPHY, C. T. & BARR, M. M. 2015. Cell-Specific Transcriptional Profiling of Ciliated Sensory Neurons Reveals Regulators of Behavior and Extracellular Vesicle Biogenesis. *Curr Biol,* 25**,** 3232-8.
WANG, J., TOKARZ, R. & SAVAGE-DUNN, C. 2002. The expression of TGFbeta signal transducers in the hypodermis regulates body size in C. elegans. *Development,* 129**,** 4989-98.
WANG, X., LI, W. G., YU, Y., XIAO, X., CHENG, J., ZENG, W. Z., PENG, Z., XI ZHU, M. & XU, T. L. 2013b. Serotonin facilitates peripheral pain sensitivity in a manner that depends on the nonproton ligand sensing domain of ASIC3 channel. *J Neurosci,* 33**,** 4265-79.
WANG, Y., APICELLA, A., JR., LEE, S. K., EZCURRA, M., SLONE, R. D., GOLDMIT, M., SCHAFER, W. R., SHAHAM, S., DRISCOLL, M. & BIANCHI, L. 2008. A

glial DEG/ENaC channel functions with neuronal channel DEG-1 to mediate specific sensory functions in C. elegans. *EMBO J,* 27**,** 2388-99.
WANG, Y., D'URSO, G. & BIANCHI, L. 2012. Knockout of glial channel ACD-1 exacerbates sensory deficits in a C. elegans mutant by regulating calcium levels of sensory neurons. *J Neurophysiol,* 107**,** 148-58.
WANG, Y., MATTHEWMAN, C., HAN, L., MILLER, T., MILLER, D. M., 3RD & BIANCHI, L. 2013c. Neurotoxic unc-8 mutants encode constitutively active DEG/ENaC channels that are blocked by divalent cations. *J Gen Physiol,* 142**,** 157-69.
WARD, S., THOMSON, N., WHITE, J. G. & BRENNER, S. 1975. Electron microscopical reconstruction of the anterior sensory anatomy of the nematode Caenorhabditis elegans.?2UU. *J Comp Neurol,* 160**,** 313-37.
WARE, R. W., CLARK, D., CROSSLAND, K. & RUSSELL, R. L. 1975. Nerve Ring of Nematode Caenorhabditis-Elegans - Sensory Input and Motor Output. *Journal of Comparative Neurology,* 162**,** 71-110.
WEMMIE, J. A., ASKWITH, C. C., LAMANI, E., CASSELL, M. D., FREEMAN, J. H., JR. & WELSH, M. J. 2003. Acid-sensing ion channel 1 is localized in brain regions with high synaptic density and contributes to fear conditioning. *J Neurosci,* 23**,** 5496-502.
WEMMIE, J. A., CHEN, J., ASKWITH, C. C., HRUSKA-HAGEMAN, A. M., PRICE, M. P., NOLAN, B. C., YODER, P. G., LAMANI, E., HOSHI, T., FREEMAN, J. H., JR. & WELSH, M. J. 2002. The acid-activated ion channel ASIC contributes to synaptic plasticity, learning, and memory. *Neuron,* 34**,** 463-77.
WHITE, J. G., SOUTHGATE, E., THOMSON, J. N. & BRENNER, S. 1976. The structure of the ventral nerve cord of Caenorhabditis elegans. *Philos Trans R Soc Lond B Biol Sci,* 275**,** 327-48.
WHITE, J. G., SOUTHGATE, E., THOMSON, J. N. & BRENNER, S. 1986. The structure of the nervous system of the nematode Caenorhabditis elegans. *Philos Trans R Soc Lond B Biol Sci,* 314**,** 1-340.
WIEMUTH, D., ASSMANN, M. & GRUNDER, S. 2014. The bile acid-sensitive ion channel (BASIC), the ignored cousin of ASICs and ENaC. *Channels (Austin),* 8**,** 29-34.
WIEMUTH, D. & GRUNDER, S. 2010. A single amino acid tunes Ca2+ inhibition of brain liver intestine Na+ channel (BLINaC). *J Biol Chem,* 285**,** 30404-10.
WOLKOW, C. A. & HALL, D. H. 2015. DIntroFIG 1: C. elegans life cycle with dauer branch, Overview. *Wormatlas*.
WU, P. Y., HUANG, Y. Y., CHEN, C. C., HSU, T. T., LIN, Y. C., WENG, J. Y., CHIEN, T. C., CHENG, I. H. & LIEN, C. C. 2013. Acid-sensing ion channel-1a is not required for normal hippocampal LTP and spatial memory. *J Neurosci,* 33**,** 1828-32.
XIE, J., PRICE, M. P., WEMMIE, J. A., ASKWITH, C. C. & WELSH, M. J. 2003. ASIC3 and ASIC1 mediate FMRFamide-related peptide enhancement of H+-gated currents in cultured dorsal root ganglion neurons. *J Neurophysiol,* 89**,** 2459-65.
XIONG, Z. G., PIGNATARO, G., LI, M., CHANG, S. Y. & SIMON, R. P. 2008. Acid-sensing ion channels (ASICs) as pharmacological targets for neurodegenerative diseases. *Curr Opin Pharmacol,* 8**,** 25-32.
XIONG, Z. G., ZHU, X. M., CHU, X. P., MINAMI, M., HEY, J., WEI, W. L., MACDONALD, J. F., WEMMIE, J. A., PRICE, M. P., WELSH, M. J. & SIMON, R. P. 2004. Neuroprotection in ischemia: blocking calcium-permeable acid-sensing ion channels. *Cell,* 118**,** 687-98.

YAGI, J., WENK, H. N., NAVES, L. A. & MCCLESKEY, E. W. 2006. Sustained Currents Through ASIC3 Ion Channels at the Modest pH Changes That Occur During Myocardial Ischemia. *Circ Res,* 99**,** 501-509.
YANG, L. & PALMER, L. G. 2014. Ion conduction and selectivity in acid-sensing ion channel 1. *J Gen Physiol,* 144**,** 245-55.
YEMINI, E., JUCIKAS, T., GRUNDY, L. J., BROWN, A. E. & SCHAFER, W. R. 2013. A database of Caenorhabditis elegans behavioral phenotypes. *Nat Methods,* 10**,** 877-9.
YOUNGER, M. A., MULLER, M., TONG, A., PYM, E. C. & DAVIS, G. W. 2013. A presynaptic ENaC channel drives homeostatic plasticity. *Neuron,* 79**,** 1183-96.
YU, Y., CHEN, Z., LI, W. G., CAO, H., FENG, E. G., YU, F., LIU, H., JIANG, H. & XU, T. L. 2010. A nonproton ligand sensor in the acid-sensing ion channel. *Neuron,* 68**,** 61-72.
ZALLOT, R., OBERG, N. & GERLT, J. A. 2019. The EFI Web Resource for Genomic Enzymology Tools: Leveraging Protein, Genome, and Metagenome Databases to Discover Novel Enzymes and Metabolic Pathways. *Biochemistry,* 58**,** 4169-4182.
ZALLOT, R., OBERG, N. O. & GERLT, J. A. 2018. 'Democratized' genomic enzymology web tools for functional assignment. *Curr Opin Chem Biol,* 47**,** 77-85.
ZANIN, E., DUMONT, J., GASSMANN, R., CHEESEMAN, I., MADDOX, P., BAHMANYAR, S., CARVALHO, A., NIESSEN, S., YATES, J. R., 3RD, OEGEMA, K. & DESAI, A. 2011. Affinity purification of protein complexes in C. elegans. *Methods Cell Biol,* 106**,** 289-322.
ZENG, W. Z., LIU, D. S., LIU, L., SHE, L., WU, L. J. & XU, T. L. 2015. Activation of acid-sensing ion channels by localized proton transient reveals their role in proton signaling. *Sci Rep,* 5**,** 14125.
ZHANG, P. & CANESSA, C. M. 2002. Single channel properties of rat acid-sensitive ion channel-1alpha, -2a, and -3 expressed in Xenopus oocytes. *J Gen Physiol,* 120**,** 553-66.
ZHANG, X., NOGUEZ, J. H., ZHOU, Y. & BUTCHER, R. A. 2013. Analysis of ascarosides from Caenorhabditis elegans using mass spectrometry and NMR spectroscopy. *Methods Mol Biol***,** 71-92.
ZHAO, B. & SCHAFER, W. R. 2013. Neuropeptide signaling: from the gut. *Curr Biol,* 23**,** R481-3.
ZHENG, Z., LAURITZEN, J. S., PERLMAN, E., ROBINSON, C. G., NICHOLS, M., MILKIE, D., TORRENS, O., PRICE, J., FISHER, C. B., SHARIFI, N., CALLE-SCHULER, S. A., KMECOVA, L., ALI, I. J., KARSH, B., TRAUTMAN, E. T., BOGOVIC, J. A., HANSLOVSKY, P., JEFFERIS, G., KAZHDAN, M., KHAIRY, K., SAALFELD, S., FETTER, R. D. & BOCK, D. D. 2018. A Complete Electron Microscopy Volume of the Brain of Adult Drosophila melanogaster. *Cell,* 174**,** 730-743 e22.
ZUO, Z., SMITH, R. N., CHEN, Z., AGHARKAR, A. S., SNELL, H. D., HUANG, R., LIU, J. & GONZALES, E. B. 2018. Identification of a unique Ca(2+)-binding site in rat acid-sensing ion channel 3. *Nat Commun,* 9**,** 2082.